



Macro-Scale Molecular Communications

Thesis submitted in accordance with the requirements of
the University of Liverpool for the degree of Doctor in Philosophy by

Daniel Tunç McGuiness

February, 2020

Abstract

The use of electromagnetic (EM) waves to transmit information has allowed our society to collaborate and share information on a scale that was unimaginable just a few decades ago. But as with any technology, there are areas where EM-based communications do not function well. For example, underwater and underground communications where EM waves experience high attenuation. This limitation has generated interest in an alternative mode of information transmission, molecular communications.

In this thesis, after giving a survey of micro- and macro-scale molecular communications, the two most important aspects of molecular communications are identified: macro-scale molecular communications and the experimental analysis of molecular communications. Molecular communication has been dominated so far by interest in the nano-scale, where the application focus is on drug-delivery and DNA communications, etc. Studies in the macro-scale are relatively rare compared to nano- and micro-scale research. This thesis looks closely at macro-scale molecular communication and attempts to improve our understanding of this novel communication paradigm. To achieve this, a mathematical model was developed, based on the advective-diffusion equation (ADE). The model was compared with experimental results, and showed a strong correlation. In addition, a model was developed to simulate molecular communication in both 1D and 3D environments.

To generate the modulated chemicals and transmit them in the environment, an in-house-built odour generator was used, and to detect the chemicals in the environment a mass spectrometer (MS) with a quadrupole mass analyser (QMA) was employed. Mass spectrometers have the ability to distinguish multiple chemicals in the environment concurrently, making them ideal detectors for use in molecular communications. Based on the experimental setup, various aspects of the communication paradigm are investigated in the three main sections. The first section focuses on the fundamental parameters that govern the propagation of molecules in a flow. The second section delves into the communication properties of this new form of information transfer. The final section studies aspects of simultaneous multiple-chemical transmission. Based on this multiple-chemical transmission, modulation methods are developed that exploit this new approach for use in molecular communications.

Acknowledgements

This thesis could have not been completed without the encouragement, collaboration, and support of a tremendous number of people.

First and foremost, I would like to extend my sincere thanks to my advisor, Professor Alan Marshall and Professor Stephen Taylor for their encouragement, support, and patience throughout my Ph.D. studies. I would definitely not reach this point without their support and encouragements. It was a privilege for me to work with extraordinary supervisors like them.

A special thanks to my family. Words can not express how grateful I am to my mother and my father for all the sacrifices that they have made for me throughout the years.

My special thanks goes to my dear girlfriend, Iris, for her unlimited love and endless support. Iris has supported me constantly during all these years, and without her support I would not have been as successful during my studies.

I would also like to thank my fellow collaborators, Valerio Selis and Stamatis Gianoukos for all the help and support they provided in this multidisciplinary research work.

Contents

Abstract	iii
Acknowledgements	v
Notations	xxiii
Preface	xxix
Glossary	xxix
1 Thesis Overview	1
1.1 Introduction	1
1.2 Contributions	3
1.3 Organisation of the Thesis	5
1.4 Publications	6
1.4.1 Journal Publications	6
1.4.2 Conference Proceedings	6
1.4.3 Poster Presentations	7
2 Background and Related Work	9
2.1 Introduction	9
2.1.1 Research History	11
2.1.2 Micro-Scale Molecular Communication	13
2.1.3 Macro-Scale Molecular Communication	13
2.2 Review Structure	14
2.3 Channel Theory	14
2.4 Propagation Speed	17
2.5 Methods of Propagation	18
2.5.1 Diffusion	18
2.5.1.1 Stochastic Approach	19
2.5.1.2 Analytical Approach	20
2.5.2 Advection	22
2.5.2.1 Stochastic Approach	22
2.5.2.2 Analytical Approach	22
2.5.3 Turbulent Flows	25
2.6 Modulation	26

2.6.1	Particle Quantity	27
2.6.2	Type and/or the structure of Particles	28
2.6.3	Time of Release	28
2.6.4	Hybrid Modulation Methods	30
2.7	Inter-symbol Interference (ISI)	30
2.7.1	Single Messenger Chemical	31
2.7.2	Multiple Messenger Chemicals	31
2.8	Error Correction	32
2.9	Information Security	33
2.10	Receivers	33
2.10.1	Micro-Scale Molecular Communication	34
2.10.2	Macro-Scale Molecular Communication	34
2.10.2.1	Electronic Nose	35
2.10.2.2	Mass Spectrometer	36
2.10.3	MIMO Applications	37
2.11	Experimental Analysis	37
2.12	Applications	40
2.12.1	Micro-Scale Molecular Communication	40
2.12.2	Macro-Scale Molecular Communication	40
2.13	Simulations	41
2.13.1	BiNS	43
2.13.2	N3Sim	43
2.13.3	COMSOL	43
2.13.4	NS2 and NS3	43
2.13.5	BNSim	44
2.13.6	NCSim	44
2.13.7	HLA	44
2.13.8	AcCoRD Simulator	44
2.13.9	Other Works	45
2.14	Standardisation	45
2.15	Conclusion	45
3	Experimental Setup	47
3.1	Introduction	47
3.2	Experimental Setup	49
3.2.1	Transmitter	49
3.2.2	Chemicals	49
3.2.3	Receiver	49
3.2.3.1	Membrane Inlet	52
3.2.3.2	Quadrupole Mass Analyser	53
3.3	Conclusion	58
4	Theory of Macro-Scale Molecular Communications	59
4.1	Introduction	59
4.2	Transmission of Molecules	59
4.2.1	Proposed Transmission Model	64
4.2.2	Open-Air Transmission	64

4.2.3	Closed-Boundary	66
4.2.4	The Radial-Advection-Diffusion Equation	67
4.2.4.1	Boundary Conditions	67
4.2.4.2	Absorption/Desorption Process	69
4.2.5	Calculation of the coefficient of Diffusivity	71
4.2.5.1	Entrance Length	72
4.2.5.2	Longitudinal Diffusivity	72
4.2.5.3	Transverse Diffusion	72
4.3	Simulation Framework	73
4.4	Conclusions	77
5	Analysis of Macro-Molecular Communications Parameters	79
5.1	Introduction	79
5.2	Noise Analysis	80
5.3	Signal Flow	81
5.3.1	Experiment Methodology	81
5.3.2	Signal Properties	82
5.3.3	Signal Energy and SNR	84
5.3.4	Modelling the Signal	85
5.4	Carrier Flow	86
5.4.1	Experimental Methodology	87
5.4.2	Signal Properties	87
5.4.3	Signal Energy and SNR	89
5.4.4	Modelling the Signal	89
5.5	Transmitted Bit Duration	91
5.5.1	Experimental Methodology	91
5.5.2	Signal Properties	91
5.5.3	Signal Energy and SNR	93
5.5.4	Modelling the Signal	94
5.6	Open-air Transmission	94
5.6.1	Experimental Methodology	95
5.6.2	Signal Properties	96
5.6.3	Signal Energy and SNR	97
5.6.4	Modelling the Signal	97
5.7	Closed-air Transmission	99
5.7.1	Experimental Methodology	100
5.7.2	Signal Properties	100
5.7.3	Signal Energy and SNR	101
5.7.4	Modelling the Signal	103
5.8	Conclusions	104
6	Modulation Analysis of Molecular Communications in the Macro-Scale	105
6.1	Introduction	105
6.2	M-ary Transmission	106
6.2.1	2-Ary Transmission	106
6.2.2	4-Ary Transmission	107
6.2.3	8-Ary Transmission	108

6.3	Molecular Inter-Symbol Interference (Mo-ISI)	109
6.3.1	One-to-Zero (o/z) Experiments	110
6.3.2	k Experiments	110
6.3.3	Residual Background Signal	111
6.4	Message Transmission Experiment	115
6.4.1	Results	115
6.5	Channel Capacity	117
6.6	Symbol-Error Rate (SER)	118
6.7	Theoretical Results	119
6.7.1	Symbol Duration	120
6.7.2	Coefficient of Diffusivity	121
6.7.3	Transmission Distance	122
6.7.4	Advection Flow	123
6.8	Bit Distribution	123
6.8.1	Symbol Period	124
6.8.2	Advection Flow	124
6.8.3	Diffusivity	125
6.8.4	Transmission Distance	126
6.9	Conclusion	126
7	Multi-Chemical Transmission	129
7.1	Introduction	129
7.2	Multi Chemical Transmission	130
7.3	Multi Chemical Noise	131
7.4	Molecular Quadrature Amplitude Modulation (MQAM)	132
7.4.1	Advection Flow	134
7.4.2	Coefficient of Diffusivity	136
7.4.3	Transmission Distance	137
7.5	Chemical Time Offset Keying (ChToK)	137
7.5.1	Experimental Analysis	138
7.6	Chemical Ratio Modulation (CRM)	140
7.6.1	Calculation of the modulation matrix	141
7.6.2	Experimental Analysis	143
7.7	Conclusion	145
8	Summary and Future-Work	147
8.1	Future Research Directions	149
8.1.1	Different Receivers	149
8.1.2	Turbulent Environments	149
8.1.3	Complex Geometries	150
8.1.4	Secure Chemical Communications	150
8.1.5	Novel Modulation Methods	150
A	Derivation of the Thin-Film Solution	151
B	Derivation of the Taylor-Aris Dispersion	155

C Photographs of the Experimental Setups	159
C.1 Experimental Setup	159
C.2 Transmitter	160
C.2.1 Odour Generator	160
C.2.2 Evaporation Chamber	161
D Derivation of the Optimal Sampling Time for 1D	163
Bibliography	165

Illustrations

List of Figures

1.1	Generalised diagram of molecular communication in the macro-scale.	1
1.2	Diagram showing the various aspects of molecular communication.	3
2.1	Diagram of the scale of molecular communications. (A) At the smaller scales of communication DNA is used to store information to pass it on to the next generation. (B) In blood vessels hormones and other signal chemicals are transmitted to maintain a living organism. (C) Large creatures use pheromones to locate mating partners across long distances (D) Mass transport can also be seen on a global scale such as the Gulf stream.	10
2.2	The significant points of molecular communications development.	11
2.3	Deoxyribonucleic acid (DNA) is used in biological systems to store genetic information. The prospect of storing and accessing information on a small and dense scale shows the possibility of implementing information transmission and storage on small scales [1]. An engineering approach to use DNA in molecular communication is to use it as a protocol between nanomachines [2].	13
2.4	Molecular communication can also be seen on the macro-scale. In moths, calling females attract their mates late at night with intermittent release of a species-specific sex-pheromone blend [3]. [Photo: Male Gypsy Moth, Credit: Ilona L/Flickr]	14
2.5	Diagram of a generalised communication system.	16
2.6	Types of modulation methods developed for use in molecular communications: Particle Quantity, Type and/or Structure of Particle and Time of Release.	26
2.7	A natural process in error correction occurs in DNA replications. The error correction in DNA is a collection of processes by which a cell identifies and corrects damage to the DNA molecules that encode its genome [4].	32
2.8	A block diagram of an electronic nose.	35
2.9	The principle diagram of the quadrupole mass analyser used in chemical detection: (1) Once the samples are introduced into the detector via the membrane inlet the chemicals are ionised and passed through a focus lens. (2) The analyser is made up from four hyperbolic rods with applied potentials. Based on the electric potential applied to the rods, which the connection diagram can be seen in (5), the ions can be separated based on their mass-to-charge values. Ions with stable trajectories, such as (4) will travel through the electric field and will arrive at the detector shown in (6), whereas ions with unstable trajectories (non-resonant ion), e.g. (3), will collide with the quadrupole and will be filtered out from the detection. Detected ions are amplified and presented visually as mass chromatogram shown in (7).	36

2.10	A representative diagram of the implementation of MIMO for use in molecular communications.	37
2.11	Experimental test beds used in literature.	38
2.12	Applications of molecular communication can be implemented both in micro-scale and macro-scale. At smaller scales, understanding of particle propagation and reception can be used to control bacteria and be used in implementing drug delivery systems. At larger scales, molecular communication can be used in studying animal behaviour.	41
3.1	The diagram of the experimental setup: (1) (N_2) gas is used as the carrier flow (Q) and is transferred into the MFC that control both the carrier flow (blue line) (Q) and the signal flow (yellow line) (q), (2) Modulation information is generated using computer software, (3) generated modulation is transmitted into an automation platform where it sends the modulation to the MFC's to create pulses, (4) MFC for the carrier flow, (5) MFC for the signal flow, (6) Evaporation Chamber (EC) where the signal chemical is injected, (7) Mixing chamber where the signal chemicals arrive and initiate the transmission from the transmitter to the receiver (8) Propagation medium (9) The inlet of the mass spectrometer, (10) Electronics control unit (ECU) which controls the mass analyser, (11) Pressure gauge, (12) Controller and the regulator cables for the mass spectrometer, (13) Data acquisition and analysis.	48
3.2	The working diagram of the odour generator (OG). [5] (1) Introduction of the carrier gas (Q) into the mixing chamber. (2) Mixing chamber where the evaporated chemicals from the chamber and the carrier gas are mixed. (3) Evaporation chamber (Figure 3.3). (4) Transmitted chemicals that are released from the chamber. (5) A modulation sequence that is used to create gas pulses.	50
3.3	Diagram of the evaporation chamber (EC): (1) inlet of the N_2 gas into the evaporation chamber. (2) Inlet where the sample is introduced. (3) Thermo-resistant septum that allows the multiple introduction of a sample via a micro syringe. (4) An absorptive material that holds the liquid sample analyte. (5) N_2 from the inlet carries the evaporated chemicals from the chamber. (6) The cumulated gas is transferred into the mixing chamber via a 6.35 mm inch Teflon tube.	50
3.4	Mass spectra of the signal chemicals used in the study. The mass spectra of the chemicals are obtained via the use of electron ionisation (EI) [NIST Chemistry WebBook (https://webbook.nist.gov/chemistry)].	51
3.5	Diagram that illustrates the process of pervaporation.	53

3.6	A diagram of the inner workings of the QMA. The sample is introduced into the system via a conduit, in which case is the membrane inlet and the sample is then bombarded with electrons in the EI to ionise. The ionised particles are then transferred into the quadrupole area via the focus lens which is fed with a DC voltages. The ions then travel the duration of the path inside the quasi-static electric field generated via the quadrupole. Only the ions with the correct mass-to-charge ratio have stable trajectories within the field generated via RF/DC applied to the electrodes. These ions are safely transported from the initial introduction to the electron multiplier. Ions with unstable trajectories, however, collide with the rods, or the walls of the chamber and are neutralised. Each ion passing through the mass analyser has a stability profile which is related to the DC and RF voltages applied to the rods. By adjusting these voltage values only specific ions can be monitored. This process, which is used in this study, is single ion monitoring (SIM).	54
3.7	(A) Equipotential lines generated by the quadrupoles (B) Electric vector field generated by the quadrupoles.	55
3.8	Examples of stable and unstable ion trajectories in a quadrupole.	56
3.9	The stability diagram for the Mathieu equation considering x and y coordinate directions. Four stability areas are shown in circles. The most common area that is used in quadrupole mass spectrometry is (A).	57
3.10	Stability diagrams plotted in RF-DC space, showing a straight scan line through the origin.	58
4.1	A diagram of the model used in the study. (A) At $t = 0$ s mass is injected into the environment. This is defined by the initial boundary condition $c(x_0, t_0) = M_0 \delta(x)$. (B) As the transmission evolves, the particles start propagating via advection and diffusion. (C) When the specified period is passed the transmitter stops releasing particles and transmits only advective flow. (D) The flow then forces the particles to be transferred from the detector to the outside environment. (E) After a finite amount has passed the particles are removed from the detector and transferred to the outside environment. However, some particles are left in the detector, which can cause inter-symbol interference for future transmissions (θ_{ISI}).	63
4.2	A Diagram showing the effect of open-air transmission.	65
4.3	A descriptive diagram of the model used in the study. At the initial stage of the experiment ($t = 0$ s) a mass is injected into the environment. Once the mass is injected, to simulate the effect of physical boundary of the environment ($A^{(0)}$), additional gas pulses are generated in the y -coordinates with positive sides being $y = 2L, y = 4R, \dots, y = 2nR$ ($A^{(1,2,\dots,\infty)}$). This is also carried out in the x -coordinates. As transmission evolves, the gas pulses transcend the boundary of the propagation medium, at which point the mirror pulses are added to the actual transmission to create the effect of the boundary.	68

4.4	Experimentally measured chemical detection with comparison to empirical fitting (linear $R^2 = 0.9891$)	71
4.5	A diagram of the algorithm used to simulate on-off keying (OOK) for macro-scale molecular communications	73
4.6	A representative diagram of how the transmission is simulated with an example transmission of a bit sequence of 011100111000 with states of the transmission (Γ_S) shown above the transmission. The first part of the simulation is to analyse the sequence based on the states. In this context the states are defined as a bit value, which in this example are 0 and 1. In this example there are five states which are 0-1-0-1-0 with durations of $1T_S$ - $3T_S$ - $2T_S$ - $3T_S$ - $3T_S$. After this assessment the system carries out the following procedures to initiate the simulation. In this example at time-point (1), the detector starts absorbing particles with the absorbing function θ_1 and this function continues until the time period of the state concludes at (4) in which the duration of the state is shown as the feedback loop to the state itself, with each bit-1 value having the absorbed mass value of $\theta_1(x, T_S)$, $\theta_1(x, 2T_S)$ and $\theta_1(x, 3T_S)$, respectively. When the time duration passes the time mark (4), the removal function (θ_0) initiates and starts removing the particles from the detector based on how many particles it has absorbed in the previous state.	76
5.1	(A) Experimental data (—) along with the theoretical fit (—) of the environmental noise. (B) FFT analysis of the noise.	80
5.2	Experimental diagram of the signal flow study	82
5.3	(A) Experimental results of the signal flow study. (B) Experimental along with theoretical comparison of signal amplitude. (Equations used in modelling: Eq. 4.11c and Eq. 4.14c)	82
5.4	(A) Signal variance of the experimental data (●) with approximation (Eq. (5.5) (—). (B) Signal correlation values (●)	83
5.5	Experimental (●) along with theoretical comparison (—) of: (A) signal energy, (B) signal-to-noise ratio (SNR)	85
5.6	Experimental and theoretical comparison of the signal shape in the signal flow study: (A) odd numbered signal flow values, (B) even numbered signal flow values. (Equations used in modelling: Eq. 4.11c and Eq. 4.14c)	86
5.7	Experimental diagram of the carrier flow study	87
5.8	Experimental results of the carrier flow (Q) experiments	88
5.9	Comparison of the maximum signal amplitude of the transmitted signal (●) and the values generated by the theoretical model (—). (Equations used in modelling: Eq. (5.12))	88
5.10	(A) Signal variance of the carrier flow study. (B) Signal correlation values of the carrier flow study	89
5.11	Experimental (●) along with theoretical (—) comparison of (A) signal energy, (B) signal-to-noise ratio	90

5.12	Experimental along with theoretical comparison of the bulk flow study. (Equations used in modelling: Eq. 4.11c and Eq. 4.14c)	90
5.13	Experimental diagram of the bit duration study.	92
5.14	Results of the bit duration study.	93
5.15	Experimental (●) along with theoretical (—) comparison of (A) maximum signal amplitude, (B) leftover signal from the bit duration study. (Equations used in modelling: Eq. 4.11c and Eq. 4.14c)	93
5.16	Experimental (●) along with theoretical (—) comparison of (A) Signal Energy (B) Signal-to-Noise ratio.	94
5.17	Experimental along with theoretical comparison of the bit duration study. (Equations used in modelling: Eq. 4.11c and Eq. 4.14c)	94
5.18	Experimental diagram of the open-air transmission study.	96
5.19	(A) Experimental results of the open-air study. (B) Experimental (●) along with theoretical (—) values of maximum signal amplitude.	96
5.20	Experimental (●) along with theoretical (—) comparison of; (A) comparison of experimental along with theoretical values of signal energy, (B) experimental along with theoretical values of signal to noise.	97
5.21	Open-Air transmission along with theoretical comparison (A) 2.5 cm (B) 5 cm (C) 7.5 cm (D) 10 cm (E) 12.5 cm (F) 15 cm	98
5.22	Experimental diagram of the closed-distance study.	100
5.23	(A) Experimental results of closed-boundary transmission. (B) Experimental results along with the theoretical comparison of the maximum signal amplitude of closed boundary transmission.	101
5.24	(A) Experimental results along with the theoretical comparison of the signal energy of closed boundary transmission (B) Experimental results along with the theoretical comparison of the Signal-to-Noise ratio (SNR) of closed boundary transmission.	102
5.25	Experimental results along with theoretical comparison for each experimental transmission (A) 0.5 m (B) 1 m (C) 1.5 m (D) 2 m (E) 2.5 m (F) 3 m.	103
6.1	Experimental (—) along with theoretical (—) comparison of M-ary experiments. (A) 2-ary transmission with bit duration of 30s. (B) 2-ary transmission with bit duration of 60s. (C) 2-ary transmission with bit duration of 90s. (D) 4-ary transmission with bit duration of 30s. (E) 4-ary transmission with bit duration of 60s. (F) 4-ary transmission with bit duration of 90s. (G) 8-ary transmission with bit duration of 30s. (H) 8-ary transmission with bit duration of 60s. (I) 8-ary transmission with bit duration of 90s. (Equations used in modelling: Eq. 4.11c and Eq. 4.14c)	108

6.2	Experimental (—) along with theoretical (—); (A) Bit transmission of 11111 0 11111 pairs. (B) Bit transmission of 11111 00 11111 pairs. (C) Bit transmission of 11111 000 11111 pairs. (D) Bit transmission of 11111 0000 111111 pairs. (E) Bit transmission of 11111 00000 11111 pairs. (F) Bit transmission of 1 0 1 pairs. (G) Bit transmission of 11 00 11 pairs. (H) Bit transmission of 111 000 111 pairs. (I) Bit transmission of 1111 0000 1111 pairs. (Equations used in modelling: Eq. 4.11c and Eq. 4.14c)	110
6.3	A diagram of possible transmissions that can create leftover chemicals (θ_{ISI}). In each sub-plot the bits are shown as circle diagrams and their duration is defined as Γ_S . In this model, shown in Chapter 4, the bits are defined as the continuation of the θ function. For example, a transmission of 111 will have absorbed mass values of $\theta_1(x, T)$, $\theta_1(x, 2T)$ and $\theta_1(x, 3T)$, respectively. Based on this behaviour, each different bit is defined as a state and can be seen in the sub-plots. (A) A sequential transmission of 1's and 0's continuously (e.g., 110011001100...) (B) A transmission of uneven amounts of 1's and 0's (e.g., 100010001001...) (C) A transmission where the transmission ends with chemical introduction into the environment (e.g., 101100011101111...)	112
6.4	(A) Experimental results of the leftover chemicals from k experiment along with theoretical comparison. (B) Experimental results of the o/z bit transmission with comparison to the theoretical model. (Equations used in modelling: Eq. 4.11c and Eq. 4.14c)	113
6.5	Experimental (—) along with theoretical (—) transmission of the message “ <i>Call Me Ishmael</i> ”. (Equations used in modelling: Eq. 4.11c and Eq. 4.14c)	116
6.6	Representative diagram of a binary asymmetric channel.	117
6.7	(A) Theoretical results of the Symbol-Error Rate (SER) of M_C -ary transmission. (B) Theoretical results of the achievable mutual information (MI) rate of M_C -ary transmission. ($x_d = 2.5$ cm, $u_x = 0.2$ cm/s, $D_L = 0.124$ cm ² /s, $T_S = 60$ s, $M = 0.4$ ng)	118
6.8	(A) Experimental (—) along with theoretical (—) comparison of the SER experiment. (B) Achievable mutual information based on the theoretical model shown in (A).	120
6.9	(A) SER of different durations of symbol time (T_S) values with respect to SNR. (B) Achievable MI of different durations of symbol time (T_S) values with respect to SNR.	120
6.10	(A) SER with increasing symbol duration (T_S). (B) Achievable MI with increasing symbol duration (T_S).	121
6.11	(A) SER of different coefficients of diffusivity (D_L) values with respect to SNR. (B) Achievable MI of different coefficients of diffusivity (D_L) values with respect to SNR.	121
6.12	(A) SER with increasing coefficients of diffusivity (D_L). (B) Achievable MI with increasing coefficients of diffusivity (D_L).	122

6.13	(A) SER of different transmission distance (x_d) values with respect to SNR. (B) Achievable MI of different transmission distance (c_d) values with respect to SNR.	122
6.14	(A) SER with increasing transmission distance (x_d). (B) Achievable MI with increasing transmission distance (x_d).	123
6.15	(A) SER of different advective flow (u_x) values with respect to SNR. (B) Achievable MI of different advective flow (u_x) values with respect to SNR.	123
6.16	(A) SER with increasing advective flow (u_x). (B) Achievable MI with increasing advective flow (u_x).	124
6.17	Simulation results of the symbol distribution of the transmitted symbol. In the plot μ are the mean value of the received mass of their respective symbol.	124
6.18	Simulation results of the symbol distribution of the transmitted symbol. In the plot μ are the mean value of the received mass of their respective symbol.	125
6.19	Simulation results of the symbol distribution of the transmitted symbol. In the plot μ are the mean value of the received mass of their respective symbol.	125
6.20	Simulation results of the symbol distribution of the transmitted symbol. In the plot μ are the mean value of the received mass of their respective symbol.	126
7.1	(A) Experimental results along with theoretical results of multi-chemical transmission. (Equations used in modelling: Eq. 4.11c and Eq. 4.14c) (B) Experimental along with theoretical fitting of multi-chemical noise.	131
7.2	A constellation diagram for use in molecular quadrature amplitude modulation (MQAM).	133
7.3	(A) Simulation results of the SER of MQAM transmission. (B) Simulation results of the MI of MQAM transmission.	134
7.4	Simulation results of molecular communication using molecular quadrature amplitude modulation (MQAM): (A) Constellation diagram of MQAM with different advective flow rates. (B) Constellation diagram of MQAM with longitudinal diffusivity rates. (C) Constellation diagram of MQAM with different transmission distance rates. (D) Distribution of received θ_I and θ_Q masses with different advective flow rates. (E) Distribution of received θ_I and θ_Q masses with different longitudinal diffusivity rates. (F) Distribution of received θ_I and θ_Q masses with different transmission distance rates. [Ideal R_X value (●)]	135
7.5	(A) Simulation results of the SER of MQAM transmission for different advective flows. (B) Simulation results of the MI of MQAM transmission for different advective flows.	136
7.6	(A) Simulation results of the SER of MQAM transmission for different longitudinal diffusion. (B) Simulation results of the MI of MQAM transmission for different longitudinal diffusion.	136
7.7	(A) Simulation results of the SER of MQAM transmission for different transmission distance. (B) Simulation results of the MI of MQAM transmission for different transmission distance.	137
7.8	Diagram representing the chemical shift keying (ChSK).	138

7.9	Experimental transmission of acetone and methanol using ChToK.	139
7.10	Experimental transmission of the acetone (—) along with the theoretical comparison (—). (Equations used in modelling: Eq. 4.11c and Eq. 4.14c)	140
7.11	Diagram representing the chemical ratio keying (CRK).	140
7.12	(A) Comparison of the unique values of the ratio modulation (—) comparison to the function $\phi_A\phi_B \frac{\pi^2}{6}$. (—)(B) Relative error ($\eta\%$) of the $\phi_A\phi_B \frac{\pi^2}{6}$ approximation.	143
7.13	(A) Experimental transmission with increasing distance of (A) acetone (B) cyclopentane (C) n-hexane.	144
7.14	Experimental results of chemical ratio keying (ChRK) by using three different chemicals: acetone, cyclopentane and n-hexane. The figures above show the signal strength with increasing distance: (A) 0.5 m, (B) 1.0 m, (C) 2.0 m and (D) 4.0 m.	144
7.15	Experimental ratio values from the ratio modulation study: (A) Signal amplitudes of the three transmitted chemicals relative to distance. (B) Amplitude values of chemicals relative to 0.5 m signal current values.	145
7.16	Experimental ratio values from the ratio modulation study: (A) cyclopentane/acetone, (B) acetone/n-hexane.	145
A.1	Diffusion process in time of a localized mass injection. As the mass concentration distributes along the x -axis, the area under the curve is preserved	152
C.1	(A), (B)Experimental setup for long distance transmission. (C) Experimental setup for short distance transmission.	159
C.2	(A) The odour generator with three evaporation chambers and mass flow controllers attached. (B) A close-up of the evaporation chambers connected to the odour generator. (C) A close-up of the mass flow controllers connected to evaporation chambers. (D) An odour generator with a single evaporation chamber and mass flow controller attached.	160
C.3	(A) Evaporation chamber. (B) Evaporation chamber disassembled. (C) Evaporation chamber from a different angle. (D) Evaporation chamber disassembled from a different angle.	161

List of Tables

2.1	Comparison of communication systems.	15
2.2	Speed comparison examples between micro-scale and macro-scale molecular communication methods.	17
2.3	Comparison of modulation methods.	29
2.4	Experimental test beds used to study molecular communications.	39
2.5	Simulation platforms for use in molecular communications.	42
3.1	Chemicals used throughout the thesis.	52
5.1	Parameters for signal flow study	81
5.2	Correlation (ρ) results of signal flow study	85
5.3	Parameters for carrier flow study	86
5.4	Correlation (ρ) results of bulk flow study	91
5.5	Parameters for bit duration experiment	92
5.6	Correlation (ρ) results of bit duration study	95
5.7	Parameters for open-air transmission study.	95
5.8	Correlation (ρ) results of open-air transmission study	99
5.9	Parameters in the closed-distance study	99
5.10	Correlation results of closed-air transmission study.	104
6.1	Parameters for M_C -ary transmission study.	107
6.2	Parameters for Mo-ISI transmission study.	109
6.3	Parameters for the message transmission study.	116
6.4	Parameters for symbol error rate (SER) transmission study.	119
6.5	Theoretical parameters for symbol error rate (SER) and mutual information (MI) study.	120
7.1	Parameters for multi-chemical transmission study.	130
7.2	parameters for multi-chemical noise study.	132
7.3	Theoretical parameters of molecular quadrature amplitude modulation (MQAM).	134
7.4	Parameters for chemical time offset keying transmission study.	139
7.5	Particular values of the Riemann-Zeta function.	142
7.6	Experimental parameters for chemical ratio keying (ChRK).	143

Notations

The following notations and abbreviations are found throughout this thesis:

Constants	Definitions	Units	Chapters
π	Circle's circumference to diameter ratio	—	2,4
c_l	Speed of light in a vacuum	m/s	2
k_B	Boltzmann's constant	J/K	2
e	Electric charge of an electron	Coulombs	3
Constants	Definitions	Units	Chapters
$\beta^O(\cdot)$	Signal energy (open-transmission)	Watts	5
$\beta^C(\cdot)$	Signal energy (closed-transmission)	Watts	5
$\Gamma(\cdot)$	State array	—	4
Γ_S	State duration	s	4
Γ_u	Mathieu umbrella term	—	3
Δ	Change of changeable quantity	—	2
$\delta(\cdot)$	Dirac delta function	—	2,4
η	Dynamic viscosity of a fluid	N · s/m ²	2
θ_i	Angular position of random walk	rad	2
$\theta_A(\cdot)$	Captured mass function	kg	4, 5
$\theta_E(\cdot)$	Particles in the environment	kg	4
$\theta_{ISI}(\cdot)$	Leftover particles in the detector	kg	4
$\theta_1(\cdot)$	Mass absorption function	kg	4
$\theta_0(\cdot)$	Mass removal function	kg	4
λ_n	Hankel transform parameter	—	2
$\lambda_x, \lambda_y, \lambda_z$	Reference Frame	m	2
λ_D	Decay function of open-air transmission	1/s	4
μ	Expected value of a data set	—	2
$\mu_D(\cdot)$	Drag forces (i.e. drift velocity)	m/s	2
ξ	Mathieu equation transform parameter	—	3
ρ_D	Density of fluid	kg/m ³	2
ρ_r	Radius of the cylindrical system	m	2
$\rho_{X,Y}$	Pearson coefficient of X and Y	—	5
σ	Variance of a data set	—	2

ζ_k	i.i.d random variable	—	2
τ	Wall shear stress	Pa	4
τ_s	Static threshold value	—	2
v	Dimension number	—	2
ϕ	Porosity	—	2
ϕ_A, ϕ_B	Chemical identities	—	7
ϕ_i	Angular position of random walk	rad	2
Φ_0	Applied potential to quadrupole	Volts	3
φ	Phase of a wave	rad	2
ψ	Scalar field	—	2
ω	Angular frequency	rad/s	3
Roman Letters	Definitions	Units	Chapters
A	Cross-sectional area	m^2	4
A_w	Amplitude of the wave	—	2
A_{yz}	Area-scale constant	m^2	4
a	Decay parameter	—	4
a_u	Mathieu parameter	—	3
B_F	Bulk flow	ml/min	3
$B(\cdot)$	Bit array	—	4
b	Decay parameter	—	4
C	Channel capacity	bits/channel	2, 6, 7
Ch	Number of chemicals	—	7
c	Concentration function	kg/m^v	2, 3, 4
D	Coefficient of diffusivity	m^2/s	2,3,4
D_x, D_y, D_z	Cartesian coefficient of diffusivity	m^2/s	4
D_H	Hydraulic diameter	m	2
D_L	Longitudinal coefficient of diffusivity	m^2/s	2
D_R	Radial coefficient of diffusivity	m^2/s	2
D_V	Random forces on a particle	m^2/s	2
D_n	Kolmogorov-Smirnov test	—	5, 7
d	Diameter	m	2, 5
E	Experimental data set		5
E_b	Energy per bit	W	7
E_S	Energy per symbol	W	6
F	Theoretical CDF		5
F_n	Empirical CDF		5
F_x, F_y	Force acting on ion in x and y axis	$\text{kg} \cdot \text{m}/\text{s}^2$	3
f	Frequency	Hz	2
f_D	Darcy-Weisbach friction factor		2
f_N	Noise present in the environment		2

$I(\cdot; \cdot)$	Mutual information	bits/symbol	2
i	Loop operator	—	4
$J(x, t)$	Diffusion flux	$1/\text{m}^2 \cdot \text{s}$	3
j	Loop operator	—	4
\vec{j}	Flux	—	2
K	Eddy coefficient of diffusivity	m^2/s	2
k	number of mirror images	—	4
$k(\cdot)$	frequency array	—	4
N_0	Noise Power	Watts	2
$\mathcal{N}(\mu, \sigma^2)$	Gaussian Distribution	—	2, 5, 6 7
L_D	Characteristic dimension	m	2
L_z	Length-scale constant	m	4
$H(\cdot)$	Information entropy function	—	6
$M(\cdot)$	Ratio modulation matrix	—	7
h	Loop operator	—	4
M_0	Injected mass to the environment	kg	2,4
M_C	Constellation number	—	7
M_n	Adjusted mass	kg	2,4
M_R	Absorbed mass by the detector	kg	2,4
m	Mass a particle	kg	2,3
N_0	Energy of the noise	—	2,7
n	Block size	—	2
$P(\cdot)$	Frequency conversion array	—	4
P_E	Pressure of the environment	atm	2,6,7
P_F	Carrier flow pressure	—	6
P_S	Probability of symbol error	—	7
P_V	Vacuum pressure	atm	2
$p_v^n(t)$	Particle position	m	2
Q	Carrier flow	ml/min	3
$Q(t)$	Simulation mass function	kg	4
q	Signal flow	ml/min	3
q_u	Mathieu parameter	—	3
R	Sink/Source	—	2,4
$R(\cdot)$	State conversion array	—	4
R_D	Detector radius	m	4,5,6,7
R_M	Boundary radius	m	4,5
$R(\cdot)$	State conversion array	—	4
r	Radius	m	2
$2r_0$	Quadrupole distance	m	3
S	Signal Power	Watts	2
T_E	Temperature of the environment	K	2

T_t	Simulation time parameters	s	4
T_s	Symbol period	s	4
T_{OSP}	Optimal sampling period	s	4
t_0	Time of instant release	s	2
t_b	Duration of the bit	s	5
t_d	Chemical detection delay	s	5, 6, 7
t_p	Propagation delay of the chemical	s	4
t	Time	s	2,3,4
U	Direct potential	V	3
u	Advective flow	m/s	2,4
u_*	Shear flow	m/s	4
\vec{u}	Advective flow vector	m/s	2
u_x, u_y, u_z	Vector elements	m/s	2
u_{avg}	Average flow	m/s	4
u_{max}	Maximum flow	m/s	4
V	RF voltage	V	3
W_n	Wiener Process		2
w	Loop operator	—	4
x, y, z	Cartesian coordinates	m	2,3
x_0, y_0, z_0	Injection point	m	4
x_e, y_e, z_e	backward propagation	m	4
x_d, y_d, z_d	forward propagation	m	4
\mathcal{X}	Signal flow values		6
Y	Discrete Variable		2
\mathcal{Y}	Symbol values		6

Mathematical Notation	Definitions	Units	Chapters
\sum	Sum	—	
\prod	Product	—	
$x \triangleq y$	x equal by definition to y	—	
∇	Del operator	—	
∇^2	Laplace operator	—	
$\text{erf}(\cdot)$	Laplace operator	—	
P_{XY}	Joint probability of X given Y	—	
$P_{X Y}$	Conditional probability of X given Y	—	
J_0	Bessel function of the 0 th kind	—	
J_1	Bessel function of the 1 st kind	—	
$\text{Var}(\cdot)$	Variance	—	
$\text{cov}(\cdot)$	Covariance	—	
$E_1(\cdot)$	Exponential integral	—	
$B_n(\cdot)$	Bernoulli number	—	

\sup	Supremum	—	6, 7
\mathbb{N}	Set of natural numbers	—	7
\mathcal{R}	Set of real numbers	—	7
card	Cardinality of a set	—	5, 7

Preface

All of the work presented henceforth was conducted in the Advanced Network Research Group (ANRG) and the Mass Spectrometry Laboratory at the department of Electrical Engineering & Electronics, University of Liverpool, UK.

A version of Chapter 4 has been published in the journal IEEE Access as *Parameter Analysis in Macro-Scale Molecular Communications Using Advection-Diffusion*, in IEEE Communication Letters as *Experimental Results on the Open-Air Transmission of Macro-Molecular Communication Using Membrane Inlet Mass Spectrometry* and in IEEE Access as *Modulation analysis in Macro-Molecular Communications*. I was the lead investigator, responsible for all major areas of concept formation, mathematical modelling and analysis, as well as manuscript composition. Professor Alan Marshall was the supervisory author on this project and was involved throughout the project in concept formation and manuscript edits.

A version of Chapter 5 has been published in the journal IEEE Access as *Parameter Analysis in Macro-Scale Molecular Communications Using Advection-Diffusion* and in IEEE Communication Letters as *Experimental Results on the Open-Air Transmission of Macro-Molecular Communication Using Membrane Inlet Mass Spectrometry*. I was the lead investigator, responsible for all major areas of concept formation, data collection and analysis, as well as manuscript composition. Professor Alan Marshall was the supervisory author on this project and was involved throughout the project in concept formation and manuscript edits.

A version of Chapter 6 has been published in the journal IEEE Access as *Modulation analysis in Macro-Molecular Communications* and presented in ACM Nanocom 2018 under the name *Asymmetrical Inter-Symbol Interference in Macro-Scale Molecular Communications*. I was the lead investigator, responsible for all major areas of concept formation, data collection and analysis, as well as the majority of manuscript composition. Professor Alan Marshall was the supervisory author on this project and was involved throughout the project in concept formation and manuscript edits.

I was the lead investigator for the projects located in Chapters 7 where I was responsible for all major areas of concept formation, data collection and analysis, as well as the majority of manuscript composition. Professor Alan Marshall was the supervisory author on this project and was involved throughout the project in concept formation and manuscript edits.

All simulations presented throughout the thesis were conducted using MATLAB 2018b (v9.5) by MathWorks.

Glossary

R_X	Receiver.
T_X	Transmitter.
AC	Acoustic Communications.
AcCoRD	Actor-based Communication via Reaction-Diffusion.
ADE	Advection-Diffusion Equation.
ANN	Artificial Neural Network.
ASK	Amplitude Shift Keying.
AWGN	Additive White Gaussian Noise.
BiNS	Biological and Nano-Scale communication simulator.
CDF	Cumulative Density Function.
ChRK	Chemical Ratio Keying.
CPU	Central Processing Unit.
CSI	Channel State Information.
CSK	Concentration Shift Keying.
CtS	Communication through Silence.
D-MoSK	Depleted Molecular Shift Keying.
DC	Direct Current.
DNA	Deoxyribonucleic acid.
DPPE	1,2-Dipalmitoyl-sn-glycero-3-phosphoethanolamine.
EC	Evaporation Chamber.
EEG	Electroencephalography.
EI	Electron Ionizer.
EM	Electromagnetic.
EMI	Electromagnetic Interference.
FEA	Finite Element Analysis.
FSK	Frequency Shift Keying.

GPU	Graphical Processing Unit.
HLA	High Level Architecture.
HMS-D1	Hybrid Modulation Scheme Design 1.
HMS-D2	Hybrid Modulation Scheme Design 2.
I-CSK	Isomer based Concentration Shift Keying.
I-MoSK	Isomer based Molecular Shift Keying.
IEEE	Institute of Electrical and Electronics Engineers.
IRSK	Isomer Ratio Shift Keying.
ISI	Inter-Symbol Interference.
MAM	Multilevel Amplitude Modulation.
MC	Molecular Communications.
MCDF	Molecular Coding Distance Function.
MFC	Mass Flow Controller.
MI	Mutual Information.
MIMO	Multiple Input Multiple Output.
MIMS	Membrane Inlet Mass Spectrometer.
MOSFET	Metal-Oxide-Semiconductor Field-Effect Transistor.
MoSK	Molecular Shift Keying.
MS	Mass Spectrometer.
MSSK	Molecular Spatial Shift Keying.
NSN	Nanoscale Sensor Networks.
OEIS	On-Line Encyclopaedia of Integer Sequences.
OG	Odour Generator.
OO-MoSK	On-Off Molecular Shift Keying.
OOK	On-Off Keying.
OPDE	Ordinary Partial Differential Equation.
OSI	Open Systems Interconnection model.
PAM	Pulse Amplitude Modulations.
PDE	Partial Differential Equation.
PDMS	polydimethylsiloxane.
PPM	Pulse Position Modulation.
PSK	Phase Shift Keying.
QMA	Quadrupole Mass Analyzer.

QMS	Quadrupole Mass Spectrometry.
QMSSK	Quadrature Molecular Spatial Shift Keying.
RF	Radio-Frequency.
RM	Rate Modulation.
SCW	Strongly Constant Weight Code.
SDE	Stochastic Differential Equation.
SER	Symbol Error Rate.
SNR	Signal to Noise Ratio.
SPION	Super Paramagnetic Iron Oxide Nanoparticles.
TCP	Transmission Control Protocol.
TEC	Time-Elapsed Communication.
TS	Type Based Sign.
TSH	Thyroid Stimulating Hormone.
VOC	Volatile Organic Compound.
VR	Virtual Reality.
Wi-Fi	Wireless Fidelity.

Chapter 1

Thesis Overview

1.1 Introduction

The need to convey messages has always been an important aspect of our society and the ability to send information across vast distances has allowed our cities to grow, our connections to widen and turned our civilisation into a global entity. Nowadays, communication systems provide a constant information access through the use of Electromagnetic (EM) signals. Even though, the benefits brought by EM are too numerous to count, there are still environments where the communication may not be reliable or even feasible. Examples of environments hostile towards EM waves are pipelines, tunnels or salt-water environments. The uneven salinity of the water can make connection unpredictable and the pipelines can absorb the energy of the waves, causing high attenuation. The drawbacks of EM are not limited in macro-scale (cm – m), as limitations also exist in small scales, especially in the micro-scale (nm – μ m) where EM is physically limited due to the ratio of the antenna size to the wavelength of the EM signal [6].

An approach that shows promise in overcoming the problems EM faces in both scales is the use of molecular communications. Molecular communications is an approach to transmit information where the transmitter releases to the environment particles (i.e., molecules, gas, pheromones etc.) that are encoded with information and are propagated through the environment until it is detected by a receiver. A diagram that represents a molecular communications process can be seen in Figure 1.1.

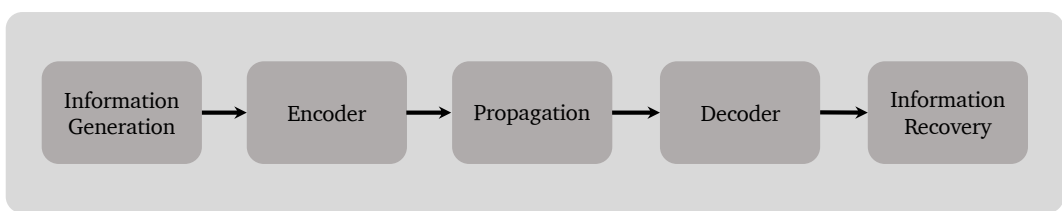


FIGURE 1.1: Generalised diagram of molecular communication in the macro-scale.

The applications of molecular communication in the macro-scale can be realised in fields such as robotics and infrastructure monitoring (e.g., pipes). It has been proposed that molecular communications can be used as a communication link for monitoring confined environments when the environment cannot act as a waveguide for EM¹. For robotics, molecular communication has been proposed to be used for distress signalling by defective robots² and for chemical trails for robot guidance³. There molecular communications can also benefit in environments where search and rescue operations can be harsh to EM waves and in infrastructure monitoring the same can be said of the pipelines in buildings that need to be monitored.

Nature, unlike our society, prefers the use of molecular communication over EM communication. Various examples can be seen in the animal kingdom, where communication is via the use of pheromones between the same species to convey information. The use of molecular communication is not bounded to macro-scale as the use of chemical communication can also be observed in bacteria, especially in quorum sensing⁴. Quorum sensing is a bacteria-to-bacteria chemical communication mechanism whereby bacteria share information it gathers (e.g., chemical concentration) and shares this information with surrounding bacteria⁵. Another benefit of using molecular communication over EM is its energy efficiency in the propagation of the chemical, where under some circumstances (i.e., diffusion), the system can be completely independent from external energy sources. The scale in which it can operate and its ability to be energy independent makes molecular communication a possible alternative to EM for harsh environments.

However, there are drawbacks to this novel communication paradigm. The biggest one being the propagation speed and the maximum achievable throughput. The low speed also increases the diffusion time, which decreases the signal amplitude, and generates more errors in the communication system. The system, therefore, may not be suitable for long range communication and EM is the better alternative.

Due to the potential of molecular communication at the micro-scale (i.e., drug delivery, in-vivo communication), research efforts have predominantly been focused on understanding the underlying principles of micro-scale molecular communication, leaving the macro-scale communication, ranging from **cm to meters**, mostly uninvestigated. Hence, there are still many problems needed to be solved and principles to be understood in the large-scale counterpart of molecular communication. In addition, while the mathematical definitions are well defined for micro-scale, macro-scale has different dominant aspects (i.e., advection, dimensional diffusivity) that change the behaviour of the communication. Micro-scale

¹Qiu, S., Guo, W., Wang, S., Farsad, N., and Eckford, A. A molecular communications link for monitoring in confined environments in *2014 IEEE International Conference on Communications Workshops (ICC)* IEEE, 2014

²Purnamadja AH, Russell RA. "Pheromone Communication in a Robot Swarm: Necrophoric Bee Behaviour and its Replication" *Robotica* vol. 23 pp. 731–742

³Sousa P, Marques L, De Almeida A Toward chemical-trail following robots. In, *Seventh International Conference on Machine Learning and Applications (ICMLA08)*. pp. 489–494. doi: 10.1109/ICMLA.2008.133

⁴B. L. Bassler, "How Bacteria Talk to Each Other: Regulation of Gene Expression by Quorum Sensing" *Current Opinion in Microbiology*, vol. 2, no. 6, pp. 582–587, 1999, doi:10.1016/S1369-5274(99)00025-9.

⁵Tissera, P. S. S., and S. Choe. "Brownian-motion-based molecular communication network using quorum sensing mechanism" in *International Conference on Information and Communication Technology Convergence (ICTC)* IEEE, 2017, doi:10.1109/ICTC.2017.8190938.

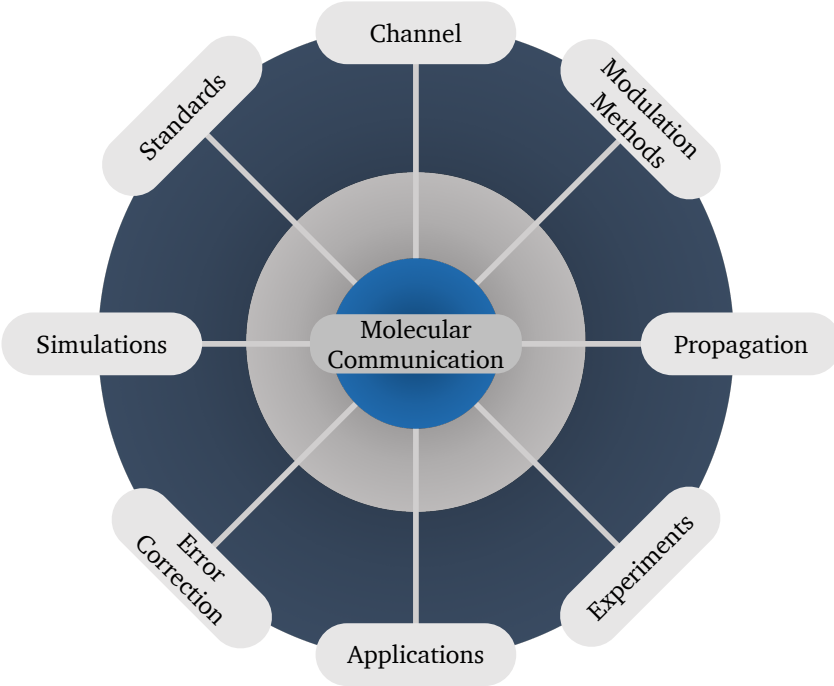


FIGURE 1.2: Diagram showing the various aspects of molecular communication.

communication, due to its scale, relies on diffusion to transmit the particles. In describing the diffusion element, it is generally modelled as Brownian motion (i.e., random walk) and is unbiased towards any dimension where the diffusion action takes place. In macro-scale, however, diffusion alone is not sufficient to carry out reliable transmission. Therefore, advection element is required. The presence of the advection element changes the behaviour of the diffusive element as diffusion in which advection takes place (i.e., transverse) is significantly higher than dimensions perpendicular to the advection (i.e., radial). Therefore, the study presented in this thesis approaches molecular communications with a heavy emphasis on understanding the principles of macro-scale communication. The research plan of the study can be categorised into two major aspects. The first aspect of the study is to establish a mathematical model that is able to accurately correlate with experimental data and to be able to predict the communication with different parameters. The second major aspect is the emphasis of experimental study of macro-scale molecular communication. As mentioned previously, molecular communication is currently a research field dominated by theoretical studies, with only a few experimental test beds designed. Therefore, this study is heavily focused on the experimental analysis of macro-scale molecular communications.

1.2 Contributions

The contributions of the thesis are as follows;

- **Review on Molecular Communications:** A literature survey on the topic of molecular communication was carried out focusing on the numerous topics of communication

properties: modulation, channel capacity, error correction, propagation methodologies etc. Additional research was undertaken regarding the simulation frameworks designed to study the various aspects and scales of molecular communication, as well as the application prospect of this novel communication method.

A diagram showing the various aspects of molecular communication given in the survey is presented in Figure 1.2.

- **Simulation Framework [8–10]:** To analyse the communication system and generate accurate predictions of macro-scale molecular communication behaviour, a simulation framework was developed based on the Advection-Diffusion Equation (ADE). The developed simulation was used to describe the numerous aspects of molecular communication in 3D macro-scale environments.
- **Parameter analysis of Molecular Communications [8]:** Macro-scale molecular communication is still in its infancy compared to micro-scale molecular communication. The parameters that govern the macro-scale molecular communication were analysed. These include, the signal flow, carrier flow and the bit duration. To further increase understanding a mathematical model of molecular communication propagation is developed and compared with experimental results.
- **Distance Analysis of Molecular Communications [9]:** Unlike signal flow, carrier flow and bit duration, distance plays a significantly different role due to the method of propagation. Based on the communication in question, there are two types of communication medium; open space (i.e., no boundary) and closed space (i.e., boundary). Experiments were done to analyse both communication mediums and mathematical models were developed to explain these effects.
- **Modulation Analysis [10]:** An important aspect of any communication method is its ability to convey information, making modulation an essential part of molecular communication. Based on traditional modulation methods for EM transmission, experiments were analysed on M_C -ary modulation and its Symbol Error Rate (SER) with different levels of modulation ($M_C = 2, M_C = 4, M_C = 8$). In addition, experimental analysis was carried out on the leftover chemicals lingering in the medium to better understand the effect of inter-symbol interference (ISI) on the communication and based on experimental studies, mathematical descriptions were derived to explain and predict the residual chemicals in the channel. The channel where the transmission occurs is described and mutual information (MI) of the communication is measured. Theoretical comparisons for SER, MI and symbol distribution are carried out for four key parameters in molecular communication: advection, distance, coefficient of diffusivity and symbol period.
- **Multi-Chemical Analysis of Molecular Communications:** One of the defining aspects of molecular communication, and its possible advantage over EM-based communications, is its use of chemical species to convey information. This prospect opens up

new possibilities of increasing the throughput of the communication. To understand this behaviour and to increase the throughput, experimental studies were carried out. Noise caused by multiple chemical species present in the transmission medium is investigated also. Finally, modulation methods were developed to take advantage of the multi-channel transmission by mathematically defining the four modulation methods.

1.3 Organisation of the Thesis

The organisation of the thesis is as follows;

- Chapter 2 presents an overview of numerous aspects of molecular communication. These includes the differences of approach for two types of molecular communications scale; micro (nm - μm) and macro scale (cm - m). The proposed propagation methods used in the literature are reviewed in addition to other aspects of the communications paradigm. These include; modulation methods, ISI mitigation techniques, error correction, simulation frameworks, proposed applications and possible standardisations.
- Chapter 3 focuses on the experimental approach of macro-scale molecular communication. The approach to the problem is described and a detailed description of the various parts of the experimental setup is given. A section is also dedicated to the theory of the detector used in the experiments: quadrupole mass analyser (QMA).
- Chapter 4 is the main mathematical chapter of the thesis where the model used in Chapters 5, 6 and 7 is described. To model the communication system a modified version of the mass transport equation, Advection-Diffusion Equation (ADE) is used as the basis.
- Chapter 5 analyses different types of parameters and their effect on the signal. These are: signal flow, carrier flow and bit duration. In addition, two types of distances were studied: open distance and closed distance. All the aforementioned parameters are then compared to the model described in Chapter 4.
- Chapter 6 emphasises the communication characteristics of the novel communication paradigm. These include analysis of M_C -ary modulation and ISI, based on empirical data obtained from experiments and linked to mathematical theory. A theoretical analysis of SER, achievable MI and symbol distribution for four key parameters were analysed. These are: transmission distance, advective flow, coefficient of diffusivity and symbol period. An experimental transmission of a message is conducted and compared with the theoretical model presented in Chapter 4.
- Chapter 7 experiments on multiple chemical transmissions. A proof-of-concept transmission was carried out with multiple chemicals along with noise analysis. Transmission of multiple chemicals opens up new possibilities and, to exploit these, new modulation methods were developed and experimented upon.

- Chapter 8 discusses the implications of the studies done in the thesis and proposes future-work related to the topic.

1.4 Publications

The following are the publications which resulted from this dissertation research and follow up work.

1.4.1 Journal Publications

1. D. T. McGuiness, S. Giannoukos, A. Marshall and S. Taylor "Experimental Results on the Open-Air Transmission of Macro-Molecular Communication Using Membrane Inlet Mass Spectrometry" in *IEEE Communications Letters*, vol. 22, no. 12, pp. 2567 – 2570, 2018. [doi:10.1109/LCOMM.2018.2875445](https://doi.org/10.1109/LCOMM.2018.2875445)
2. D. T. McGuiness, S. Giannoukos, A. Marshall and S. Taylor "Parameter Analysis in Macro-Scale Molecular Communications Using Advection-Diffusion" in *IEEE Access*, vol. 6, pp. 46706 – 46717, 2018. [doi:10.1109/ACCESS.2018.2866679](https://doi.org/10.1109/ACCESS.2018.2866679)
3. S. Giannoukos, D. T. McGuiness, A. Marshall, J. Smith and S. Taylor "A Chemical Alphabet for Macromolecular Communications" in *Analytical Chemistry*, vol. 90, no. 12, pp. 7739 – 7746, 2018. [doi:10.1021/acs.analchem.8b01716](https://doi.org/10.1021/acs.analchem.8b01716)
4. D. T. McGuiness, S. Giannoukos, A. Marshall and S. Taylor "Modulation Analysis in Macro-Molecular Communications" in *IEEE Access*, vol. 7, pp. 11049 – 11065, 2019. [doi:10.1109/ACCESS.2019.2892850](https://doi.org/10.1109/ACCESS.2019.2892850)
5. D. T. McGuiness, V. Selis and A. Marshall "Molecular-Based Nano-Communication Network: a Ring Topology Nano-bots for In-Vivo Drug Delivery System" in *IEEE Access*, vol. 7, pp. 12901 – 12913, 2019. [doi:10.1109/ACCESS.2019.2892816](https://doi.org/10.1109/ACCESS.2019.2892816)
6. D. T. McGuiness, S. Giannoukos, S. Taylor and A. Marshall "Experimental and Analytical analysis of Macro-Scale Molecular Communications in Closed Boundaries" in *IEEE Transactions on Molecular, Biological and Multi-Scale Communications*, vol. 5, pp. 44 – 55, 2019. [doi:10.1109/TMBMC.2019.2955094](https://doi.org/10.1109/TMBMC.2019.2955094)

1.4.2 Conference Proceedings

1. D. T. McGuiness, A. Marshall, S. Taylor and S. Giannoukos "Asymmetrical Inter-Symbol Interference in Macro-Scale Molecular Communications" in *5th International Conference on Nanoscale Computing and Communication*, ACM, 2018. [doi:10.1145/3233188.3233194](https://doi.org/10.1145/3233188.3233194)
2. V. Selis, D. T. McGuiness and A. Marshall "Nano-machine to Nano-machine Molecular Communications for Drug Delivery Systems" in *6th International Conference on*

Nanoscale Computing and Communication, ACM, 2019.
[doi:10.1145/3345312.3345471](https://doi.org/10.1145/3345312.3345471)

3. **D. T. McGuiness**, S. Giannoukos, S. Taylor and A. Marshall “Experimental Study of the Flush Dynamics of Macro-Scale Molecular Communications” in *6th International Conference on Nanoscale Computing and Communication*, ACM, 2019.
[doi:10.1145/3345312.3345489](https://doi.org/10.1145/3345312.3345489)

1.4.3 Poster Presentations

1. **D. T. McGuiness**, S. Giannoukos, F. P. M. Jjunju, J. Smith, A. Marshall and S. Taylor “Investigating Mass Spectromic Communication Approaches for Odor Transmission over Data Networks” in *ASMS*, 2017.
2. F. P. M. Jjunju, S. Giannoukos, **D. T. McGuiness**, A. Marshall, V. Selis, J. Smith, S. Maher and S. Taylor “Scent Transmission over the Internet Using Mass Spectrometry” in *ASMS*, 2017.

Chapter 2

Background and Related Work

2.1 Introduction

Sending information from one point to another is a well-established concept. The use of mobile phones and the internet have shown the importance of information transmission, and this is currently achieved via the utilisation of electromagnetic (EM) waves. Even though the achievements are numerous, there are shortcomings, for which alternative methods of communications can be utilised.

In nature the transmission of information can happen at the macro-scale, where communication can be achieved by using both chemical and EM, and at micro-scale, where communication is mostly done chemically. Commercial communication technologies rely on EM waves ranging from radio to optical bands. However, there are problems that conventional EM communications face (electromagnetic-interference (EMI), crosstalk etc.), where alternative approaches could be utilised, which do not suffer from the mentioned hindrances. An example of EM-harsh environments could be the use of EM waves in closed environments (e.g., tunnels, pipelines) or in aqueous environments, where the signal attenuation can be very high [11–13]. In water, EM waves do not travel as effectively as they would do in air. The signal experiences a high propagation delay and if the travelling medium has additional chemicals present (salt, minerals etc.), the conductivity of the medium is changed. This can add to the already high attenuation and increase the complexity of modelling the system [13]. There have been alternative techniques studied to overcome this problem. One of them being acoustic communications (AC): sending information using sound waves. The fundamental difference between AC and EM is the former uses pressure waves as the information carrier and the latter uses EM waves. AC is utilised in many ways in nature, such as in invertebrates and fish [14, 15]. It is primarily used in underwater communication where EM communications suffer from high diffraction loss; however, compared to EM, AC has low data rates and has problems such as multi-path propagation, time variations of the channel, small available bandwidth and high signal attenuation over long distances [16]. An alternative example would be the use of EM communication in nano-scale applications. At these scales, it is possible to produce nano-scale antennas for high-frequency communications. However, the complexity of the transceiver design, and the integration of the antennas to

nano-machines, still remain substantial engineering problems. Even if the integration were possible, the output power of the transceiver would not be powerful enough to establish a bidirectional communication channel [17, 18]. In addition, the ratio of antenna size to the EM wave also poses a major problem [6, 19]. Optical communication would also not be efficient, since it either requires a guided medium (i.e., an optical fiber) or a line-of-sight (i.e., free-space optical communications [20]). The handicaps of using EM communication can be summed up as [12]:

- Ratio of the antenna size to the wavelength
- High absorption losses of EM waves
- Propagation difficulties without using waveguides
- Limitations caused by spectrum availability

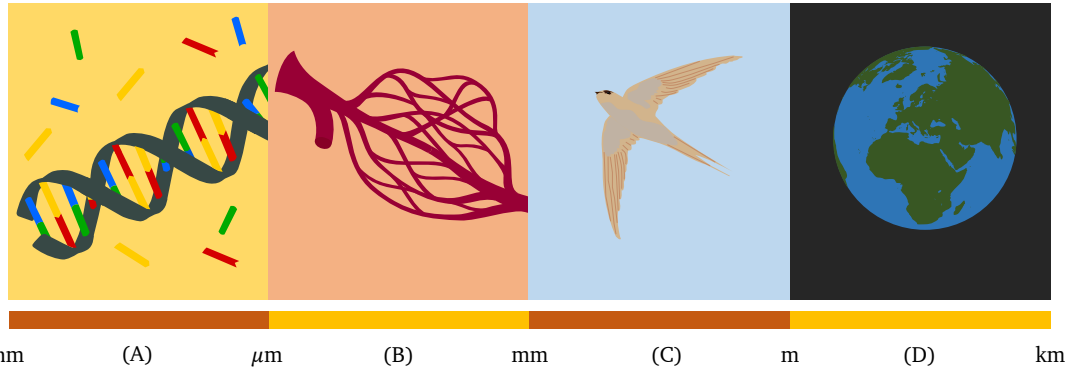


FIGURE 2.1: Diagram of the scale of molecular communications. (A) At the smaller scales of communication DNA is used to store information to pass it on to the next generation. (B) In blood vessels hormones and other signal chemicals are transmitted to maintain a living organism. (C) Large creatures use pheromones to locate mating partners across long distances (D) Mass transport can also be seen on a global scale such as the Gulf stream.

In order to overcome these problems an alternative communication paradigm can be used. Instead of using EM waves to send information, chemical signals can be employed. This type of transmission is called molecular communication [11]. In harsh environments, where the path loss is very high for EM waves, chemical signals may prove more reliable [12, 21]. In molecular communication, a transmitter releases information particles (e.g., proteins, molecules) into an aqueous or a gaseous medium, where the particles can propagate using either passive (diffusion) or active transport (advection). The receiver then decodes the information particles based on predefined communication protocols [22].

In nature, the use of molecular communication can be seen in various events. At ranges of micro-scale (nm to μm), chemical signals are used for inter-cellular communications [23]. Whereas in macro-scale (cm to m), pheromones are used for long-range communications between the same species [24]. However, in nature the transmission of pheromones is normally used to send limited determined messages. The engineering prospect of sending reliable data by using molecules is the main challenge of this communication paradigm [25].

In Table (2.1), page 15, the three types of communication mentioned in the introduction are compared. A scale which molecular communication can be achieved can be seen in Figure 2.1. Since molecular communication relies on particles (i.e., molecules, pheromones) to transmit information, there are scales where this is already achieved; from small scales such as DNA replication (i.e., semiconservative replication) to grand scales such as migratory patterns [26].

2.1.1 Research History

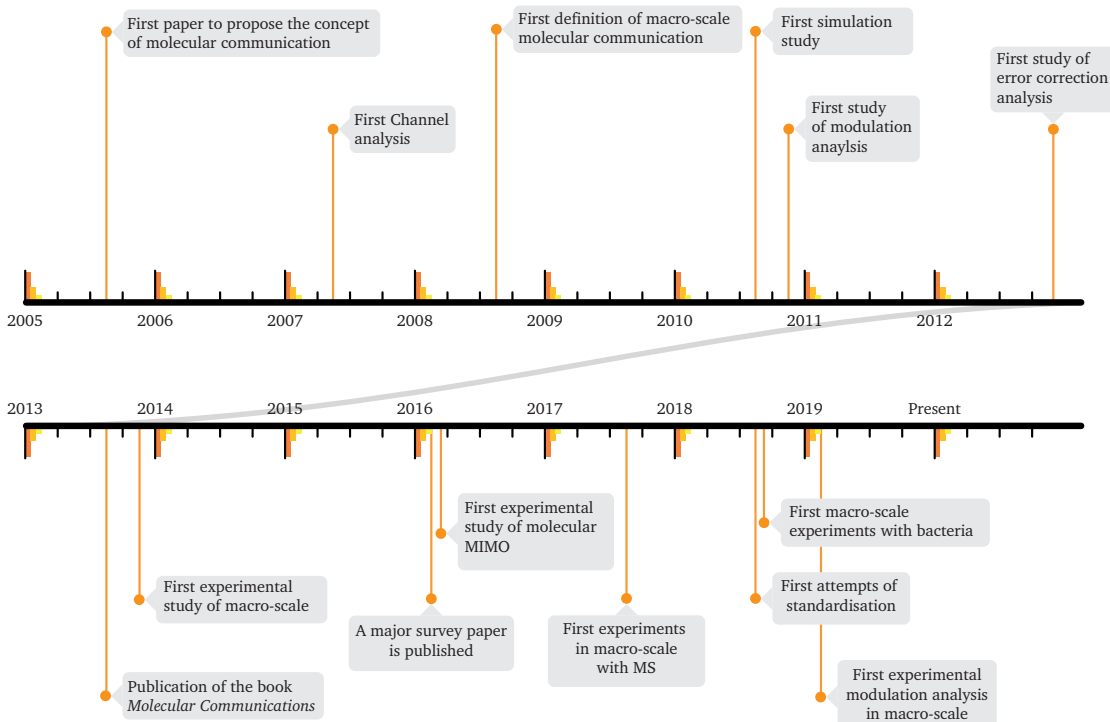


FIGURE 2.2: The significant points of molecular communications development.

While the concept of chemicals as a means of communication in the biological domain existed in some form for over a billion years, the use of molecular communication in engineering terms was first described by T. Nakano, et. al in 2005 [27]. This work proposed a method for nanomachines to communicate using signalling network (i.e., calcium signalling) in an aqueous environment and designed a simple network with an encoder and a decoder. As it mostly focused on a biological environment, molecular communication evolved and improved with the concept of biocompatibility in mind. Following this work, different aspects of molecular communications were studied. One of the first aspects studied were the channel itself. In a biological environment, the channel is generally an aqueous environment. A. W. Eckford in 2007 presented a channel capacity analysis with Brownian motion [25]. While this study was done in an idealised environment, following works started to fill in the spaces.

These works mentioned previously have all been done under micro-scale, where the communication range happens from nm to μm . However, as there are animals that can

communicate in distance up to kms, possibility exist where communication can be established using chemicals in engineering terms. One of the first papers to create a definition of macro-scale molecular communication was presented by I. F. Akyildiz et. al in 2008 [18]. While this paper focused mostly on nano communications a substantial amount of work was describing a system of pheromonal molecular communication.

Along with the channel analysis, modulation analysis was carried out for micro-scale molecular communication by M. U. Mahfuz et. al. in 2010 [21], where on-off keying was introduced and studied. As more and more aspects of molecular communications were being scrutinised, simulation analysis was starting to appear with a study conducted by E. Gul et. al. being one of the firsts [28]. The study implemented an already established network simulator NS-2 for use in micro-scale molecular communications. Error correction analysis soon followed with a study implementing already established principles for molecular communications with a work published by M. S. Leeson et. al. in 2012 [29].

Aforementioned works have all been theoretical. As micro-scale would entail the implementation of sensor and detector relative to the size of a red-blood cell, work has been carried out theoretically. However, macro-scale work in human scale (cm-km) and therefore sensors and detectors already present can be used to design an experimental platform to study the communication paradigm. The first "proof-of-concept" experimental study of molecular communication in macro-scale was carried out by N. Farsad et. al. in 2013. The proposed system uses a modified spray and an off-the-counter MQ3 spray to initiate a transmission. Following these culmination of the previous work a comprehensive survey was published by N. Farsad in 2016 [22]. This body of work presented an overview of the work carried on molecular communication with more emphasis on the micro-scale communication with respect to theory and applications. All the experimental research up-to now has been focused on a single input single output system and in 2016 the first experimental study in multi-input multi output system is conducted [252]. It has shown that molecular communication performance can be expanded via the use of MIMO. As experimental approach to study macro-scale gained traction, different receivers were tested. One being mass spectrometer where in 2017 it was used to test long range molecular communication by transmitting different chemicals as information concurrently [45]. Mass spectrometers, unlike a MQ3 sensors, are capable of distinguishing numerous chemicals concurrently and shown to be viable receivers for use in macro-scale applications. As more experiments starts to surface, the need to standardise the procedures also becomes a problem which was addressed in [327]. In this work a procedure was described to increase readability across many scientists by creating a standard for experimentation.

These receivers mentioned shown to be viable for use in large scales but one of the big push in studying molecular communication is its bio-compability and its possible use in in-vivo applications. A study conducted in 2018 shown a system where the bacteria is used in molecular communication[261]. By giving specific light pulses the chemical concentration generated by the bacterica can be changed and this can be received by a pH sensor. While this system is a proof-of-concept, it has shown the possibility for using organisms as a means

of information transfer. A recent study was done in 2019 to analyse both experimentally and theoretically the modulation properties of macro-scale molecular communications [10].

2.1.2 Micro-Scale Molecular Communication

The use of molecules to transmit information on the micro-scale has been employed, being perfected in each iteration, by evolutionary processes such as protein creation and DNA replication [30] in a cell. In addition, being bio-compatible makes it a perfect choice for use in medical applications, and if transmission is solely by diffusion, the system does not require any energy from an external source. The transmission can also be made using active methods such as advection-diffusion (i.e., convection) [31], which will be discussed in section 2.5.2 in detail. A diagram of the biological application, DNA, can be seen in Figure 2.3 and a paper published in 2018 has developed a protocol where information is encoded with DNA strands for use in nanomachines [2].

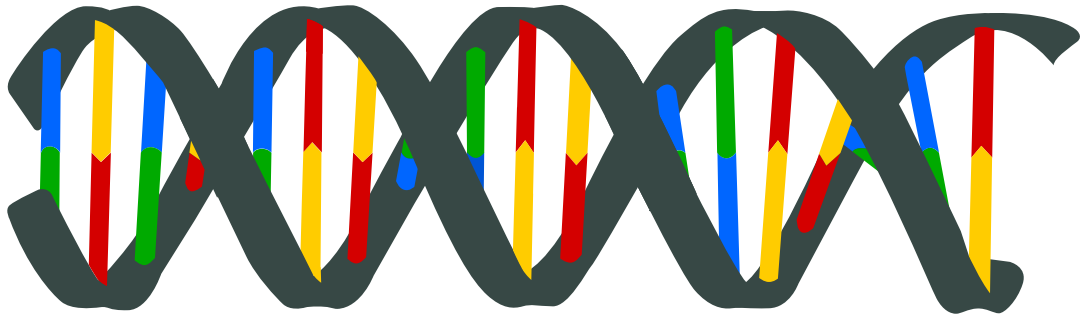


FIGURE 2.3: Deoxyribonucleic acid (DNA) is used in biological systems to store genetic information. The prospect of storing and accessing information on a small and dense scale shows the possibility of implementing information transmission and storage on small scales [1]. An engineering approach to use DNA in molecular communication is to use it as a protocol between nanomachines [2].

2.1.3 Macro-Scale Molecular Communication

The possibility of molecular communications at the macro-scale was first described in [32], where macro-scale is defined as a communication system with a transmission distance of a “few cm and more” [32]. Similar to the micro-scale, nature has been utilising the macro-scale for a long time. The application of pheromones [24] can be given as an example and a representation of this application can be seen in Figure 2.4. In addition, the use of chemicals to deter predators, to define locations can be given as further examples. Even though in principle the mechanics of the macro-scale are similar to the micro-scale, the problems that have to be overcome are different.



FIGURE 2.4: Molecular communication can also be seen on the macro-scale. In moths, calling females attract their mates late at night with intermittent release of a species-specific sex-pheromone blend [3]. [Photo: Male Gypsy Moth, Credit: Ilona L/Flickr]

2.2 Review Structure

The structure of the review is as follows. In Section 2.1, the topic is introduced. The historical development of molecular communication is presented in Section 2.2. Section 2.3 focuses on the channel theory of molecular communications. Propagation is further analysed based on how it is accomplished: diffusion or advection-diffusion in Section 2.5. In Section 2.6, types of modulation that were developed for the field are discussed along with the inter-symbol interference (ISI) and error-correction methods in Section 2.7 and Section 2.8, respectively. Section 2.10 discusses the reception process in molecular communications based on the scale of the communication. In Section 2.11, various experiments done in molecular communication are reviewed. This is then followed by the application of this new communication paradigm in Section 2.12. Section 2.13 is the review of numerous simulation platforms used in the study of molecular communication and Section 2.14 focuses on the standardisation effort of the communication method. The review concludes with Section 2.15.

2.3 Channel Theory

Information theory provides an invaluable insight into the workings of a communication system [82] and this also holds true with molecular communication, where the application of information theory is relatively new and has recently become a research interest [83]. One of the most important aspects of this field is the application of channel modelling. A generalised block diagram that represents a channel can be seen in Figure 2.5.

In a physical sense, a communication channel can be described as the environment in which the signal travels (i.e., air, space, water, etc.).

TABLE 2.1: Comparison of communication systems.

Property	Electromagnetic Communication	Macro Molecular Communication	Micro Molecular Communication
Communication type	Wave		Particle
Transmission distance	mm - km	cm - m [32]	nm - μ m [11]
Transmission medium	Air (EM Radiation) and Cable		Liquid and Gas
Transmission speed	up to $3 \cdot 10^8$ m/s (speed of light)	Passive Flow (Diffusion): $\leq 1 \text{ cm}^2/\text{s}$	Active flow (Advection): $\ll 3 \cdot 10^8 \text{ m/s}$
Propagation	Line-of-Sight		Diffusion [33] and Advection [34]
Methods	Ground Wave, Sky Wave	Convection, Turbulent Flow [35] [31]	Gap Junctions [36], Molecular Motors [37]
Transmitter & Receiver	Antennae (T_x/R_x) Laser Diodes (T_x) Photodetector (R_x)	Sprays (T_x) [38] & Arduino Uno (T_x/R_x) Electronic Noses ¹ (R_x) [42] & pH Sensors (R_x) Mass Spectrometers (MS) (R_x) [8, 45–47] Biomimicry Sensors ¹ (R_x) [50, 51] Peristaltic Pump (T_x) & Susceptometer coil (R_x) Odour Generator (T_x) [8, 45–47]	Genetically modified cells ¹ (T_x/R_x) [39–41] Artificial Cells ¹ (T_x/R_x) [43, 44] Synthesizing Receptors ¹ (R_x) [48, 49] Novel Materials ¹ (T_x/R_x) [52]
Information element	Electrical Signals, EM Waves + Light	Odours [8, 45–47], Scent [42]	DNA , Proteins [53] [54]
Power Source	Electrical (external)	Chemical, Thermal (internal/external) & Flow (external)	
Energy Consumption	High	Low [55]	
Used in Nature	Platypus [51] Eel [51]	Hormone (TSH) [56] Plant-to-Plant communication [58] Pheromone (Fish, Ants, etc.) [24, 60, 61]	Cell-to-Cell communication [57] Intra-cell communication [59]
Predictability	Accurate, Linear		Stochastic, non-linear
Applications	Cellular communication Radio Television Internet Computer	Infrastructure Monitoring [62] Underground Communication [64] Transmission through pipes [12] Studying animal behaviour [24] Odour tracking robots [68–76] Pheromone based communication [50, 79–81]	Medicinal [52, 63] Targeted drug delivery [65] Nanorobots [66] Disease diagnosis and treatment [63, 67] Nanorobot communication[77, 78]

¹ Theorized

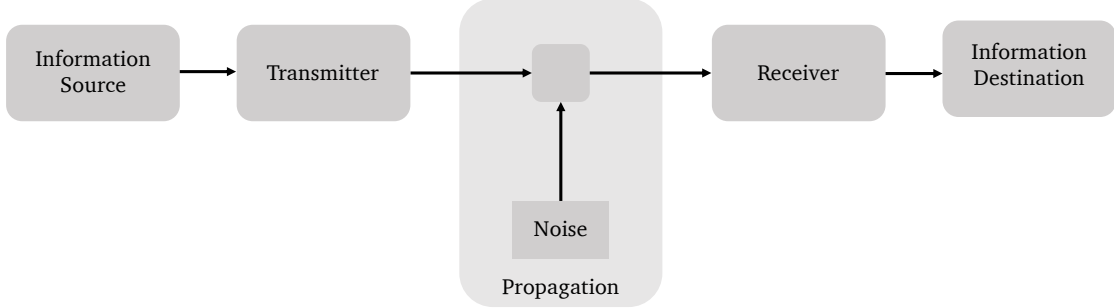


FIGURE 2.5: Diagram of a generalised communication system.

In a mathematical sense, the channel is a function that bridges the information definition between input and output. In theory, the transmitted signal (X) and the received signal (Y) can be the same. This would be called a noiseless channel. In a practical sense though, there are uncertainties that arise from the environmental noise, interferences from other devices (e.g., EMI) or worse, interference from itself (i.e., ISI). In molecular communication, the noise can be caused by the detector, diffusion of the messenger chemicals, particle collisions etc. This can cause a problem when estimating the channel for a reliable communication [84]. As any communication needs an environment to send information, no transmission method is immune from disturbances [85] and these limitations impose a tight upper bound on the amount of information that can be reliably transmitted. This is also known as the channel capacity (C). This limitation is shown in Shannon's channel capacity of a communication system with additive white Gaussian noise (AWGN) [85]:

$$C = \log_2 \left(1 + \frac{S}{N_0} \right), \quad (2.1)$$

where S is the signal power (W) and the N_0 is the power of the noise (W). However, in molecular communication, there are ways in which the effect of noise can be diminished as some propagation methods produce less variance (e.g., advection) compared to others (e.g., diffusion).

In a noisy system, the channel capacity plays a prominent role in modelling the communication [82]. For a discrete memory-less channel, where the received signal is independent of all the previous transmitted symbols, the achievable mutual information rate can be calculated from $P_{XY}(x, y)$, $P_X(x)$ and $P_Y(y)$ in Eq. (2.2) [83, 85] :

$$I(X; Y) = \sum_{x,y} P_{XY}(x, y) \log \left[\frac{P_{XY}(x, y)}{P_X(x)P_Y(y)} \right], \quad (2.2)$$

where $I(X; Y)$ is the mutual information, $P_{XY}(x, y)$ is the joint probability distribution and X and Y are two discrete variables. If the transmission possesses no memory effect, the capacity of the channel can be written as [82, 85] :

$$C \triangleq \max_{p(x)} I(X; Y). \quad (2.3)$$

TABLE 2.2: Speed comparison examples between micro-scale and macro-scale molecular communication methods.

Macro-Scale Molecular Communication			
Example	Chemical	Speed	Reference
Morphogen	EGF	$1 \cdot 10^{-7} \text{ cm}^2/\text{s}$	[104]
Airstream	Bombykol	0.6 m/s	[105]
Hormonal Signalling	TSH	5 cm/s	[56]
Neural Signalling	Active Potential	10-100 m/s	[23]
Southern Ocean	Particles	$1 \cdot 10^4 \text{ m}^2/\text{s}$	[106]
Cyclone Olivia	Particles	408 km/h	[107]
The Great Red Spot	Particles	618 km/h	[108]

Micro-Scale Molecular Communication			
Example	Chemical	Speed	Reference
Vesicular trafficking	Proteins	1 $\mu\text{m}/\text{s}$	[53, 109, 110]
Bacterial Migration	DNA	10-20 $\mu\text{m}/\text{s}$	[54, 111]
Calcium Signalling	Ca^{+2} Wave	10-30 $\mu\text{m}/\text{s}$	[112, 113]
Chemotactic Signalling	Protein	1-10 $\mu\text{m}^2/\text{s}$	[114]
Membrane Diffusion	DPPE (lipid)	11.58 m^2/s	[115]
Molecular Motors	Kinesin	6400 Å/s	[116]

However, if memory begins to play an effective role, the mathematical expression for the channel capacity of a block size of n with memory is given as [82, 86] :

$$C \triangleq \lim_{n \rightarrow \infty} \sup \frac{1}{n} I(X^n; Y^n). \quad (2.4)$$

For a discrete memory-less channel the channel capacity can be calculated using special algorithms if $p(y|x)$ is known beforehand. [82, 87, 88]. However, as will be mentioned in the ISI section, molecular communication shows memory effects, and this changes the calculation method considerably [89].

The channel characteristics of molecular communication have been studied for various properties. These include channel modelling [90–96], channel capacity [97–99] and noise [100, 101].

2.4 Propagation Speed

The speed with which the symbols are transmitted from one point to another is an important factor in any communication system. In a traditional EM-based communication the speed at which a signal can propagate can reach up to the speed of light ($c_l = 299,792,458 \text{ m/s}$) in a perfect vacuum.

The speed of an EM wave is governed by the refraction index of the medium. For example, an EM wave travelling in air has a refractive index of 1.0003 so the speed of propagation is $\sim 100\%$; however, in an aqueous environment such as water the index is 1.33, slowing the speed of propagation to 75 % of the speed of light. Communication can also be made with conductive materials such as copper or optical fibre, in which the speed can range from 50 % up to 99 % of c_l .

Molecular communication, however, is based on particles instead on waves and therefore, due to the principals of special relativity, a transmission speed of c_l is not possible. To transmit particles, the speed can be generated by two methods of propagation. It can be generated from internal forces (diffusion) or from external forces (advection). A combination of both these forces can also be utilised in propagation (advection + diffusion). These methods are discussed in detail in the following section.

2.5 Methods of Propagation

2.5.1 Diffusion

Also known as Brownian motion, diffusion is a process of random particle motion caused by collisions of other fast-moving atoms or particles in a gaseous or aqueous medium [33, 117]. Even though this process is random by nature, information can be transmitted from one point to another solely by diffusion. The main advantage of this technique is that the energy required for propagation is sourced from the thermal energy of the environment, and can be tapped into without the need for any external energy source. The application of this method can be observed in numerous biological processes. An example would be the exchange of O_2 and CO_2 in the lungs. While inhaling, the alveoli are flooded with O_2 -rich air and are only separated from the CO_2 -rich bloodstream by a 1-2 μm of membrane. The close proximity of the two different concentrations causes the diffusion process. There are other examples of diffusion in a biological system, such as DNA replication [118], protein production [119], etc.

Diffusion is a characteristic property of a chemical in a specific environment. As the temperature increases, the diffusivity also increases, and in an aqueous environment the diffusion propagation is also slower compared to the gaseous environment. The diffusivity coefficient in water can be estimated using the Stokes-Einstein relation [120] :

$$D = \frac{k_B T_E}{6\pi\eta r}, \quad (2.5)$$

where k_B is Boltzmann's constant (J/K), T_E is the temperature (K), η is the dynamic viscosity ($N \cdot s / m^2$) and r is the radius of the sphere (m). For the gas phase the diffusion coefficient can be expressed as [121] :

$$D = \frac{2}{3} \sqrt{\frac{k_B^3}{\pi^3 m} \frac{T_E^{3/2}}{P_E d^2}}, \quad (2.6)$$

where m is the mass of the gas (kg), d is the diameter of the gas molecule (m) and P_E is the pressure (Pa). For two different gases (A and B) their diffusivity relative to each other can be expressed as :

$$D_{AB} = \frac{2}{3} \sqrt{\frac{k_B^3}{\pi^3}} \sqrt{\frac{1}{2m_A} + \frac{1}{2m_B}} \frac{4T_E^{\frac{3}{2}}}{P_E(d_A + d_B)^2}, \quad (2.7)$$

where m_A and m_B are the molecular masses of gas A and B (kg), d_A and d_B are the molecular diameters of gas A and B (m), respectively. However, defining diffusion as one thing that can be applied to all circumstances may not be correct. There are other types of diffusion that explain this propagation in different circumstances, which are governed by different mathematical concepts and models. A major aspect of diffusion is the environment it is initiated. For example, diffusion happening through a biological membrane behaves differently to diffusion happening in a turbulent environment. These affect the mathematics used to model the diffusion. Examples of different types of diffusion can be seen below.

- **Anomalous Diffusion [122]:** Diffusive behaviour with a non-linear relation to time. Can be seen in protein diffusion in cells and porous media
- **Eddy Diffusion (i.e., Turbulent Diffusion) [123]:** Diffusive behaviour caused by eddy motion. Seen in turbulent environments.
- **Facilitated Diffusion [124]:** Diffusion caused by spontaneous passive transport. Can be seen in the transportation of molecules across a biological membrane
- **Knudsen Diffusion [125]:** Diffusion occurring in porous media where the pore length is comparable or smaller than the mean free path. This effect is observed in porous membrane environments.

The speed range of molecular communication can range from $\mu\text{m/s}$ to m/s . In addition, since propagation can involve flows, the speed can theoretically be increased further. A comparison of various speeds of molecular communication in nature can be seen in Table 2.2.

2.5.1.1 Stochastic Approach

Diffusion is based on random movements and therefore can be modelled based on its probabilistic behaviour. There have been studies to model this effect, such as using Markov Chains [126, 127] and Monte Carlo [128]. The diffusion process can be modelled mathematically using the following model [22, 129]:

$$\begin{bmatrix} \Delta x_i \\ \Delta y_i \\ \Delta z_i \end{bmatrix} = \begin{bmatrix} x_{i-1} \\ y_{i-1} \\ z_{i-1} \end{bmatrix} + \Delta r \cdot \begin{bmatrix} \cos \theta_i \sin \phi_i \\ \sin \theta_i \sin \phi_i \\ \cos \phi_i \end{bmatrix}, \quad (2.8)$$

where Δr is the displacement (m), both θ_i and ϕ_i represent the 3D angular position and x, y, z represent the spatial coordinates (m). However, there are other methods in which diffusion is modelled in the literature.

One way of approaching the problem of random propagation is to model the process as a stochastic continuous-time problem. This process, known in literature as the Wiener process, has been used in modelling Brownian motion and, as a reflection, has been utilised in modelling the propagation for use in molecular communication [101]. Let $\varsigma_1, \varsigma_2, \dots$ be independent and identically distributed random variables with an expected value of 0 and a variance of 1. For each n , the continuous time stochastic process can be defined as :

$$W_n(t) = \frac{1}{\sqrt{n}} \sum_{1 \leq k \leq \lfloor nt \rfloor} \varsigma_k, \quad t \in [0, 1], \quad (2.9)$$

The above equation represents a random step function with each increment of W_n being independent of one another. For large values of n the stochastic process approaches a normal distribution of $\mathcal{N}(0, t)$ due to the central limit theorem.

Another approach is to apply the Langevin equation [130], which describes the time evolution of a subset of the degrees of freedom. Based on the equation, the position ($p_v^n(t)$) of a particle n with a mass of m at time t along any of the dimensions (v) obeys the following interpretation of the equation :

$$m \frac{\partial^2 p_v^n(t)}{\partial t^2} = -6\pi\eta r \frac{\partial p_v^n(t)}{\partial t} + f_N(t), \quad (2.10)$$

where $f_N(t)$ is the noise present in the environment (i.e., particles present in the environment). Stochastic approaches of diffusion in molecular communication can be seen in many studies; such as modelling the complete system of molecular communications [131], noise analysis in ligand-binding [132] and channel capacity in a fluid medium [133]. Finally, point process theory was also studied for use in molecular communications [134].

2.5.1.2 Analytical Approach

The second approach to modelling the propagation is to model the system as a partial differential equation (PDE). The diffusion-only equation, also known as Fick's 2nd law, which is described in [135] can be expressed as;

$$\frac{\partial c}{\partial t} = D \left(\frac{\partial^2 c}{\partial x^2} \right), \quad (2.11a)$$

$$\frac{\partial c}{\partial t} = D \left(\frac{\partial^2 c}{\partial x^2} + \frac{\partial^2 c}{\partial y^2} \right), \quad (2.11b)$$

$$\frac{\partial c}{\partial t} = D \left(\frac{\partial^2 c}{\partial x^2} + \frac{\partial^2 c}{\partial y^2} + \frac{\partial^2 c}{\partial z^2} \right), \quad (2.11c)$$

where D is the diffusion coefficient (cm^2/s) and c is the concentration at a given point in space (kg/m^3). Therefore, the concentration of the molecules is dependent on the spatial coordinates as well as the time.

The PDE given in Eq. (2.11) can have numerous solutions, based on the boundaries of the system. One of the minimalist approaches of solving Eq. (2.11) is to solve it at the point of release of the chemicals (t_0). If M_0 is the initial number of molecules, or mass, released from the transmitter at the time t_0 then the initial conditions for the molecular concentration $c(x, t)$ for 1D, also known as the “*thin film solution*” in the literature, diffusion process can be expressed as:

$$c(|x| > 0, t_0) = 0, \quad (2.12a)$$

$$c(x = 0, t_0) = M_0 \delta(x), \quad (2.12b)$$

$$c(|x| \rightarrow \infty, t) = 0. \quad (2.12c)$$

In these equations $\delta(x)$ represents the continuous Dirac delta function for a given spatial dimension (x, y, z) and is defined as [136]:

$$\int_{-\infty}^{+\infty} \delta(x) dx = 1. \quad (2.13)$$

By implementing the boundary conditions given in Eq. (2.12) to Eq. (2.11), the PDE can be solved and the solutions for the each dimension are:

$$c(x, t) = \frac{M_0}{\sqrt{4\pi Dt}} \exp\left(-\frac{x^2}{4Dt}\right), \quad (2.14a)$$

$$c(x, y, t) = \frac{M_0}{\sqrt{(4\pi Dt)^2}} \exp\left(-\frac{x^2 + y^2}{4Dt}\right), \quad (2.14b)$$

$$c(x, y, z, t) = \frac{M_0}{\sqrt{(4\pi Dt)^3}} \exp\left(-\frac{x^2 + y^2 + z^2}{4Dt}\right). \quad (2.14c)$$

The derivation of this solution can be seen in Appendix A. There are other ways the diffusion equation can be solved with different initial conditions [119]. The channel response can be obtained by changing the conditions of the boundary if there is an absorbing receiver [137]. The capture function of the system can be derived by the integration of the channel response from the differential equation with a boundary [138]. By calculating the impulse response differentiation with respect to time, it is possible to calculate the peak concentration at the peak time [138, 139].

2.5.2 Advection

Advection is defined as the transportation of material or heat by using the flow of another fluid [34]. In molecular communications, introducing a velocity element to the propagation can be mathematically described with two approaches. The former being a stochastic approach and latter being an analytical approach.

2.5.2.1 Stochastic Approach

An approach to modelling the diffusion with an advection element is to introduce a velocity vector to random-walk simulations. This process can be modelled by using the Monte Carlo method [128] by introducing a velocity component (\mathbf{u}) to the diffusion process presented in Eq. (2.15) [22]:

$$\begin{bmatrix} \Delta x_i \\ \Delta y_i \\ \Delta z_i \end{bmatrix} = \begin{bmatrix} u_{x,i-1} \\ u_{y,i-1} \\ u_{z,i-1} \end{bmatrix} \cdot \begin{bmatrix} x_{i-1} y_{i-1} z_{i-1} \end{bmatrix} + \Delta r \cdot \begin{bmatrix} \cos \theta_i \sin \phi_i \\ \sin \theta_i \sin \phi_i \\ \cos \phi_i \end{bmatrix}. \quad (2.15)$$

As mentioned in the diffusion stochastic process, stochastic differential equations (SDEs) can also be implemented to model the advective element. A different approach to modelling is to use the Fokker-Planck (aka. Smoluchowski) equation [140]. This equation describes the time evolution of the probability density function of the velocity of a particle under the influence of drag forces ($\mu_D(x, t)$) (i.e., drift) and random forces ($D_V(x, t)$) (i.e., diffusion) in space and time. The mathematical equation for the Fokker-Planck is given in Eq. (2.16):

$$\frac{\partial p}{\partial t}(x, t) = -\mu_D(x, t) \frac{\partial p}{\partial x}(x, t) + D_V(x, t) \frac{\partial^2 p}{\partial x^2}(x, t). \quad (2.16)$$

To solve this ordinary partial differential equation (OPDE), different types of boundaries have been proposed that can produce different solutions: such as infinite environment [141, 142], infinite source [29, 143] or long-term capture [144]. This approach was used in [144] to analyse macro-scale communications and the aspect of the sensor cleaning from a theoretical point of view.

2.5.2.2 Analytical Approach

In this approach the system is modelled deterministically. However, to model the propagation the advection term must be mathematically defined. In this definition of propagation, some aspects of the transported substances are conserved, such as energy. An example would be the pollutants in a river or the gas flow through pipelines. The mathematical expression of advective flow can be seen as [145] :

$$\mathbf{u} \cdot \nabla = u_x \frac{\partial}{\partial x} + u_y \frac{\partial}{\partial y} + u_z \frac{\partial}{\partial z}, \quad (2.17)$$

where $\mathbf{u} = (u_x, u_y, u_z)$ is the velocity field and the ∇ is the del operator. The advection equation for a conserved quantity for a scalar field of ψ is expressed by the continuity equation [146]:

$$\frac{\partial \psi}{\partial t} + \nabla \cdot (\psi \mathbf{u}) = 0. \quad (2.18)$$

With the advection defined, the final approach would be to reintroduce diffusion to this propagation. Convection is the sum action of both diffusion and advection and mathematically this phenomenon is modelled using the advection-diffusion equation. This equation can be derived from the continuity equation given below:

$$\frac{\partial c}{\partial t} + \nabla \cdot \vec{j} = R, \quad (2.19)$$

where \vec{j} is the total flux and the R is the source or the sink for the function c . In this system, there are two flux sources. The former being the diffusive flux from the diffusion of particles and the latter being the advective flux due to the motion created by the flow:

$$\begin{aligned} \vec{j}_D &= -D \nabla c, \\ \vec{j}_A &= \mathbf{u}c. \end{aligned} \quad (2.20)$$

By inserting these equations into the continuity equation the advection-diffusion equation can be obtained. In the literature this is also known as the convection-diffusion equation and drift-diffusion equation [147], which is expressed as [148]:

$$\frac{\partial c}{\partial t} = \underbrace{\nabla \cdot (D \nabla c)}_{\text{Convection}} - \underbrace{\nabla \cdot (\mathbf{u}c)}_{\text{Advection}} + R, \quad (2.21)$$

where;

- c is the concentration of mass transfer (kg/m^3).
- D is the diffusivity coefficient (i.e., mass diffusivity for particle motion) (m^2/s).
- \mathbf{u} is the velocity field that the quantity is moving with (m/s). For example, if c is the salt concentration in a river, \mathbf{u} is the velocity of the water flow.
- R is the “sink/source” of the quantity c . In chemical processes, $R > 0$ means the system is creating more chemicals (i.e., sources) and $R < 0$ means the system is destroying more chemicals (i.e., a sink).

An approach to solve the equation is to change the frame of reference from stationary coordinates (x, t) to moving coordinates (λ_x, t) . This reference frame can be mathematically expressed as [149]:

$$\lambda_x = (x - u_x t). \quad (2.22)$$

If this frame is inserted into Eq. (2.21)

$$\frac{\partial c}{\partial t}(\lambda_x, t) = \frac{\partial c}{\partial \lambda_x} \frac{\partial \lambda_x}{\partial t} + \frac{\partial c}{\partial t} \frac{\partial t}{\partial t} = -u_x \frac{\partial c}{\partial \lambda_x} + \frac{\partial c}{\partial x} t, \quad (2.23a)$$

$$\frac{\partial c}{\partial x}(\lambda_x, t) = \frac{\partial c}{\partial \lambda_x} \frac{\partial \lambda_x}{\partial t} + \frac{\partial c}{\partial t} \frac{\partial t}{\partial x} = \frac{\partial c}{\partial \lambda_x}, \quad (2.23b)$$

$$\frac{\partial^2 c}{\partial x^2}(\lambda_x, t) = \frac{\partial^2 c}{\partial \lambda_x^2}. \quad (2.23c)$$

By substituting from Eq. (2.23) for $\partial c / \partial t$, $\partial c / \partial x$ and $\partial^2 c / \partial x^2$ to Eq (2.21) becomes :

$$\frac{\partial c}{\partial t} = D \frac{\partial^2 c}{\partial \lambda_x^2}. \quad (2.24)$$

As can be observed Eq. (2.24) this equation is Fick's 2nd law, with the only difference being having a moving reference frame λ_x . By using the same boundary conditions described in Eq. (2.12), the solution for the equations becomes:

$$c(x, t) = \frac{M_0}{\sqrt{4\pi Dt}} \exp\left(-\frac{\lambda_x^2}{4Dt}\right). \quad (2.25)$$

Converting back to the stationary frame of reference, the final equation is obtained and can be seen in Eq. (2.26a). The 2D and 3D solutions can be seen in Eq. (2.26b) and (2.26c), respectively.

$$c(x, t) = \frac{M_0}{\sqrt{4\pi Dt}} \exp\left(-\frac{(x - u_x t)^2}{4Dt}\right), \quad (2.26a)$$

$$c(x, y, t) = \frac{M_0}{\sqrt{(4\pi Dt)^2}} \exp\left(-\frac{(x - u_x t)^2}{4Dt}\right) \exp\left(-\frac{(y - u_y t)^2}{4Dt}\right), \quad (2.26b)$$

$$c(x, y, z, t) = \frac{M_0}{\sqrt{(4\pi Dt)^3}} \exp\left(-\frac{(x - u_x t)^2}{4Dt}\right) \times \exp\left(-\frac{(y - u_y t)^2}{4Dt}\right) \exp\left(-\frac{(z - u_z t)^2}{4Dt}\right). \quad (2.26c)$$

Eq. (2.11c) represents the diffusion of a chemical in a 3D unbounded space. However, on a macro-scale, the propagation of the chemicals can be made in a bounded domain. This has benefits over the boundary-less methods. The most important being that by using a closed system, more chemicals will arrive at the receiver and make it possible to increase the distance of communication.

For using a bounded communication a cylindrical shape has a few advantages. The most important one being that because it does not have any corners to act as stress concentrators, and it helps the fluid flow to be smoother compared to other geometric shapes. The cylindrical coordinate representation of the advection-diffusion equation (ADE) can be seen in Eq. (2.27) [150]:

$$\frac{\partial c}{\partial t} = D_L \frac{\partial^2 c}{\partial z^2} - u \frac{\partial c}{\partial z} + \frac{D_R}{r} \left(r \frac{\partial c}{\partial r} \right), \quad (2.27)$$

where r , θ and z are the cylindrical coordinates, D_L is the longitudinal diffusivity (cm^2/s) and D_R is the radial diffusivity (cm^2/s). θ is omitted since it is assumed that the system has angular symmetry.

The solution for this kind of equation with initial and boundary conditions can be obtained by implementing the Hankel [151] and Laplace Transforms [150]. One such solution is shown below [150]:

$$c(r, z, t) = \frac{M_0}{\phi \rho_r^2 \sqrt{D_L \pi^3 t}} \sum_{n=0}^{\infty} \frac{1}{\lambda_n} \left\{ \exp \left[-\frac{(ut-z)^2}{4D_L t} - D_R \lambda_n^2 t \right] \right. \\ \left. - \frac{u}{2D_L} \exp \left[-\frac{uz}{D_L} - D_L \lambda_n^2 t \right] \operatorname{erfc} \left(\frac{z+ut}{\sqrt{4D_L t}} \right) \right\} \left(\frac{\rho_r^2}{r^2} + \frac{2\rho_r J_1(\lambda_n \rho_r) J_0(\lambda_n r)}{r^2 |J_0(\lambda_n r)|^2} \right), \quad (2.28)$$

where r is the radius of the cylindrical system (m), ρ_r is the radius of the inner injected zone, ϕ is the porosity of the material and λ_n is the Hankel transform parameter determined by the following transcendental equation:

$$\frac{J_0(\lambda_n r)}{dr} = 0. \quad (2.29)$$

As can be seen, defining boundaries unto the propagation greatly increases the complexity of the analytical solution, relying on different methods for solving the PDE, such as separation of variables [152] or change of variables [153]. Studies in boundary medium transmission in molecular communication has seen interest both experimentally [45, 47] and theoretically [154].

2.5.3 Turbulent Flows

Turbulent flows are caused by the random fluctuations in a flow caused by the chaotic motions of particles [35]. These movements of particles in the flow are called eddy diffusion, because of their similarity to molecular diffusion. In molecular diffusion, the random motion of molecules themselves from the thermal energy from the environment cause the diffusion, whereas in turbulent diffusion it is the motion of the fluid that causes the propagation [155–157].

Turbulence is heavily dependent on the bulk flow, as the turbulence only happens if the flow is above a critical number. This critical number is defined as Reynolds number and is calculated by the ratio of the inertial forces to the viscous forces of the fluid in question [158] :

$$\operatorname{Re} = \frac{\rho u L_D}{\eta}, \quad (2.30)$$

where ρ is the density of the fluid (kg/m^3), u is the velocity of the fluid (kg/m), L_D is the characteristic linear dimension of the environment (m) and η is the dynamic viscosity of the fluid ($\text{Pa} \cdot \text{s}$). Distribution of particles in a turbulent environment is analogous to heat diffusion in a solid [159]. The equations which explain this phenomenon are similar to Eq. (2.11) and can be written for spherical coordinates. Modelling the system in spherical coordinates has the advantage of possessing spherical symmetry. In addition, in nature, communication using molecules has been done using spherical puffs of particles (i.e. plant-to-plant [58]). In light of this, Eq. (2.11) can be converted to spherical coordinates with spherical symmetry:

$$\frac{\partial c}{\partial t} = \frac{K}{r^2} \frac{\partial}{\partial r} \left(r^2 \frac{\partial c}{\partial r} \right), \quad (2.31)$$

where K is the coefficient of eddy-diffusion (m^2/s), c is the concentration function (kg/m^3) and r is the radius of the transmission (m) with the following identity:

$$r^2 = x^2 + y^2 + z^2. \quad (2.32)$$

By applying the boundary conditions defined in [160] a solution can be derived:

$$c(x, t) = \frac{M_0}{\sqrt{(4\pi Kt)^3}} \exp\left(-\frac{r^2}{4Kt}\right), \quad (2.33)$$

Turbulence in molecular communications is a new field of study with experimental work only recently gaining traction to analyse this kind of propagation in macro-scale aqueous propagation [161, 162].

2.6 Modulation

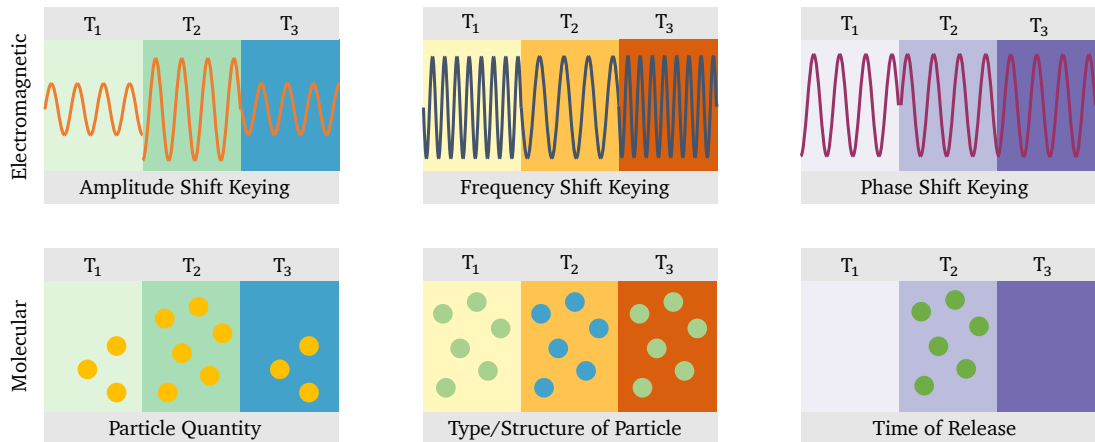


FIGURE 2.6: Types of modulation methods developed for use in molecular communications: Particle Quantity, Type and/or Structure of Particle and Time of Release.

Modulation is the process of changing the property of a periodic waveform with a modulating signal that typically contains information to be transmitted. The symbols are encoded

into the carrier signal properties. In an EM-based communication system, the carrier waves are sinusoids and can be expressed mathematically as;

$$s(t) = A_w \sin(2\pi f t + \varphi), \quad (2.34)$$

where A_w is the wave amplitude, f is the wave frequency (Hz) and φ is the wave phase (rad). The amplitude is the peak-to-peak height of the signal, f affects the number of oscillations that the signal makes in a given second and the phase is the shift the signal makes from the origin. Based on this, information can be encoded onto a sine wave by using any of the three properties mentioned above: Amplitude-Shift Keying (ASK), Frequency-Shift Keying (FSK) and Phase-Shift Keying (PSK). However this is not limited to using only one modulation scheme and hybrid modulations can be utilised.

Compared to EM-based communication systems, in molecular communication, the information carriers are particles (i.e. molecules) that are very tiny (range of Å). By using the EM modulation methods as a basis, the information can be encoded into molecules based on its following properties.

In this section 2.4, the main modulation methods developed for use in molecular communication will be discussed in detail. In further sections, the ISI and error-correction properties of different modulation methods will be analysed. Finally, a comparison of all the modulation methods described in the section can be seen in Table (2.3).

In this review, modulation methods are categorised into four distinct sections.

- Those that primarily utilise particle quantity.
- Those that exploit particle differences for modulation.
- Those that modulate information based on the release times of particles.
- Those that utilise more than a single property for modulation (aka., hybrid).

2.6.1 Particle Quantity

By implementing the quantity of the molecules as the method of modulations, the information can be encoded into the quantity of molecules used for transmission. An alternative approach would be to use a concentration based approach (mol/m^3). This could be a better approach for use in macro-scale because of the scale of communication.

One of the first works carried out on molecular modulation can be traced back to [21]. This paper proposed two different modulation methods for use in diffusion-based propagation channels. The former is analogous to On-Off Keying (OOK) of EM communication systems where the bit 0 was defined as the concentration level of 0 ($Q_0 = 0$) and the bit 1 was defined as the concentration level of Q ($Q_1 = Q$).

In [163] and [164] two novel modulation methods were discussed for use in diffusion based propagation channels. The first method was based on the number of molecules arriving at the receiver below or above a certain threshold (τ_s). This method was given the term Concentration Shift Keying (CSK) and is similar to ASK in an EM communication system;

and the number of bits per transmitted symbol can be increased (Binary CSK 2-bits, Quadruple CSK 4-bits, ...). The CSK modulation scheme mentioned is designed for a transmitter and a receiver with fixed positions. In [165], the CSK modulation/demodulation is analysed when the transmitter and/or the receiver becomes mobile.

2.6.2 Type and/or the structure of Particles

By using the chemical characteristic of the molecules, chemical formulas can be used as individual symbols for transmission. An example would be the use of acetone ($(CH_3)_2 CO$) to encode the symbol 00 and n-hexane (C_6H_{14}) to encode 11. The first proposed modulation discussed in [163] and [164] relies on the chemical difference of messenger molecules passing a certain threshold (τ_s). This has been named Molecular Shift Keying (MoSK) and hydrofluorocarbon based chemicals were given as information carrying molecule examples (1-florobutane as 00, 1,3 - difluorobutane as 10 etc.). This method can also increase its transmitted bits in a similar fashion to CSK (Binary MoSK 2-bits, Quadruple MoSK 4-bits, ...)

There has also been research done on modulation methods for use in in-body molecular communication. In [166], it has been proposed to use aldohexose isomers as information carriers, called isomer based molecular shift keying (I-MoSK). The authors have also stressed that for the molecular communication to be bio-compatible, harmless compounds should be chosen as information carriers unlike the hydrofluorocarbons used in [164]. The advantages of using isomers in a molecular communication system is that isomers have the same type of atoms, which decreases the complexity of synthesis. Based on isomers, the authors have considered using isomers in CSK, I-CSK and MoSK, I-MoSK. Another approach would be to use isotopes which were studied in [167]. In [168] a modulation technique called depleted MoSK (D-MoSK) was proposed, which requires reduced number of the types of molecules for encoding compared to MoSk to reduce the complexity on the nano-machines.

A novel approach is to have two chemicals representing (+) and (-) signals which was studied in [169] where two chemicals are transmitted A and B, respectively, defined as type based sign (TS) modulation. In addition a variation of this modulation was proposed to implement it to utilise chemical reactions [170].

2.6.3 Time of Release

Information can be encoded to the time in which the chemicals are either released or received by the transmitter [25]. An example would be to send Acetone at $t = 0s$ to encode 00 and at $t = 5s$ to encode 11. However, encoding information into timing can be a challenging task since the propagation of chemicals is random for diffusive (i.e., Brownian motion) channels in micro-scale and therefore this type of modulation may be more suited for application on macro-scale.

A variation on OOK is studied in [171]. The study was conducted on Pulse Amplitude Modulation (PAM). In this scheme, the bit-1 is encoded as a spike in the beginning of the time frame and the bit-0 is encoded as total silence in the time frame.

TABLE 2.3: Comparison of modulation methods.

Modulation Type	Modulation Method	Acronym	Principle			Reference
			Mass	Type	Time	
Particle Quantity	On-Off Keying	OOK	×	.	.	[21]
	Concentration-Shift Keying	n - CSK	×	.	.	[163, 164], [165]
Particle Type	Molecular-Shift Keying	n - MoSK	.	×	.	[163, 164]
	Isomer based Molecular-Shift Keying	I - MoSK	.	×	.	[163, 164]
Isomer based Concentration-Shift Keying	I - CSK	.	×	.	[163, 164]	
	Isotropic based Molecular-Shift Keying	n - MoSK	.	×	.	[167]
Depleted Molecular Shift Keying	D - MoSK	.	×	.	[168]	
	Type Based Sign	TS	.	×	.	[170]
Time of Release	Pulse Amplitude Modulation	PAM	.	.	×	[171]
	Molecular Frequency Shift Keying	—	.	.	×	[21]
Time-elapsed Communication	TEC	.	.	×	[172]	
	SMART Time-elapsed Communication	SMART - TEC	.	.	×	[172]
Pulse Position Modulation	PPM	.	.	×	[171]	
	Concentration through Silence	CtS	.	.	×	[171]
Rate Modulation	RM	.	.	×	[171]	
	Multilevel Amplitude Modulation	M-AM	×	×	.	[21]
Isomer-Based Ratio-Shift Keying	IRSK	×	×	.	[166]	
	Molecular ARray-based COmmunication	MARCO	.	×	×	[173]
Molecular Transition-Shift Keying	MTSK	.	×	×	[174]	
	Power-Adjusted MTSK	MTSK - PA	.	×	×	[174]
Hybrid Molecular Scheme 1	HMS D1	×	×	.	[175]	
	Hybrid Molecular Scheme 2	HMS D2	×	×	.	[175]
Molecular Space Shift Keying	MSSK	×	×	.	[176]	
	Quadrature Molecular Space Shift Keying	QMSSK	×	×	.	[176]
Molecular Spatial Modulation	MSM	×	×	.	[176]	

In [21], the concentration levels of the chemicals is varied in accordance to the sinusoidal signal in a given frequency similar to FSK in EM communications. This would add up to the already available concentration in the environment (Q_{avg}) an additional element is sent to the environment ($Q_{amp} \sin(2\pi f)$) to make the chemical amplitude behave like a wave. With this the modulation is analogous to that of FSK.

Bacteria have the ability to behave as transceivers, known as quorum sensing [177], which enables them to interact with one another. A method that utilises this is the time-elapsed communication (TEC) discussed in [172] and proposed for use in biological applications (i.e., bacteria) to increase the natural data rate of 10^{-5} bit/s. This is for very slow networks (i.e., on-chip bacterial communication). In this method, information is encoded into the time intervals between pulses. This method was tested on genetically engineered *Escherichia coli* (*E. coli*) bacteria. These bacteria would produce fluorescence light proportional to the information particle concentration however, the method experiences bit errors in transmission. In order to overcome that, the authors have proposed an improved TEC called SMART-TEC [172].

In [171] a modulation method based on the time property of the chemical emission is proposed. Pulse position modulation (PPM), relies on the emission of particles in an ordered manner to define the symbol. In a two bit system, the bit - 1 would be defined as a short pulse then silence for the remainder of the timeframe, whereas bit - 0 would be defined

as a short pulse in the middle of the time frame. In [178], the concept of PPM is further developed and higher order ($M_C > 2$) values were shown to outperform CSK.

A second modulation method proposed in [171] is named Communication through Silence (CtS), where the symbol is encoded between the start pulse and the stop pulse. The final emission-based modulation scheme proposed in [171] is Rate Modulation (RM). This modulation relies on the number of pulses in a given time frame. An example would be, encoding “9” with 9 pulses in a time frame t and “12” with 12 pulses in the same time frame t .

2.6.4 Hybrid Modulation Methods

In this review, hybrid modulation describes a method that utilises two or more types of modulation methods. In [21] a combination of OOK and molecular FSK was implemented to increase the throughput of the communication named multilevel amplitude modulation (MAM). This is achieved by modulation Q_{avg} in conjunction with $Q_{amp} \sin(2\pi f)$ to achieve a higher rate of encoding. In [166] the authors have proposed using isomer ratios to encode information, which has been named IRSK. This method relies on the ratios of the quantity of isomers the detector absorbs. The authors have stressed that this kind of modulation would be more robust, since the ratios are the encoding element rather than the quantity. In [179], a method based on the combination of type and the time of release was proposed. This method, being asynchronous, could achieve higher information rates compared to time based methods. To define the model, the method was presented as an event-driven system. In addition a hybrid modulation scheme based on CSK and MoSK, named run-length aware hybrid modulation have been proposed that reduces the ISI of the communication [175].

Another work on modulation in continuous diffusion was [180], a pulse based modulation scheme was proposed. This modulation scheme, however is used to send simple commands to adjoining nano-machines (i.e., detection of unwanted particles) and based on fast change of concentration in a given environment. In [181] a modulation was proposed combining the properties of concentration shift keying (CSK) and molecular-shift keying (MoSK) into a single modulation method for use in high data rates. Another modulation method that combines CSK and MoSK was proposed in [175]; these are, modulation method hybrid modulation scheme design 1 (HMS-D1) and 2 (HMS-D2). In [176] novel modulation methods for use in MIMO application was developed. Fist, named molecular space shift keying (MSSK) uses the antennae indices as the information source. Second, quadrature MSSK (QMSSK) uses two types of chemical and finally a molecular spatial modulation which is a combination of MoSK and MSSK.

2.7 Inter-symbol Interference (ISI)

In molecular communications the noise of the environment behaves differently compared to an EM communication. In EM, the environmental noise (N_0) generally stays stable, however molecular communication is based on particles and because of that, particles may remain

in the propagation medium and may affect future transmissions and may or may not arrive at an unintended time slot. This causes a decrease in molecular communication channel capacity and creates a memory effect [22].

The memory effect can be a major problem if there is a continuous stream of transmission, which makes ISI a big problem in molecular communication since continuing transmission would eventually decrease the channel capacity to such extent that information transmission would become infeasible. Because of this, reduction of ISI should be a primary concern when designing a modulation method. Due to this hindrance, the property of ISI has been studied extensively [46, 164, 182–186].

There are methods in which ISI can be reduced. Based on the literature and the research done in this problem, ISI reduction can be classified into two types:

- Single type of messenger chemical.
- Multiple types of messenger chemicals.

In the following sections (2.7.1 and 2.7.2), both approaches will be discussed in detail.

2.7.1 Single Messenger Chemical

The approach of utilising only a single chemical has the limit of only having a single messenger molecule type to work with. Increasing the time slot of each symbol in the communication can be given as an example. However this would sacrifice the throughput of the channel for transmission reliability. This method, however, would make the already slow molecular communication even slower, which has forced new methods to mitigate ISI in an efficient way.

Another approach of ISI mitigation is to remove the leftover chemicals in the communication channel. A method to accomplish this is to use enzymes or inhibitor chemicals [187–191]. In this method, the enzymes that are present in the channel degrade the information particles as they are transmitted, thereby reducing the ISI and the receiver error probability. Alternative approaches are also present in the literature such as; ISI mitigation by calculating of the optimum reception delay [192], adaptive detection [193] and photolysis reactions [194].

2.7.2 Multiple Messenger Chemicals

Utilisation of multiple chemicals for messenger particles has advantages over a single chemical messenger system. One being that since chemicals are independent of each other, more symbol time can be given to the chemical without hindering the throughput.

In [174] an approach to reduce the ISI was proposed by combining CSK and MoSK and calling it molecular transition shift keying (MTSK). In its binary form two types of molecules were implemented, defined as type-A and type-B. The modulator then decided which molecule to send based on the previously sent bit and the current bit. If type-A is sent the system sends type-B and vice versa. In the same paper, a power efficient version

(MTSK-PA) is also proposed where the residual molecules from the previous symbols are utilised to reduce the energy consumption.

An alternative ISI reduction method is to utilise the order of released information particles [173]. This method, called MARCO by the authors, defines bit-0 as releasing first particle *A* and then later *B*. For bit - 0 the release is vice versa. This method was shown to reduce the ISI. In [195], a similar idea was implemented in which alternating molecules were used to reduce ISI (e.g., type-a molecule for even time slots and type-b molecules for odd time slots). By using more chemicals, more rotations can be made between time slots and this can help reduce ISI greatly.

2.8 Error Correction

By definition, error correction is used to diminish the effects of noise on the transmitted signal that could be caused by the environment or sensors and correct the errors by introducing redundancy [22]. This redundancy can later be detected to check whether information was changed or not. For example, in a repetition code, bit - 0 is encoded as 00000 and bit - 1 as 11111 when this code is received as 00101 and 10111, it can easily be identified and decoded correctly [196].

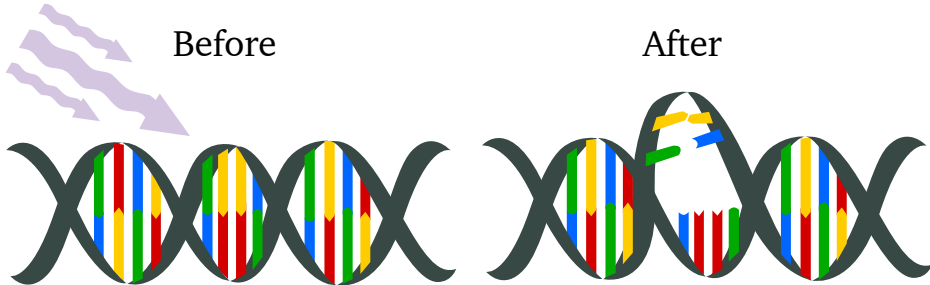


FIGURE 2.7: A natural process in error correction occurs in DNA replications. The error correction in DNA is a collection of processes by which a cell identifies and corrects damage to the DNA molecules that encode its genome [4].

One of the first attempts to use error correcting codes was to implement one based from EM systems. A Hamming code [29] was applied to On-Off Keying (OOK) with diffusion based molecular communications. It was shown that by implementing such codes and by using a large number of molecules the system outperformed communication without redundancy. However, if fewer particles were used the inverse became true. This happens because of the extra ISI added by the parity bits. The authors also expressed that it is not an energy efficient solution if the separation distance between the transmitter and the receiver is small. Based on this energy issue work was done to introduce energy efficient codes for use in molecular communication [197] and in [198] energy comparison of Self-Orthogonal Convolutional Codes (SOCCs) was conducted.

Another attempt was made in [199, 200] where an alternative to the already established Hamming distance is proposed, named Molecular Coding Distance Function (MCDF). In

this function, the coding distance is not defined as a static value, but based on a transition probability. It was shown that this method shows better performance than Hamming coding in molecular communications. Finally applications of already existing error-correction code methods have been reported: High-order Hamming Code [197], Minimum Energy Codes [201], Reed-Muller Codes [202] and Reed-Solomon Codes [203].

In [197], a new family of channel codes have been proposed called ISI - free codes that takes the limited decoding ability of the sensors in mind. These coding schemes have been simulated in a diffusion environment by the use of Brownian motion. In [202] a comparison study of the recently proposed channel coding schemes were reviewed.

A problem of modelling the channel is the inconsistency across a given distance. This is caused by numerous properties of the environment (temperature, molecule collision etc.). To overcome this, channel state information is calculated. This method helps to describe how the signal propagates. The channel state information (CSI) can be classified based on which knowledge is known; either the current condition instantaneous CSI or the statistical knowledge statistical CSI. In [84], it was shown that in a CSK modulation the strongly constant weight code (SCW) can be used in molecular communication to improve transmission. In [204] constant-composition codes were used to mitigate the use of channel state information (CSI). In [205], error performance analysis of diffusion based molecular communication with OOK was done. In [206] zero error codes were implemented for molecular communications. In [207] error-correction via-amplitude width encoding was done. In [208] the performance of Bose-Chaudhuri-Hocquenghem [209] and Reed-Solomon codes [210] for molecular communication with diffusion are evaluated by simulation and results are analysed.

2.9 Information Security

An important aspect of any communication system is the security it gives to its users. Information transmission and encryption is a heavily studied topic in EM communication; however, in molecular communication, it has yet to gain the interest of researchers. A study was made in [102] to analyse the implementation of a secure channel for molecular communications and in [103] security and privacy were discussed for use in molecular communication.

2.10 Receivers

In order to decode the message, a receiver must be used. The receiver can be any device that is able to detect chemical concentrations and be able to convert them into electrical impulses. For use in macro-scale molecular communication, an electronic nose (section 2.10.2.1) or a mass spectrometer (MS) (section 2.10.2.2), which are already common place in many industrial applications, can be utilised. In micro-scale the sensor and applications are still a new concept and are a current research interest.

2.10.1 Micro-Scale Molecular Communication

The use of sensors in the micro-scale is still a relatively new concept. The use of nanoscale sensor networks (NSN) was first proposed in [18], where sensors are defined as nodes at nano-scale sizes. These small scale devices can be used as a network and can be used in applications such as medicine or military [211]. However the conceptualisation and the production of these kind of sensors is hard to produce to the same performance standard compared to their macro-scale sensor counterparts because of their dimensions. In [212] networking schemes for these kind of sensors were discussed. Recently there have been developments of nano-sensors that can be utilised for micro-scale [213, 214], one of the ideas being the use of biological circuits, based on chemical reaction networks and DNA transcription processes [215, 216].

An alternative way of implementing sensors for use in micro-scale can be derived from organic systems. In [217] the use of artificial neural networks (ANN) was proposed for use in micro-scale. These ANNs could be interfaced to a nano-device and achieve communication in a small size. In [172], quorum sensing in bacteria were utilised to transmit information, which can further be used as sensors in future applications.

In literature, sensors are generally categorised as either passive or active [218]. A passive receiver is defined as a receiver that does not interfere with the environment such that particles that are detected are not removed from the environment [219–224]. An active receiver, on the other hand, directly interferes with the particles in the environment such that the particles are absorbed and removed from the system [138, 225–227].

An important part of any communication is synchronisation and arrival time [228, 229]. A communication that has synchronisation stops slips from occurring and maintains performance. Based on this there have been studies done on the possibility of synchronisation in molecular communications with diffusion [230, 231] and with advection [232].

Deep Learning has been gaining traction as an impressive tool in optimisation and therefore has been used in numerous fields on real-life applications. Recently, molecular communication has also seen deep learning in decoding transmitted signals [233, 234] and receivers [235].

In [236], a detection network was devised for molecular communications. In [237] a new pre-coding algorithm was introduced at transmitter side to mitigate the ISI for adaptive threshold detectors was shown and applied. In [238] signal detection based on derivation for high-data rate molecular communication is done. In [239] the effect of spatial partitioning on the variance of the output signal is investigated and in [240] the receiver performance for molecular communication is improved by use of an adaptive weighted algorithm.

2.10.2 Macro-Scale Molecular Communication

An advantage of macro-scale over micro-scale is that there are technologies already available that can be implemented as detectors. The information particle of a macro-scale can utilise gas particles and there are various types of detectors in the market that can be used. An

important group of gases are volatile organic compounds (VOCs). These types of gasses are used in nature by plants mostly for communication purposes [58]. These chemicals are mostly in their gas phase at room temperature and they can be detected using electronic noses or the use of mass spectrometers (MS) which are discussed below in detail.

2.10.2.1 Electronic Nose

An electronic nose is defined as a sensory tool used to detect chemical odour/scent. The first conceptualisation of this device was made by Persaud and Dodd in 1982 [241]. From [242] an electronic nose has the following:

- sensor matrix to simulate a human olfactory system.
- pattern recognition system that recognises the olfactory pattern data processing unit which can perform similar function as an olfactory bulb.

The ability of discriminating and recognising a variety of gases and odours using small numbers of sensors led the electronic nose to be used in various areas, such as medical and diagnostics [243–245], food [246–248] and cosmetics sectors [249]. A block diagram of an electronic nose can be seen in Figure 2.8.

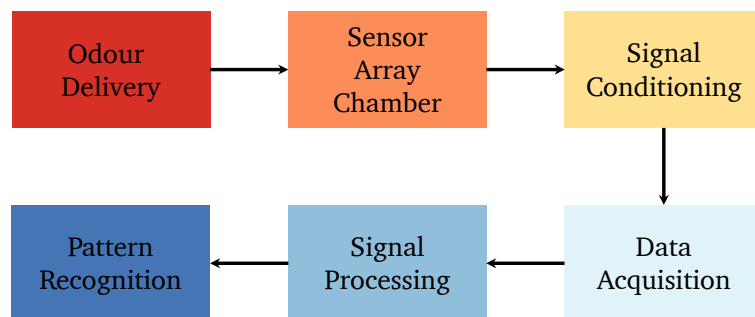


FIGURE 2.8: A block diagram of an electronic nose.

The basic prospect of an electric nose is to convert the chemical footprint into a detectable electrical signal. This could be achieved using different properties of a type of material (change of resistance, temperature etc.). However, some measurement of characteristics are suited better for certain applications. In [42] the use of electronic noses was deemed to be the best candidate for use in an odour communication system due to their portability compared to mass spectrometers. However, as it will be mentioned in the next part, mass spectrometers provide specific qualities that can make the MS a de facto standard for use in macro-scale molecular communication experimentation.

2.10.2.2 Mass Spectrometer

Mass Spectrometers (MSs) have played a key part in many phases of drug discovery and the identification of proteins. This is all possible because of the MS's sensitivity and speed of analysis. Aside from its importance in the drug industry, MS is also a vital part in many fields. Examples would be identifying and monitoring bio-markers in physiological fluids, rapid screening of drug-target binding and other biochemical analysis. As a result of its vast usage in most fields and for its versatility, MS has became a routinely used technique. MS have the ability to detect numerous chemicals concurrently and with high resolution making it a valuable option for use in molecular communications as a receiver. A detailed description of a type of MS, quadrupole mass analyser (QMA) is given in Chapter 3.

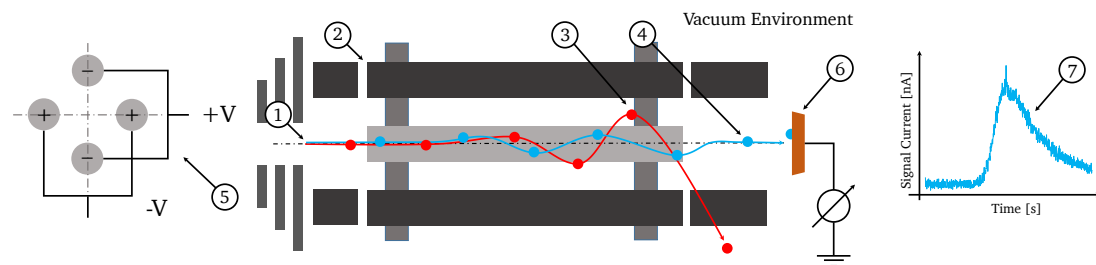


FIGURE 2.9: The principle diagram of the quadrupole mass analyser used in chemical detection: (1) Once the samples are introduced into the detector via the membrane inlet the chemicals are ionised and passed through a focus lens. (2) The analyser is made up from four hyperbolic rods with applied potentials. Based on the electric potential applied to the rods, which the connection diagram can be seen in (5), the ions can be separated based on their mass-to-charge values. Ions with stable trajectories, such as (4) will travel through the electric field and will arrive at the detector shown in (6), whereas ions with unstable trajectories (non-resonant ion), e.g. (3), will collide with the quadrupole and will be filtered out from the detection. Detected ions are amplified and presented visually as mass chromatogram shown in (7).

The name “*Mass Spectrometry*” gives an unclear definition of the name. The measurement is not done on the mass of the sample (kg) but on the mass-to-charge (m/z) ratio. A mass-spectrum is defined as the relative ion abundance (%) vs. m/z . The spectrum is using the units of Dalton (Da) per unit charge (q) [250]. In a MS analysis, all information comes from gas-phase ions. There are three primary components of a mass spectrometer: an ionisation source, a mass analyser and a detector.

The use of MS in molecular communication is relatively new with proof-of-concept transmission first reported 2017 in [45]. To utilise the experiments, a membrane inlet mass spectrometer (MIMS) with a QMA is used. In [47] the study was further developed and the modulation methods of OOK and CSK were investigated. In [46] an experimental message was sent using a MIMS and [8] an extensive analysis was done on the parameters of the macro-scale. In [9], the noise was analysed to be additive white Gaussian noise (AWGN) and the open-air transmission of macro-scale was analysed.

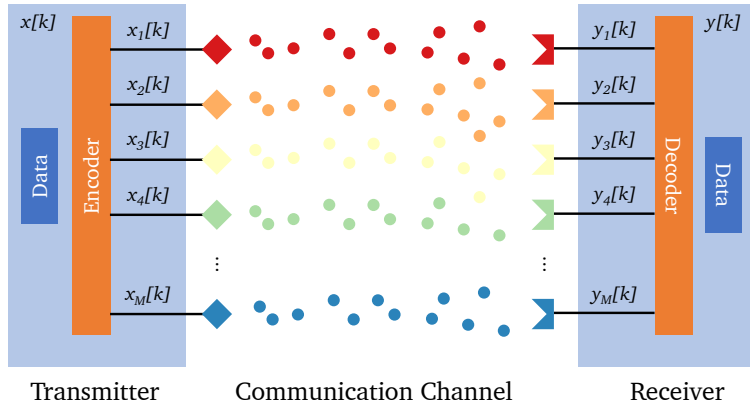


FIGURE 2.10: A representative diagram of the implementation of MIMO for use in molecular communications.

2.10.3 MIMO Applications

In radio applications, multiple input multiple output (MIMO) is a method to increase the capacity of a radio link using multiple antennas and receivers [251]. This technique is widely used in traditional communication such as IEEE 802.11n (Wi-Fi), IEEE 802.11ac (Wi-Fi) etc.

There have been studies to implement this method for use in molecular communications. In a study conducted in [142], one of the first instances of MIMO use in molecular communication was conducted. However, in this study, the effects of ISI were not considered. The first study that considered both MIMO and ISI was in [252]. The main drive of the utilisation of MIMO is to increase the already slow communication of molecular communication. Based on this premise various studies were realised on the properties of molecular MIMO, such as detection [253–256], modulation analysis [176], channel analysis [257–259] and cooperative relaying [260].

2.11 Experimental Analysis

The study of molecular communication has mostly been done on the theoretical aspects. However, macro-scale molecular communications have seen the use of practical experimental test-beds to study the aspects of the methods of communication.

One of the first test beds to study the effect of molecular communications is shown in [38]. In this study, as a transmitter an electrical spray controlled by an Arduino is used and for detector a MQ-3, MQ303A and MR513 sensors were utilised. The transmitted chemical was chosen as isopropyl alcohol (C_3H_8O). In [262], an experimentally validated end-to-end channel model for molecular communication systems based on the setup in [38] was developed and experimented.

Another approach uses the characteristics of the molecules to convey information which was accomplished in [263]. In this research the pH values were used. The carriers of information are designated to be hydrogen ions and the detection of these particles is achieved

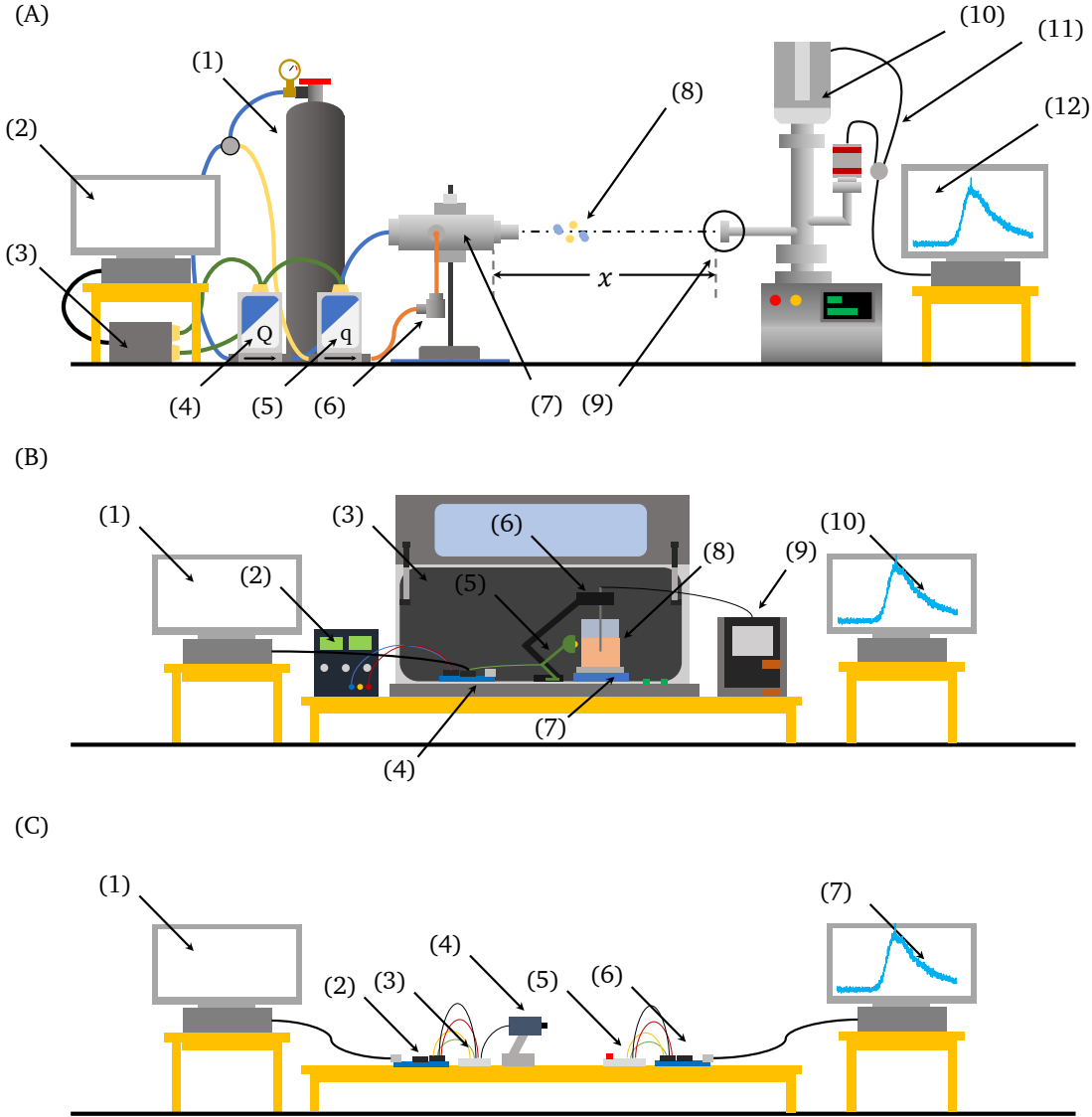


FIGURE 2.11: Experimental test beds used in literature

- (A) The diagram of the odour generator-MS experimental setup [8–10, 46, 47]: (1) N₂ gas; (2) modulation information; (3) automation platform; (4) MFC for the carrier flow; (5) MFC for the signal flow; (6) evaporation chamber (EC); (7) mixing chamber; (8) propagation medium; (9) MS inlet; (10) electronics control unit; (11) pressure gauge; (12) controller and the regulator cables; (13) data acquisition and analysis.
- (B) Bench-top experimental setup [261]: (1) transmitter; (2) voltage source; (3) incubator; (4) arduino; (5) LED; (6) pH sensor; (7) magnetic stirrer; (8) bacteria in glass tube; (9) pH meter; (10) Receiver.
- (C) Tabletop Molecular Communication [38]: (1) Transmitter; (2) Arduino; (3) Adafruit LCD shield kit; (4) DuroBlast electrical spray; (5) MQ-3 sensor; (6) Arduino; (7) receiver.

by use of a pH sensor. The transmitter is made up from a series of peristaltic pumps which compresses the tube to create a flow. The propagation channel is a silicon tube and the receiver is a pH meter interacting with an Arduino Uno. From experimental results it was demonstrated that transmission speeds of 4 bps could be achieved.

In [264] an alternative approach was considered, where instead of propagating the particles in a gaseous environment an aqueous environment was chosen and the transmitter chemical was chosen to be lauric acid coated SPIONs (superparamagnetic iron oxide nanoparticles), which were employed in drug delivery applications [265]. Propagation and transmission is accomplished by a peristaltic pump and the detection is done by susceptometer coil which generates an electrical signal when there are magnetic materials in close proximity.

A short study was conducted in [162] where the information rate of molecular communication is studied in laminar and turbulent flow.

A recent study was done in [261] where a biological approach was considered. The setup utilised a colony of bacteria (*E. Coli*) expressing bacteriorhodopsin in their cell membrane for easy-to-control optical signal conversion. Based on the input from the photo sensor, bacteria change the pH of the environment and the transmission is detected via a pH sensor.

In [266] a similar experimental setup to [38] was used to study and analyse anti-ISI demodulation schemes for diffusion based molecular communications.

A study was done in [267] where a proof-of-concept multi-input multi output (MIMO) molecular communication was conducted. This MIMO application was further analysed in [252] and in [268] the application was studied with an additional advection element.

In [269] the first controlled information transfer through an in-vivo nervous system by modulating digital data from macro-scale devices onto the nervous system of common earthworms and conducting successful transmissions was demonstrated.

While the experimental studies conducted rely on different principles of operation (electronic sprays, bacteria colonies etc.) most of the experiments conducted are short distance transmission ($< 1 \text{ m}$). Long distance ($> 1 \text{ m}$) transmission is only studied by either using an Arduino or a MS as a receiver. While the approach using Arduino allows transmission over long distances, it relies on external fans to propagate and utilises liquid chemicals to send its information. This approach may not be suitable for systems where the transmission needs to be conducted in a boundary (i.e., pipe). This is caused by the gravitational forces acting on the liquid chemical.

The last approach, MS, overcomes this problem by utilising gas-phase-only transmission with pressurised N_2 gas to create propulsion. This approach allows transmission in closed environments over long distances ($> 1 \text{ m}$).

TABLE 2.4: Experimental test beds used to study molecular communications.

Transmitter	Propagation Medium	Messenger Particles	Detector	Distance	bps	Reference
Odour Generator	Gaseous	VOCs	Mass Spectrometer	4 m	0.05	[8, 45–47]
Arduino with Electrical Spray	Gaseous	Water Droplets	MQ-3 with Arduino	4 m	0.5	[38, 262]
LED with Arduino	Aqueous	<i>E. Coli</i> Bacteria	pH Sensor	$< 1 \text{ m}$	0.016	[261]
Peristaltic Pump	Aqueous	Superparamagnetic Iron Oxide Nanoparticles	Susceptometer coil	5 cm	0.25	[264]
Peristaltic Pump	Gaseous	Ions	pH Sensor	$< 1 \text{ m}$	4	[263]

2.12 Applications

2.12.1 Micro-Scale Molecular Communication

Micro-scale molecular communications can be used in fields such as drug delivery systems/medicine [17, 270–273]. In addition, studying micro-scale molecular communications gives insight to the communication done in the nm to μm range. This knowledge could further be used to develop bio-computers [274, 275].

An important application of micro-scale is the manipulation of biological processes from an engineering perspective. This can be done by using quorum sensing [177]. By mimicking this stimuli system, self-organising collective sensors (SECOAS) can be improved to be used in environmental monitoring system. This is a swarm made by individual nodes, which chooses a node to transmit in order to save on limited energy [276]. This molecular application can also be applied to ad-hoc networks [277]. There are biological approaches in which micro-scale molecular communication can be applied such as Ca^{+2} signalling [278], ligand-receptor binding mechanism [279, 280], synthetically engineered bacteria [281] and electroencephalogram (EEG) waves [282].

Molecular communications can be used to analyse in-vessel transport. It was proposed in [32] that vessel-like structures provide a boundary to the transportation and guides propagation to the desired destination. This aspect of communications has been studied in literature on its various properties, such as decoding method [283], channel geometry [284, 285] and channel model [286].

2.12.2 Macro-Scale Molecular Communication

The current applications of macro-scale are limited since most of the conventional large scale communications are dominated by traditional communication methods (EM) that have been well developed and established. However, there are areas where EM communication is not desirable and an alternative might prove to be a better choice. A study has shown that EM based sensors have limited reliability in infrastructure monitoring [62]. In addition, environments where EM communication is limited because of obstacles [64] (i.e. caves, mines) macro-scale can be a good alternative and can also be used in sending information using pipes. In [12], it was shown that under specific conditions molecular communications outperforms electromagnetic communication in terms of signal quality in a pipe where EM has higher attenuation per distance in a copper pipe.

In addition to being a tool for communication, macro-scale molecular communication can also be used for studying biological processes such as pheromone communication in animals [24]; ants using chemical trails for navigation [60] or moths using chemical signalling over several km [51]. Based on these biological processes, much research has been done to implement this biological application and make it applicable as an engineering approach [50, 287–289].

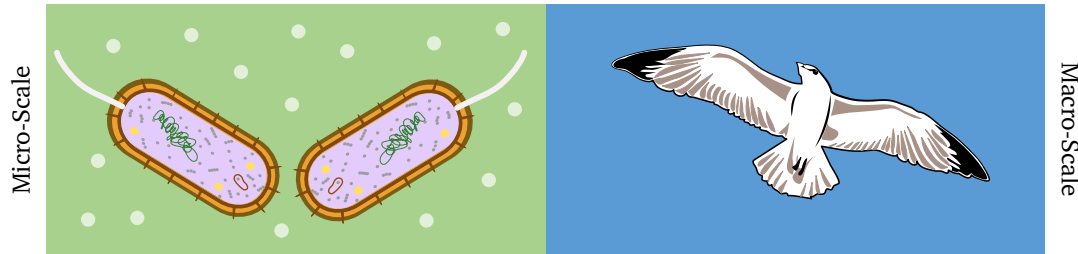


FIGURE 2.12: Applications of molecular communication can be implemented both in micro-scale and macro-scale. At smaller scales, understanding of particle propagation and reception can be used to control bacteria and be used in implementing drug delivery systems. At larger scales, molecular communication can be used in studying animal behaviour.

Another application of macro-scale is in robotics. By utilising pheromone communication and olfaction [68, 79, 290] communication between robots can be established. The research field for this application can be divided based on two distinct approaches:

- Chemical (odour) tracking robots [68–76].
- Pheromone based communication [79–81, 291].

A different approach to the use of macro-scale molecular communication would be odour transmission using digital medium [42]. The topic has been known since the 1950s and deals with sending and receiving scent in digital medium; it has become more important with the mass availability of virtual reality (VR) hardware [292]. These hardware are impressive in simulating the reality for both audio and video but the sensory input for odour is still a problem to emulate. The transmission of audio and video are well understood, however the transmission of odour from transmitter to the receiver is still a topic of research [293, 294]. The knowledge gained on studying macro-scale chemical propagation can be further implemented to this topic which can be used to create realistic scent streams to further improve the illusion of reality of a VR environment.

2.13 Simulations

Simulation is the imitation of an operation of a real world process [295]. As it plays a very important part in many fields of engineering, molecular communication has also seen a fair share of simulation platforms designed to simulate the process of propagation and detection. One of the limitations of micro-scale over macro-scale is the scarcity of experimental analysis. This is due to size of the scale and lack of equipment able to carry out the experiments. Based on these drawbacks simulations play an important role in the analysis and the study of numerous parameters of the communications.

As mentioned there are a variety of simulation models designed to analyse specific properties of this novel communication paradigm. In this section each simulation platform will be briefly discussed and their comparison can be seen in Table 2.5.

TABLE 2.5: Simulation platforms for use in molecular communications.

Simulator Name	Customisation	License	Function	User Interface	Implementation	References
BiNS2	Customisable Domains	Open	Diffusion based	Command Line	Java	[296, 297]
CalComSim	via Python	Open	Calcium Signalling in tissues	Command Line	Python	[298]
N3Sim	via Config File	Open	Diffusion	Command Line	Java	[299, 300]
Comsol	Script based module	Commercial	Multipurpose	Graphical	N/A	[285]
NS-3	via C++ & Python	Open	Network Simulator	Command Line	C++ & Python	[298, 301]
NanoNS	via C ++ & OTcl	Open	Diffusion Based	Command Line	C++	[28]
NanoNS3	via C ++ & OTcl	Open	Diffusion Based	Command Line	C++	[302]
BNSim	via Java	Open	Bacteria Networks	Command Line	Java	[303]
NCSim	via C++ & Python	Open	Flagellated Bacteria Networks	Command Line	C++	[299]
HLA	via C++ & Python	Open	Flagellated Bacteria Networks	Command Line	C++	[304]
AccORD	via C++ & Python	Open	Flagellated Bacteria Networks	Command Line	C++	[194, 218, 305–308]
MUCIN	via MatLAB	Commercial	Diffusion	Graphical	MatLAB	[309]

2.13.1 BiNS

Biological and nano-scale communication simulator (BiNS) is a multi-threaded simulation package for molecular communication systems developed by the researchers from the University of Perugia [296]. Its customisable design provides a set of tools for generating objects and allows modelling the behaviour of biological entities, including the collision handling and the modelling of diffusion with advective flow propagation onto both constrained and open space environments.

2.13.2 N3Sim

N3Sim is a java-based simulation framework that used diffusion only molecular communications. This platform allows the analysis of molecular networks possessing several transmitters and receivers [299]. The diffusion process through the medium is modelled as Brownian motion, which takes account of particles' inertia and collisions among particles as they travel through the medium. The simulation is based on a three-layer architecture:

- User interface layer.
- Data layer.
- Domain layer.

The simulation parameters are defined by the text configuration file.

2.13.3 COMSOL

COMSOL multiphysics is a commercial multi-purpose platform designed for simulating and analysing physics-based problems through a unified work flow for electrical, mechanical, fluid, and chemical applications [310]. It implements finite element analysis (FEA), to study different physics and engineering applications. An example of the use of COMSOL multiphysics for simulating a molecular communication drug delivery system is presented in [310] and is also used in simulating micro-fluidic environments [285].

2.13.4 NS2 and NS3

NS2 and NS3 are discrete-event network simulators. Even though they were not originally developed for molecular communications, their flexible structure has allowed implementing some basic elements of molecular communications.

NanoNS [28] is an NS-2 based simulator for diffusion based molecular communication in aqueous environments, with continuous thermal motion of molecules.

NS-3 is a simulation tool that has been developed in the framework of the IEEE P1906.1 working group [311]. User programs can be written in C++ or Python programming languages.

2.13.5 BNSim

BNSim is a multi-threaded Java-based simulation platform for analysing bacteria networks [303]. These networks interconnect engineered bacteria that communicate at the nano-scale.

BNSim functions by integrating three simulation methods:

- Gillespie stochastic simulation algorithm [312].
- Stochastic differential equations (SDEs), used to model large-scale chemical system with a controlled level of approximation.
- Hybrid algorithm which integrates the above methods.

2.13.6 NCSim

NCSim is a simulation platform for molecular communications that utilises flagellated bacteria for transmission of information [313]. The simulations primary objective is on the analysis of different message encoding techniques. It can simulate several simultaneous links between the nano-machines. NCSim incorporates the stochastic model for bacteria mobility, and the plasmid/chromosome transfer between bacteria through the conjugation process. NCSim consists of three modules:

- Physical layer of bacterial nano-networks.
- Scenario generator and simulation monitor.
- Plot generation.

2.13.7 HLA

High level architecture (HLA), which is standardised under IEEE 1516, is used to design and develop a distributed simulation tool for molecular communication and in [304], the authors introduced a simulator design based on the HLA model focusing on scalability. It is used to design a distributed simulation tool for molecular communications, so that different scalability options can be used to include additional processing power to reduce the execution time. This model allows the design of large systems, which could be difficult to do otherwise.

2.13.8 AcCoRD Simulator

AcCoRD (actor-based communication via reaction-diffusion) is a molecular communication simulator and designed as a generic reaction-diffusion solver for flexible system configuration. Actors are placed as sources (i.e., transmitters) or observers (i.e., receivers) of molecules. Environments can be defined with a combination of microscopic and mesoscopic regions [194, 218, 305–308].

2.13.9 Other Works

Aside from simulation platform there are other studies which aid in the simulation studies of molecular communication, such as; algorithms [314–317], multithreaded CPU and GPU implementation [318], parallel processing [319], analytical analysis [320–322], modelling [323, 324] and frameworks [325].

2.14 Standardisation

Standardisation is defined as the process and the implementation of technical standards based on the consensus of different parties [326]. Molecular communication is a relatively new field of study compared to EM where most of the technologies are standardised. However, there are attempts at standardising aspects of molecular communications.

One of these attempts is the unification of the research of molecular communications into a single architecture, named molecular communication markup language (MolComML) [327]. This standardisation is similar and influenced by the systems biology markup language (SBML) which is the de-facto standard for representing biological processes through computational models in systems biology [328] and in [329] a new metric was proposed for the performance evaluation of molecular signal within the context of molecular communications.

Aside from the research standardisation, there are also works on implementing standards for the communication aspect of the system. In [211] the communication system was analysed based on the open systems interconnection (OSI) model and each layer was discussed in detail and in [330], transmission control protocol (TCP) was implemented and studied for molecular communications.

Another approach is to standardise how information is transmitted. This is done in EM communications as packets where information is encoded to the package to define its numerous properties; beginning, end, where it is headed to etc. This approach was also recently studied in [331] where data frames in molecular communication are envisioned.

2.15 Conclusion

In this Chapter, a review into the molecular communications is undertaken. Molecular communications is still novel and still being experimented upon, and there are aspects of the field where studies need to be conducted. One of these fields is information security. Information security is a pivotal aspect of modern communication and becomes ever more important as time passes. However, aside from a few preliminary studies, research is required. Studies have been done into modulation methods, ISI mitigation and mathematical modelling of the propagation. These properties are mostly based on already established principles in EM. There are still aspects of molecular communication yet to be discovered that is intrinsic to its particle properties that cannot be implemented to a wave-based communication system. Experimental studies have recently gained traction and have shown physical proof of the

validity of molecular communication both biological and mechanical. Simulation platforms were developed to increase the speed of progress of this field. Applications exist where molecular communications is a better alternative to already existing communication methods and in the future, molecular communications shows promise in improving our ability to communicate in areas where the current methods (i.e., EM) struggle by fundamentally changing the method of communication.

Chapter 3

Experimental Setup

3.1 Introduction

Molecular communication, as discussed in the previous chapters, is an emerging field, and compared to traditional communication methods (i.e., EM) is still in its infancy regarding the understanding of its physical properties. To analyse this novel communication paradigm experimentally, a test-bed must be established. Unlike EM or AC, molecular communication does not rely on the propagation of waves. Instead, it relies on the momentum of travelling particles. Therefore, to realise the communication, a receiver that can distinguish chemicals must be implemented. This can be accomplished in two ways.

The first method is to use sensors that physically interact with the particles and produce current from the interaction (i.e., MOSFETs). Consider, as an example, tin-oxide (SNO_2) sensors. The gates of these MOSFETs are covered with SNO_2 and by interacting with the O_2 in the air it produces a current, depending on the concentration value of the introduced chemical species. However, this can cause a bottleneck in the communication where the interaction of the chemical and the sensor can decrease the sensitivity of the future transmissions and make it unsuitable for long transmissions. Due to the mechanics of SNO_2 (redox) the sensor can reach saturation point where the sensor lacks O^- ions to interact with the signal chemical in the transmission medium [332].

The second approach, is the utilisation of mass spectrometers (MS). A MS is an instrument capable of analysing and distinguishing charged ions based on their motion in an applied electric and/or magnetic field. The analyser of the MS allows the detection of ions with a particular mass-to-charge (m/z) ratio [250, 333], making it a useful tool for use in molecular communication, as described in Section 2.10.2.2.

In this chapter, different parts of the experimental setup are described in detail. Section 3.2 gives an overview of the experimental test bed. Section 3.2.1 discusses the operation of the transmitter. In Section 3.2.2 the chemical species used throughout the thesis are given. Section 3.2.3 is dedicated to the receiver, where the operating principle of the QMA is given in detail.

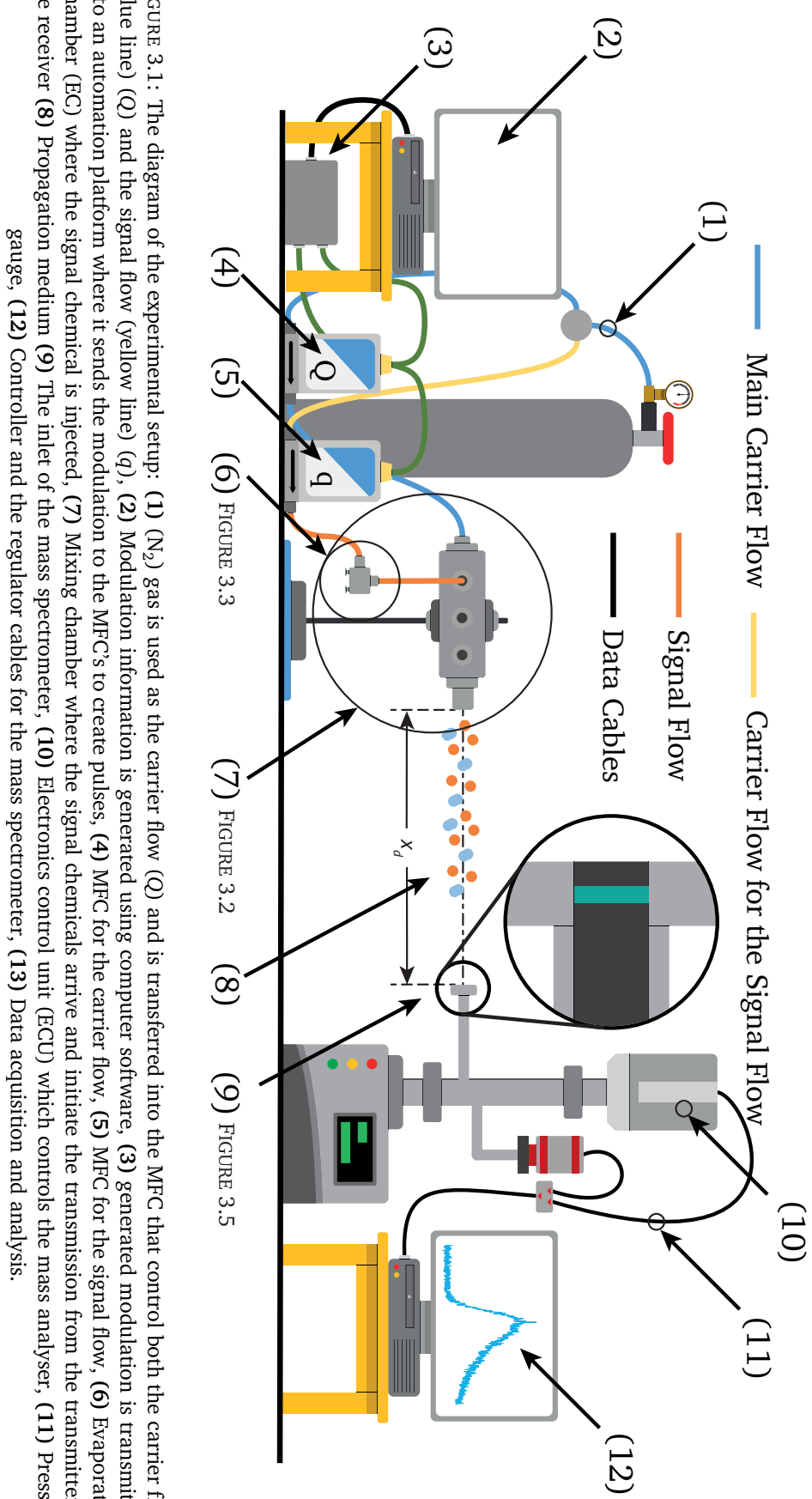


FIGURE 3.1: The diagram of the experimental setup: (1) N_2 gas is used as the carrier flow (Q) and is transferred into the MFC that control both the carrier flow (blue line) (Q) and the signal flow (yellow line) (q), (2) Modulation information is generated using computer software, (3) generated modulation is transmitted into an automation platform where it sends the modulation to the MFC's to create pulses, (4) MFC for the carrier flow, (5) MFC for the signal flow, (6) Evaporation Chamber (EC) where the signal chemical is injected, (7) Mixing chamber where the signal chemicals arrive and initiate the transmission from the transmitter to the receiver (8) Propagation medium (9) The inlet of the mass spectrometer, (10) Electronics control unit (ECU) which controls the mass analyser, (11) Pressure gauge, (12) Controller and the regulator cables for the mass spectrometer, (13) Data acquisition and analysis.

3.2 Experimental Setup

The generation and transmission of chemicals based on a message was made using an in-house-built odour generator, and the detection of the chemical was made using a mass spectrometer (MS), namely a quadrupole mass analyser (QMA). The diagram for the experimental setup used in the study can be seen in Figure 3.1. In the following section, each of the major parts of the experimental study is discussed in detail.

3.2.1 Transmitter

A gas dispenser that is controlled by mass flow controllers (MFCs) releases volatile organic compounds (VOCs) (placed into an evaporation chamber) called the signal flow, whereas the flow passing through the mixing chamber is called the carrier flow (N_2) [5, 45]. VOCs are chemicals that can transmit from the liquid to the gas phase at ordinary room temperature and pressure. This property is due to the low boiling point of the chemical, which forces a large number of molecules to evaporate from its liquid or sublimate from its solid phase and mix-in with the surrounding air; known as volatility. Most odours are made up of VOCs.

The MFCs are connected directly into the N_2 gas cylinder and controlled directly by a computer and an automation platform. The automation platform sends digital commands to the MFC and the internal valve inside can be controlled to create gas pulses. In this setup, there are two flows present: one is responsible for transporting the samples from the evaporation chamber into the mixing chamber (signal flow q); the second one is responsible for carrying the signal chemicals from the mixing chamber to the transmission medium (carrier flow Q). A diagram of the odour gas generator can be seen in Figure 3.2, and the evaporation chamber can be seen in Figure 3.3. When the gas leaves the mixing chamber and transmits through the medium it is defined as bulk flow (B_F) [5, 45]:

$$B_F = Q + q. \quad (3.1)$$

3.2.2 Chemicals

In this study four types of chemicals were used. A zero-grade N_2 (% 99.998 purity with 1 bar pressure) was chosen for the carrier gas (Q) that carries both the signal chemical from the transmitter to the receiver and transports the signal chemical from the evaporation chamber to the transmitter. The properties of the signal gas (q) used in this study are given in detail in Table 3.1. The mass spectrum of the chemicals used throughout the thesis can be seen in Figure 3.4.

3.2.3 Receiver

In the studies following the chapter, to detect the chemicals that are released by the odour generator (OG), a portable membrane-inlet mass spectrometer (MIMS), from Q Technologies Ltd., was used as the primary sensor. MIMS is a method of introducing analytes into the MS's

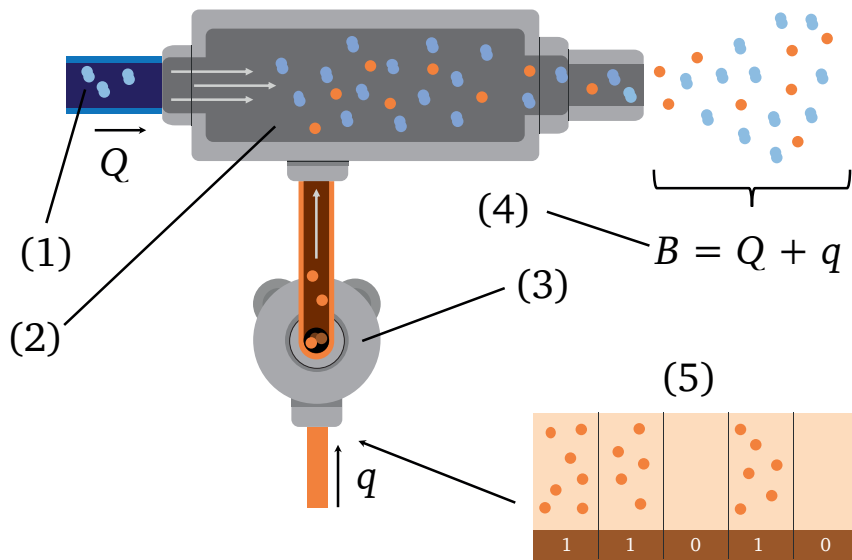


FIGURE 3.2: The working diagram of the odour generator (OG). [5] (1) Introduction of the carrier gas (Q) into the mixing chamber. (2) Mixing chamber where the evaporated chemicals from the chamber and the carrier gas are mixed. (3) Evaporation chamber (Figure 3.3). (4) Transmitted chemicals that are released from the chamber. (5) A modulation sequence that is used to create gas pulses.

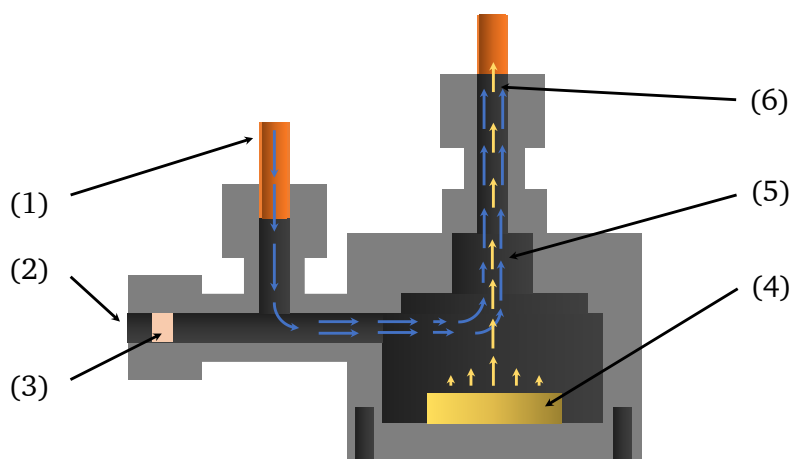


FIGURE 3.3: Diagram of the evaporation chamber (EC): (1) inlet of the N_2 gas into the evaporation chamber. (2) Inlet where the sample is introduced. (3) Thermo-resistant septum that allows the multiple introduction of a sample via a micro syringe. (4) An absorptive material that holds the liquid sample analyte. (5) N_2 from the inlet carries the evaporated chemicals from the chamber. (6) The cumulated gas is transferred into the mixing chamber via a 6.35 mm inch Teflon tube.

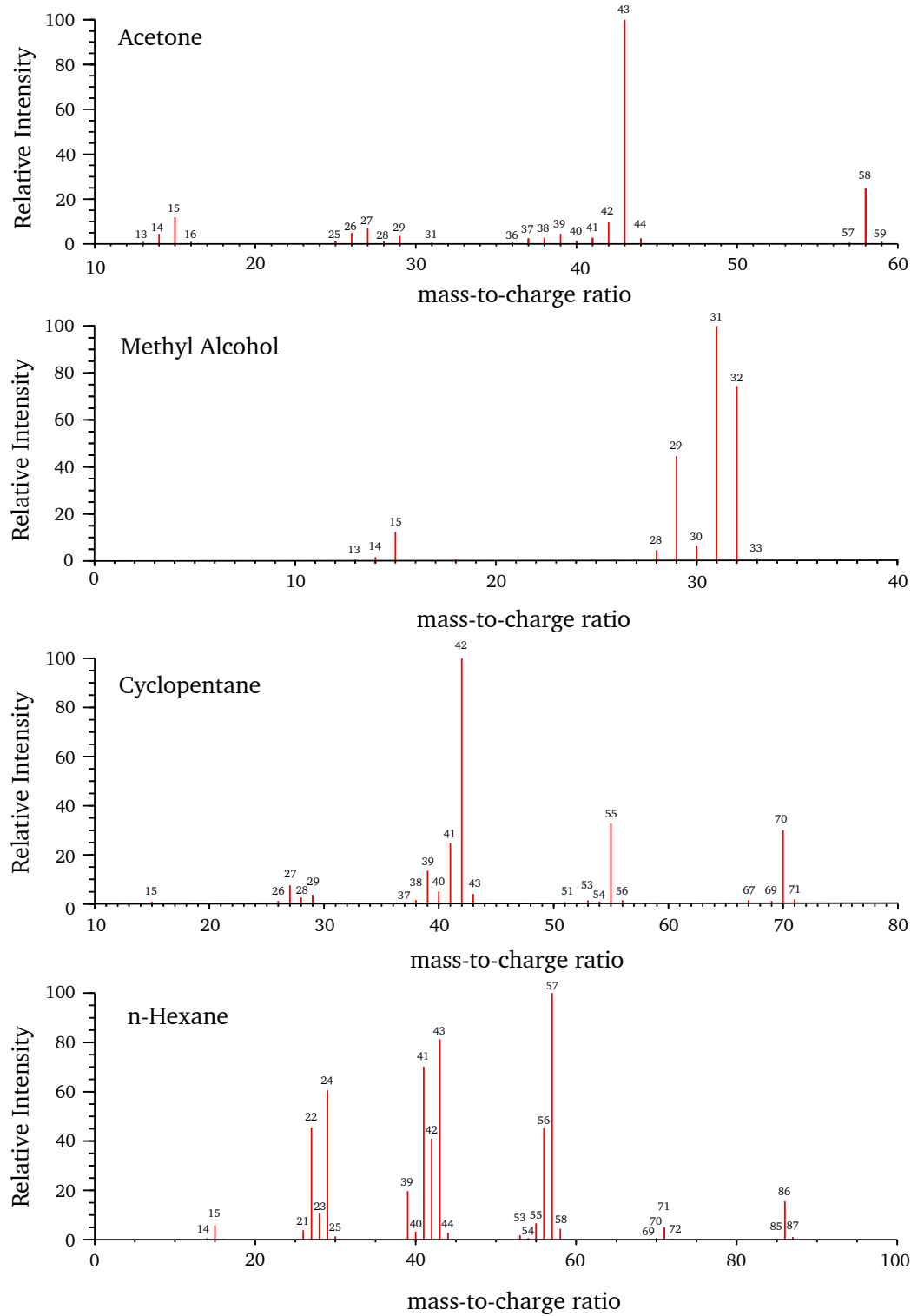


FIGURE 3.4: Mass spectra of the signal chemicals used in the study. The mass spectra of the chemicals are obtained via the use of electron ionisation (EI) [NIST Chemistry WebBook (<https://webbook.nist.gov/chemistry>)].

TABLE 3.1: Chemicals used throughout the thesis.

Parameters	Acetone	Methanol	Cyclopentane	n-Hexane
Molecular Formula	(CH ₃)COCH ₃	(CH ₃)OH	C ₅ H ₁₀	C ₆ H ₁₄
Molecular Weight	58.08 g/mol	32.04 g/mol	70.135 g/mol	86.18 g/mol
CAS Number	67-64-1	67-56-1	287-92-3	110-54-3
Vapour Density ¹	1.56	1.11	2.4	2.97
Vapor Pressure ²	184 mmHg	97.68 mmHg	317.8 mmHg	153 mmHg
Boiling Point	56 °C	64.7 °C	49.2°C	68.5°C
Melting Point	-17.2 °C	-98 °C	-94°C	-96 °C
Diffusivity in air	0.124 cm ² /s	0.15 cm ² /s	0.0919 cm ² /s	0.2 cm ² /s
Chapters used in	5, 6 and 7	5, 6 and 7	7	7

¹ Relative to the density of the air (air = 1) ² Normal Temperature and Pressure

vacuum chamber via a semi-permeable membrane [334, 335]. The membrane is usually a thin, gas-permeable, hydrophobic material such as polydimethylsiloxane (PDMS), which is also used in this study. Samples can be almost any fluid, including water, air or sometimes even solvents. The great advantage of the method of sample introduction is its simplicity. MIMS can be used to measure a variety of analytes in real-time, with little or no sample preparation. MIMS is most useful for the measurement of small, non-polar molecules (< 200 Da), since molecules of this type have a greater affinity for the membrane material than the sample.

A MIMS consists of three primary parts: a sampling probe that lets the gas sample pass the membrane for the MS to analyse, a triple filter quadrupole mass spectrometer, which in turn consists of an electron ionisation (EI) source, QMA and a detector, and finally a vacuum system. The inlet of the system, consists of a fine non-sterile flat PDMS membrane [45, 336]. In the following subsections 3.2.3.1 and 3.2.3.2 major parts of the MIMS are described in detail.

3.2.3.1 Membrane Inlet

The initial analysis of the chemical species begins with the interaction of the signal chemicals with the membrane present in the inlet of the QMA. This process, called *pervaporation*, involves three distinct actions [337].

1. Absorption of sample molecules into the membrane (absorption),
2. Diffusion of sample molecules through the membrane (diffusion),
3. Evaporation of the molecules from membrane surface to the vacuum (desorption).

The pervaporation process can be described using Fick's two laws of diffusion. The 1st law describes the relation between the diffusive flux ($J(x, t)$) and the concentration of the molecules in the given environment. The diagram of the pervaporation phenomena can be seen in Figure 3.5.:

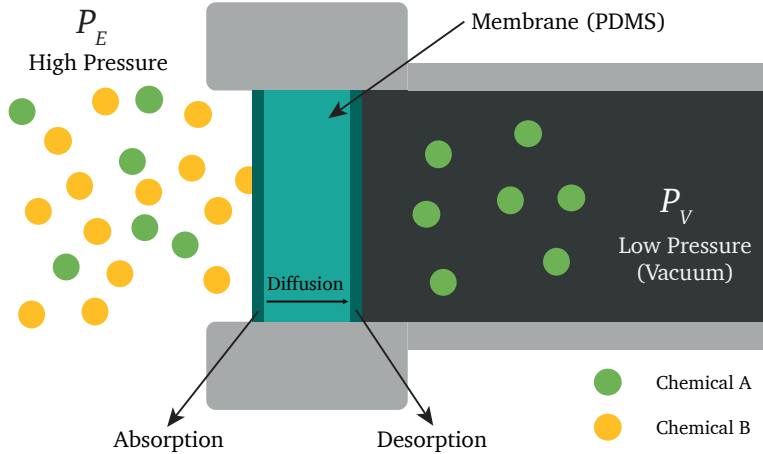


FIGURE 3.5: Diagram that illustrates the process of pervaporation.

$$J(x, t) = -D \frac{\partial c(x, t)}{\partial x}, \quad (3.2)$$

and the concentration gradient can be explained by Fick's 2nd law :

$$\frac{\partial c(x, t)}{\partial t} = D \frac{\partial^2 c(x, t)}{\partial x^2}. \quad (3.3)$$

The applications and the properties of the MIMS are described in the literature [336, 338–342]. Due to the presence of the membrane, each chemical can interact with the membrane differently, and this in turn can cause different absorption rates [45]. Additional details of the membrane and its applications can be seen in [336].

3.2.3.2 Quadrupole Mass Analyser

Developed at the beginning of the 1950s by Wolfgang Paul and Steinwegen from the University of Bonn, the QMA relies on the manipulation of ion trajectories by controlling the RF voltage applied to the quadrupole rods [343]. Since then, QMAs have become an important instrument in analysing samples. The principle theory of QMAs is given in the following paragraph and a functional diagram of the workings of a QMA can be seen in Figure 3.6.

Ions travelling along the z -axis (axial axis) are under the influence of an electric field generated by four parallel metal rods with their centre at the origin. The potential lines and the vectorial lines of the quadrupole field can be seen in Figure 3.7.

The potentials applied to the rods are given below:

$$+\Phi_0 = +(U - V \cos \omega t), \quad (3.4a)$$

$$-\Phi_0 = -(U - V \cos \omega t), \quad (3.4b)$$

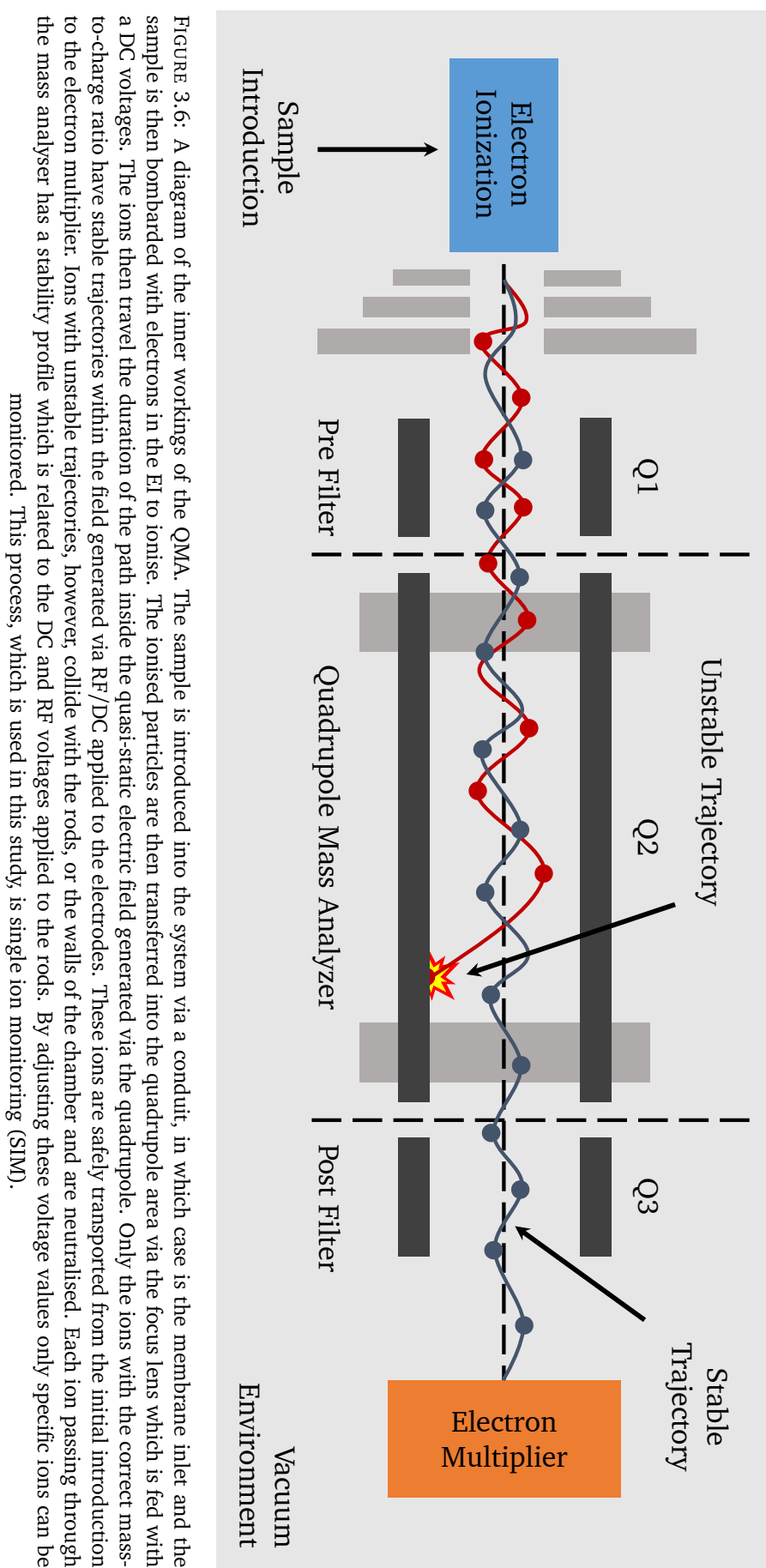


FIGURE 3.6: A diagram of the inner workings of the QMA. The sample is introduced into the system via a conduit, in which case is the membrane inlet and the sample is then bombarded with electrons in the EI to ionise. The ionised particles are then transferred into the quadrupole area via the focus lens which is fed with a DC voltages. The ions then travel the duration of the path inside the field generated via the quasi-static electric field generated via the quadrupole. Only the ions with the correct mass-to-charge ratio have stable trajectories within the field generated via RF/DC applied to the electrodes. These ions are safely transported from the initial introduction to the electron multiplier. Ions with unstable trajectories, however, collide with the rods, or the walls of the chamber and are neutralised. Each ion passing through the mass analyser has a stability profile which is related to the DC and RF voltages applied to the rods. By adjusting these voltage values only specific ions can be monitored. This process, which is used in this study, is single ion monitoring (SIM).

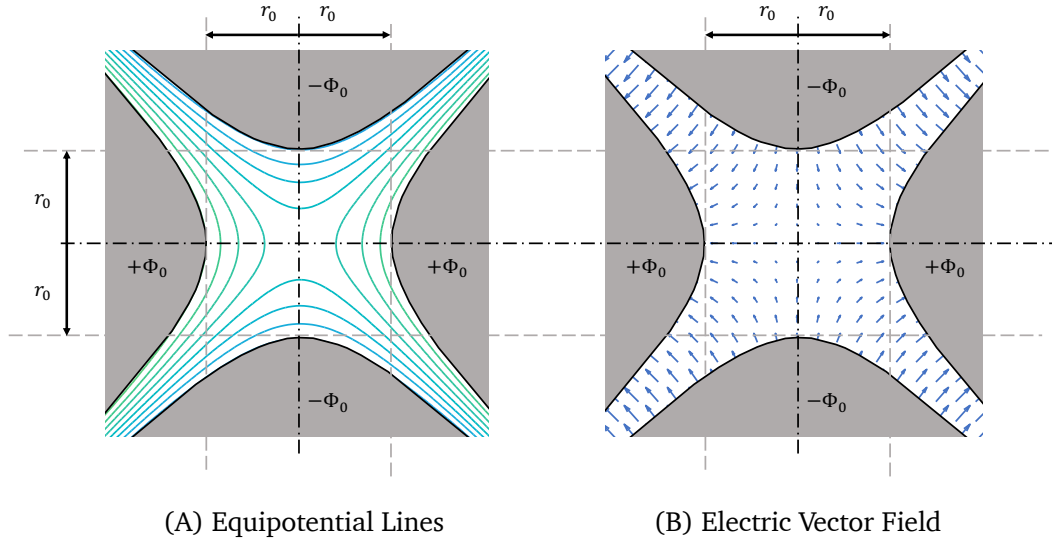


FIGURE 3.7: (A) Equipotential lines generated by the quadrupoles (B) Electric vector field generated by the quadrupoles.

where $Φ_0$ defines the potential applied to the rods (V), $ω$ is the angular frequency (rad/s), U is the direct potential (V) and V is the “zero-to-peak” amplitude of the RF voltage (V).

The accelerated ions enter the space between the quadrupoles, which align along the z -axis. The force acting on the accelerating ions is caused by the quadrupole electric fields. The possible trajectories of the ion inside a quadrupole field can be seen in Figure 3.8.

$$F_x = m \frac{d^2x}{dt^2} = -ze \frac{\partial \Phi}{\partial x} = -2ze x \frac{(U - V \cos \omega t)}{r_0^2}, \quad (3.5a)$$

$$F_y = m \frac{d^2y}{dt^2} = -ze \frac{\partial \Phi}{\partial y} = +2ze y \frac{(U - V \cos \omega t)}{r_0^2}, \quad (3.5b)$$

where m is the mass of an ion and e is the electric charge of a single electron (Coulombs). The electric potential (Φ) can be represented as a function of ($Φ_0$):

$$\Phi_{(x,y)} = (x^2 - y^2) \frac{\Phi_0}{r_0^2}, \quad (3.6)$$

where $2r_0$ is the closest distance between the four electrodes. By rearranging the equations given in Eq. (3.5), the movement equations (aka., Paul equation) is obtained:

$$\frac{d^2x}{dt^2} + \frac{2ze}{mr_0^2}(U - V \cos \omega t)x = 0, \quad (3.7a)$$

$$\frac{d^2y}{dt^2} - \frac{2ze}{mr_0^2}(U - V \cos \omega t)y = 0. \quad (3.7b)$$

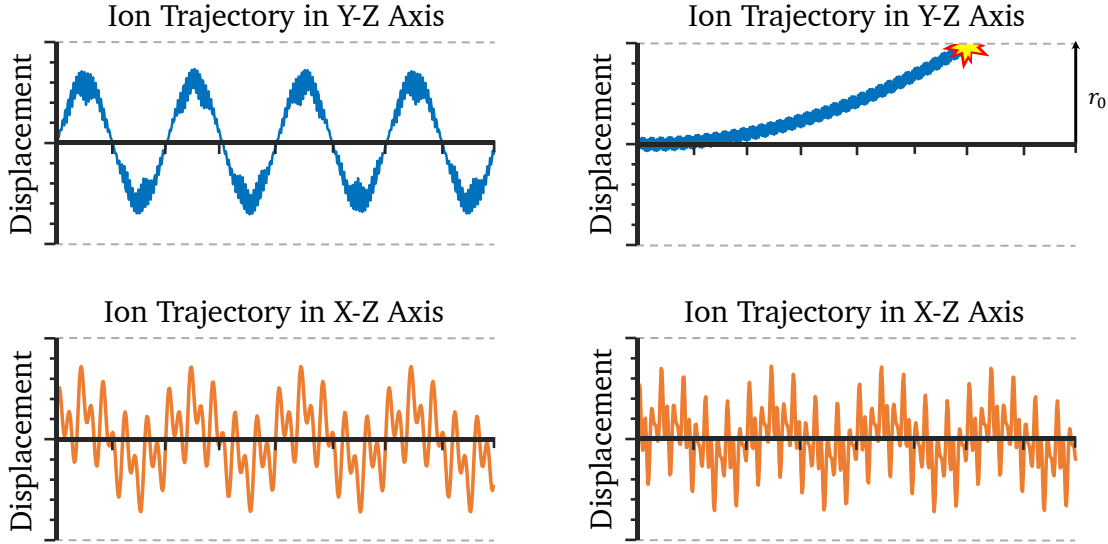


FIGURE 3.8: Examples of stable and unstable ion trajectories in a quadrupole.

The equations above describe the movement of an ion in a 3D environment within the influence of a quadrupole electric field. The ion's trajectory will stay stable if the x and y values never reach r_0 . If the values exceed r_0 the ion will collide with the quadrupole and never arrive at the detector. To solve the equations with respect to x and y the Eq. (3.7) needs to be integrated. To solve these sets of equations, the following conversions are used:

$$\xi = \frac{\omega t}{2}, \quad \xi^2 = \frac{\omega^2 t^2}{4}. \quad (3.8)$$

To simplify the equations given in (3.7), an umbrella term of Γ_u is given with the following identity with the redefined equation:

$$\Gamma_u = x = -y, \quad (3.9a)$$

$$\frac{d^2\Gamma_u}{dt^2} + \frac{2ze}{mr_0^2}(U - V \cos \omega t)\Gamma_u = 0. \quad (3.9b)$$

Including the transformation given in Eq. (3.8) to Eq. (3.9) yields the following expression:

$$\frac{\omega^2}{4} \frac{d^2\Gamma_u}{d\xi^2} + \frac{2ze}{mr_0^2}(U - V \cos 2\xi)\Gamma_u = 0. \quad (3.10)$$

The introduction of the parameter $\omega^2/4$ can be removed by multiplying both sides of the equation by $4/\omega^2$:

$$\frac{d^2\Gamma_u}{d\xi^2} + \frac{8ze}{m\omega^2 r_0^2}(U - V \cos 2\xi)\Gamma_u = 0, \quad (3.11)$$

A final simplification of Eq (3.11) by grouping the parameters into two definitions:

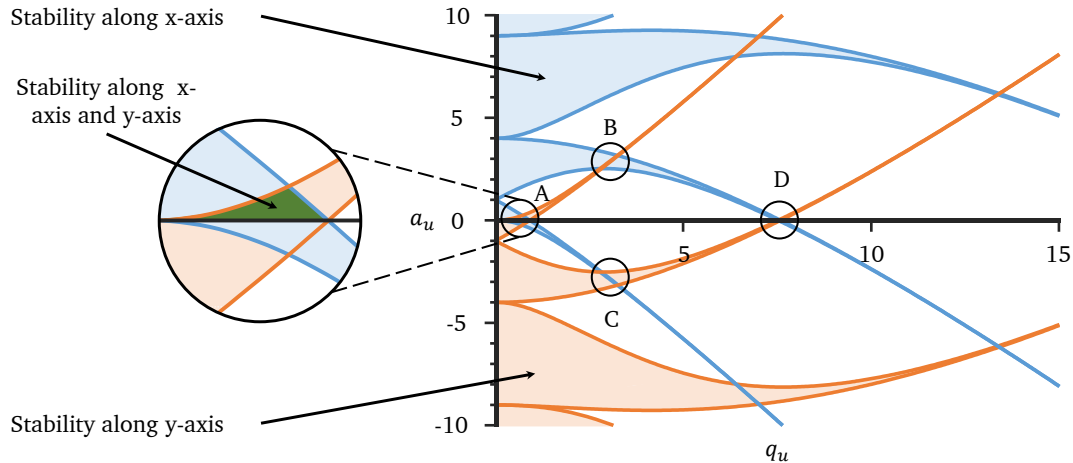


FIGURE 3.9: The stability diagram for the Mathieu equation considering x and y coordinate directions. Four stability areas are shown in circles. The most common area that is used in quadrupole mass spectrometry is (A).

$$a_u = a_x = -a_y = \frac{8zeU}{m\omega^2 r_0^2}, \quad q_u = q_x = -q_y = \frac{4zeV}{m\omega^2 r_0^2}. \quad (3.12)$$

The current description of the motion equation can be shown as:

$$\frac{d^2\Gamma_u}{d\xi^2} + (a_u - 2q_u \cos 2\xi)\Gamma_u = 0 \quad (3.13)$$

This equation is known in the literature as the Mathieu equation, which was introduced in 1868 by mathematician *Emile Mathieu* to solve problems related to vibrating elliptic membranes.

In a quadrupole the distance between the rods (r_0) is constant due to construction and the angular frequency (ω) is kept constant during operation. Therefore, U and V are the two variables of the analysis. The stability diagram, which Eq. (3.13) generates, can be seen in Figure 3.9 with the x and y axes being q_u and a_u . In the figure, there are two distinct areas that can be observed. These coloured areas represent the stability of the travelling ion in the x or y axis. The ion will traverse the quadrupole safely only if the parameters of motion lie in the joint area of both x and y area (i.e., the green area). Rearranging the parameters in Eq. (3.12) gives:

$$U = a_u \frac{m \omega^2 r_0^2}{8e} \quad V = q_u \frac{m \omega^2 r_0^2}{4e} \quad (3.14)$$

In operation, the $(\omega^2 r_0^2/e)$ part of both U and V is constant, making m/z the only variable. By increasing the m/z value linearly (i.e., switching from one mass to another) the a_u and q_u will also experience a change in values. This change will cause the triangular area seen in Figure 3.9, making every mass an individual area in the V - U space. This change in the stability area can be seen in Figure 3.10.

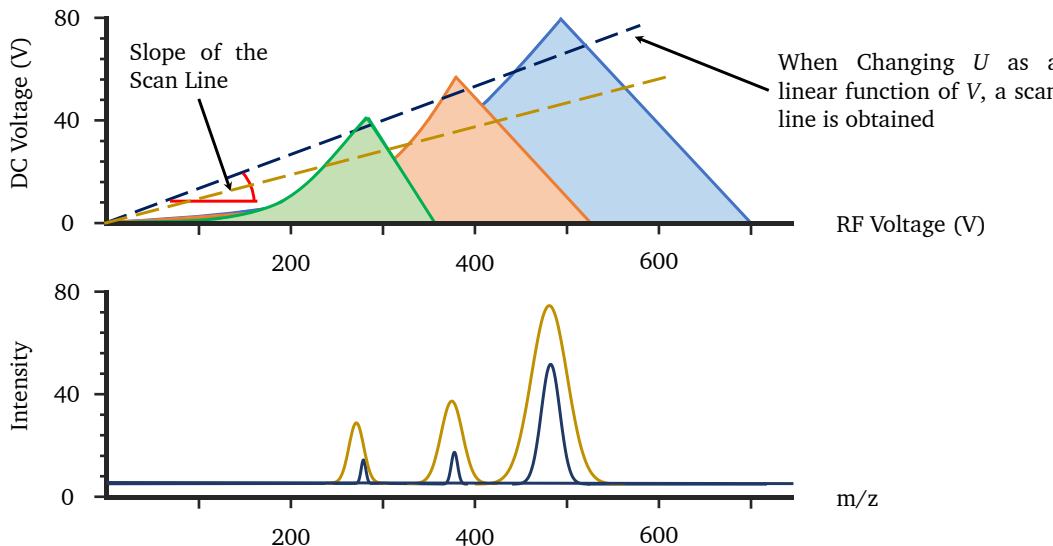


FIGURE 3.10: Stability diagrams plotted in RF-DC space, showing a straight scan line through the origin.

Decreasing the slope of the mass scan line allows the scan line to pass through a major area of the stability diagram. This, in turn, widens the mass peak. The outcome of this characteristic shape of the stability diagram is that, as the resolution is reduced (making the peak wider), the position of the leading edge of the mass peak moves to lower apparent mass three times more quickly than the trailing edge of the mass peak moving to a higher apparent mass. This moves the mass peak centre to a lower apparent mass. Therefore, instrument calibration is necessary.

3.3 Conclusion

This chapter establishes the principal experimental parts used throughout the thesis. The transmitter used in the experimental analysis exploits the chemical properties of highly volatile chemicals (VOCs) to generate the chemical signals and the propulsion is generated by N₂ tank. A descriptive section was dedicated to the underlying theory of QMA along with the membrane inlet technology. As mentioned before, the mass spectrometer (MS) has the ability to detect multiple chemicals simultaneously making MS a valuable receiver for use in molecular communication experimental analysis.

In chapter 4, the mathematical modelling of molecular communications on the macro-scale is described for different environments.

Chapter 4

Theory of Macro-Scale Molecular Communications

4.1 Introduction

This chapter focuses on the mathematical modelling of the macro-scale molecular communication. As mentioned, macro-scale is seldom studied compared to micro-scale therefore mathematical models describing the macro-scale effects (i.e., advection) are rare. In this chapter, mathematical descriptions used throughout the study are given. Depending on the environment (i.e., boundary-less, open-air) models are revised. Each Cartesian dimension (x, y, z) is considered in modelling the communication using the advective-diffusion equation (ADE).

4.2 Transmission of Molecules

A communication based on the transmission of particles (i.e., molecules, silt, pollutants etc.) can be explained using the mass transport phenomena. This can be briefly explained as the exchange of mass, energy, charge and momentum between observed systems. Since molecular communications utilises the mass of the particles in the exchange between systems, Fick's 2nd law can be used to describe the system when there is no additional flow present in the system [135]:

$$\frac{\partial c}{\partial t} = D \nabla^2 c, \quad (4.1)$$

The derivation of the Fick's 2nd law can be seen in Appendix A. At micro scales (nm to μm) the above equation can be used to model and explain the whole system. However, at macro-scales (cm to m) the system needs external propulsion to transmit the chemicals. Therefore, an additional parameter, the advection flux, is needed to introduce the flow component into the system. To describe the system, a generalised expression of advection-diffusion (general scalar transport [344]) is used:

$$\frac{\partial c}{\partial t} = D \nabla^2 c - \nabla \cdot (\mathbf{u}c) + R. \quad (4.2)$$

The derivation of the ADE from the continuity equation is shown in Chapter 2. To simplify the equation, it is assumed that the diffusion coefficient is constant ($\partial D / \partial t = 0$), there are no sources or sinks ($R = 0$), and the velocity has zero divergence ($\mathbf{u} \equiv 0$). Based on these definitions, the equation can be rewritten as:

$$\frac{\partial c}{\partial t} = D \nabla^2 c - \nabla \cdot (\mathbf{u}c). \quad (4.3)$$

The solution for this equation can be derived based on the following initial boundary conditions, known as “*thin-film solution*”:

$$c(|x| > 0, |y| > 0, |z| > 0, t_0) = 0, \quad (4.4a)$$

$$c(x = 0, y = 0, z = 0, t_0) = M_0 \delta(x) \delta(y) \delta(z), \quad (4.4b)$$

$$c(|x| \rightarrow \infty, |y| \rightarrow \infty, |z| \rightarrow \infty, t) = 0. \quad (4.4c)$$

where M_0 is the initial mass injected into the environment (kg), x, y, z are the dimensions in which the propagation takes place, t_0 is the initial time (s) and $\delta(x), \delta(y), \delta(z)$ are the Dirac delta functions of their respective dimensions. The mathematical definition of Dirac delta function is given below [345]:

$$\delta(x) = \begin{cases} 1, & x = 0, \\ 0, & x \neq 0. \end{cases} \quad (4.5)$$

Based on these boundaries to the PDE, the solution with no physical boundaries applied to the propagation can be expressed as:

$$c(\lambda_{x_0}, t) = \frac{M_0}{A_{yz} \sqrt{4\pi D_x t}} \exp\left(-\frac{\lambda_{x_0}^2}{4D_x t}\right), \quad (4.6a)$$

$$c(\lambda_{x_0}, \lambda_{y_0}, t) = \frac{M_0}{L_z 4\pi t \sqrt{D_x D_y}} \exp\left(-\frac{\lambda_{x_0}^2}{4D_x t} - \frac{\lambda_{y_0}^2}{4D_y t}\right), \quad (4.6b)$$

$$c(\lambda_{x_0}, \lambda_{y_0}, \lambda_{z_0}, t) = \frac{M_0}{(4\pi t)^{3/2} \sqrt{D_x D_y D_z}} \exp\left(-\frac{\lambda_{x_0}^2}{4D_x t} - \frac{\lambda_{y_0}^2}{4D_y t} - \frac{\lambda_{z_0}^2}{4D_z t}\right). \quad (4.6c)$$

where D_x, D_y and D_z are the diffusive coefficients in x, y and z coordinates respectively (cm^2/s), A_{yz} and L_z are the area-scale (m^2) and length-scale (m) of the neglected dimensions. t is the duration of the experiment (s), c is the concentration of the chemical in 1D, 2D and 3D ($\text{kg}/\text{m}, \text{kg}/\text{m}^2$ and kg/m^3) and $\lambda_{x_0}, \lambda_{y_0}$ and λ_{z_0} are the moving reference frames with the following descriptions:

$$\lambda_{x_0} = x - (x_0 + u_x t), \quad (4.7a)$$

$$\lambda_{y_0} = y - (y_0 + u_y t), \quad (4.7b)$$

$$\lambda_{z_0} = z - (z_0 + u_z t), \quad (4.7c)$$

where x_0 , y_0 and z_0 are the injection points of the mass (m), u_x , u_y and u_z are the mean flow velocity (m/s) and $u_x t$, $u_y t$ and $u_z t$ are the distances the centre of mass of the cloud travelled (m) in a given time of t (s).

In macro-scale molecular communications, the diffusion (D_x , D_y and D_z) caused by the particles may be governed by a combination of momentum and turbulent diffusion.

The equations given in Eq. (4.6) quantify the concentration value of the sample in a given time (t) and space (x , y , z). By integrating the concentration function with respect to distance (x , y , z) the particles that are present in the environment (θ_E) in a given time t can be calculated:

$$\theta_E(x_d, t) = \int_{-x_\epsilon}^{+x_d} c(x, t) dx, \quad (4.8a)$$

$$\theta_E(x_d, y_d, t) = \int_{-x_\epsilon}^{+x_d} \int_{-y_\epsilon}^{+y_d} c(x, y, t) dx dy, \quad (4.8b)$$

$$\theta_E(x_d, y_d, z_d, t) = \int_{-x_\epsilon}^{+x_d} \int_{-y_\epsilon}^{+y_d} \int_{-z_\epsilon}^{+z_d} c(x, y, z, t) dx dy dz, \quad (4.8c)$$

where x_d , y_d , z_d are the distances from the detector to the origin point (m) and x_ϵ , y_ϵ , z_ϵ are the distance that particles travel against the flow (m) in Cartesian coordinates (x , y , z). As the system has no sink nor source ($R = 0$), the chemicals that are used in the transmission can either be in transmission (θ_E) or have been absorbed by the detector (θ_1). Therefore, both the aforementioned mass values must add up to the initial introduction of mass (M_0) at the beginning of the transmission:

$$M_0 = \theta_E + \theta_1. \quad (4.9)$$

The mass absorbed by the detector (θ_1), therefore, can be calculated by simply subtracted from the initial mass (M_0) [8, 9, 144]:

$$\theta_1(x_d, t) = M_0 - \int_{-x_\epsilon}^{+x_d} c(x, t) dx, \quad (4.10a)$$

$$\theta_1(x_d, y_d, t) = M_0 - \int_{-x_\epsilon}^{+x_d} \int_{-y_\epsilon}^{+y_d} c(x, y, t) dx dy, \quad (4.10b)$$

$$\theta_1(x_d, y_d, z_d, t) = M_0 - \int_{-x_\epsilon}^{+x_d} \int_{-y_\epsilon}^{+y_d} \int_{-z_\epsilon}^{+z_d} c(x, y, z, t) dx dy dz. \quad (4.10c)$$

The closed-form solution for the mass absorption in 1D, 2D and 3D can be seen in Eq. (4.11):

$$\theta_1(x_d, t) = M_0 - \frac{M_0}{2} \left[\operatorname{erf}\left(\frac{x_d - u_x t}{\sqrt{4D_x t}}\right) + \operatorname{erf}\left(\frac{x_\epsilon + u_x t}{\sqrt{4D_x t}}\right) \right], \quad (4.11a)$$

$$\begin{aligned} \theta_1(x_d, y_d, t) = M_0 - \frac{M_0}{4} & \left[\operatorname{erf}\left(\frac{x_d - u_x t}{\sqrt{4D_x t}}\right) + \operatorname{erf}\left(\frac{x_\epsilon + u_x t}{\sqrt{4D_x t}}\right) \right] \\ & \times \left[\operatorname{erf}\left(\frac{y_d - u_y t}{\sqrt{4D_y t}}\right) + \operatorname{erf}\left(\frac{y_\epsilon + u_y t}{\sqrt{4D_y t}}\right) \right], \end{aligned} \quad (4.11b)$$

$$\begin{aligned} \theta_1(x_d, y_d, z_d, t) = M_0 - \frac{M_0}{8} & \left[\operatorname{erf}\left(\frac{x_d - u_x t}{\sqrt{4D_x t}}\right) + \operatorname{erf}\left(\frac{x_\epsilon + u_x t}{\sqrt{4D_x t}}\right) \right] \\ & \times \left[\operatorname{erf}\left(\frac{y_d - u_y t}{\sqrt{4D_y t}}\right) + \operatorname{erf}\left(\frac{y_\epsilon + u_y t}{\sqrt{4D_y t}}\right) \right] \left[\operatorname{erf}\left(\frac{z_d - u_z t}{\sqrt{4D_z t}}\right) + \operatorname{erf}\left(\frac{z_\epsilon + u_z t}{\sqrt{4D_z t}}\right) \right], \end{aligned} \quad (4.11c)$$

where $\operatorname{erf}(\cdot)$ is the error function with the following definition [346]:

$$\operatorname{erf}(x) = \frac{1}{\sqrt{\pi}} \int_{-x}^{+x} \exp(-t^2) dt. \quad (4.12)$$

The chemicals that are absorbed by the detector (θ_1) in a given period of T_S are given in Eq. (4.13):

$$M_R = \theta_1(x_d, t = T_S) - \theta_1(x_d, t = 0), \quad (4.13a)$$

$$M_R = \theta_1(x_d, y_d, t = T_S) - \theta_1(x_d, y_d, t = 0), \quad (4.13b)$$

$$M_R = \theta_1(x_d, y_d, z_d, t = T_S) - \theta_1(x_d, y_d, z_d, t = 0). \quad (4.13c)$$

Therefore, the removal of chemicals from the detector (θ_0) to the outside environment can be expressed by the following expression:

$$\theta_0(x_d, t) = \frac{M_R}{2} \left[\operatorname{erf}\left(\frac{x_d - u_x t}{\sqrt{4D_x t}}\right) + \operatorname{erf}\left(\frac{x_e + u_x t}{\sqrt{4D_x t}}\right) \right], \quad (4.14a)$$

$$\begin{aligned} \theta_0(x_d, y_d, t) &= \frac{M_R}{4} \left[\operatorname{erf}\left(\frac{x_d - u_x t}{\sqrt{4D_x t}}\right) + \operatorname{erf}\left(\frac{x_e + u_x t}{\sqrt{4D_x t}}\right) \right] \\ &\quad \times \left[\operatorname{erf}\left(\frac{y_d - u_y t}{\sqrt{4D_y t}}\right) + \operatorname{erf}\left(\frac{y_e + u_y t}{\sqrt{4D_y t}}\right) \right], \end{aligned} \quad (4.14b)$$

$$\begin{aligned} \theta_0(x_d, y_d, z_d, t) &= \frac{M_R}{8} \left[\operatorname{erf}\left(\frac{x_d - u_x t}{\sqrt{4D_x t}}\right) + \operatorname{erf}\left(\frac{x_e + u_x t}{\sqrt{4D_x t}}\right) \right] \\ &\quad \times \left[\operatorname{erf}\left(\frac{y_d - u_y t}{\sqrt{4D_y t}}\right) + \operatorname{erf}\left(\frac{y_e + u_y t}{\sqrt{4D_y t}}\right) \right] \left[\operatorname{erf}\left(\frac{z_d - u_z t}{\sqrt{4D_z t}}\right) + \operatorname{erf}\left(\frac{z_e + u_z t}{\sqrt{4D_z t}}\right) \right]. \end{aligned} \quad (4.14c)$$

As can be seen from Eq. (4.11) and Eq. (4.14) the mass parameter is different in each equation: former being the mass injected into the environment (M_0) and the latter is the mass that is absorbed by the detector (M_R). While the injected mass is a predefined value, M_R dynamically changes as the transmission evolves [8, 9].

The model that represents the transmission can be seen in Figure 4.1.

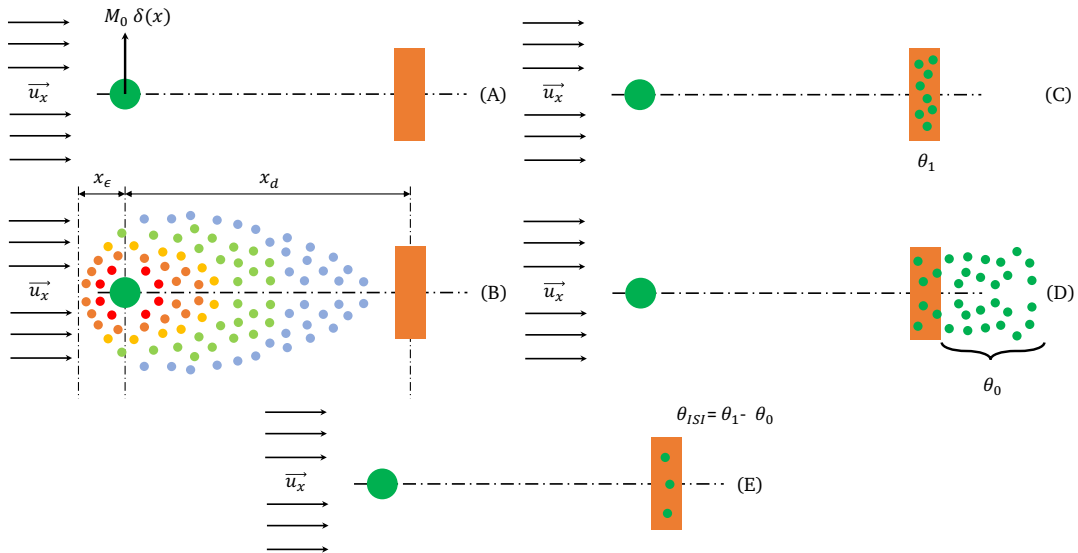


FIGURE 4.1: A diagram of the model used in the study. (A) At $t = 0$ s mass is injected into the environment. This is defined by the initial boundary condition $c(x_0, t_0) = M_0 \delta(x)$. (B) As the transmission evolves, the particles start propagating via advection and diffusion. (C) When the specified period is passed the transmitter stops releasing particles and transmits only advective flow. (D) The flow then forces the particles to be transferred from the detector to the outside environment. (E) After a finite amount has passed the particles are removed from the detector and transferred to the outside environment. However, some particles are left in the detector, which can cause inter-symbol interference for future transmissions (θ_{ISI}).

4.2.1 Proposed Transmission Model

Based on the interaction of chemicals with the environment and the detector mentioned in Section 4.2, experimental work was carried out and was validated by the use of the aforementioned model in 3D. In the experimental setup, the flow occurs in the x -direction only. Therefore (u_y) and (u_z) are assumed to be negligible :

$$u_y = 0, \quad u_z = 0. \quad (4.15)$$

The y and z coordinates of the environment are given the value of the radius of the detector (R_D):

$$y_d = y_e = R_D, \quad z_d = z_e = R_D. \quad (4.16)$$

In the propagation there are two types of diffusion, former being the longitudinal diffusion (D_L) and the latter being the radial diffusion (D_T). Because the advective flow (u_x) occurs in the x -direction, the particles propagate in the x -direction (i.e., increases the diffusion in the x -direction). A final note is that the diffusion occurring along the x -axis is the longitudinal diffusion and the diffusion happening in the y and z axes are defined as radial diffusion (D_T):

$$D_L = D_x, \quad D_T = D_y = D_z, \quad D_L \gg D_T. \quad (4.17)$$

Based on these definitions the equation that gives the absorbed mass by the detector from the outside environment (θ_1) and the mass removed from the detector to the outside environment (θ_0) given can be shown as:

$$\theta_1(x_d, R_D, t) = M_0 - \frac{M_0}{2} \operatorname{erf}\left(\frac{R_D}{\sqrt{4D_T t}}\right)^2 \left[\operatorname{erf}\left(\frac{x_d - u_x t}{\sqrt{4D_L t}}\right) + \operatorname{erf}\left(\frac{x_e + u_x t}{\sqrt{4D_L t}}\right) \right], \quad (4.18a)$$

$$\theta_0(x_d, R_D, t) = \frac{M_R}{2} \operatorname{erf}\left(\frac{R_D}{\sqrt{4D_T t}}\right)^2 \left[\operatorname{erf}\left(\frac{x_d - u_x t}{\sqrt{4D_L t}}\right) + \operatorname{erf}\left(\frac{x_e + u_x t}{\sqrt{4D_L t}}\right) \right] \quad (4.18b)$$

4.2.2 Open-Air Transmission

To model the effect of open air transmission an additional parameter, decay (λ_D), is required. Therefore, to include this parameter in the model, the ADE is revisited.

$$\frac{\partial c}{\partial t} = \nabla \cdot (D \nabla c) - \nabla \cdot (\mathbf{u}c) + R. \quad (4.19)$$

The system has no defined boundary (i.e., pipe), therefore the amount introduced by the system will not be equal to the amount detected by the receiver since some amount of particles will stray away from the path of the detector. This property can be modelled by introducing a sink ($R = -\lambda_D c$) to the equation. Inserting this parameter to Eq. (4.19) yields:

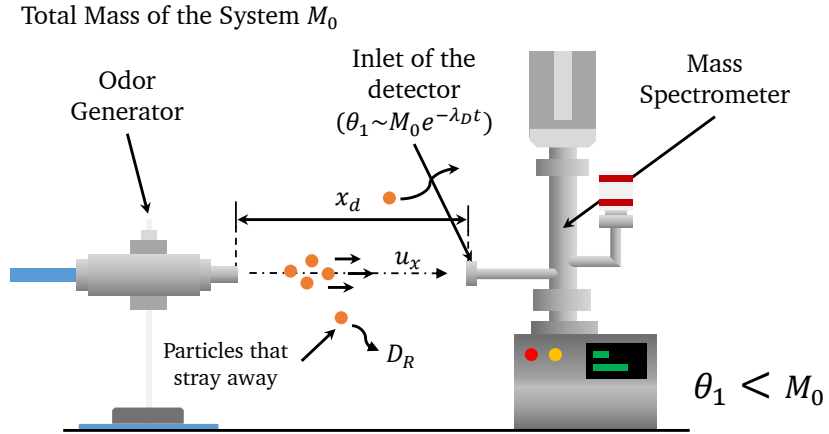


FIGURE 4.2: A Diagram showing the effect of open-air transmission.

$$\frac{\partial c}{\partial t} = \nabla \cdot (D \nabla c) - \nabla \cdot (\mathbf{u}c) - \lambda_D c, \quad (4.20)$$

where λ_D is the decay parameter of the function (s^{-1}). The prototypical solution ($c(x = 0, t = 0) = M_0 \delta(x)$) to the given expression in Eq. (4.20) is given in Eq. (4.21):

$$c(x, y, z, t) = \frac{M_0}{(4\pi t)^{3/2} \sqrt{D_x D_y D_z}} \times \exp\left(-\frac{(x - u_x t)^2}{4D_x t} - \frac{(y - u_y t)^2}{4D_y t} - \frac{(z - u_z t)^2}{4D_z t} - \lambda_D t\right). \quad (4.21)$$

The equation above represents the concentration of the introduced sample in a given time and space. By integrating the concentration function with respect to distance the particles that are present in the environment can be calculated. To calculate the chemicals absorbed by the detector, the integration function is subtracted from the injected mass [144]:

$$\theta_1(x_d, y_d, z_d, t) = M_0 - \int_{-x_\epsilon}^{+x_d} \int_{-y_\epsilon}^{+y_d} \int_{-z_\epsilon}^{+z_d} c(x, y, z, t) dx dy dz. \quad (4.22)$$

The solution to the above Eq. (4.22) for open distance transmission with decay can be obtained by integrating the concentration function in 3D Cartesian dimensions and subtracting the original mass. This solution is given in Eq. (4.23):

$$\theta_1(x_d, R_D, t) = M_0 \exp(-\lambda_D t) \times \left\{ 1 - \frac{1}{2} \operatorname{erf}\left(\frac{R_D}{\sqrt{4D_T t}}\right)^2 \left[\operatorname{erf}\left(\frac{x_d - u_x t}{\sqrt{4D_L t}}\right) + \operatorname{erf}\left(\frac{x_\epsilon + u_x t}{\sqrt{4D_L t}}\right) \right] \right\}. \quad (4.23)$$

The chemicals that are absorbed by the detector from the outside environment (θ_1) in a given period of T_S is given in Eq. (4.24):

$$M_R = \theta_1(x_d, R_D, t = T_S) - \theta_1(x_d, R_D, t = 0). \quad (4.24)$$

Therefore, the removal of chemicals from the detector (θ_0) to the outside environment can be expressed by the following Eq. (4.25):

$$\theta_0(x_d, r, t) = M_R \exp(-\lambda_D t) \times \left\{ \frac{1}{2} \operatorname{erf} \left(\frac{r}{\sqrt{4D_T t}} \right)^2 \left[\operatorname{erf} \left(\frac{x_d - u_x t}{\sqrt{4D_L t}} \right) + \operatorname{erf} \left(\frac{x_d + u_x t}{\sqrt{4D_L t}} \right) \right] \right\}. \quad (4.25)$$

As can be seen from Eq. (4.23) and Eq. (4.25) the mass parameter is different in each equation: former being the mass injected into the environment (M_0) and the latter is the mass that is absorbed by the detector (M_R). This process of introduction/removal of particles can be seen in detail in [8]. To model the detrimental effects of open air transmission, the decay parameter (λ_D) with respect to transmission distance (x_d) is approximated using a power equation with a and b being fitting parameters [347, 348]. The parameters of the decay equation (a, b) can be influenced by numerous parameters, such as the temperature and the pressure of the environment, particles and eddies present in the transmission medium.

$$\lambda_D(x_d) = ax_d^b, \quad a = 6.743 \times 10^{-5}, \quad b = 2.616. \quad (4.26)$$

While this decay function along with the equations developed are used in open-distance transmission, the problems faced with closed source are different a different approach needs to be implemented.

4.2.3 Closed-Boundary

To describe the closed boundary effect on the communication, the 3D solution to the PDE given in Eq. (4.6c) is revisited:

$$c(x, y, z, t) = \frac{M_0}{\sqrt{(4\pi D_x D_y D_z t)^3}} \times \exp \left(-\frac{(x - u_x t)^2}{4D_x t} - \frac{(y - u_y t)^2}{4D_y t} - \frac{(z - u_z t)^2}{4D_z t} \right), \quad (4.27)$$

where D_x , D_y and D_z are diffusion coefficients of their respective dimensions (m^2/s) and u_x , u_y and u_z are the advective flow in x , y and z dimensions respectively (m/s). The equation given in Eq. (4.27) shows the solution of system that has no boundaries, where the chemicals are free to disperse or diffuse in any direction possible. To create a boundary

effect on the propagation, the Cartesian definition of the function needs to be converted to cylindrical coordinates which the following section focuses on.

4.2.4 The Radial-Advection-Diffusion Equation

Eq. (4.27) represents the concentration function in 3D Cartesian space and to describe the cylindrical geometry of the transmission medium, the equation is converted to cylindrical coordinates with the following transformations:

$$x = R_M \cos \theta, \quad y = R_M \sin \theta \quad z = z, \quad (4.28a)$$

$$D_x = D_y = D_T, \quad D_z = D_L, \quad (4.28b)$$

$$u_x = u_y = u_r, \quad u_z = u_z. \quad (4.28c)$$

where R_M is the radius of the propagation medium (m). Following this conversion process, Eq. (4.27) can be written in its cylindrical form:

$$c(R_M, \theta, z, t) = \frac{M}{\sqrt{(4\pi D_T^2 D_L t)^3}} \exp\left(-\frac{(R_M \cos \theta - u_r t)^2}{4D_T t} - \frac{(R_M \sin \theta - u_r t)^2}{4D_T t} - \frac{(z - u_z t)^2}{4D_L t}\right). \quad (4.29)$$

This equation can be further simplified by using trigonometric identities (i.e., $R_M^2 = R_M^2 \cos^2 \theta + R_M^2 \sin^2 \theta$) and omitting the radial advective flow ($u_r = 0$) to the following expression:

$$c(R_M, z, t) = \frac{M}{\sqrt{(4\pi D_T^2 D_L t)^3}} \exp\left(-\frac{R_M^2}{4D_T t} - \frac{(z - u_z t)^2}{4D_L t}\right). \quad (4.30)$$

4.2.4.1 Boundary Conditions

To create a boundary condition for this function, the method of mirror images is used. This is a mathematical tool for solving PDEs by adding the mirror image of the function with respect to the symmetry hyperplane.

For example to have a boundary at $x = x_0$ in 1D, the same function is added at $x = 2x_0$. This ensures that the change of concentration at the defined boundary x_0 equal to zero (i.e., zero flux at the radial boundary of the pipe). However, as the transmission evolves, more images are needed to maintain the accuracy of the function. Therefore, continuing the example, mirror images are added at distances $x = 4x_0, x = 6x_0, \dots$.

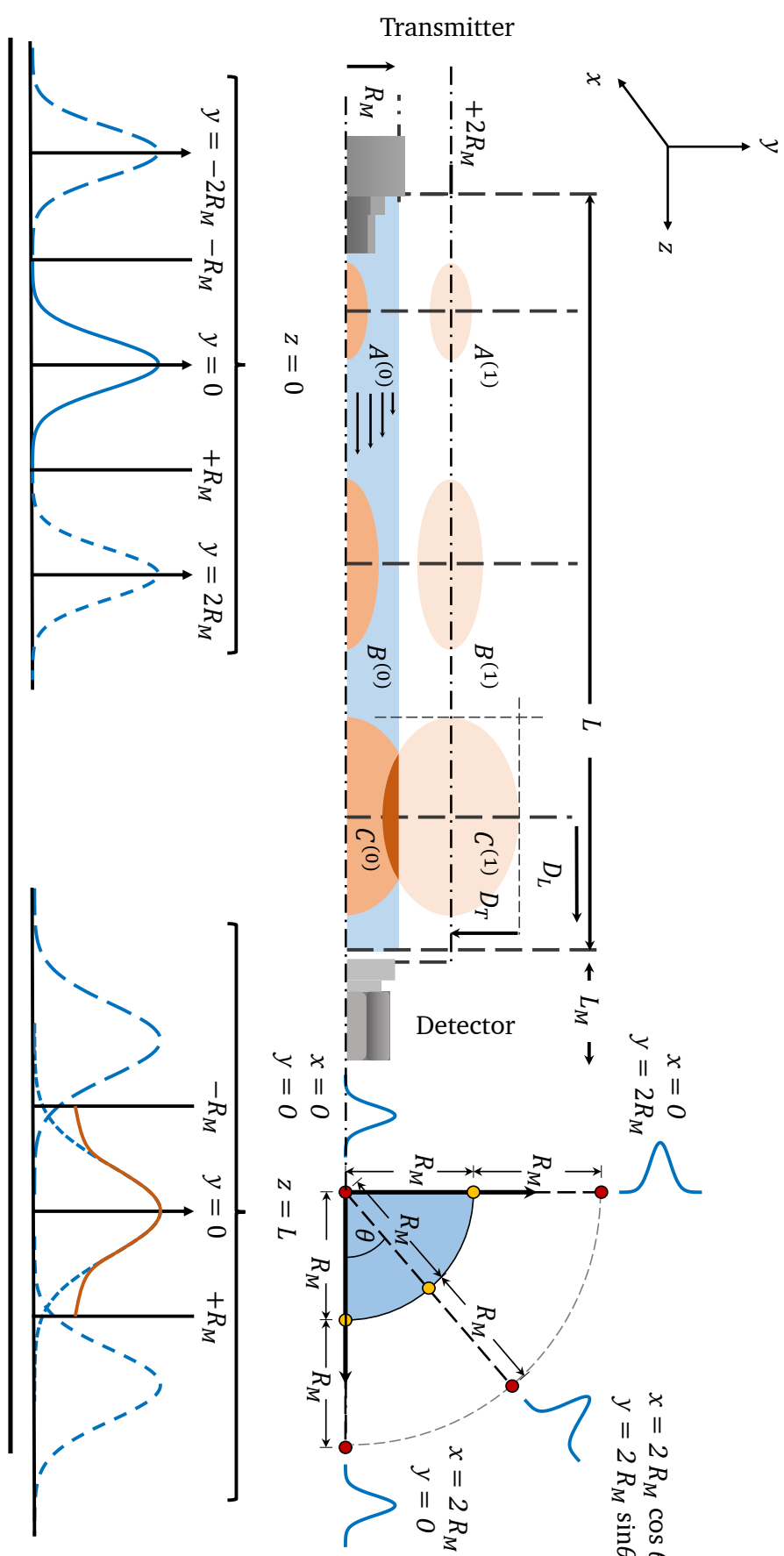


FIGURE 4.3: A descriptive diagram of the model used in the study. At the initial stage of the experiment ($t = 0$ s) a mass is injected into the environment. Once the mass is injected, to simulate the effect of physical boundary of the environment ($A^{(0)}$), additional gas pulses are generated in the y -coordinates with positive sides being $y = 2L$, $y = 4R$, ..., $y = 2nR$ ($A^{(1,2,\dots,\infty)}$). This is also carried out in the x -coordinates. As transmission evolves, the gas pulses transcend the boundary of the propagation medium, at which point the mirror pulses are added to the actual transmission to create the effect of the boundary.

In the environment used in this study, there is only the radial no-flux boundary at R_M , where R_M is the radius of the boundary (m). If the transmission of particles is assumed to be in z -direction, the boundary condition can be expressed as:

$$\left. \frac{\partial c}{\partial r} \right|_{r=R_M} = 0. \quad (4.31)$$

4.2.4.2 Absorption/Desorption Process

Based on the boundary condition described in Eq. (4.31), the mirror functions can be implemented to the concentration function in 3D which is given as:

$$c(r, z, t) = \frac{M}{\sqrt{(4\pi t)^3 D_T^2 D_L}} \sum_{n=0}^{\infty} \exp \left(-\frac{(r - 2nR_M)^2}{4D_T t} - \frac{(z - u_z t)^2}{4D_L t} \right), \quad (4.32)$$

where n is the summation index. As can be seen in the equation above, the function is independent from θ as it possesses angular symmetry. By integrating the concentration function with respect to the cylindrical volume element the particles that are present in the environment, (θ_E) can be calculated.

$$\theta_E = \iiint_V c \, dz \, r \, dr \, d\theta. \quad (4.33)$$

As the system has no sink/source ($R = 0$), the chemicals that are used in the transmission can either be in the environment (θ_E) or have been absorbed by the detector (θ_1). Therefore, both the aforementioned mass values must add upto the initial introduction of mass in the beginning of the transmission,

$$M = \theta_E + \theta_1. \quad (4.34)$$

The mass absorbed by the detector (θ_1), can be calculated by subtracting from the initial mass (M) [8, 10],

$$\theta_1(r, \theta, z, t) = M - \theta_E(r, \theta, z, t), \quad (4.35a)$$

$$\theta_1(r, \theta, z, t) = M - \int_0^{2\pi} \int_0^R \int_0^L c(r, \theta, z, t) \, dz \, r \, dr \, d\theta, \quad (4.35b)$$

where x_d is the distance between the transmitter and the detector (m). The solution to this equation, which expresses the absorbed particles by the detector, can be expressed as:

$$\begin{aligned}\theta_1(R_M, x_d, t) = M - \frac{M}{i\sqrt{4D_T t}} & \left[\operatorname{erf}\left(\frac{u_z t}{\sqrt{4D_L t}}\right) + \operatorname{erf}\left(\frac{x_d - u_z t}{\sqrt{4D_L t}}\right) \right] \\ \sum_{n=0}^{\infty} \exp\left(-n^2 \frac{R_M^2}{D_T t}\right) & \left\{ i\sqrt{D_T t} \left[1 - \exp\left((4n-1) \frac{R_M^2}{4D_T t}\right) \right] + nR\sqrt{\pi} \exp\left(n^2 \frac{R_M^2}{D_T t}\right) \right. \\ & \left. \times \left[\operatorname{erfi}\left(n \frac{iR_M}{\sqrt{D_T t}}\right) - \operatorname{erfi}\left(\frac{(2n-1)}{2} \frac{iR_M}{\sqrt{D_T t}}\right) \right] \right\}, \quad (4.36)\end{aligned}$$

where i is the imaginary unit with the identity $i^2 = -1$ and $\operatorname{erfi}(\cdot)$ is the imaginary error function with the following identity [346]:

$$\operatorname{erfi}(x) = -i\operatorname{erf}(ix) = \frac{2}{\sqrt{\pi}} \int_0^x e^{t^2} dt. \quad (4.37)$$

Once the chemicals are absorbed by the detector, the removal process can be initiated. To begin the calculation of the desorption process the particles that have been absorbed need to be quantified. To achieve this, the travel time of the signal has to be taken into account. As the chemical travels long distances, the response time is also delayed considerably and therefore the removal of particles from the detector to the outside environment is also delayed by the same amount of time. Therefore, the particles that are absorbed by the detector (M_R) can be calculated as:

$$M_R = \theta_1(R_M, L, T_S + t_{\text{emp}}) - \theta_1(R_M, L, t_{\text{emp}}), \quad (4.38)$$

where T_S is the symbol period (s) and t_{emp} is the empirically measured time for the detection of chemical with respect to distance. The empirical fitting of this equation is given below and the fitting process can be seen in Figure 4.4.

$$t_{\text{emp}}(L) = p_1 L + p_2, \quad (4.39a)$$

$$p_1 = 27.6, \quad p_2 = 16.51, \quad (4.39b)$$

where p_1 and p_2 are the fitting parameters to the empirical fitting function. This parameter would change depending on the chemical that is used for sending information and in this study the function is based on acetone being the signal chemical. Based on these preliminary definitions, the removal of particles from the detector to the outside environment can be defined by the following function:

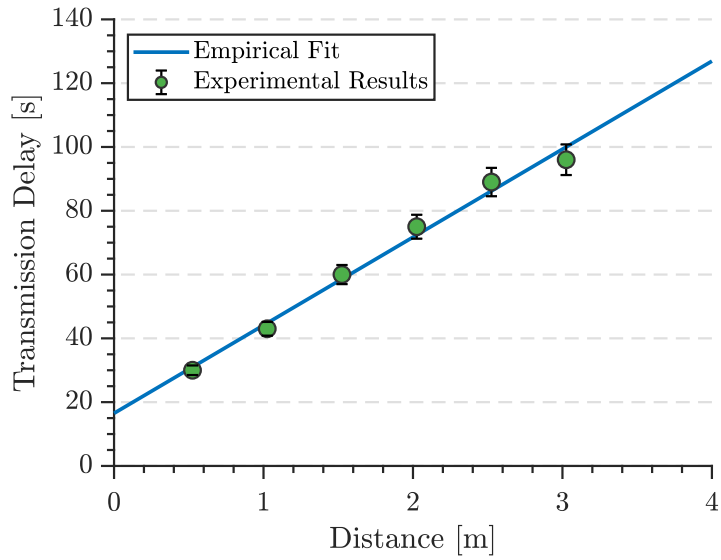


FIGURE 4.4: Experimentally measured chemical detection with comparison to empirical fitting (linear $R^2 = 0.9891$).

$$\theta_0(R_M, L_M, t) = \frac{M_R}{i\sqrt{4D_T t}} \left[\operatorname{erf}\left(\frac{u_z t}{\sqrt{4D_L t}}\right) + \operatorname{erf}\left(\frac{L_M - u_z t}{\sqrt{4D_L t}}\right) \right] \\ \sum_{n=0}^{\infty} \exp\left(-n^2 \frac{R_M^2}{D_T t}\right) \left\{ i\sqrt{D_T t} \left[1 - \exp\left((4n-1) \frac{R_M^2}{4D_T t}\right) \right] + n R_M \sqrt{\pi} \exp\left(n^2 \frac{R_M^2}{D_T t}\right) \right. \\ \left. \times \left[\operatorname{erfi}\left(n \frac{iR_M}{\sqrt{D_T t}}\right) - \operatorname{erfi}\left(\frac{(2n-1)}{2} \frac{iR_M}{\sqrt{D_T t}}\right) \right] \right\}, \quad (4.40)$$

where L_M is the distance between the membrane and the detector (m). It must be noted that unlike the absorption process, where chemicals travel long distances to reach the detector, in the desorption process the chemical propagation begins from the detector membrane and ends at the outside environment ($L \gg L_M$). A detailed description of introduction/removal of particles can be seen in [8, 10] and a diagram of the model used in the study is presented in Figure 4.3.

4.2.5 Calculation of the coefficient of Diffusivity

To calculate the longitudinal diffusivity coefficient of the propagation (D_L), which plays a pivotal role in this type of communication transmission, the characteristic properties of the fluid motion must be established.

In a communication where particles are propagated through a medium, the main propeller of these particles is the volumetric flow rate (Q). This is defined as the amount of volume transported in a given amount of time (m^3/s) and the velocity parameter (u) can be obtained by dividing the volumetric flow rate by the cross-sectional area of the tube (A):

$$u_{\max} = \frac{Q}{A} = \frac{Q}{4\pi R^2}, \quad u_{\text{avg}} = \frac{1}{2}u_{\max}. \quad (4.41)$$

After obtaining the velocity parameter, the next characteristic of a fluid motion to be established is whether the motion is laminar or turbulent. To calculate this value, the Reynolds number (Re) is used. The equation for Reynolds number can be seen below [349]:

$$\text{Re} = \frac{\rho u_{\text{avg}} L_D}{\eta}, \quad (4.42)$$

where ρ is the density of the fluid (kg/m^3), u_{avg} is the mean velocity of the fluid (m/s), L_D is the characteristic linear dimension of the environment (m). For the system in question it is the diameter of the pipe, and η is the dynamic viscosity of the fluid ($\text{N} \cdot \text{s}/\text{m}^2$).

4.2.5.1 Entrance Length

Entrance length is defined as the distance a flow travels after entering a pipe before the flow becomes fully developed. Since the Reynolds number is low ($\text{Re} < 2000$) the flow can be considered laminar and the entrance length for the system is calculated by the the following equation [349]:

$$L_E = 0.1 R_M \text{Re}. \quad (4.43)$$

4.2.5.2 Longitudinal Diffusivity

Longitudinal diffusivity is defined as diffusion paralel to the advective vector. As the flow is laminar ($\text{Re} < 2000$) the longitudinal diffusivity can be calculated as [350]:

$$D_L = D_m + \left(\frac{u_{\text{avg}}^2 R_m^2}{48 D_m} \right), \quad (4.44)$$

where D_m is the molecular diffusion (cm^2/s). The derivation of this equation can be seen in Appendix B.

4.2.5.3 Transverse Diffusion

The presence of the membrane affects the transverse diffusion more profoundly than longitudinal since the main propagator of motion along the radial axis is diffusion rather than advection aided diffusion seen in longitudinal diffusion. To calculate the coefficient, mean squared displacement is used [351]:

$$D_T = \lim_{t \rightarrow \infty} \frac{d}{dt} \sum_{n=1}^N \frac{1}{2N} ((x_n(t) - x_n(0))), \quad (4.45)$$

where $x_n(0)$ is the initial position coordinate of the gas molecules and $x_n(t)$ is the position coordinate of the gas molecule after time, t .

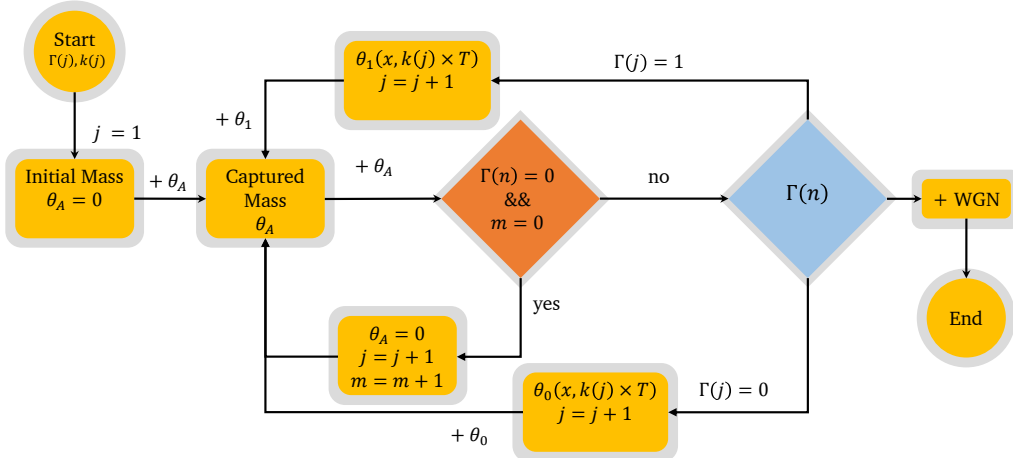


FIGURE 4.5: A diagram of the algorithm used to simulate on-off keying (OOK) for macro-scale molecular communications.

4.3 Simulation Framework

Based on the equation derived from Eq. (4.20), a simulation of the macro-scale molecular communications is developed. The flowchart for the simulation can be seen in Figure 4.5 and the description of the simulation is as follows;

1. A state array of Γ and a frequency array k with a length of j is generated. The state array describes the possible states (i.e., in OOK there are two states; 0 and 1) and the frequency array describes the duration of occurrence of each state before changing into a new state.
2. An initial definition of the captured mass (θ_A) is generated and given the value of $\theta_A = 0$ before any transmission commences.
3. The system checks the array to see if the first transmitted state in the array is 0. This is done since the definition of the removal of particles (θ_0) relies on the mass absorbed by the detector (M_R). Therefore, the removal of particles is not initiated and the captured mass value stays $\theta_A = 0$ and the simulation continues to the next state in the array. This process continues until the system detects a 1 in the state array (Γ) and moves the transmission window by the period of T_S times the frequency array with the same index. This check is carried out by the m parameter and once the simulation switches from 0 to 1 for the first time the m parameter is assigned the value of $m = 1$ and stops this loop until the termination of the simulation.

$$\theta_A = [0_{1, (x, k(1) \times T_S)}] \quad (4.46)$$

4. The system checks the states in the array $\Gamma(j)$. If the bit value is 1, the system introduces the chemicals into the system. The duration of the bit-1 is dependent on the value of the frequency array $k(j)$ with the same index value. For example, for a symbol duration of T_S with three bit-1s, the total mass accumulated by the system is $\theta_1(x, 3T_S)$ with each bit-1 value having $\theta_1(x, T_S)$, $\theta_1(x, 2T_S)$ and $\theta_1(x, 3T_S)$ respectively. Based on this behaviour the captured mass is updated accordingly.

$$\theta_A = [0_{1,(x,k(1)\times T_S)} \quad \theta_1(x, k(2) \times T_S)] \quad (4.47)$$

This process can be seen in detail in Figure 4.6.

5. After the system has accumulated particles from the bit-1 transmission (θ_1), when the next state is 0 and based on the value the system flushes the chemicals relative to the particles already in the system (M_R) and continues to remove the particles from the detector until state array moves to the next value.

$$\theta_A = [0_{1,(x,k(1)\times T_S)} \quad \theta_1(x, k(2) \times T_S) \quad \theta_0(x, k(3) \times T_S)] \quad (4.48)$$

6. When the next bit-1 is to be transmitted, the leftover chemicals are added to the particle introduction.
7. The operation continues until the count operator (j) reaches the length of the state and frequency arrays.

$$\theta_A = [0_{1,(x,k(1)\times T_S)} \quad \theta_1(x, k(2) \times T_S) \quad \dots \quad \theta_{\Gamma(j)}(x, k(j) \times T_S)] \quad (4.49)$$

8. Before the simulation concludes, additive white Gaussian noise (AWGN) is added to the simulated signal [9].

The pseudo-code for an OOK transmission 3D environment is given overleaf. The first part of the algorithm converts a given bit array into two different arrays: (i) state array (ii) frequency array. The second part of the algorithm is to simulate the transmission based on

the two generated arrays.

Algorithm 1: Macro-Scale Molecular Simulation

Input: x_d (distance), x_e (distance), u_x (advective flow), D_L, D_T (diffusivity), M_0 (injected mass), T_S (bit duration), B (bit array)

```

1  $i = 0; w = 1; h = 1;$  // Definition of loop parameters
2 Converting the message ( $B$ ) array to state and frequency ( $k$ ) arrays
3 for  $h = 1$  to  $\text{card}(B)$  do
4   if  $h=1$  then
5      $i = i + 1; R(w) = B(h); P(w) = i;$ 
6   else if  $B(h-1) = B(h)$  then
7      $i = i + 1; P(w) = B(h); R(w) = i;$ 
8   else if  $B(h-1) \neq B(h)$  then
9      $P(w) = i; w = w + 1;$ 
10     $R(w) = B(h); i = 1;$ 
11   if  $h = \text{card}(B)$  then
12      $P(w) = 1; w = w + 1;$ 
13   end
14 end
15  $\Gamma = [0 \ R]; k = [0 \ P];$ 
16  $\theta_A = 0;$  // Initialisation of the transmission
17 for  $j = 2$  to  $\text{card}(\Gamma)$  do
18   if  $\Gamma(j) > \Gamma(j-1)$  then // When state 1 is detected
19      $M_A = \theta_A(\text{end});$ 
20     for  $t = 1$  to  $k(j) \times T_S$  do
21        $Q(t) = M_A + \Gamma(j) - \Gamma(j-1) -$ 
22          $\frac{1}{2}(\Gamma(j) - \Gamma(j-1)) \operatorname{erf}\left(\frac{R_D}{\sqrt{4D_T t}}\right)^2 \left[ \operatorname{erf}\left(\frac{x_e - u_x t}{\sqrt{4D_L t}}\right) + \operatorname{erf}\left(\frac{x_d + u_x t}{\sqrt{4D_L t}}\right) \right];$ 
23        $\theta_1(t + T_S) = Q(t);$ 
24     end
25   else // When state 0 is detected
26      $M_R = \theta(\text{end});$ 
27     for  $t = 1$  to  $k(j) \times T_S$  do
28        $Q(t) = \frac{1}{2}(M_R - \Gamma(j)) \operatorname{erf}\left(\frac{R_D}{\sqrt{4D_T t}}\right)^2 \left[ \operatorname{erf}\left(\frac{x_e - u_x t}{\sqrt{4D_L t}}\right) + \operatorname{erf}\left(\frac{x_d + u_x t}{\sqrt{4D_L t}}\right) \right];$ 
29        $\theta_1(t + T_S) = Q(t);$ 
30     end
31   end
32    $T_t = k(j) \times T_S + T_t;$ 
33 end
34  $\theta_1 = \theta_1 + \mathcal{N}(\mu_N, \sigma_N^2);$  // Addition of white Gaussian noise

```

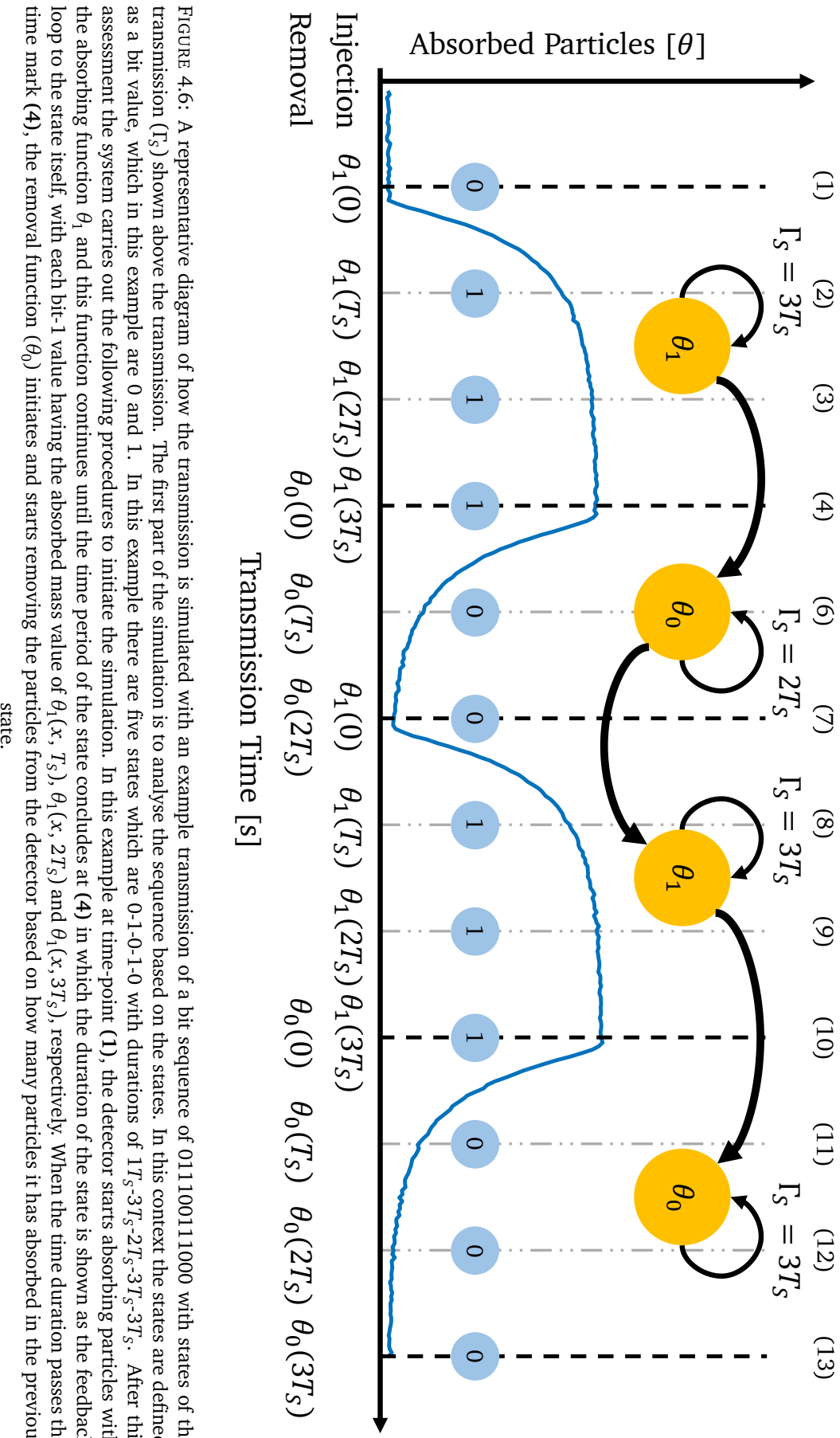


FIGURE 4.6: A representative diagram of how the transmission is simulated with an example transmission of a bit sequence of 011100111000 with states of the transmission (Γ_S) shown above the transmission. The first part of the simulation is to analyse the sequence based on the states. In this context the states are defined as a bit value, which in this example are 0 and 1. In this example there are five states which are 0-1-0-1-0 with durations of $1T_S$ - $3T_S$ - $2T_S$ - $3T_S$ - $3T_S$. After this assessment the system carries out the following procedures to initiate the simulation. In this example at time-point (1), the detector starts absorbing particles with the absorbing function θ_1 and this function continues until the time period of the state concludes at (4) in which the duration of the state is shown as the feedback loop to the state itself, with each bit-1 value having the absorbed mass value of $\theta_1(x, T_S)$, $\theta_1(x, 2T_S)$ and $\theta_1(x, 3T_S)$, respectively. When the time duration passes the time mark (4), the removal function (θ_0) initiates and starts removing the particles from the detector based on how many particles it has absorbed in the previous state.

4.4 Conclusions

In this chapter, the mathematical description that is used throughout the thesis is described. The process of particle transport across an environment can be explained by the use of the advective-diffusion equation (ADE). The model is based on the mass exchange between the detector and the environment. Depending on the environment (i.e., boundary, open space) the equation that describes the evolution can change, and are described for both open distance and closed distance. In addition, the diffusion parameter for closed-distance transmission is investigated in detail. The chapter concludes by describing the simulation framework used throughout the study.

Three chapters follow that use the experimental setup described in Chapter 3 and theoretical model developed in Chapter 4. The next chapter describes the fundamental parameters of macro-scale molecular communication. These parameters play a pivotal role in describing the limit of the communications. From these limitations, reliable communication methods can be developed and analysed which are studied in Chapter 6. Chapter 7 focuses on further improving the communication speed and the mutual information of the system by using multiple chemicals for simultaneous transmission.

Chapter 5

Analysis of Macro-Molecular Communications Parameters

5.1 Introduction

Molecular communication at the macro-scale (cm to m) is still in its infancy compared to micro-scale and experimentally the parameters that govern the communication are yet to be studied analytically and experimentally. As with any communication paradigm, parameters play a pivotal role in the communication performance and the limits in which communication can be achieved. In this chapter, the properties of macro-scale molecular communication are investigated both experimentally and theoretically. These include:

- **Environmental Noise:** Non-messaging chemicals in the transmission medium.
- **Signal Flow:** Mass of the messaging chemical species.
- **Carrier Flow:** The speed in which the chemicals propagate.
- **Pulse Duration:** Duration in which the chemicals are released from the transmitter.
- **Open Distance Transmission:** Chemicals propagating in a medium with no boundary.
- **Closed Distance Transmission:** Chemicals propagating in a medium with a boundary.

To test these parameters, an in-house-built odour generator (OG) was used to generate the chemicals pulses and a quadrupole massanalyser (QMA) for detection. The experimental setup used in the chapter can be seen in detail in Chapter 3. The theoretical comparisons done in this chapter are based on the mathematical model given in Chapter 4.

The chapter is organised as follows. Section 5.2 focuses on the noise present in the environment and analysis was carried out on the determination and the characteristics of the noise. In Section 5.3 the signal flow (q) is analysed in terms of signal amplitude, signal shape, signal energy and signal-to-noise ratio (SNR), the same approach is applied to carrier flow (Q) and pulse duration (t_b) which can be seen in Section 5.4 and Section 5.5, respectively.

The second part of the chapter (5.6 and 5.7) focuses on the distance parameter as it is the defining character that influences the signal attenuation. To analyse this effect on the communication two types of distances were analysed: open-air transmission discussed in section 5.6 and closed-air transmission discussed in section 5.7. Both scenarios were experimented with 6 different lengths and repeated 3 times to determine stabilised variation.

5.2 Noise Analysis

To analyse the noise of the environment, the detector was left monitoring the background noise. The background noise of the system can be caused by numerous parameters such as leftover chemicals within the MS vacuum chamber, pressure differences in the inlet of the MS or ambient chemicals in the air that produce a similar m/z ratio to the m/z ratio value of the signal chemical. The cumulative density function (CDF) of the observed background noise can be seen in Figure 5.1a and the frequency spectrum of the noise can be seen in Figure 5.1b.

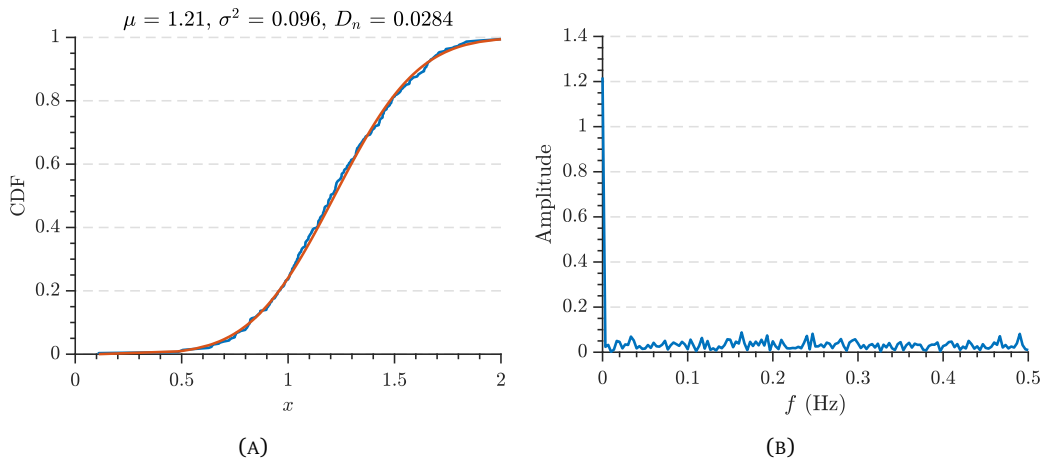


FIGURE 5.1: (A) Experimental data (—) along with the theoretical fit (—) of the environmental noise. (B) FFT analysis of the noise.

In order to quantify the fitting of the distribution, $F(x)$, to the empirical CDF, $F_n(x)$, the Kolmogorov-Smirnov test is used [352]:

$$D_n = \sup_x |F_n(x) - F(x)|. \quad (5.1)$$

As can be seen from the distribution fit of data (Figure 5.1a), the results strongly suggest a Gaussian distribution (i.e., normal distribution) for the noise in the system. Aside from having a DC offset value (caused by the particles present in the environment) which can be seen in Figure 5.1b, the noise is behaving as white noise, where there is no discernible dominant frequency component. Therefore, in a macro-scale molecular communication with a MIMS detector, the model of the noise can be defined as AWGN with the following expression:

$$\mathcal{N}(\mu_N, \sigma_N^2). \quad (5.2)$$

5.3 Signal Flow

Signal flow (q), for the communication in question, is defined as the concentration value of the chemical that is used in the transmission of the information. In this experiment the signal flow is generated from volatile organic compounds (VOCs) in gas form. In addition, since this property in the experimental setup is by nature flow, and not a direct injection of particles, the absorbed mass by the detector can change if the carrier flow (Q) property is varied which will be discussed in Section 5.4.

TABLE 5.1: Parameters for signal flow study

Experimental Parameter	Symbol	Value	Unit
Tracked signal flow ion	m/z	43	Da
Carrier flow	Q	750	ml/min
Bit duration	t_b	300	s
Acetone detection delay [45]	t_d	15	s
Flush duration	t_f	90	s
Transmission distance	x_d	2.5 ± 0.1	cm
Carrier flow pressure	P_F	1	bar
Diffusivity of acetone in air	D	0.124	cm^2/s
Theoretical Parameter	Symbol	Value	Unit
Advective flow in x -axis	u_x	0.02	cm/s
Advective flow in y -axis and z -axis	u_y & u_z	0	cm/s
Transmission distance	x_d	2.5	cm
Longitudinal diffusivity	D_L	0.15	cm^2/s
Radial diffusivity	D_T	1×10^{-3}	cm^2/s
Detector radius	R_D	0.3	cm
Noise mean & variance	μ_N, σ_N^2	1.21, 0.096	pA, W/ion

In the setup, discussed in detail in chapter 3, this property is controlled by using mass flow controllers (MFCs) and an automation platform. The details of the experimental setup can be seen in Chapter 3.

An experiment was conducted to test the communication properties of the signal flow (q) for molecular communications in macro-scale. Both theoretical and experimental parameters for the study are given in Table 5.1. The theoretical model is described in detail in Chapter 4.

5.3.1 Experiment Methodology

The experiment start by transmitting only carrier flow (Q) to the inlet of the detector for 90s, defined as t_f to clear the detector from any residual chemicals present in the inlet or the environment. After t_f time has passed, the transmitter initiates the signal flow (q) transmission, along with the carrier flow for propagation ($q + Q$), for the duration of 300s.

This time frame is defined as t_b . The experiment concludes by transmitting only carrier flow for 90 s, defined as t_f . The diagram for the experiment can be seen in Figure 5.2

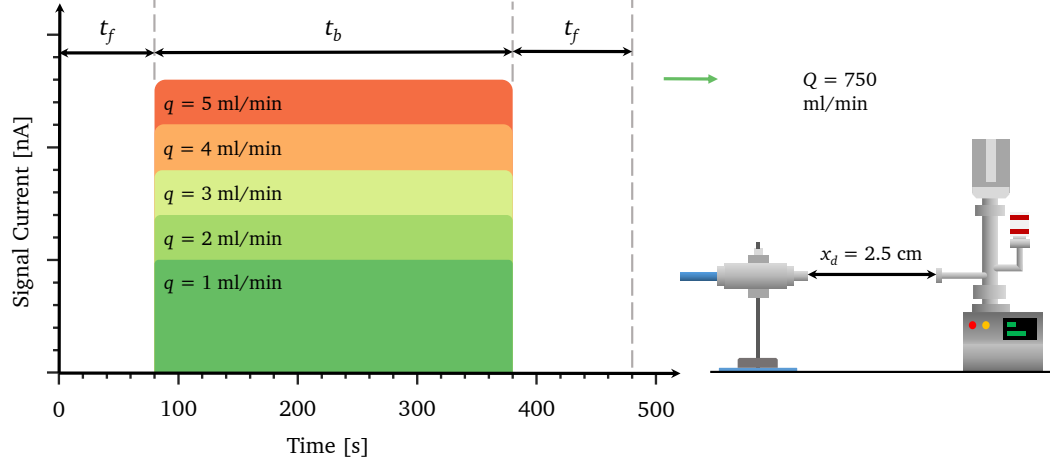


FIGURE 5.2: Experimental diagram of the signal flow study.

5.3.2 Signal Properties

The results for the signal flow study can be seen in Figure 5.3a for the transmitted signal and Figure 5.3b for the maximum amplitude of the signal current compared with the theoretical model discussed in Chapter 4.

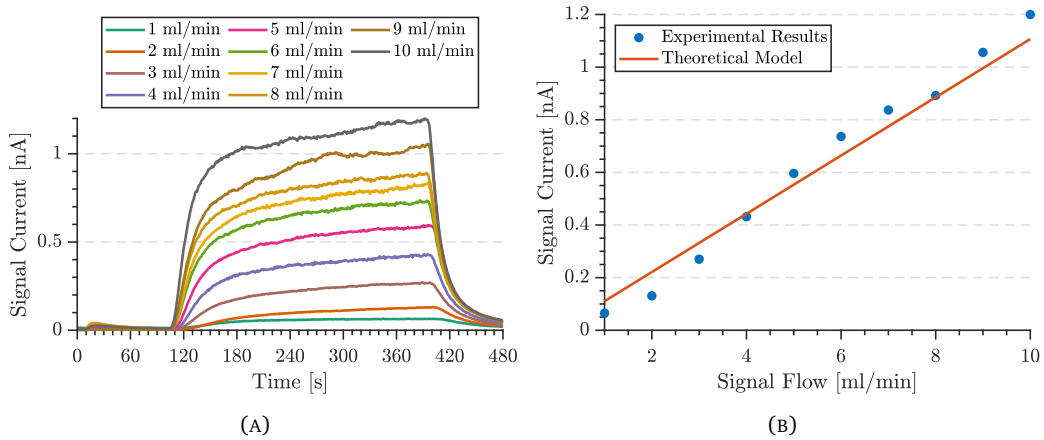


FIGURE 5.3: (A) Experimental results of the signal flow study. (B) Experimental along with theoretical comparison of signal amplitude. (Equations used in modelling: Eq. 4.11c and Eq. 4.14c)

As can be seen, the signal current increases in amplitude in relation to the introduced signal flow and the relation between these parameters is linear as seen in Figures 5.3a and 5.3b. However, the increase of signal creates increased distortion which can be observed in Figure 5.3a. Therefore to quantify this distortion, the variance (σ^2) of the signal when signal flow is varied is measured.

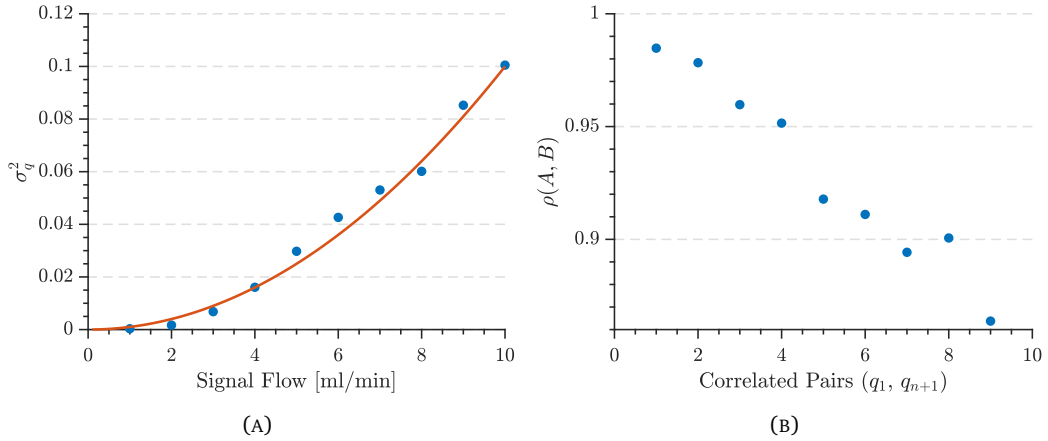


FIGURE 5.4: (A) Signal variance of the experimental data (●) with approximation (Eq. (5.5)) (—). (B) Signal correlation values (●).

The variance is calculated as:

$$\text{Var}(E) = \frac{1}{n} \sum_{i=1}^n (E_i - \mu)^2, \quad (5.3)$$

where E is the experimental data, n is the size of the experimental set and μ is the average value:

$$\mu = \frac{1}{n} \sum_{i=1}^n E_i. \quad (5.4)$$

Based on the experimental results, the variance ($\text{Var}(E)$) of the signal with respect to the signal flow (q) can be seen in Figure 5.4a. The relation between the variance and the signal flow can be approximated as:

$$\text{Var}(E) \approx 0.001q^2. \quad (5.5)$$

The rise of variance with increased signal flow is due to the fact that as the signal flow (q) increases, the chemicals present in the communication increase as well, which increases the number of particles diffused in a way that is detrimental to the transmitted signal.

To measure whether the signal retains the shape as the signal flow changes the Pearson correlation coefficient [353] is used. The equation of the coefficient is given:

$$\rho_{E,T} = \frac{\text{cov}(E, T)}{\sigma_E \sigma_T}, \quad (5.6)$$

where E represents the experimental data and T represents the theoretical data. The results can be seen in Figure 5.4b. As it can be seen the signal quantity increase has a negative effect on the correlation to the original signal ($q = 1 \text{ ml/min}$). This is caused by the diffusion of particles which in turn is caused by increased introduction of chemicals into the system.

5.3.3 Signal Energy and SNR

When a sample is to be analysed by a MS, the sample is ionised and detected by a detector. The detector produces current from the introduction of the samples (θ_A). Therefore, the energy of a continuous signal (β), can be calculated as:

$$\beta(x_d, R_D, t) = \int_{-\infty}^{+\infty} |\theta_A(x_d, R_D, t)|^2 dt. \quad (5.7)$$

When the sample is introduced into the detector (θ_1), the energy generated by the sample can be calculated as:

$$\beta_1(x_d, R_D, t) = \int_{-\infty}^{+\infty} \left| M_0 - \frac{M_0}{2} \operatorname{erf}\left(\frac{R_D}{\sqrt{4D_T t}}\right)^2 \left[\operatorname{erf}\left(\frac{x_d - u_x t}{\sqrt{4D_L t}}\right) + \operatorname{erf}\left(\frac{x_e + u_x t}{\sqrt{4D_L t}}\right) \right] \right|^2 dt, \quad (5.8a)$$

$$\beta_1(x_d, R_D, t) = M_0^2 \int_{-\infty}^{+\infty} \left| 1 - \frac{1}{2} \operatorname{erf}\left(\frac{R_D}{\sqrt{4D_T t}}\right)^2 \left[\operatorname{erf}\left(\frac{x_d - u_x t}{\sqrt{4D_L t}}\right) + \operatorname{erf}\left(\frac{x_e + u_x t}{\sqrt{4D_L t}}\right) \right] \right|^2 dt. \quad (5.8b)$$

When the introduction is finalised and the mass remaining in the detector starts propagating from the inlet to the outside environment due to bulk flow (θ_0) the sample energy is defined as:

$$\beta_0(x_d, R_D, t) = \int_{-\infty}^{+\infty} \left| \frac{M_R}{2} \operatorname{erf}\left(\frac{R_D}{\sqrt{4D_T t}}\right)^2 \left[\operatorname{erf}\left(\frac{x_d - u_x t}{\sqrt{4D_L t}}\right) + \operatorname{erf}\left(\frac{x_e + u_x t}{\sqrt{4D_L t}}\right) \right] \right|^2 dt, \quad (5.9a)$$

$$\beta_0(x_d, R_D, t) = M_R^2 \int_{-\infty}^{+\infty} \left| \frac{1}{2} \operatorname{erf}\left(\frac{R_D}{\sqrt{4D_T t}}\right)^2 \left[\operatorname{erf}\left(\frac{x_d - u_x t}{\sqrt{4D_L t}}\right) + \operatorname{erf}\left(\frac{x_e + u_x t}{\sqrt{4D_L t}}\right) \right] \right|^2 dt. \quad (5.9b)$$

Therefore, the the energy generated by the signal can be expressed as:

$$\beta(x_d, R_D) = \int_{t_f}^{t_f + t_b} |\theta_1(x_d, R_D, t)|^2 dt + \int_{t_f + t_b}^{2t_f + t_b} |\theta_0(x_d, R_D, t)|^2 dt. \quad (5.10)$$

Based on Eq. (5.7) - (5.10), it can be seen that the signal flow parameter (M_0 and M_R) has a quadratic relation to the energy the signal produces. However due to the presence of error functions in the equation, the comparison of experimental results to derived data was done numerically, which can be seen in Figure 5.5a.

To calculate the signal-to-noise ratio of the system the following equation is used:

$$SNR_{dB} = 10 \log_{10} \left(\frac{\beta}{N_0} \right), \quad (5.11)$$

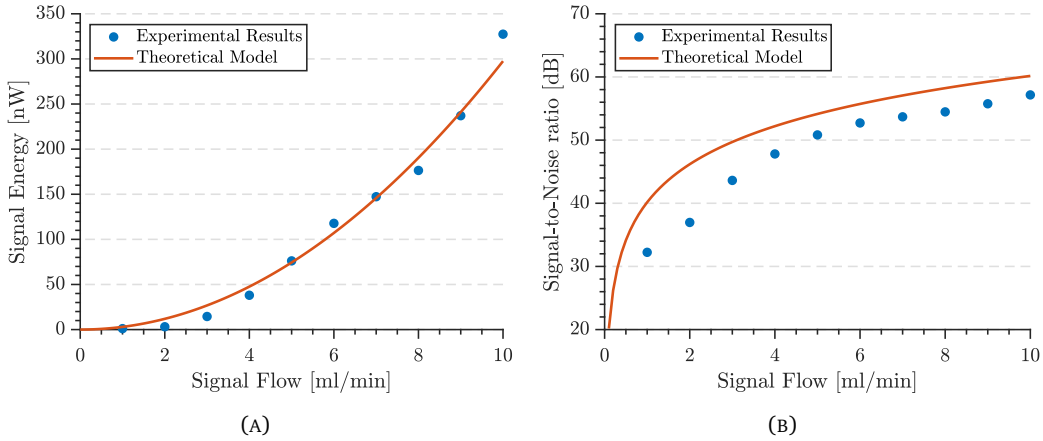


FIGURE 5.5: Experimental (●) along with theoretical comparison (—) of: (A) signal energy, (B) signal-to-noise ratio (SNR).

where N_0 is the power of the noise (W). In this study, the noise power is used as the variance σ_N^2 calculated in the noise analysis done in Section 5.2. The results for the SNR value comparison can be seen in Figure 5.5b. As can be seen, the theoretical model shows reasonably strong agreement with the experimental results with small deviations from the model caused by the complex interactions with the membrane.

5.3.4 Modelling the Signal

To test the validity of the model described in Chapter 4, experimental values ($q = 1 \text{ ml/min} \dots 10 \text{ ml/min}$) are compared to the the theoretical model of their respective signal flow values. The result of this comparison can be seen in Figure 5.6a and Figure 5.6b. As can be seen, the model shows agreement with the experimental results. However, it should be pointed out that the chemicals that are “removed”(i.e., depleted) from the the system occur in a faster rate than the model would normally predict. This can be caused by the membrane in the inlet sampling probe of the detector.

The Pearson correlation, given in Eq. (5.6), for the signal flow study can be seen in Table 5.2. As can be seen in the Table, the model is able to predict the signals that were generated experimentally with acceptable accuracy ($\rho \geq 0.9$), whereas the model shows high accuracy in predicting the maximum signal amplitude and signal energy ($\rho \geq 0.99$). The following section will focus on the effect of the carrier flow (Q) on the transmitted signal.

TABLE 5.2: Correlation (ρ) results of signal flow study .

Signal Parameters		Signal Modelling				
Signal amplitude	1 ml/min	1 ml/min	2 ml/min	3 ml/min	4 ml/min	5 ml/min
0.9962	0.9043	0.8809	0.9580	0.9808	0.9847	
Energy	SNR	6 ml/min	7 ml/min	8 ml/min	9 ml/min	10 ml/min
0.9950	0.9924	0.9955	0.9953	0.9958	0.9943	0.9920

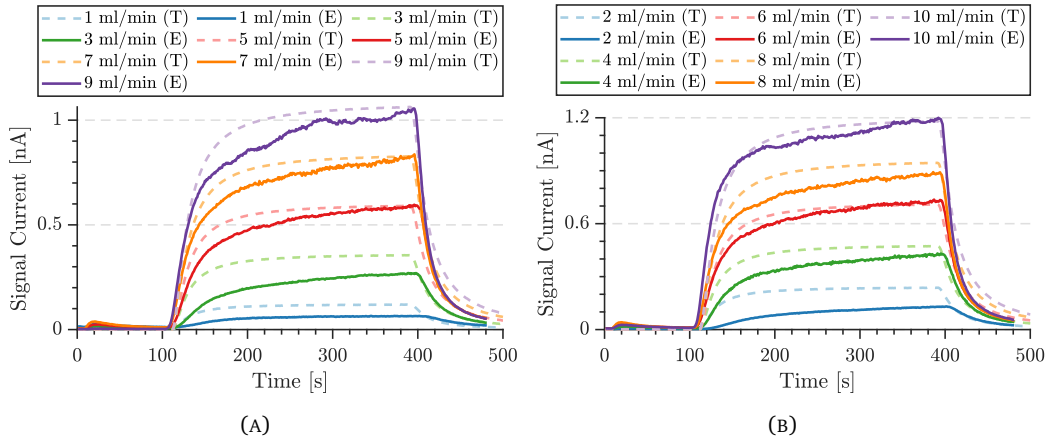


FIGURE 5.6: Experimental and theoretical comparison of the signal shape in the signal flow study: (A) odd numbered signal flow values, (B) even numbered signal flow values. (Equations used in modelling: Eq. 4.11c and Eq. 4.14c).

5.4 Carrier Flow

Carrier flow can be defined as the flow which aids the transmission from the transmitter to the receiver. The flow decreases the amount of time needed to travel the distance thereby increasing the transmission speed, however the introduction of a carrier flow decreases the concentration of the signal flow which decreases the amplitude of the signal. To test the effect of the carrier flow on the transmission, an experiment was conducted. The parameters for the experiment are given in Table 5.3.

TABLE 5.3: Parameters for carrier flow study

Experimental Parameter	Symbol	Value	Unit
Tracked signal flow ion	m/z	43	Da
Signal flow	q	8	ml/min
Bit duration	t_b	300	s
Acetone detection delay [45]	t_d	15	s
Flush duration	t_f	90	s
Transmission distance	x_d	2.5 ± 0.1	cm
Carrier flow pressure	P_F	1	bar
Diffusivity of acetone in air	D	0.124	cm^2/s
Theoretical Parameter	Symbol	Value	Unit
Introduced mass	M_0	2.4	ng
Advectional flow in y -axis and z -axis	u_y & u_z	0	cm/s
Transmission distance	x_d	2.5	cm
Detector radius	R_D	0.3	cm
Longitudinal diffusivity	D_L	0.14	cm^2/s
Radial diffusivity	D_T	1×10^{-3}	cm^2/s
Noise mean & variance	μ_N, σ_N^2	1.21, 0.096	pA, W/ion

5.4.1 Experimental Methodology

The experiment starts by transmitting only carrier flow to the detector for 90s, defined as t_f to clear the detector from any residual chemicals present in the inlet or the environment. After t_f time has passed, the transmitter initiates the signal flow transmission, along with the carrier flow for propagation, for 300 s. This time frame is defined as t_b . The experiment concludes by transmitting only carrier flow for 90 s, defined as t_f . The signal flow is kept constant at $q = 8 \text{ ml/min}$. The diagram for the experiment can be seen in Figure 5.7.

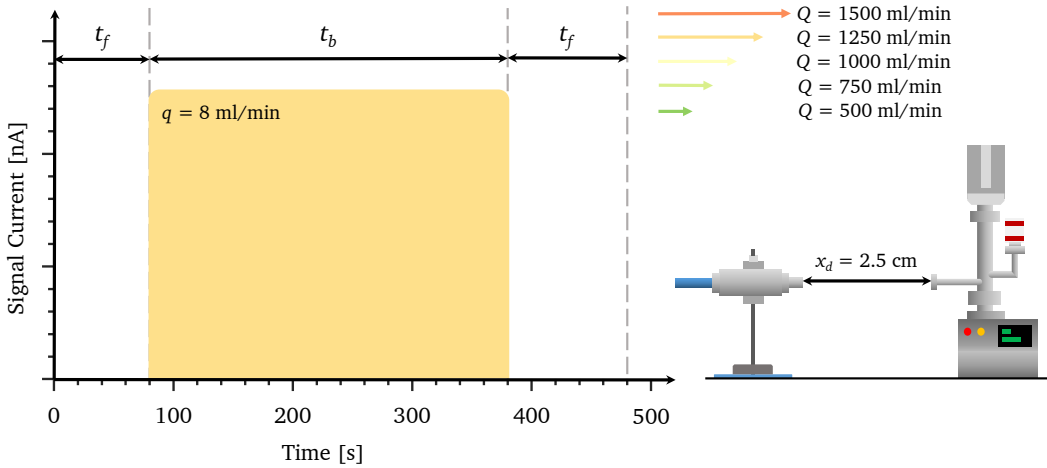


FIGURE 5.7: Experimental diagram of the carrier flow study

5.4.2 Signal Properties

The results of the carrier flow transmission experiments can be seen in Figure 5.8a and Figure 5.8b and the maximum amplitude values of each transmission can be seen in Figure 5.9.

As it can be seen, the signal sees a decrease in amplitude as the flow velocity is increased. This is due to the decrease in the concentration of the signal chemicals that are transmitted. This effect occurs due to two properties: the way chemicals are transmitted in the experimental design and the carrier flow. Increased carrier flow decreases the amount of chemicals that are transmitted from the mixing chamber to the transmission medium. As the carrier flow is increased the pressure in the mixing chamber increases as well, which in turn causes a negative effect on the introduction of the signal flow into the evaporation chamber (EC).

The carrier flow is made up from fast moving particles (N_2) that mix with the signal chemicals to aid the propagation. This in turn, however, decreases the concentration of the signal chemicals and decreases the maximum attainable signal. Since the detector is tracking a specific m/z value (i.e., 43) the detector won't pick up on any signal generated by the carrier flow, therefore high flow values are detrimental to the signal amplitude.

Both these properties can be approximated by the following equation:

$$M_n = M_0 E_1 \left(\frac{u_x x_d}{D_L} \right), \quad (5.12)$$

where E_1 is the exponential integral with the following definition [354]:

$$E_1(z) = \int_1^\infty \frac{1}{t} \exp(-tz) dt. \quad (5.13)$$

By introducing the Eq. (5.12) into the simulation framework given in Chapter 4, the new mass can be calculated. Based on this, it can be seen in Figure 5.9 that the model shows an agreement to the experimental results of the signal amplitude.

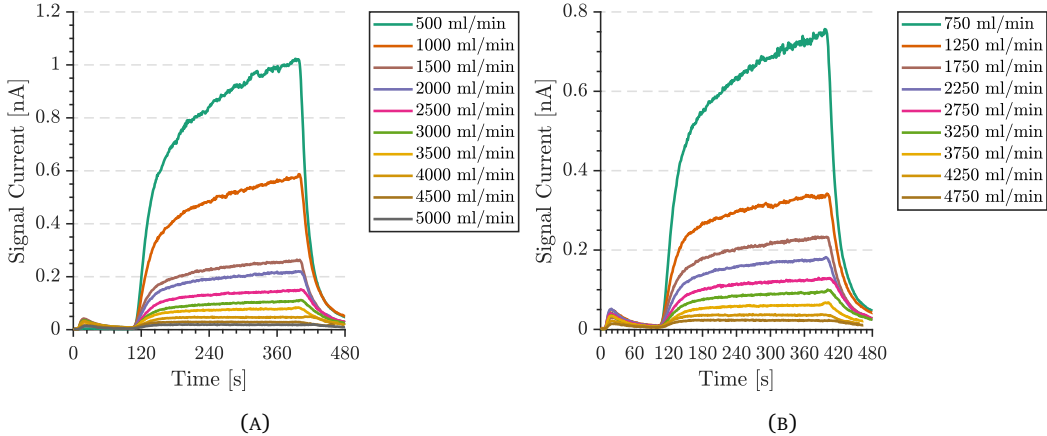


FIGURE 5.8: Experimental results of the carrier flow (Q) experiments.

As the carrier flow increases, the shape of the signal becomes similar to that of a square wave. This behaviour can be explained by taking the limit of the absorbed concentration function $\theta_1(x_d, R_D, t)$:

$$\lim_{u_x \rightarrow \infty} \theta_1(x_d, R_D, t) = M_n. \quad (5.14)$$

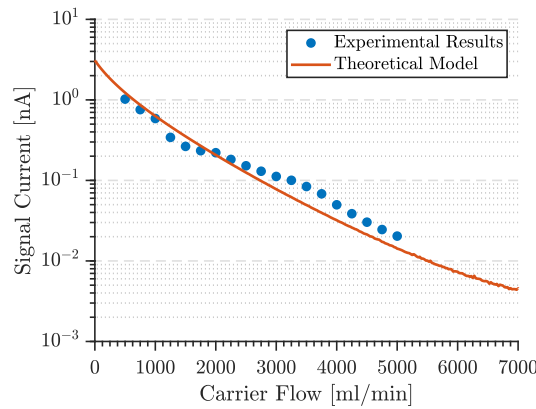


FIGURE 5.9: Comparison of the maximum signal amplitude of the transmitted signal (●) and the values generated by the theoretical model (—). (Equations used in modelling: Eq. (5.12))

This occurs due to the dominance of the flow (i.e., advection) rises and the effect of random movements (i.e., diffusion) becomes less apparent. This effect can be also seen in the variance (σ^2) of the signal in Figure 5.10a. The decrease in signal correlation can also be observed in Figure 5.10b, however unlike the signal flow where diffusion plays a role, in carrier flow the decorrelation is caused by the lack of particles in the system and the signal level approaching the background noise of the detector, therefore decreasing the correlation value.

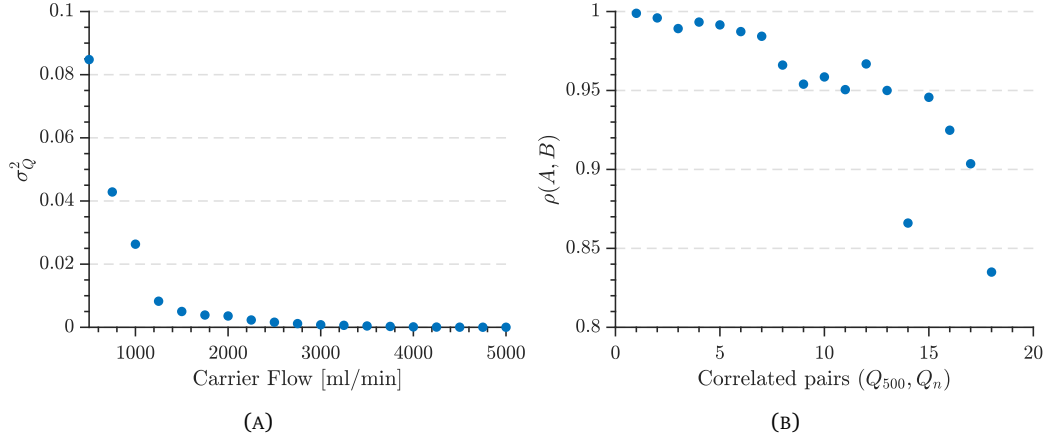


FIGURE 5.10: (A) Signal variance of the carrier flow study. (B) Signal correlation values of the carrier flow study.

5.4.3 Signal Energy and SNR

The energy generated by the transmitted signal for the carrier flow experiment can be calculated from Eq. (5.7) - (5.10). The only difference is the introduction mass needs to be recalculated based on Eq. (5.12). Due to the complexity of the equations, as mentioned in the signal flow experiment, numerical results are calculated and used for comparison to experimental data. The results can be seen in Figure 5.11a for signal energy and in Figure 5.11b for SNR values.

5.4.4 Modelling the Signal

In Figures 5.12a, 5.12b, 5.12c and 5.12d the comparison of experimental signals (E) to the modelled signals (T) for each carrier flow test are shown. As can be seen, the model is able to predict the signal in lower flow values, however as the flow is increased the model diverges from the experimental data. It must be noted of the initial pulse occurring in the beginning of the test. This initial pulse can occur due to various effects of the membrane inlet of the detector. These include, leftover chemicals in the membrane, chemicals lingering in the detector etc.

The correlation values for the carrier flow study can be seen in Table 5.4. As can be seen, the theoretical model shows acceptable prediction up to carrier flow values of 3000 ml/min ($\rho \geq 0.9$). At high flow values the model still can predict the signal, however due to the

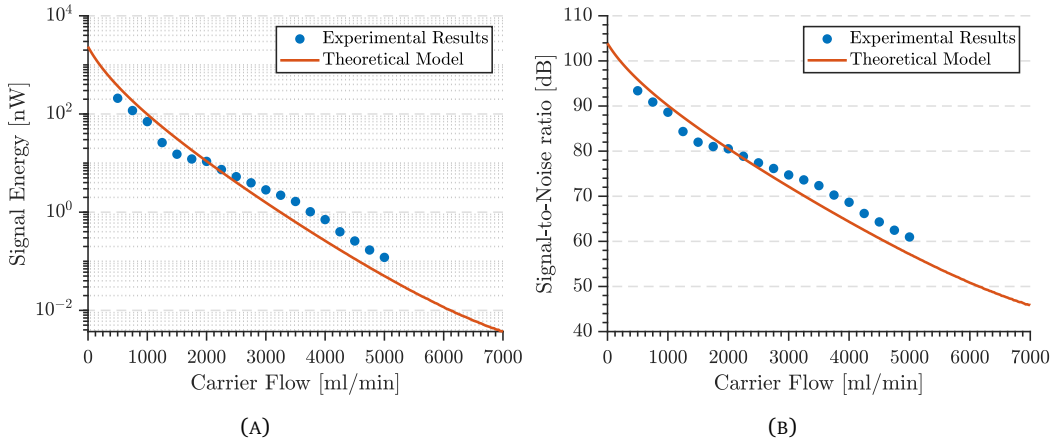


FIGURE 5.11: Experimental (●) along with theoretical (—) comparison of (A) signal energy, (B) signal-to-noise ratio.

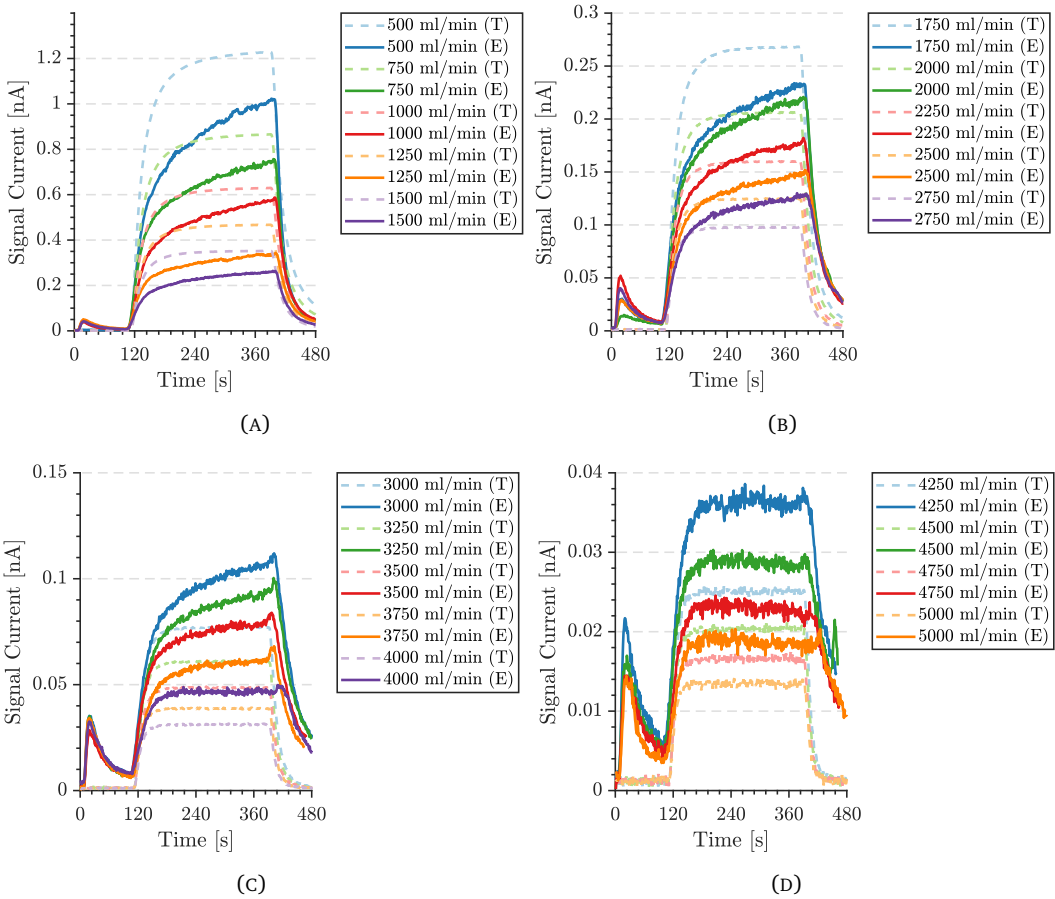


FIGURE 5.12: Experimental along with theoretical comparison of the bulk flow study. (Equations used in modelling: Eq. 4.11c and Eq. 4.14c)

increased effect of the noise, the correlation value is less than in low flow values ($\rho \geq 0.78$). The decrease of the correlation value can also be caused by the initial pulse generated by each experiment. This is caused by unwanted chemicals in the detector or in the vicinity of the detector. In low flows this effect is negligible (i.e., Figure 5.12a). However when the

flow is high, (i.e., Figure 5.12d) this initial pulse becomes significant enough to impact the correlation between the experimental data and the model.

TABLE 5.4: Correlation (ρ) results of bulk flow study

Signal Properties		Signal Modelling				
Signal Amplitude		500 ml/min	750 ml/min	1000 ml/min	1250 ml/min	1500 ml/min
0.9947		0.9867	0.9880	0.9805	0.9798	0.9791
Signal Energy	SNR	1750 ml/min	2000 ml/min	2250 ml/min	2500 ml/min	2750 ml/min
0.9966	0.9936	0.9753	0.9655	0.9594	0.9313	0.9086
		3000 ml/min	3250 ml/min	3500 ml/min	3750 ml/min	4000 ml/min
		0.9069	0.8893	0.9169	0.8830	0.8015
		4250 ml/min	4500 ml/min	4750 ml/min	5000 ml/min	
		0.9213	0.9053	0.8742	0.7824	

5.5 Transmitted Bit Duration

Transmitted bit duration (t_b) is the time each bit is given between two flushing times. Depending on the duration given, different properties of the communication system might occur and play a major role and hinder the property. One of the properties and a problem for molecular communication is the leftover chemicals influencing the next bit. This effect, known as Inter-symbol Interference (ISI), is a problem that limits the throughput of the system. The parameters for experimental and modelling used in the bit duration study are given in Table 5.5.

5.5.1 Experimental Methodology

The experiment starts by transmitting only carrier flow to the detector for 90s, defined as t_f to clear the detector from any residual chemicals present in the inlet or the environment. After t_f time has passed, the transmitter initiates the signal flow transmission, along with the carrier flow for propagation, for an initial value of 90s with 30s increments up to 360s. This time frame is defined as t_b . The experiment concludes by transmitting only carrier flow for 90 s, defined as t_f . The signal flow is kept constant at $q = 8 \text{ ml/min}$ and the carrier flow is set to $Q = 750 \text{ ml/min}$. The diagram for the experiment can be seen in Figure 5.13.

5.5.2 Signal Properties

The experimental result for the transmitted signal with varying bit duration can be seen in Figure 5.14. It can be seen that as the bit duration (t_b) is increased the signal sees an increase in its amplitude in Figure 5.15a. This arises due to the increase exposure to the signal chemicals. Since the window in which signal transmitted increases, more mass is absorbed by the detector. This effect can be observed clearly in Figure 5.14 and for the maximum amplitude in Figure 5.15a

TABLE 5.5: Parameters for bit duration experiment

Parameter	Symbol	Value	Unit
Tracked signal flow ion	m/z	43	Da
Signal flow	q	6	ml/min
Carrier flow	Q	1000	ml/min
Acetone detection delay [45]	t_d	15	s
Flush duration	t_f	90	s
Transmission distance	x_d	2.5 ± 0.1	cm
Carrier flow pressure	P_F	1	bar
Diffusivity of acetone in air	D	0.124	cm ² /s
Theoretical Parameter	Symbol	Value	Unit
Introduced mass	M_0	2.4	ng
Advective flow in x -axis	u_x	0.02	cm/s
Advective flow in y -axis and z -axis	u_y & u_z	0	cm/s
Transmission distance	x_d	2.5	cm
Detector radius	r	0.3	cm
Longitudinal diffusivity	D_L	0.14	cm ² /s
Radial diffusivity	D_T	1×10^{-3}	cm ² /s
Noise mean & variance	μ_N, σ_N^2	1.21, 0.096	pA, W/ion

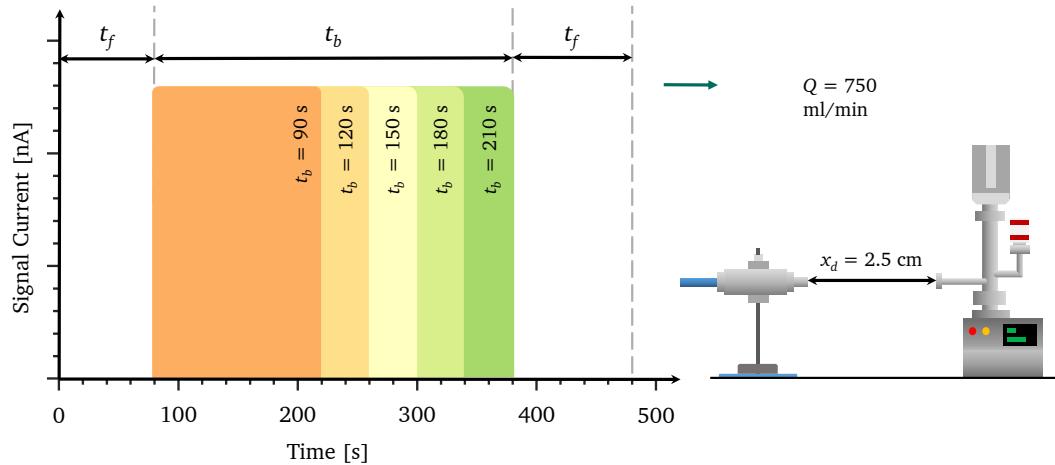


FIGURE 5.13: Experimental diagram of the bit duration study.

This increase in amplitude is better for detection. However, as more mass is absorbed by the detector, more mass needs to be removed from the detector to the outside environment as this effect of absorption/desorption was explained in Chapter 4. After flushing, whatever remains may cause ISI and decrease the performance of the communication. This increase in the background signal current (i.e., leftover from the bit transmission) can be observed in Figure 5.15b.

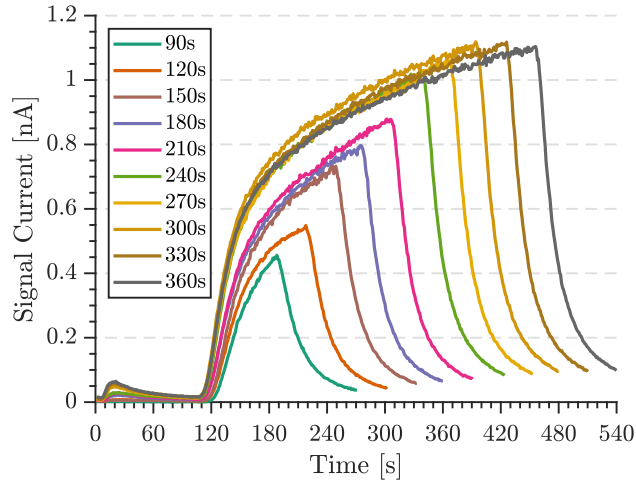


FIGURE 5.14: Results of the bit duration study.

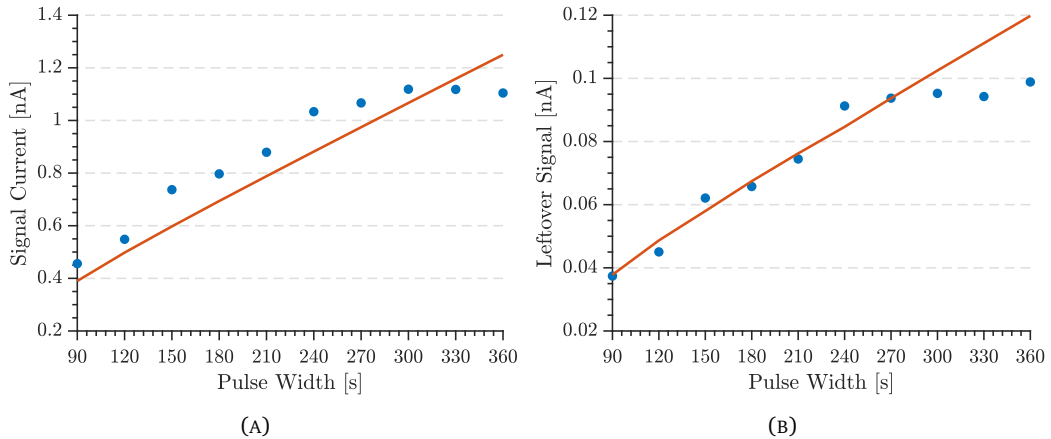


FIGURE 5.15: Experimental (●) along with theoretical (—) comparison of (A) maximum signal amplitude, (B) leftover signal from the bit duration study. (Equations used in modelling: Eq. 4.11c and Eq. 4.14c)

However the rise of both the amplitude and the background signal decreases as bit length is increased. This behaviour is due to the detector reaching the point where it absorbs all the chemicals in the bit transmission (i.e., saturation of the membrane inlet).

5.5.3 Signal Energy and SNR

Experimental results along with theoretical comparsion to signal energy and SNR can be seen in Figure 5.16a and Figure 5.16b respectively.

As can be seen the model shows acceptable prediction with experimental results up to 270 s. However, due to the membrane presence in the detector, the experimental values start saturating after this point.

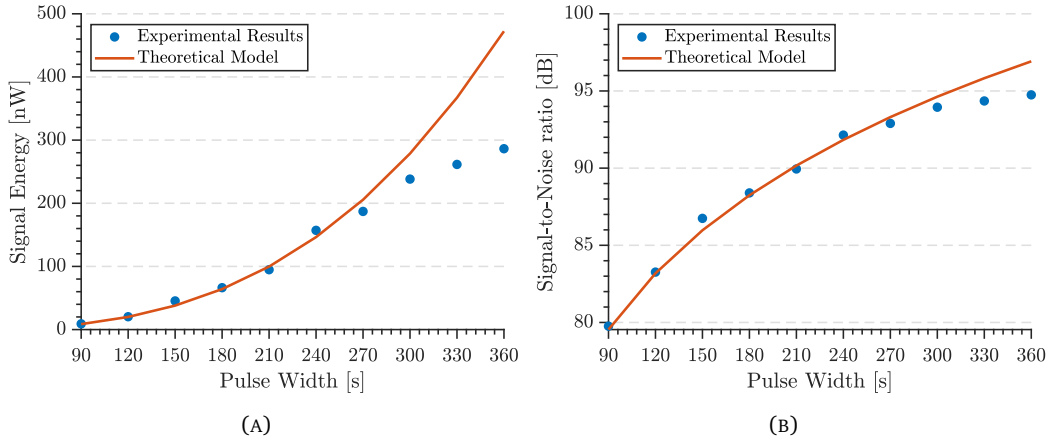


FIGURE 5.16: Experimental (●) along with theoretical (—) comparison of (A) Signal Energy (B) Signal-to-Noise ratio.

5.5.4 Modelling the Signal

The theoretical comparison with experimental data can be seen in Figure 5.17a and Figure 5.17b. The correlation values for the bit duration study can be seen in Table 5.6.

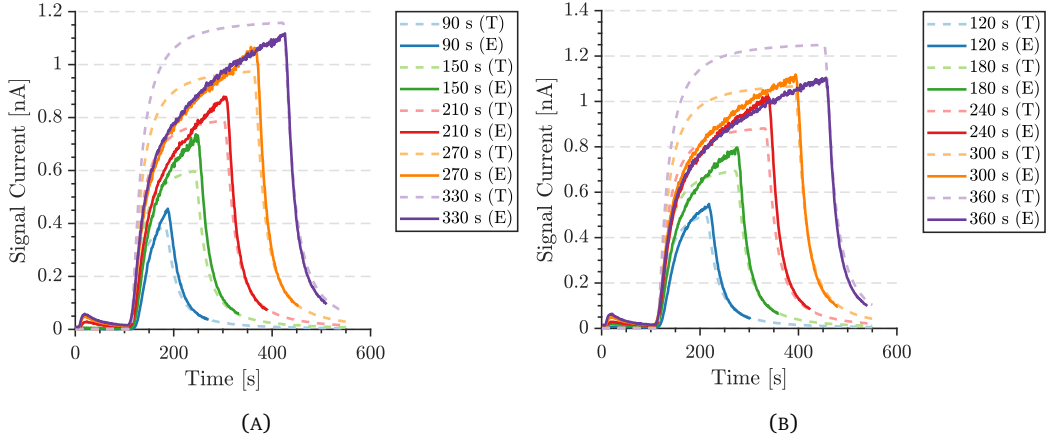


FIGURE 5.17: Experimental along with theoretical comparison of the bit duration study. (Equations used in modelling: Eq. 4.11c and Eq. 4.14c)

As can be seen from both Figures and the correlation value table, the model shows strong agreement with the experimental data ($\rho \geq 0.97$). However, it must be noted that there is a divergence between the rise rate. This can be caused by the membrane interaction between the signal chemical and the detector.

5.6 Open-air Transmission

Transmission distance plays an important role in defining the limitations of a communication method. Unlike EM type communication, propagation is done via the motion of particles

TABLE 5.6: Correlation (ρ) results of bit duration study

Signal Parameters		Signal Modelling				
Signal Amplitude	Leftover Signal	90 s	120 s	150s	180 s	210 s
0.9567	0.9570	0.9384	0.9682	0.9665	0.9806	0.9755
Signal Energy	SNR	240 s	270 s	300s	330 s	360 s
0.9682	0.9930	0.9781	0.9787	0.9853	0.9808	0.9792

TABLE 5.7: Parameters for open-air transmission study.

Experimental Parameter	Symbol	Value	Unit
Signal flow (Acetone)	q	8	ml/min
Tracked signal flow ion	m/z	43	Da
Carrier flow	Q	750	ml/min
Bit duration	t_b	60	s
Acetone detection delay [45]	t_d	15	s
Flush duration	t_f	60	s
Carrier flow pressure	P_F	1	bar
Environment pressure	P_E	1.008 ± 0.002	bar
Environment temperature	T_E	293.5 ± 0.2	K
Diffusivity of Acetone in Air	D	0.124	cm^2/s
Theoretical Parameter	Symbol	Value	Unit
Introduced mass	M_0	1.2	ng
Advective flow in x -axis	u_x	0.18	cm/s
Advective flow in y -axis and z -axis	u_y & u_z	0	cm/s
Longitudinal diffusivity	D_L	0.15	cm^2/s
Radial diffusivity	D_T	1×10^{-4}	cm^2/s
Detector radius	R_D	0.3	cm
Noise mean & variance	μ_N, σ_N^2	1.21, 0.096	pA, W/ion
Decay parameter	a	7.5×10^{-5}	-
	b	2.616	-

and therefore can experience higher attenuation, and without a guided medium (i.e., open-air) this can be even worse. To experimentally analyse the attenuation, an experiment was conducted. The experimental parameters along with the theoretical parameters used in modelling can be seen in Table 5.7.

5.6.1 Experimental Methodology

The experiment was conducted by varying the transmission distance (x_d) from 2.5 cm to 15.0 cm. The transmission of the signal starts with 60s of flush (t_f). This is done by sending only the carrier flow (Q) and is used to clean up the sensor from the leftover chemicals by the signal flow (q). This is followed by a 60s pulse (t_b) of chemicals ($Q + q$) and finally 60s

of flush (Q) at the end of the experiment. Each transmission experiment was repeated 3 times and the average values of the experiments are taken.

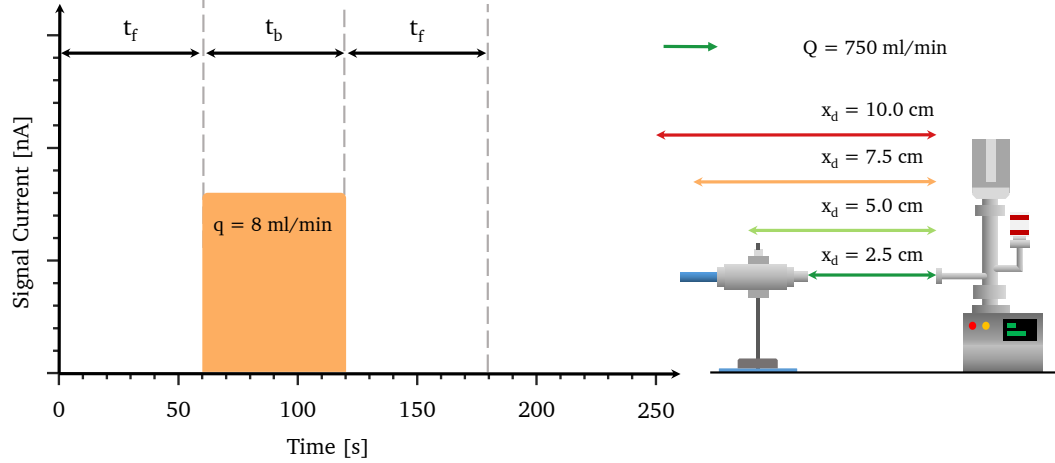


FIGURE 5.18: Experimental diagram of the open-air transmission study.

5.6.2 Signal Properties

To model the system, the equations derived in Section 4.2.2 are used. It is assumed that the noise is AWGN and present at the receiver. The experimental transmission in open-air can be seen in Figure 5.19a and the results of the open-air transmission with comparison to the theoretical model can be seen in Figure 5.21. The amplitude values compared to theoretical values for each distance is given in Figure 5.19b.

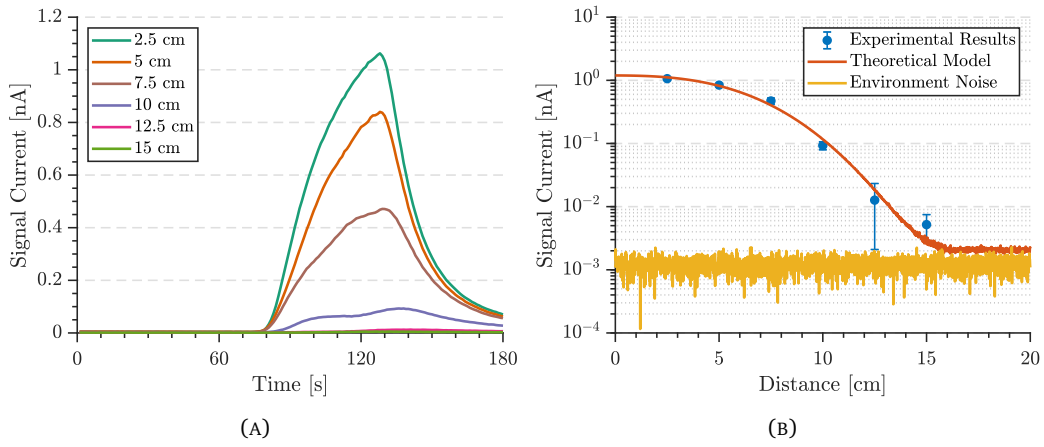


FIGURE 5.19: (A) Experimental results of the open-air study. (B) Experimental (●) along with theoretical (—) values of maximum signal amplitude.

As it can be seen in Figure 5.21 and Figure 5.19b, the model shows agreement with experimental results. However, it should be noted that as distance increases, the fluctuation in the signal sees a noticeable increase which can be seen in Figure 5.21e and Figure 5.21f.

It can also be seen that at a distance of 15 cm (Figure 5.21f) the fluctuations caused by the noise start playing a bigger role in the signal which causes a decrease in the accuracy of the model.

The signal experiences increased distortion as the distance is increased. This distortion and the loss in the amplitude are due to outside interferences affecting the transmission (particle collisions in the medium or the diffusive properties causing the chemicals to miss the detector). When the transmission distance is increased further than 10 cm, the amplitudes of the retrieved signals are measured as 12.7×10^{-12} and 5.2×10^{-12} A for 12.5 cm and 15 cm respectively which compared to amplitude at 2.5 cm, 1.06×10^{-9} A is close to two orders of magnitude lower.

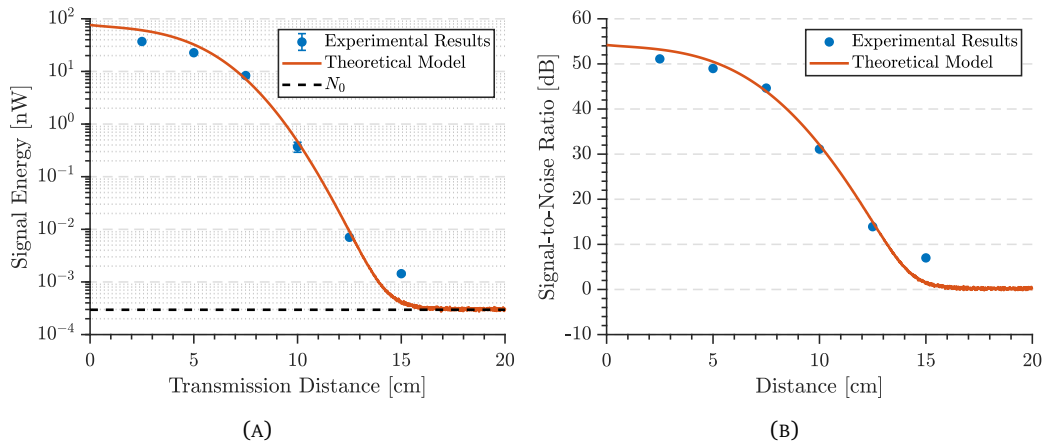


FIGURE 5.20: Experimental (●) along with theoretical (—) comparison of; (A) comparison of experimental along with theoretical values of signal energy, (B) experimental along with theoretical values of signal to noise.

5.6.3 Signal Energy and SNR

Based on Eq. (5.7) - (5.10), the energy of the transmitted signal is calculated numerically and the comparison can be seen in Figure 5.20a. As it can be seen, the theoretical model shows agreement to the experimental results and shows a non-linear behaviour as distance increases. It must also be noted that after a certain amount of distance ($x_d > 15$ cm) the energy of the transmitted signal dissipates and only the energy produced by the noise (N_0) remains which can be seen in Figure 5.20a. Unlike an EM system, where N_0 is defined as W/Hz, in molecular communications it can be defined as W/chemical or W/ion. It also must be noted that the noise power is different for different chemicals, which will be analysed in Chapter 7. The SNR comparison can be seen in Figure 5.20b.

5.6.4 Modelling the Signal

To show the validity of the model, 6 experimental results were compared with the theoretical model which can be seen in Figure 5.21a for 2.5 cm, Figure 5.21b for 5 cm, Figure 5.21c for 7.5 cm, Figure 5.21d for 10 cm, Figure 5.21e for 12.5 cm and Figure 5.21f for 15 cm.

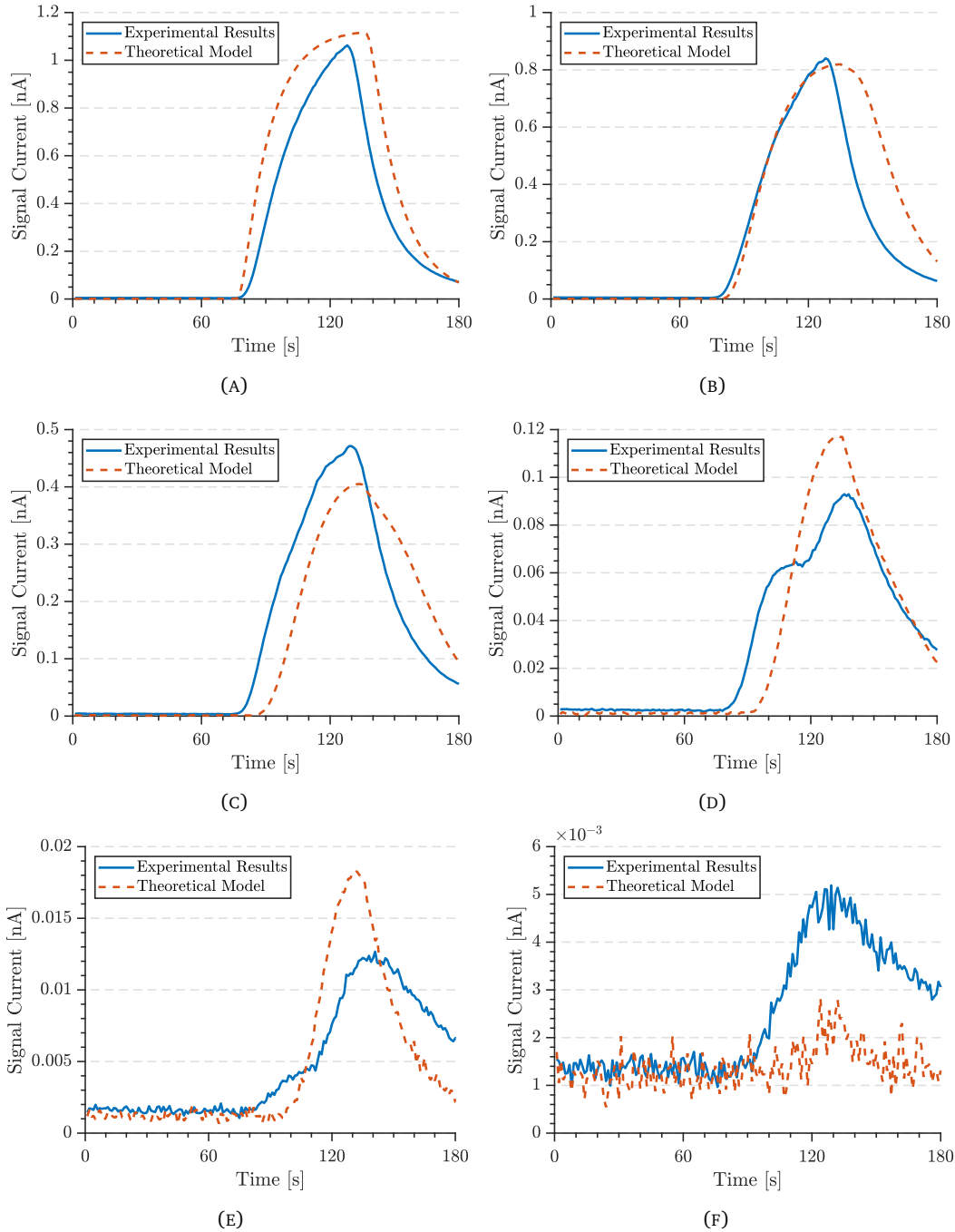


FIGURE 5.21: Open-Air transmission along with theoretical comparison (A) 2.5 cm (B) 5 cm (C) 7.5 cm (D) 10 cm (E) 12.5 cm (F) 15 cm

As can be seen for short distances the signal shape and its amplitude can be relatively be predicted by the mathematical model. However, as distance sees an increase, due to the environmental effects, the signal becomes increasingly unpredictable which results in lower correlation values that can be seen in Table 5.8.

TABLE 5.8: Correlation (ρ) results of open-air transmission study

Signal Parameters		Signal Modelling		
Signal Amplitude	2.5 cm	5 cm	7.5 cm	
0.9963	0.9696	0.9154	0.8910	
Signal Energy	SNR	10 cm	12.5 cm	15 cm
0.9935	0.9946	0.9309	0.8458	0.5951

5.7 Closed-air Transmission

One of the major problems of open-air transmission is the high attenuation the signal experiences as it propagates through space. This is caused by the diffusion of the particles and loss of direction as distance increases. To overcome this, a boundary can be implemented to the transmission medium to protect the transmitted signal from dispersing to other directions. In this parameter analysis, the attenuation of the signal travelling in a confined medium is studied.

TABLE 5.9: Parameters in the closed-distance study

Experimental Parameters	Symbol	Value	Unit
Tracked Signal Ion	m/z	43	Da
Signal Flow	q	8	ml/min
Carrier Flow	Q	750	ml/min
Carrier Flow Pressure	P_Q	1	atm
Vacuum Pump Pressure	P_V	2.4×10^{-6}	torr
Environment Pressure	P_E	1 ± 0.003	bar
Environment Temperature	T_E	297.35 ± 1.5	K
Inner Tube diameter	d_{in}	19.80	mm
Outer Tube diameter	d_{out}	24.25	mm
Acetone detection delay [45]	t_d	15	s
Theoretical Parameters	Symbol	Value	Unit
Density of the fluid	ρ_D	1.165	kg/m ³
Mean velocity of the fluid	u	2×10^{-2}	m/s
Hydraulic diameter of the pipe	D_H	2×10^{-2}	m
Dynamic viscosity of the fluid	η	1.76×10^{-5}	Ns/m ²
Reynolds Number	Re	26	-
Laminar diffusion	D_L	0.168	cm/s
Shear Stress	τ	1.4×10^{-4}	Pa
Darcy-Weisbach friction factor	f_D	2.46	-
Shear Flow	u_*	1.1×10^{-2}	m/s
Transient diffusion	D_L^T	11.2	cm/s ²

The experimental parameters along with the theoretically calculated values can be seen in Table 5.9. The mathematical model used to describe the propagation is explained in chapter 4, section 4.2.3

5.7.1 Experimental Methodology

The experiment starts by transmitting only carrier flow (Q) to the detector for 60s to clear the detector from any residual chemicals present in the inlet or the environment.

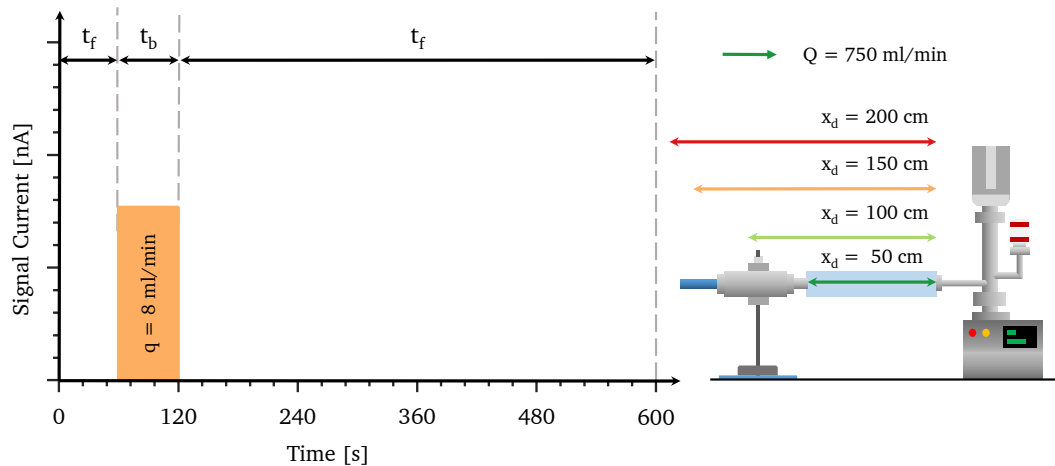


FIGURE 5.22: Experimental diagram of the closed-distance study.

After 60s has passed, the transmitter initiates the signal flow transmission, along with the carrier flow for propagation, for 60 s. This time frame is defined as t_b . The experiment concludes by transmitting only carrier flow for 480 s. The experimental setup can be seen in Figure 5.22.

5.7.2 Signal Properties

The experimental results of the closed boundary transmission can be seen in Figure 5.23a. As can be seen, the signal behaves in a non-linear fashion and with each consecutive increase in the distance, the signal amplitude decreases and causes delay in the arrival of the signal. This delay caused by the increase of distance can be seen in Figure 4.4.

As can be noted, the theoretically generated signal shows agreement with the experimentally obtained results. Finally the maximum signal amplitude generated from these transmissions with comparison to the theoretical calculations can be seen in Figure 5.23b with additional theoretical comparisons of two different radii: 0.9 cm and 1.1 cm. The effects of the radius of the boundary shows that small changes in the boundary has a significant effect on the signal arrival and the attenuation. Increasing the radius increases the attenuation and detection delay whereas decreasing the radius has the inverse effect. The reason of this observation is due to the radial diffusion propagation and particle collisions

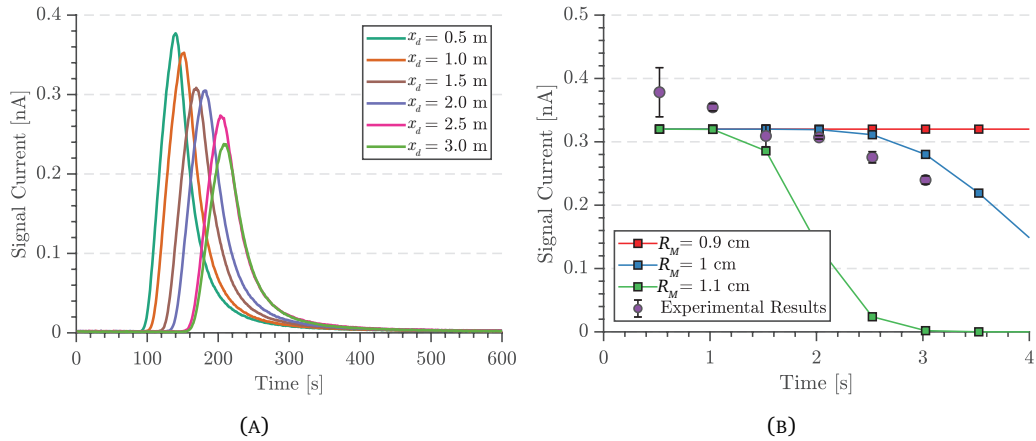


FIGURE 5.23: (A) Experimental results of closed-boundary transmission. (B) Experimental results along with the theoretical comparison of the maximum signal amplitude of closed boundary transmission.

with the boundary where bigger radius would allow more particles to disperse, decreasing the overall signal amplitude.

5.7.3 Signal Energy and SNR

In this study the energy of the theoretically generated signal is calculated using the following equations. The major change between the following calculation and the Eq. (5.7) - (5.10) is the inclusion of the propagation delay (t_{emp}). In previous section, due to the short transmission distance ($x_d \ll 1$ m) the delay caused by propagation was considered negligible. However, as distance is expressed in m instead of cm, the delay must be taken into account in calculations.

$$\begin{aligned} \beta_1(L, R_M, t) = & \int_{t_{\text{emp}}}^{T_S + t_{\text{emp}}} \left| M - \frac{M}{i\sqrt{4D_T t}} \left[\operatorname{erf}\left(\frac{u_z t}{\sqrt{4D_L t}}\right) + \operatorname{erf}\left(\frac{L - u_z t}{\sqrt{4D_L t}}\right) \right] \right. \\ & \sum_{n=0}^{\infty} \exp\left(-n^2 \frac{R_M^2}{D_T t}\right) \left\{ i\sqrt{D_T t} \left[1 - \exp\left((4n-1) \frac{R_M^2}{4D_T t}\right) \right] + nR\sqrt{\pi} \exp\left(n^2 \frac{R_M^2}{D_T t}\right) \right. \\ & \left. \times \left[\operatorname{erfi}\left(n \frac{iR_M}{\sqrt{D_T t}}\right) - \operatorname{erfi}\left(\frac{(2n-1)}{2} \frac{iR_M}{\sqrt{D_T t}}\right) \right] \right\}^2 dt \quad (5.15) \end{aligned}$$

The second is when the mass is being removed from the detector.

$$\begin{aligned} \beta_0(L_M, R_M, t) = & \int_{t_{\text{emp}}}^{T_F + t_{\text{emp}}} \left| \frac{M_R}{i\sqrt{4D_T t}} \left[\operatorname{erf}\left(\frac{u_z t}{\sqrt{4D_L t}}\right) + \operatorname{erf}\left(\frac{L_M - u_z t}{\sqrt{4D_L t}}\right) \right] \right. \\ & \sum_{n=0}^{\infty} \exp\left(-n^2 \frac{R_M^2}{D_T t}\right) \left\{ i\sqrt{D_T t} \left[1 - \exp\left((4n-1) \frac{R_M^2}{4D_T t}\right) \right] + nR\sqrt{\pi} \exp\left(n^2 \frac{R_M^2}{D_T t}\right) \right. \\ & \left. \times \left[\operatorname{erfi}\left(n \frac{iR_M}{\sqrt{D_T t}}\right) - \operatorname{erfi}\left(\frac{(2n-1)}{2} \frac{iR_M}{\sqrt{D_T t}}\right) \right] \right\}^2 dt \quad (5.16) \end{aligned}$$

where T_F is the duration of the flush.

$$\beta(L; L_M, R_M, t) = \beta_1(L, R_M, t_{\text{emp}} : T_D + t_{\text{emp}}) + \beta_0(L_M, R_M, t_{\text{emp}} : T_F + t_{\text{emp}}) \quad (5.17)$$

The experimental values obtained from this study along with theoretical comparisons can be seen in Figure 5.24a. As can be seen, the theoretical results of $R_D = 1$ cm shows agreement with experimental results and additional theoretical results show the behaviour of the signal with different radius values.

As the radius of the transmission medium is increased, the cross-sectional area of the flow is also increased, which in a system with a constant flow, would entail that the average flow u_{avg} experiences a decrease which finally would cause the signal energy to appear less.

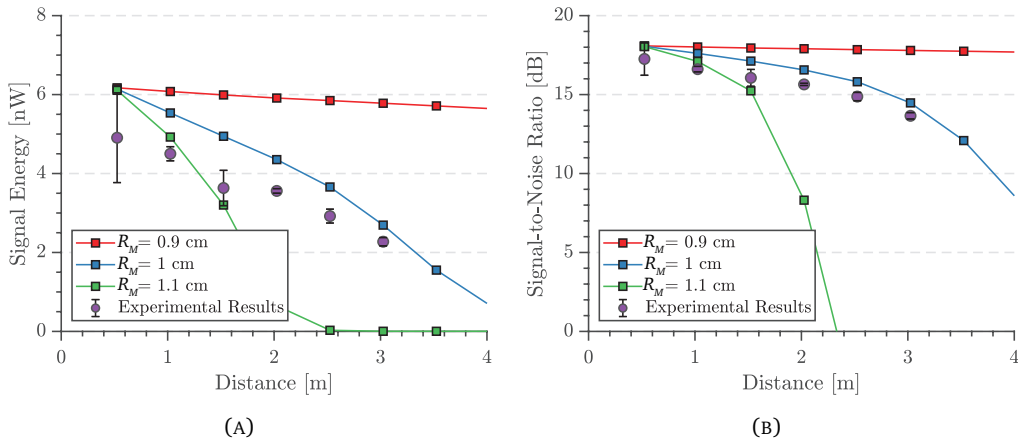


FIGURE 5.24: (A) Experimental results along with the theoretical comparison of the signal energy of closed boundary transmission (B) Experimental results along with the theoretical comparison of the Signal-to-Noise ratio (SNR) of closed boundary transmission.

To calculate the signal to noise ratio, Eq. (5.11) is used along with the plot of experimental along with theoretical comparison can be seen in Figure 5.24b. As can be seen from the plot the signal sees an increase in its SNR values as the transmission distance increases and the increase of the radius of the transmission medium further decreases the value of the SNR, however, the effect of radius on the SNR value loss seems negligible until a distance of 1 m.

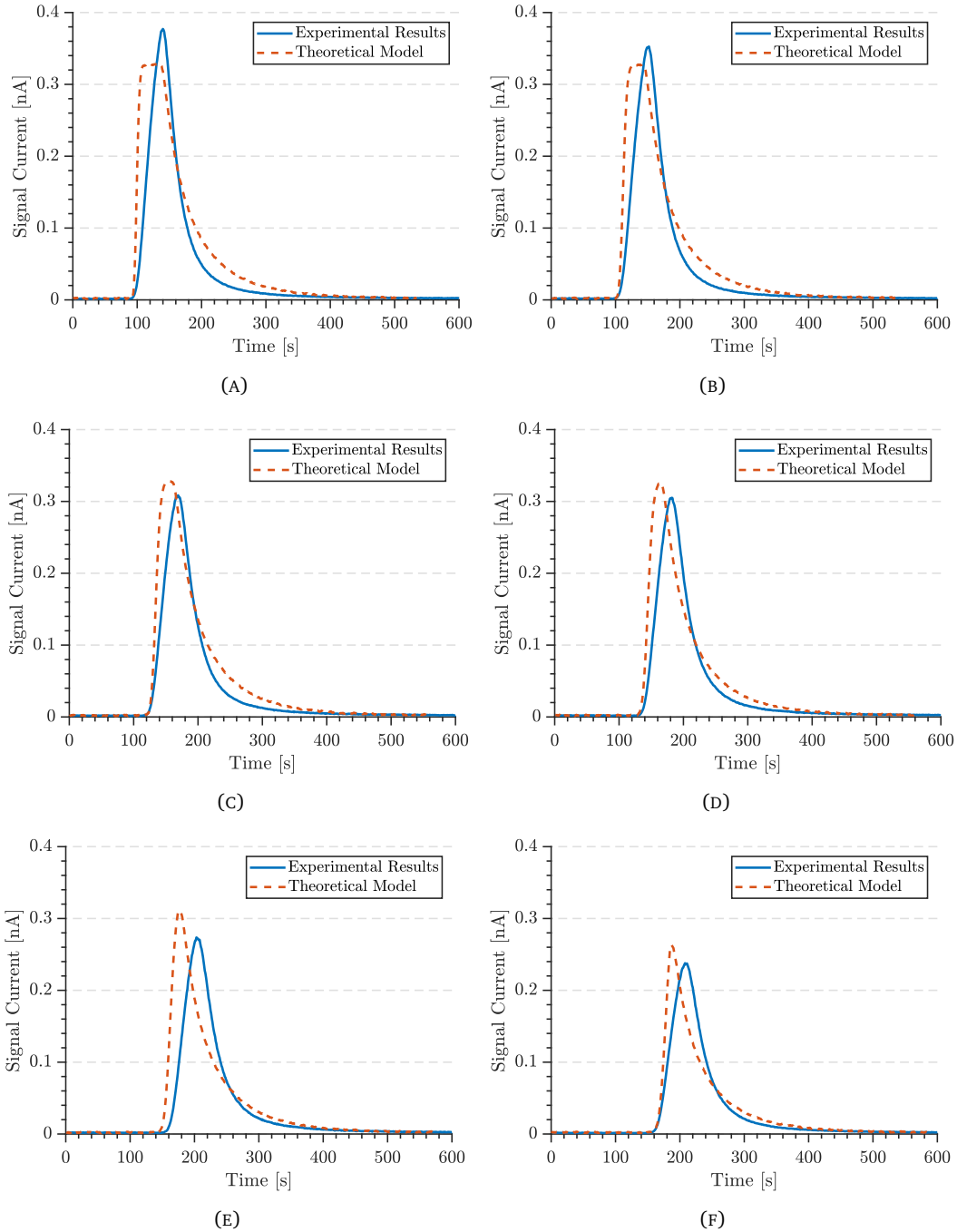


FIGURE 5.25: Experimental results along with theoretical comparison for each experimental transmission (A) 0.5 m (B) 1 m (C) 1.5 m (D) 2 m (E) 2.5 m (F) 3 m.

5.7.4 Modelling the Signal

To test the validity of the closed transmission of molecular communication in modelling the propagating signal, the model developed in chapter 4 is compared with each different transmission distance. The results for the comparison can be seen in Figures 5.25a, 5.25b, 5.25c, 5.25d, 5.25e, 5.25f for 50 cm, 100 cm, 150 cm, 200 cm, 250 cm and 300 cm, respectively. As can be seen, the model is able to predict the signal with acceptable accuracy

$(\rho > 0.87)$ up to 250 cm. However, the model starts deviating from the experimental signal, not from amplitude, but from rise and fall time. This effect can be caused by the effects of the membrane acting on the signal. The correlation values for the modelling of closed-air transmission study can be seen in Table 5.10.

TABLE 5.10: Correlation results of closed-air transmission study.

Signal Parameters		Signal Modelling		
Signal Amplitude	50 cm	100 cm	150 cm	
0.7982	0.9052	0.9170	0.9448	
Signal Energy	SNR	200 cm	250 cm	300 cm
0.9935	0.9946	0.8995	0.7685	0.9006

5.8 Conclusions

In this Chapter, five main properties of macro-molecular communications are analysed: signal flow (q), carrier flow (Q), bit duration (T) open-air transmission and closed-air transmission. Signal flow generates the signal used in transmission and the carrier flow aids in the transmission by decreasing the time of response. To test these properties an experimental setup was utilised, consisting of a in-house built odour generator that generates the necessary pulses to create chemical messages and a quadrupole mass analyser (QMA) with a membrane inlet to detect the transmitted chemical messages. Experiments on the signal analysis show that the signal energy is quadratically dependent on the signal flow introduced into the system. Carrier flow (Q) behaves in a more complex way compared to the signal flow and has both advantages and disadvantages. The presence of the carrier flow decreases the effect of the diffusive properties of the signal chemicals and makes the signal behave similar to that of a square wave, but the carrier flow also diminishes the signal amplitude and therefore the energy, which can make the detection of the signal a challenge if the transmission is along a considerable distance. An experiment was conducted to test the effects of bit duration of the communication system. The leftover chemicals from the transmission see an increase as the bit duration is increased however, after a certain bit duration length, the system reaches a stable point which may be the effect of the membrane in the system.

The open-air transmission shows that the chemical signal experiences high attenuation whereas the propagation of chemicals in a closed environment is able to transmit chemicals longer distances that are not possible using open-air transmission.

The next chapter will focus on the communication aspect of molecular communications.

Chapter 6

Modulation Analysis of Molecular Communications in the Macro-Scale

6.1 Introduction

Molecular communication at the macro scale (cm to km) is a novel way of transmitting information compared to the heavily studied micro-scale (nm to μm). While in Chapter 5 the parameters of the macro-scale were studied experimentally and theoretically, additional analysis is needed to understand this novel communication and implement it as a communication paradigm.

In this chapter, both experimental and theoretical modulation analysis of macro-scale molecular communications are conducted. The experimental studies were made on the M_C -ary $M_C = 2$ (i.e., 0, 1), $M_C = 4$ (i.e., 00, 01, 10, 11) and $M_C = 8$ level transmission. A Symbol Error Rate (SER) study of molecular communications of 2-ary modulation is also tested. In addition, a theoretical analysis of an SER study was also conducted based on the simulation model given in chapter 4, which also shows the consistency with the experimental results. Molecular Inter-Symbol Interference (Mo-ISI) is discussed and an optimal transmission duration is calculated. Finally, a channel model is developed to explain the asymmetrical nature of the communications.

The major contributions of this chapter are as follows;

1. **M_C -ary Transmission study:** A comparison was made with experimental data of M_C -ary transmission of three levels ($M_C = 2$, $M_C = 4$ and $M_C = 8$) and for three different symbol periods ($T_s = 30 \text{ s}$, $T_s = 60 \text{ s}$ and $T_s = 90 \text{ s}$) which shows that the simulation framework can be used to model molecular communications at the macro-scale.
2. **Molecular ISI (Mo-ISI):** A study was made to analyse the effects of Molecular ISI (Mo-ISI) in macro-scale molecular communications. The model developed in Chapter 4 is shown to have strong agreement with the experimental results. Mathematical equations were derived from the model to analytically calculate the residual chemicals from different types of transmissions.

3. **Optimal Symbol Duration:** An optimal symbol duration time is calculated by maximizing the error function ($\text{erf}(\cdot)$) used in the solution for the advection-diffusion equation.
4. **M_C -ary SER Analysis:** An SER analysis was conducted both experimentally ($M_C = 2$) and theoretically ($M_C = 2, 4, 8, 16$ and 32).
5. **Message Transmission Experiment:** An experimental transmission of a message encoded to chemicals was conducted. The transmitted message was compared to the theoretical model developed in Chapter 4.
6. **Molecular Channel:** The type of the channel is defined as asymmetric and the capacity of the communication is described based on the asymmetric nature of the communication.
7. **Parameter effect on SER, MI and Distribution of Received Symbol Values:** A theoretical study of the Mutual Information (MI), SER and distribution of received symbol values was made on the four parameters: transmission distance (x_d), advective flow (u_x), longitudinal diffusivity (D_L) and symbol period (T_S).

The structure of the Chapter is as follows. In Section 6.2 the experimental results along with theoretical comparisons are described for the M_C -ary transmission. In Section 6.3, Molecular ISI is studied. Two types of experiments were conducted (k and o/z) and analysed with the theoretical model developed in Chapter 4. Section 6.4 presents the experimental transmission of a message using chemicals. In Section 6.5 the channel capacity is described and MI is calculated. Section 6.6 discusses the experimental analysis of $M_C = 2$ modulation along with theoretical comparisons to $M_C = 2, M_C = 4, M_C = 8, M_C = 16$ and $M_C = 32$. In Section 6.7 the effects of various parameters on the achievable mutual information and SER are simulated based on the framework mentioned in Chapter 4. In Section 6.8 an analysis was made on the symbol distribution of a 4-ary transmission and the variance (σ^2) of the symbols is discussed. The chapter ends with conclusions in Section 6.8.

6.2 M-ary Transmission

M_C -ary transmission is a type of modulation in which instead of relying on the transmission of one bit at a given time, multiple bits are transmitted. The experimental parameters of the M-ary transmission can be seen in Table 6.1. In the experiment 3 bit durations were tested: 30s, 60s and 90s. The message that was chosen for transmission is “MCX” in American Standard Code for Information Interchange (ASCII).

6.2.1 2-Ary Transmission

In 2-ary transmission, two levels of concentration are used in the transmission the values and its corresponding bit values can be seen in Eq. (6.1).

TABLE 6.1: Parameters for M_C -ary transmission study.

Experimental Parameter	Symbol	Value	Unit
Tracked signal flow ion	m/z	43	Da
Carrier flow	Q	750	ml/min
Acetone detection delay [45]	t_d	15	s
Transmission distance	x_d	2.5 ± 0.1	cm
Environment pressure	P_E	1 ± 0.003	bar
Carrier flow pressure	P_F	1	bar
Vacuum pump pressure	P_V	1.95×10^{-6}	torr
Environment temperature	T_E	297.35 ± 1.5	K
Diffusivity of acetone in air ¹	D	0.124	cm ² /s
Theoretical Parameter	Symbol	Value	Unit
Advective flow in x -axis	u_x	0.02	cm/s
Advective flow in y -axis and z -axis	u_y & u_z	0	cm/s
Transmission distance	x_d	2.5	cm
Detector radius	R_D	0.3	cm
Longitudinal diffusivity	D_L	0.15	cm ² /s
Radial diffusivity	D_T	1×10^{-3}	cm ² /s
Noise mean & variance	μ_N, σ_N^2	1.21, 0.096	pA, W/ion

¹ Normal air and temperature

$$\mathcal{X} = \{0, 8\} \quad (6.1a)$$

$$\mathcal{Y} = \{0, 1\} \quad (6.1b)$$

The experimental results along with comparison to the theoretical model can be seen in Figures 6.1a, 6.1b and 6.1c. As it can be seen, the distinction between two states is discernible even on the shortest bit duration and the theoretical model shows strong agreement with the experimental results. Even though, the clarity between bits is high, the throughput of the communication is low since only 1 bit is transmitted during a given symbol time.

6.2.2 4-Ary Transmission

In 4-ary transmission, four levels of concentration are used in the transmission. The values and its corresponding bit values can be seen in Eq. (6.2).

$$\mathcal{X} = \{0, 3, 6, 9\} \quad (6.2a)$$

$$\mathcal{Y} = \{00, 01, 10, 11\} \quad (6.2b)$$

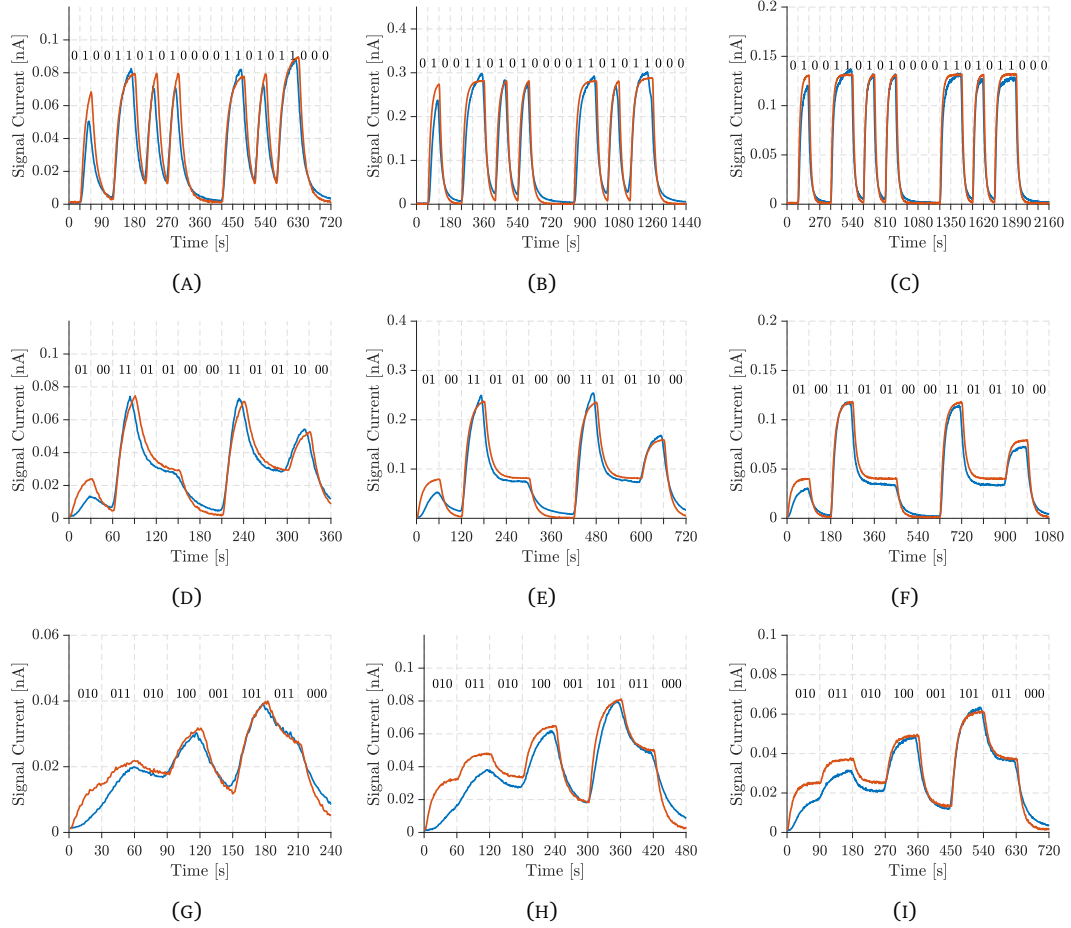


FIGURE 6.1: Experimental (—) along with theoretical (—) comparison of M-ary experiments. (A) 2-ary transmission with bit duration of 30s. (B) 2-ary transmission with bit duration of 60s. (C) 2-ary transmission with bit duration of 90s. (D) 4-ary transmission with bit duration of 30s. (E) 4-ary transmission with bit duration of 60s. (F) 4-ary transmission with bit duration of 90s. (G) 8-ary transmission with bit duration of 30s. (H) 8-ary transmission with bit duration of 60s. (I) 8-ary transmission with bit duration of 90s. (Equations used in modelling: Eq. 4.11c and Eq. 4.14c)

The experimental results along with comparison to the theoretical model can be seen in Figures 6.1d, 6.1e and 6.1f. The $M_C = 4$ level modulation transmission has shown some detrimental effect due to doubling the bits transmitted in a given second. However, the signals of 60s and 90s bit duration shows clear distinction between levels, however the level differences is smaller in 30s transmission.

6.2.3 8-Ary Transmission

In 8-ary transmission, eight levels of concentration are used in the transmission and the corresponding bit values can be seen in Eq. (6.3). The results show the effect on increasing the transmitted bits per second from 2 to 3 has increased the ISI in the system.

TABLE 6.2: Parameters for Mo-ISI transmission study.

Experimental Parameter	Symbol	Value	Unit
Tracked signal flow ion	m/z	43	Da
Carrier flow	Q	750	ml/min
Acetone Detection delay [45]	t_d	15	s
Transmission distance	x_d	2.5 ± 0.1	cm
Environment pressure	P_E	1 ± 0.003	bar
Carrier flow pressure	P_F	1	bar
Vacuum pump pressure	P_V	1.95×10^{-6}	torr
Environment temperature	T_E	297.35 ± 1.5	K
Diffusivity of acetone in air ¹	D	0.124	cm ² /s
Theoretical Parameter	Symbol	Value	Unit
Advective flow in x -axis	u_x	0.02	cm/s
Advective flow in y -axis and z -axis	u_y & u_z	0	cm/s
Transmission distance	x_d	2.5	cm
Detector radius	r	0.3	cm
Longitudinal diffusivity	D_L	0.15	cm ² /s
Radial diffusivity	D_T	1×10^{-3}	cm ² /s
Noise mean & variance	μ_N, σ_N^2	1.21, 0.096	pA, W/ion

¹ Normal air and temperature

$$\mathcal{X} = \{0, 1, 2, 3, 4, 5, 6, 7\} \quad (6.3a)$$

$$\mathcal{Y} = \{000, 001, 010, 011, 100, 101, 110, 111\} \quad (6.3b)$$

It must be noted that the initial pulse differs from the predicted signal. This can be caused by particle interaction with the membrane present in the inlet. However, as the transmission evolves, the theoretical model predicts the experimental values accurately.

6.3 Molecular Inter-Symbol Interference (Mo-ISI)

To understand the behaviour of the bit transmission and the leftover chemical it leaves in the detector, a series of experiments were conducted. In these experiments a sequence of bits were transmitted. The experimental parameters for the experiments can be seen in Table 6.2.

The first set of experiments were done by sending a single 0 bit between increasing amount of 1s ($o/z = 1$ is 10101..., $o/z = 2$ is 11011011... etc.).

The second set of experiments were conducted by sending equal amounts of 1's and 0's ($k = 1$ is 101010..., $k = 2$ is 11001100..., $k = 3$ is 111000111... etc.).

6.3.1 One-to-Zero (o/z) Experiments

The results for the o/z can be seen from Figure 6.2a to 6.2e with an additional one more zero in each following Figure. As it can be seen , the more “0” present in the transmission, less particles are left in the system. And in $o/z = 5$, the signal reaches the background noise of the system.

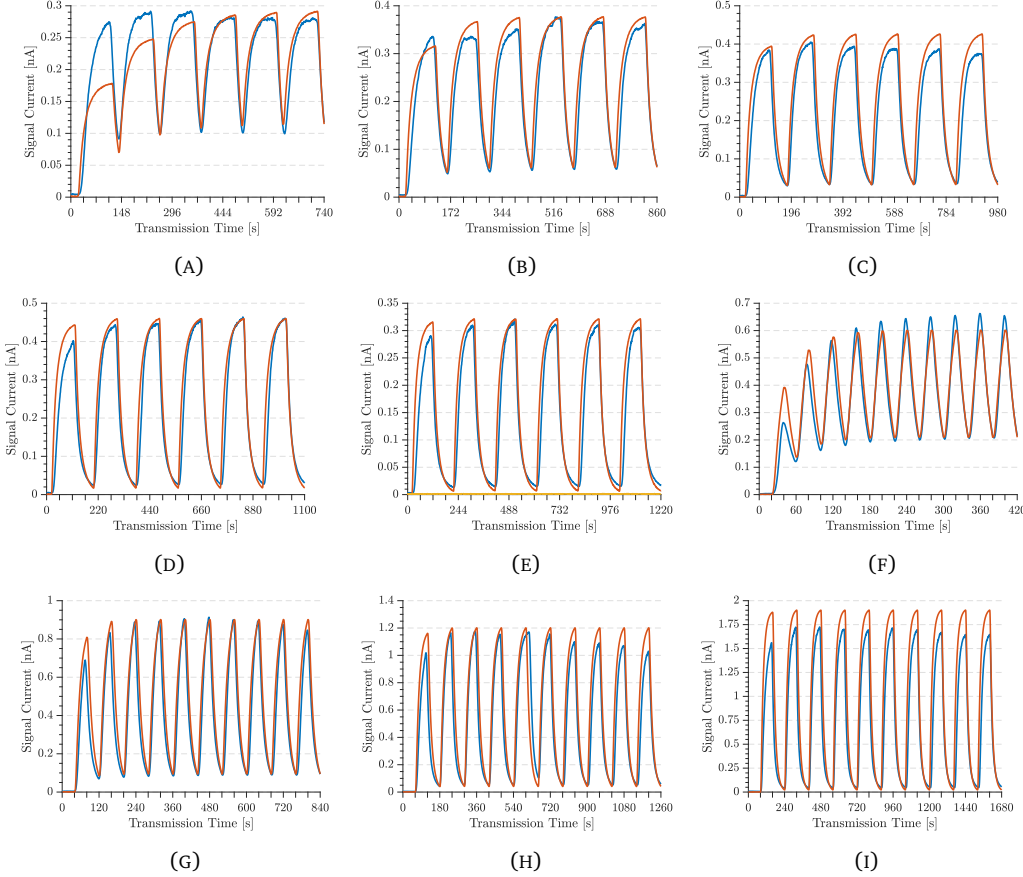


FIGURE 6.2: Experimental (—) along with theoretical (—); (A) Bit transmission of 11111 0 11111 pairs. (B) Bit transmission of 11111 00 11111 pairs. (C) Bit transmission of 11111 000 11111 pairs. (D) Bit transmission of 11111 0000 111111 pairs. (E) Bit transmission of 11111 00000 11111 pairs. (F) Bit transmission of 1 0 1 pairs. (G) Bit transmission of 11 00 11 pairs. (H) Bit transmission of 111 000 111 pairs. (I) Bit transmission of 1111 0000 1111 pairs. (Equations used in modelling: Eq. 4.11c and Eq. 4.14c)

6.3.2 k Experiments

The experimental results of sending equal amounts of 1s and 0s can be seen from Figures 6.2f, 6.2g, 6.2h and 6.2i. As it can be seen when a single sequence of 101010... is transmitted, the system takes time for the absorption/removal process to reach equilibrium. This is due to the way the system absorbs and cleans out the particles inside the detector.

When the system introduces the particles into the detector, the system absorbs based on how much the bit gives in addition to the background noise and when the system clears out

the particles from the detector, the flushing will be proportional to the already present particles in the system. This flushing will increase when the detector has more particles. This will continue until the particles in the system becomes high enough that add/remove function of the communication equalises. However, when the system introduces more particles before a flushing occurs the system needs less pairs to stabilise. This is due to the removal and absorption processes that are directly proportional to the mass injected and mass present in the detector respectively. More mass absorbed by the detector causes more mass to be removed in the removal process, decreasing the time it takes to reach equilibrium.

6.3.3 Residual Background Signal

One of the important aspects of molecular communications is the leftover particles that decrease the amount of information that can be transmitted in a given symbol period. This property is unique to molecular communications. In electromagnetic (EM) communications, the interference is normally constant (i.e., N_0 stays stable). However, in molecular communication, the residual chemicals from 1-bit symbol can gradually increase the desired level and if the symbol duration is not kept at a reasonable duration, it will cause incorrect decoding. To model the ISI the equation derived in Eq. (4.11) is used. In this model the ISI can be modelled based on the interaction of the absorption (θ_1) and the removal (θ_0) of the particles. To simplify the equation, the part of the function where the absorption occurs is defined as:

$$U_{1D}(x_d, t) = \left[\operatorname{erf}\left(\frac{x_d - u_x t}{2\sqrt{D_x t}}\right) + \operatorname{erf}\left(\frac{x_e + u_x t}{2\sqrt{D_x t}}\right) \right], \quad (6.4a)$$

$$U_{2D}(x_d, y_d, t) = \frac{1}{2} \left[\operatorname{erf}\left(\frac{x_d - u_x t}{2\sqrt{D_x t}}\right) + \operatorname{erf}\left(\frac{x_e + u_x t}{2\sqrt{D_x t}}\right) \right] \\ \left[\operatorname{erf}\left(\frac{y_d - u_y t}{2\sqrt{D_y t}}\right) + \operatorname{erf}\left(\frac{y_e + u_y t}{2\sqrt{D_y t}}\right) \right], \quad (6.4b)$$

$$U_{3D}(x_d, y_d, z_d, t) = \frac{1}{4} \left[\operatorname{erf}\left(\frac{x_d - u_x t}{2\sqrt{D_x t}}\right) + \operatorname{erf}\left(\frac{x_e + u_x t}{2\sqrt{D_x t}}\right) \right] \\ \left[\operatorname{erf}\left(\frac{y_d - u_y t}{2\sqrt{D_y t}}\right) + \operatorname{erf}\left(\frac{y_e + u_y t}{2\sqrt{D_y t}}\right) \right] \left[\operatorname{erf}\left(\frac{z_d - u_z t}{2\sqrt{D_z t}}\right) + \operatorname{erf}\left(\frac{z_e + u_z t}{2\sqrt{D_z t}}\right) \right]. \quad (6.4c)$$

In the first part of the experiment (k study) equal numbers of bits ($U_1 = U_0$) were sent in sequence. A diagram of this kind of transmission can be seen in Figure 6.3 (A). Based on this bit transmission, the total ISI caused by the transmission can be expressed as:

$$\theta_{v_{ISI}} = M_0 \sum_{i=1}^{i=n} U_v^i - \frac{M_0}{2} \sum_{i=1}^{i=n} U_v^{i+1}, \quad (6.5)$$

where v is the dimension operator (i.e., $v = 2$ for 2D). In the second part of the experiment (o/z study) an uneven amount of 1's and 0's is sent in sequence ($U_1 \neq U_0$). The diagram for

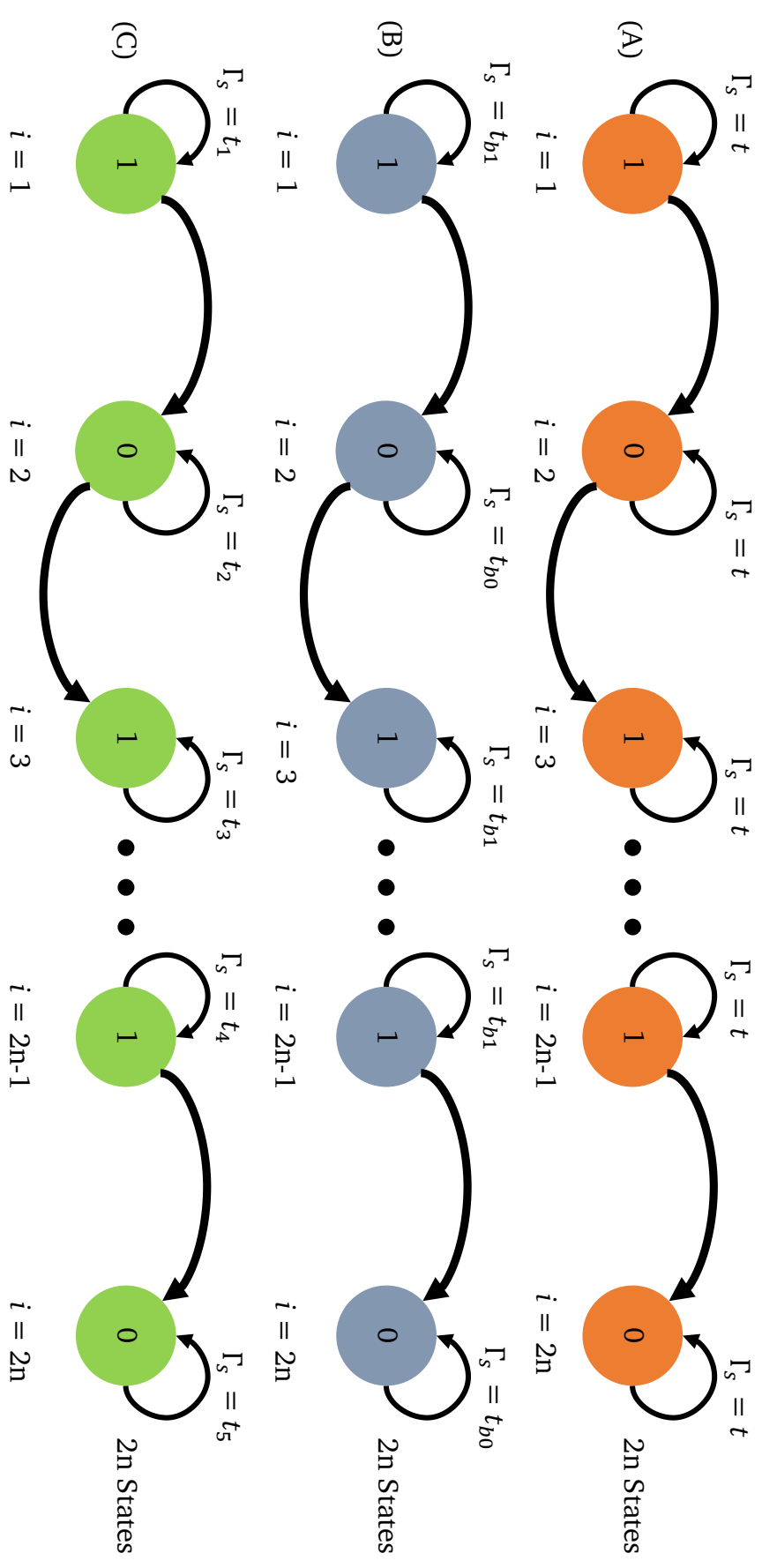


FIGURE 6.3: A diagram of possible transmissions that can create leftover chemicals (θ_{IS^t}). In each sub-plot the bits are shown as circle diagrams and their duration is defined as Γ_s . In this model, shown in Chapter 4, the bits are defined as the continuation of the θ function. For example, a transmission of 111 will have absorbed mass values of $\theta_1(x, T)$, $\theta_1(x, 2T)$ and $\theta_1(x, 3T)$, respectively. Based on this behaviour, each different bit is defined as a state and can be seen in the sub-plots. (A) A sequential transmission of 1's and 0's continuously (e.g., 110011001100...) (B) A transmission of uneven amounts of 1's and 0's (e.g., 100010001001...) (C) A transmission where the transmission ends with chemical introduction into the environment (e.g., 10110001110111...)

this transmission can be seen in Figure 6.3 (B). This change in transmission can be modelled as:

$$\theta_{v_{ISI}} = M_0 \sum_{i=1}^{i=n} U_{v_0}^i - \frac{M_0}{2} U_{v_1} \sum_{i=1}^{i=n} U_{v_0}^i. \quad (6.6)$$

If the transmission has an even amount of state changes between bits 1 and 0, which can be seen in Figure 6.3 (C), the generalised equation that gives ISI is:

$$\theta_{v_{ISI}} = M_0 \sum_{j=1}^{j=n} \prod_{i=j}^{i=n} U_{v_{2i}} - \frac{M_0}{2} \sum_{j=1}^{j=n} U_{v_{2j-1}} \prod_{i=j}^{i=n} U_{v_{2i}}, \quad (6.7)$$

and if the transmission has an odd amount of state changes, the equation can be written by including an additional absorption (θ_1) value to Eq. (6.7):

$$\theta_{v_{ISI}} = M_0 \sum_{j=1}^{j=n} \prod_{i=j}^{i=n} U_{v_{2i}} - \frac{M_0}{2} \sum_{j=1}^{j=n} U_{v_{2j-1}} \prod_{i=j}^{i=n} U_{v_{2i}} + M_0 - \frac{M_0}{2} U_{v_{2n+1}}. \quad (6.8)$$

The results of the leftover background-noise experiment compared to the theoretical model can be seen in Figures 6.4a and 6.4b for a o/z study and k study, respectively.

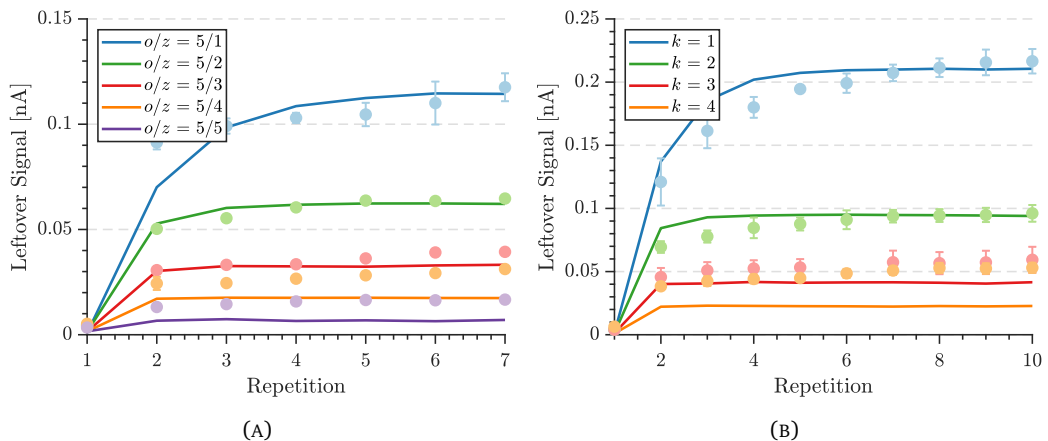


FIGURE 6.4: (A) Experimental results of the leftover chemicals from k experiment along with theoretical comparison. (B) Experimental results of the o/z bit transmission with comparison to the theoretical model. (Equations used in modelling: Eq. 4.11c and Eq. 4.14c)

As can be seen, the model agrees well with the experimental data when the leftover particles from the transmission create a large amount of interference. However, as the chemicals create less and less interference, the model prediction becomes less accurate. This is due to the effect of the ambient noise playing a more important role. To mitigate the effect, an optimal time for the symbol period can be calculated based on the equations derived in Chapter 4.

The Optimal Symbol Period (OSP) can be calculated by maximising the value in the error function $\text{erf}(\cdot)$. For the detector to retain no chemicals from transmission the error function must produce the value 1. However, due to the impracticality of this ($\text{erf}(\infty) = 1$), a finite

value must be chosen for the determination of the OSP. For a given value of $n = 2$ the error function produces the value of 0.995, which can be used for the practical cases of molecular communications.

By solving the error functions ($\text{erf}(\cdot)$) present in the absorption/removal equations given in Eq. (4.18), the optimal sampling period can be calculated. As can be seen in both equations, there are two error functions. The main differences being the distance values; former being x_d and latter being x_e . Since the distance that chemicals travel against the flow is negligible compared to the actual distance of the propagation ($x_d \gg x_e$) only the former part of the equation is used in calculation of the optimal sampling period. For a given n value the optimal symbol period (T_{OSP}) can be calculated as follows:

$$n_x = \left(\frac{x_d - u_x T_{\text{OSP}}}{2\sqrt{D_x T_{\text{OSP}}}} \right), \quad n_y = \left(\frac{y_d - u_y T_{\text{OSP}}}{2\sqrt{D_y T_{\text{OSP}}}} \right), \quad n_z = \left(\frac{z_d - u_z T_{\text{OSP}}}{2\sqrt{D_z T_{\text{OSP}}}} \right). \quad (6.9)$$

By solving the aforementioned equation with respect to T_{OSP} two solutions (T_{\max} , T_{\min}) can be derived which are presented below:

$$T_{1D_{\max}} = \frac{u_x x_d + 2D_x n_x^2 + 2n_x \sqrt{D_x (D_x n_x^2 + u_x x_d)}}{u_x^2}, \quad (6.10a)$$

$$T_{1D_{\min}} = \frac{u_x x_d + 2D_x n_x^2 - 2n_x \sqrt{D_x (D_x n_x^2 + u_x x_d)}}{u_x^2}. \quad (6.10b)$$

To calculate the 2D solution it is assumed the diffusion is homogeneous across all cartesian dimensions ($D_x = D_y = D_z$).

$$T_{2D_{\max}} = \frac{u_y x_d + 4D_x n_x n_y + u_x y_d}{2u_x u_y} + \frac{\sqrt{8D_x n_x n_y (2D_x n_x n_y + u_x y_d + u_y x_d) + (u_x y - u_y x_d)^2}}{2u_x u_y}, \quad (6.11a)$$

$$T_{2D_{\min}} = \frac{u_y x_d + 4D_x n_x n_y + u_x y_d}{2u_x u_y} - \frac{\sqrt{8D_x n_x n_y (2D_x n_x n_y + u_x y + u_y x) + (u_x y_d - u_y x_d)^2}}{2u_x u_y}, \quad (6.11b)$$

$$\max \{ \theta_{v_{ISI}} \} \quad \text{if} \quad T \leq T_{v_{\min}}, \quad (6.12a)$$

$$\theta_{v_{ISI}} > 0 \quad \text{if} \quad T_{v_{\min}} < T < T_{v_{\max}}, \quad (6.12b)$$

$$\min \{ \theta_{v_{ISI}} \} \quad \text{if} \quad T \geq T_{v_{\max}}. \quad (6.12c)$$

As long as the above criterion in Eq. (6.12c) are not met, transmission will retain the ISI during the communication. The presence of the ISI will shift the distribution of 0 bits to a higher value as the transmission evolves, and if the receiver uses a static threshold detection (τ_s), it will increasingly decode 0 wrongly as the transmission continues and will create an uneven probability between $p(1|0)$ and $p(0|1)$, making the communication asymmetric.

6.4 Message Transmission Experiment

One of the major problems of using molecules in transmission is the leftover from previous chemicals. Chemical sensors, therefore need to be cleaned in order to overcome the problem of the memory effect. However, the sensor cleaning time can be long especially with a membrane present in the detector, adding a further delay to the signal. Moreover, because of the behaviour of molecular communications, the transmission time given for a single bit may not be enough for the signal to reach to the background noise level, e.g., if there is a single 0 between a string of 1's, the 0 bit produces a higher signal current than the background noise level at the beginning of the transmission (i.e., a single 0 cannot flush all the chemicals leftover from consecutive 1's). In addition, the next "1" bit adds additional chemicals (θ_1) to the leftover chemicals (θ_{ISI}) which in turn produces even higher signal current. Therefore, if there are more 1's than 0's present in the transmission this could lead to an increase of the overall signal amplitude, making a simple threshold detector inefficient at decoding the transmission correctly.

In the experimental transmission system, the signal current values (measured by the QMA) for the "1" bit ranges from 0.1 nA to 0.53 nA and 0 ranges from 0.37 nA to 0.006 nA. The overlaps between 0 values and 1 caused by the residual chemicals from the previous bit can cause incorrect decoding of the transmitted signal. To overcome this, instead of relying on the amplitude values of each bit, the behaviour of the bits relative to the previous bit was investigated

6.4.1 Results

The properties of chemical transmission make the simple threshold detection inefficient because of varying amplitude values based on the residue chemicals from previous transmission, therefore a detection method based on relative bit value is better suited for this type of communication system. The mechanism of the algorithm is as follows;

- The initial bit is determined by a predefined threshold in which this experiment is defined as $\tau_s = 0.1$ nA.
- The second bit is then defined relative to the previous decoded bit; if it is higher it is defined as 1, lower it is defined as 0.

To avoid errors due to unpredicted signal amplitude changes (e.g., due to fluctuations in the air), the following error correction routine was implemented:

TABLE 6.3: Parameters for the message transmission study.

Experimental Parameter	Symbol	Value	Unit
Tracked signal flow ion	m/z	43	Da
Signal flow	q	8	ml/min
Carrier flow	Q	750	ml/min
Bit duration	t_b	20	s
Acetone Detection delay [45]	t_d	15	s
Transmission distance	x_d	2.5 ± 0.1	cm
Carrier flow pressure	P_F	1	bar
Diffusivity of acetone in air ¹	D	0.124	cm ² /s
Theoretical Parameter	Symbol	Value	Unit
Injected Mass	M_0	0.4	ng
Advective flow in x -axis	u_x	0.12	cm/s
Advective flow in y -axis and z -axis	u_y & u_z	0	cm/s
Transmission distance	x_d	2.5	cm
Detector radius	R_D	0.3	cm
Longitudinal diffusivity	D_L	0.124	cm ² /s
Radial diffusivity	D_T	1×10^{-3}	cm ² /s
Noise mean & variance	μ_N, σ_N^2	1.21, 0.096	pA, W/ion

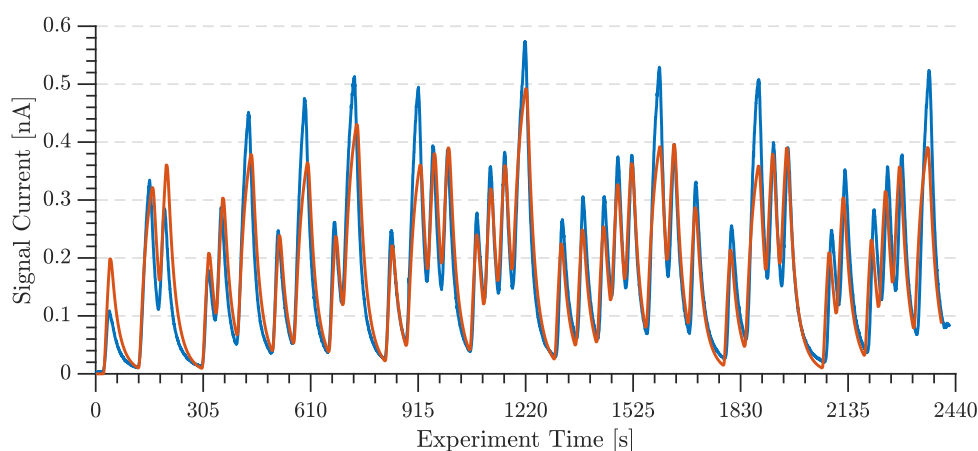
¹ Normal air and temperature

FIGURE 6.5: Experimental (—) along with theoretical (—) transmission of the message “Call Me Ishmael”. (Equations used in modelling: Eq. 4.11c and Eq. 4.14c)

- Every retrieved signal data was compared to the previous one and if the difference is within a specified range it was defined as the previous bit. The range is calculated empirically since every chemical will react differently with the detector. For acetone, the range value coefficient assigned as $k_\tau = 0.1$.

The results of the transmission can be seen in Figure 6.5. In the experiment, a message was sent in ASCII binary code. The message chosen was the first line from the novel Moby Dick “*Call me Ishmael*” [355]. The message was converted to chemical data where bit “1” was assigned as a signal gas pulse of 8 ml/min and bit “0” was with no pulse; and both bits having a carrier flow of 750 ml/min nitrogen gas was used. Using a static threshold value of $\tau_s = 0.191$ nA, 5 bits out of 120 transmitted were decoded incorrectly however, with the algorithm the decoding error value decreased to 1 bit in 120 bits. The errors occurred with the threshold detection is due to the changing amplitudes of 0’s and 1’s as the transmission evolves. The lower errors in the relative bit decoding shows that the algorithm is better at decoding a molecular message than threshold detection.

6.5 Channel Capacity

When a 1-bit symbol is introduced to the detector, unless the symbol duration is shorter than the optimal given in Eq. (6.12c), the detector will absorb less mass than it was introduced into the environment. Moreover, since the flush mechanics relies on the particles that are already in the detector, the bit 0 cannot remove all the particles in the detector in the given time. Based on the ISI properties of the communication mentioned in the previous section, the communication channel can be expressed as asymmetric. The diagram of the channel can be seen in Figure 6.6.

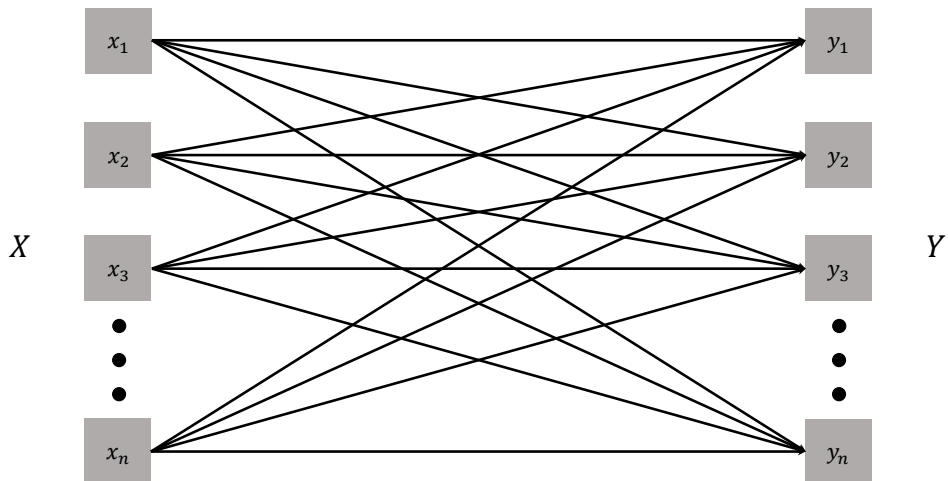


FIGURE 6.6: Representative diagram of a binary asymmetric channel.

To define the channel capacity, the mutual information ($I(\cdot; \cdot)$) must be measured. The channel capacity with a block length of n that possesses memory effects can be generalised have the following equation [82, 86]:

$$C \triangleq \lim_{n \rightarrow \infty} \sup \frac{1}{n} I(X^n; Y^n). \quad (6.13)$$

The mutual information is a measure of how much one random variable tells about another with the definition of it given below [82]:

$$I(X^n; Y^n) = H(Y^n) - H(Y^n | X^n), \quad (6.14)$$

where $H(Y^n)$ is the Shannon entropy of the probability vector Y and $H(Y^n | X^n)$ is the conditional entropy of Y given X . Based on the equations given in Eq. (6.13) and (6.14), the achievable MI is calculated by simulating the probabilities based on the simulation framework given in Chapter 4.

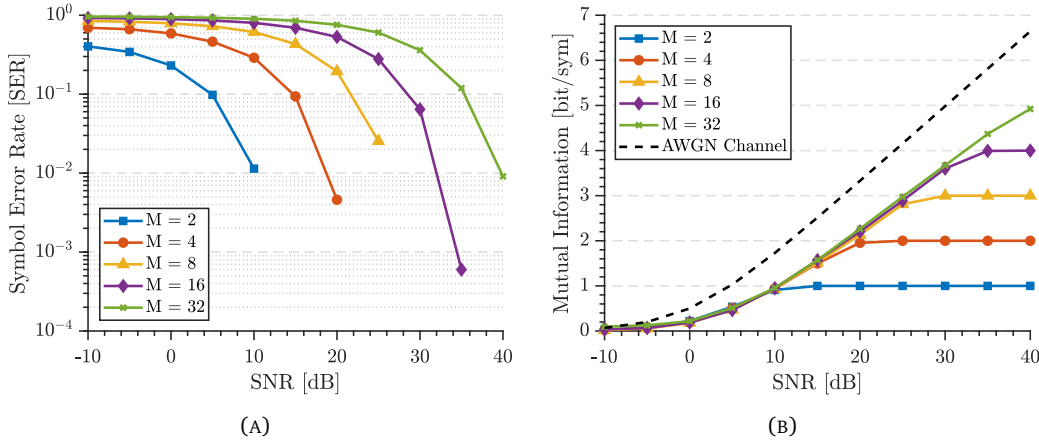


FIGURE 6.7: (A) Theoretical results of the Symbol-Error Rate (SER) of M_C -ary transmission. (B) Theoretical results of the achievable mutual information (MI) rate of M_C -ary transmission.
($x_d = 2.5$ cm, $u_x = 0.2$ cm/s, $D_L = 0.124$ cm 2 /s, $T_S = 60$ s, $M = 0.4$ ng)

6.6 Symbol-Error Rate (SER)

To analyse the symbol-error rate (SER) properties of Macro-scale molecular communications, an experiment was conducted, with the parameters of the experimental setup can be seen in Table 6.4.

Bit duration of 5s, 10s, 15s and 20s are experimented. Each experiment transmitted 100 bits randomised with equal probabilities of 1s and 0s. In each experiment 300 μ l of sample is introduced into the Evaporation Chamber (EC). 5s, 10s, 15s and 20s experiments were done 3 times and the average error is taken.

The experimental along with the theoretical comparison of SER can be seen in Figure 6.8a. The theoretically calculated MI based on the experimentally obtained SER can be seen in Figure 6.8b. As it can be seen, the experimental results show agreement with the

TABLE 6.4: Parameters for symbol error rate (SER) transmission study.

Experimental Parameter	Symbol	Value	Unit
Tracked signal flow ion	m/z	43	Da
Signal flow	q	8	ml/min
Carrier flow	Q	750	ml/min
Acetone Detection delay [45]	t_d	15	s
Transmission distance	x_d	2.5 ± 0.1	cm
Environment pressure	P_E	1 ± 0.003	bar
Carrier flow pressure	P_F	1	bar
Vacuum pump pressure	P_V	1.95×10^{-6}	torr
Environment temperature	T_E	297.35 ± 1.5	K
Diffusivity of acetone in air ¹	D	0.124	cm^2/s
Theoretical Parameter	Symbol	Value	Unit
Injected mass	M_0	1	ng
Advective flow in x -axis	u_x	0.02	cm/s
Advective flow in y -axis and z -axis	u_y & u_z	0	cm/s
Transmission distance	x_d	2.5	cm
Detector radius	R_D	0.3	cm
Longitudinal diffusivity	D_L	0.124	cm^2/s
Radial diffusivity	D_T	1×10^{-3}	cm^2/s
Noise mean & variance	μ_N, σ_N^2	1.21, 0.096	pA, W/ion

¹ Normal air and temperature

numerical results obtained from the simulation ($\rho = 0.94$). A static threshold (τ_s) was used in decoding of the received bits. The theoretical analysis of M-ary modulation in terms of SER and MI can be seen in Figure 6.7a and Figure 6.7b respectively. To calculate the mutual information for both experimental and theoretical results, the Shannon entropy along with conditional entropy are calculated individually and subtracted from each other as shown in Eq. (6.14).

6.7 Theoretical Results

In this section of the study, three parameters of the transmission are studied for symbol error rate (SER) analysis and the channel capacity. These parameters are: transmission distance (x), longitudinal diffusivity (D_L) and advective flow (u_x). Two types of comparisons were made. Firstly, a comparison was made by varying the signal-to-noise ratio (SNR) for both SER and mutual information and secondly, the parameter becomes the variable for SER and mutual information to better observe the parameters effect on these communication properties. The parameters used in the theoretical study can be seen in Table 6.5.

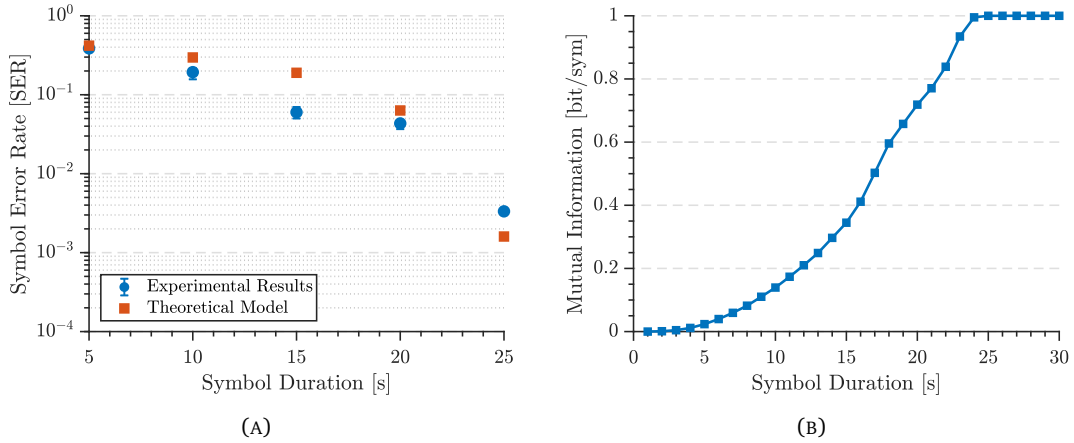


FIGURE 6.8: (A) Experimental (—) along with theoretical (—) comparison of the SER experiment. (B) Achievable mutual information based on the theoretical model shown in (A).

TABLE 6.5: Theoretical parameters for symbol error rate (SER) and mutual information (MI) study.

Theoretical Parameter	Symbol	Value	Unit
Injected mass	M_0	1	ng
Transmission distance	x_d	2.5	cm
Advective flow in x -axis	u_x	0.1	cm/s
Advective flow in y -axis & z -axis	u_y & u_z	0	cm/s
Longitudinal diffusivity	D_L	0.1	cm ² /s
Radial diffusivity	D_T	1×10^{-4}	cm ² /s
Symbol duration	T_S	60	s

6.7.1 Symbol Duration

As it can be seen in Figure 6.9a and Figure 6.9b, as the symbol period is increased, the attainable mutual information experiences an increase and the amount of errors in the system decreases.

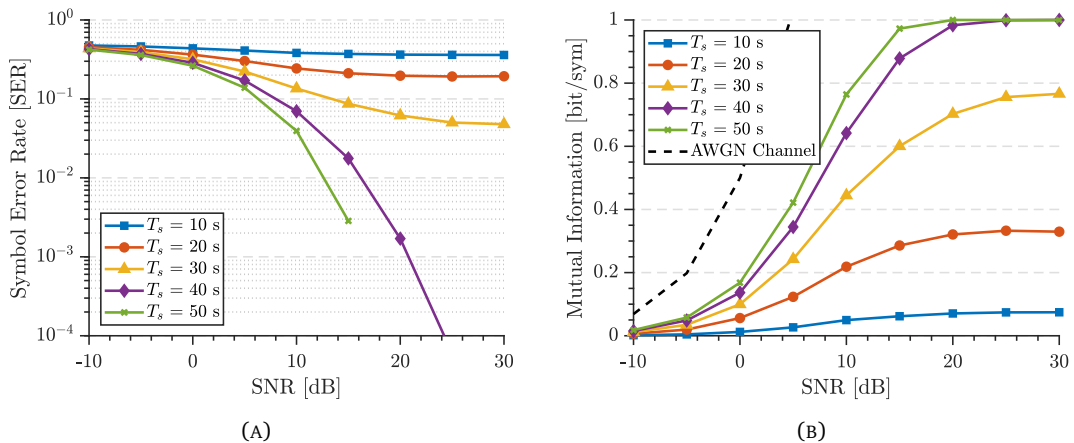


FIGURE 6.9: (A) SER of different durations of symbol time (T_s) values with respect to SNR. (B) Achievable MI of different durations of symbol time (T_s) values with respect to SNR.

This behaviour is attributed to the amount of energy given per symbol (E_s). As the symbol time increases, the average energy per symbol will see an increase which is the primary factor in improving the capacity and decreasing the produced SER. This effect can also be observed in Figure 6.10a and Figure 6.10b where the increase of symbol duration increases the MI.

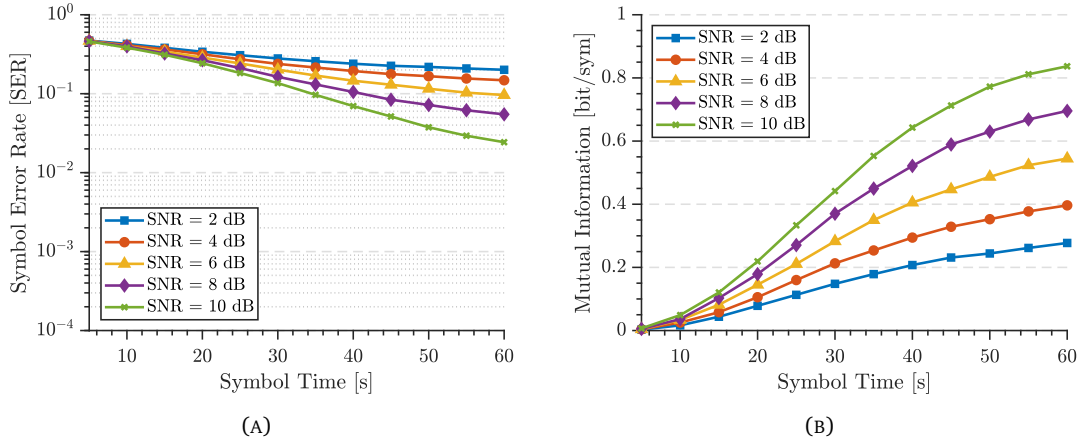


FIGURE 6.10: (A) SER with increasing symbol duration (T_S). (B) Achievable MI with increasing symbol duration (T_S).

6.7.2 Coefficient of Diffusivity

In Figures 6.11a and 6.11b, it can be seen that the increase of diffusivity has negligible effect on the SER and the MI.

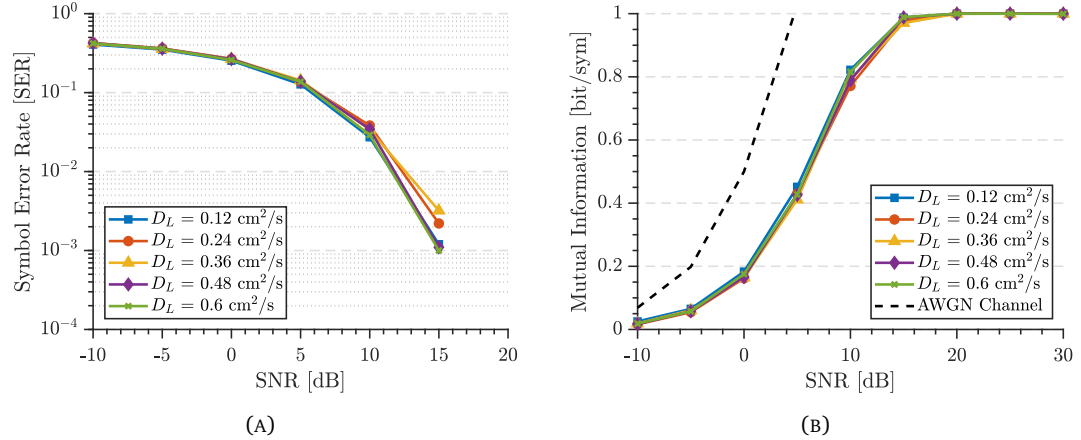


FIGURE 6.11: (A) SER of different coefficients of diffusivity (D_L) values with respect to SNR. (B) Achievable MI of different coefficients of diffusivity (D_L) values with respect to SNR.

This could be due to the fact that with the presence of an advective flow, the effect of diffusion is suppressed where the increase of the parameter plays a minor role. However in Figures 6.12a and 6.12b, it can be seen that with the increase of the SNR the effects of diffusion become more noticeable and based on the simulation results, the effect seems to increase the MI. However as stated the effect is negligible.

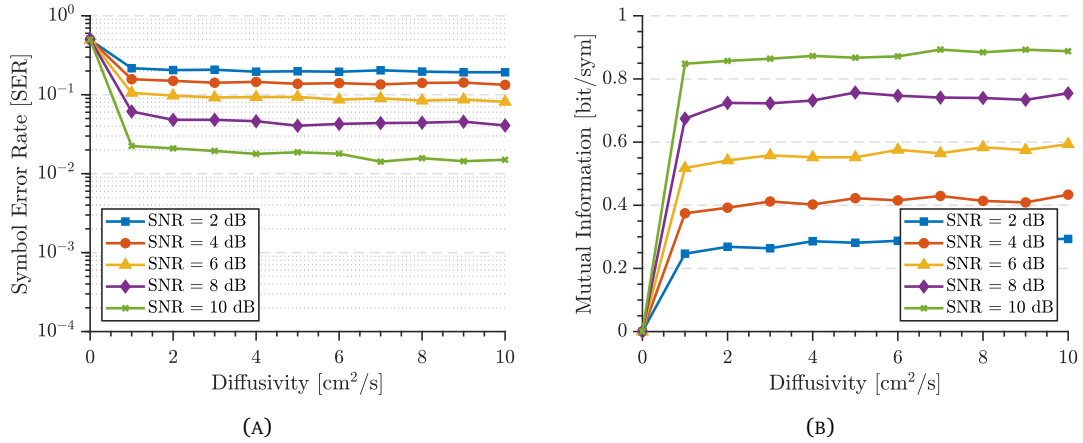


FIGURE 6.12: (A) SER with increasing coefficients of diffusivity (D_L). (B) Achievable MI with increasing coefficients of diffusivity (D_L).

6.7.3 Transmission Distance

As it can be seen in Figures 6.13a and 6.13b, as the transmission distance is increased, the attainable mutual information experiences a decrease and the amount of errors in the system sees an increase.

This is caused by the insufficient time given for the detector to detect the particles. As distance increases, the propagation time increases as well and additionally the diffusive properties dilutes the transmission, where the chemicals start propagating in directions other than the path of the advective flow, which increases the time needed to absorb all the chemicals in the medium. The effect of increased transmission distance can be seen in Figures 6.14a and 6.14b.

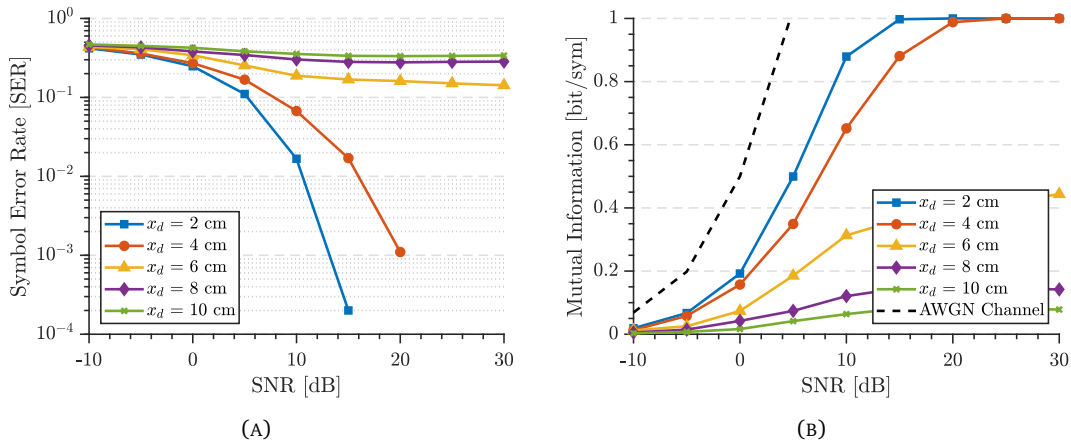


FIGURE 6.13: (A) SER of different transmission distance (x_d) values with respect to SNR. (B) Achievable MI of different transmission distance (c_d) values with respect to SNR.

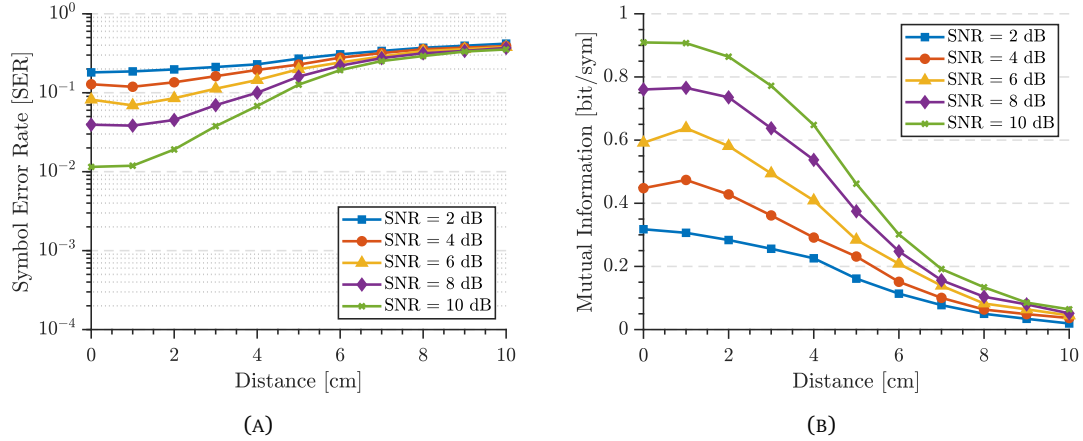


FIGURE 6.14: (A) SER with increasing transmission distance (x_d). (B) Achievable MI with increasing transmission distance (x_d).

6.7.4 Advection Flow

The effect of advective flow on the channel capacity can be seen in Figure 6.16b and 6.15b. As the velocity of the transmission is increased, the channel capacity sees an increase with a corresponding decrease in errors. This is caused by the effect of advection rather than the effect of diffusion.

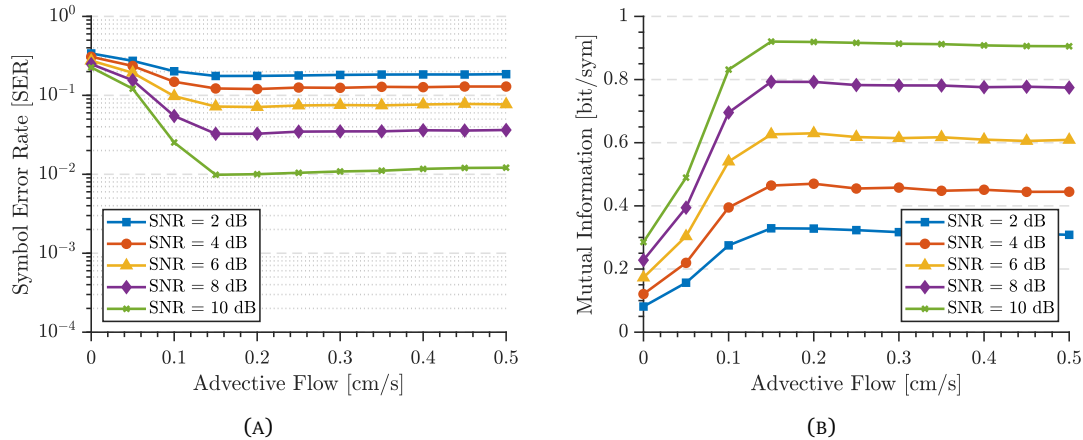


FIGURE 6.15: (A) SER of different advective flow (u_x) values with respect to SNR. (B) Achievable MI of different advective flow (u_x) values with respect to SNR.

The effect of advection has a higher increase in channel capacity than diffusion. The effect of increasing the advective flow on the increase of the MI and the reduction of the SER can be seen in Figures 6.16a and 6.15a.

6.8 Bit Distribution

To analyse the bit distribution of molecular communications, simulations were done by changing the properties of the propagation. These are: longitudinal diffusivity, advective

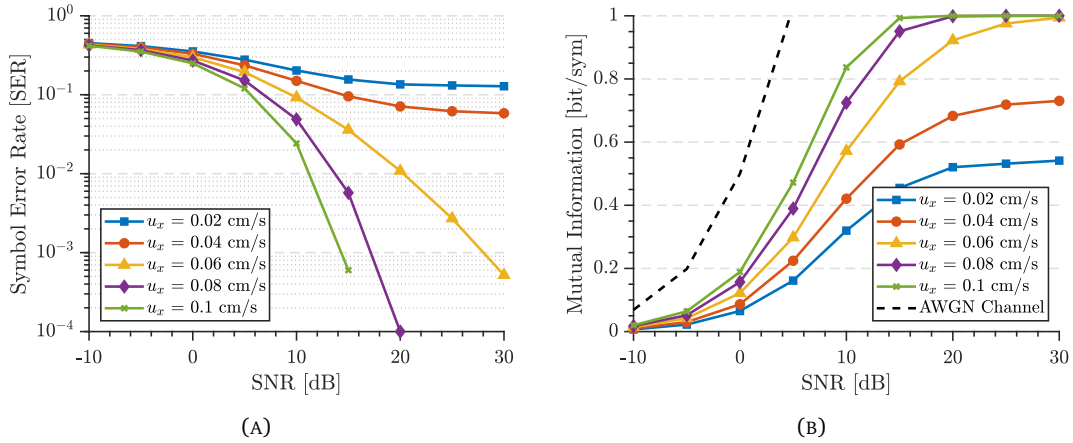


FIGURE 6.16: (A) SER with increasing advective flow (u_x). (B) Achievable MI with increasing advective flow (u_x).

flow and the transmission distance. The effect of these parameters will be analysed by transmitting 4-level transmission.

6.8.1 Symbol Period

The effect of symbol period on the symbol distribution can be seen in Figure 6.17a and distribution variance in Figure 6.17b. As can be seen from both figures, the increase of symbol period has a positive effect on the separation of the symbol distribution and decreases the variance of the distribution of the symbols.

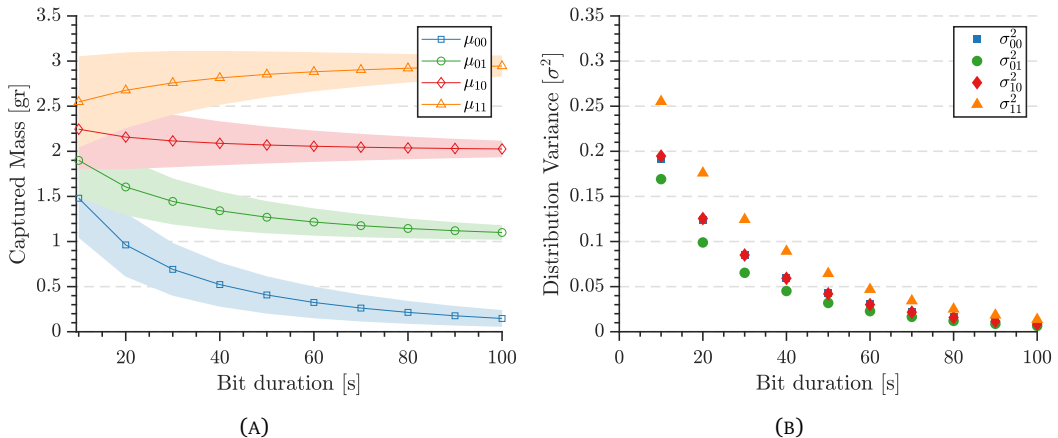


FIGURE 6.17: Simulation results of the symbol distribution of the transmitted symbol. In the plot μ are the mean value of the received mass of their respective symbol.

6.8.2 Advective Flow

Advection is defined as the transport of a substance by the use of bulk motion. In this chapter, the advection is modelled as a 1-D vector in the x -direction and the effect of the flow on bit distribution can be seen in Figure 6.18a. As can be seen, the increase in flow plays a major

role in the decrease in the variance (σ^2) of the distribution and the stability of the mean (μ) of the distribution. The results show that a small increase in the flow plays a substantial role in the separation of bits.

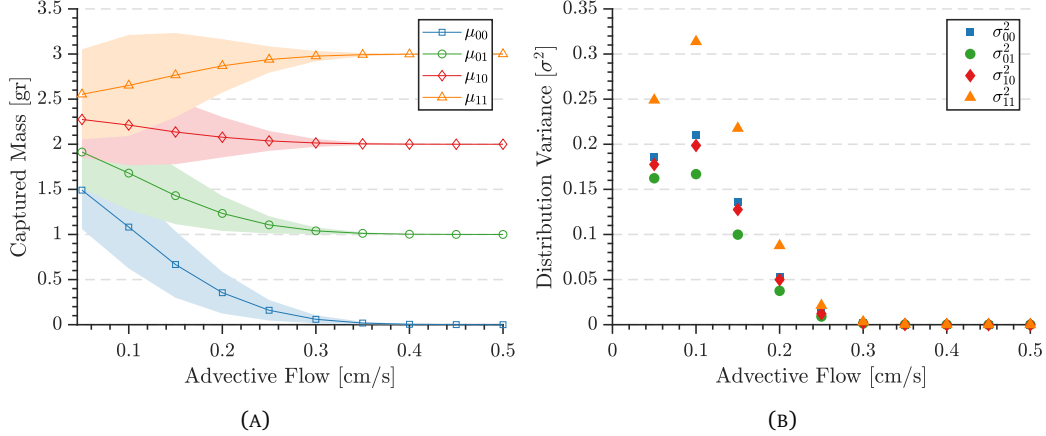


FIGURE 6.18: Simulation results of the symbol distribution of the transmitted symbol. In the plot μ are the mean value of the received mass of their respective symbol.

6.8.3 Diffusivity

Diffusivity is the action the particle take by utilising internal energy to propagate in a random fashion. Some particles will move against the direction of the flow which causes delay in the saturation and the flush of the signal, i.e. when bit 1 is introduced, the action of absorption takes longer as diffusivity is increased and flush time is increased as diffusivity is increased.

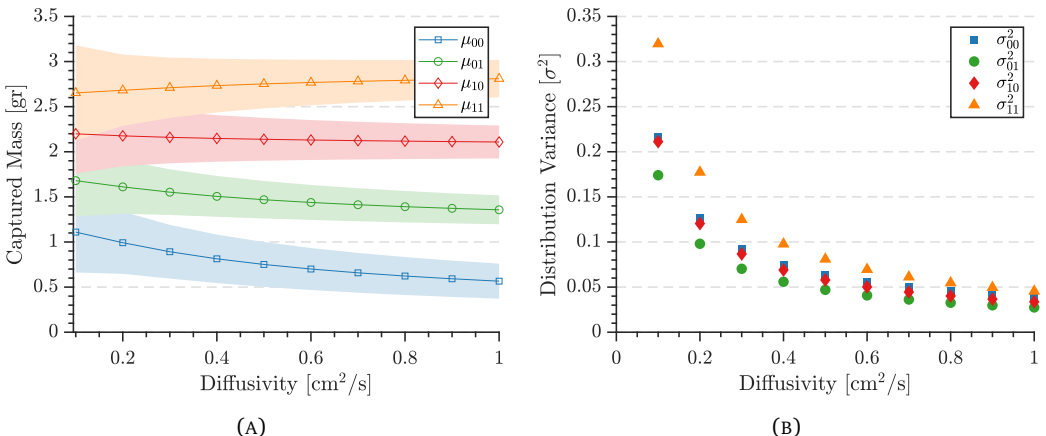


FIGURE 6.19: Simulation results of the symbol distribution of the transmitted symbol. In the plot μ are the mean value of the received mass of their respective symbol.

Because of this, the effect of increased diffusivity does not have a profound effect on the decrease of the bit distribution variance as advective flow. The results also show that an increase in advection is a much better choice for improving the detection of bits than increasing the diffusivity.

6.8.4 Transmission Distance

One of the detrimental effects of molecular communication is the distance of transmission (x_d). Because the advective flow (u_x) of the system cannot compensate for the increase in distance, the detection of the chemicals gets delayed and particles that are sent get misdirected from the transmission path so that less particles arrive at the detector. Straying from the path can be caused by numerous parameters such as diffusivity of the transmitted particles, flow or collisions with particles present in the environment.

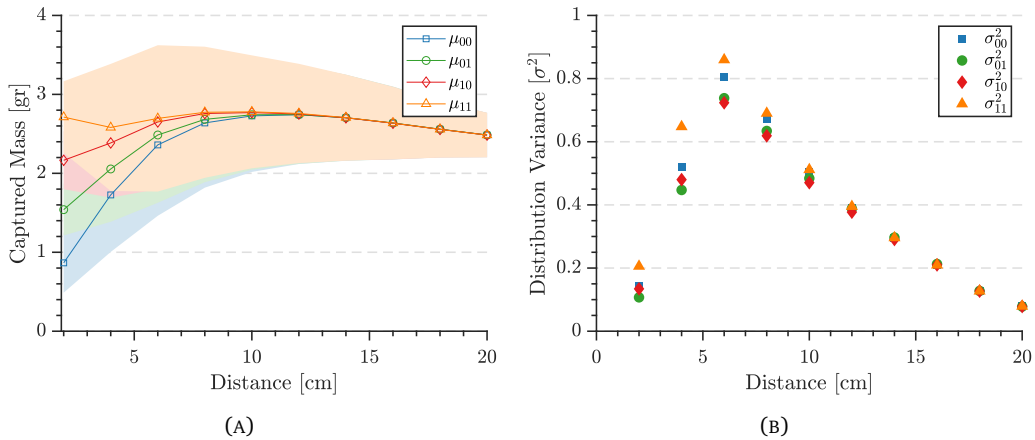


FIGURE 6.20: Simulation results of the symbol distribution of the transmitted symbol. In the plot μ are the mean value of the received mass of their respective symbol.

The distribution of chemicals with the transmission distance can be seen in Figure 6.20b and the variance can be seen in Figure 6.20a. As can be seen the increase of distance causes the bit distributions to merge. This in turn causes a decrease in correct decoding of the message and given enough distance makes communication impossible.

6.9 Conclusion

This chapter presents an experimental and analytical study on the M-ary transmission properties of macro-scale molecular communications. As a transmitter, an in-house-built odour generator was used and as a detector a mass spectrometer with a quadrupole mass analyser (QMA) was utilised. $M_C = 2$, $M_C = 4$ and $M_C = 8$ level transmissions were made experimentally using a solution of acetone and methanol as the signal chemical. A simulation model was developed based on the advection-diffusion equation and was compared to experimentally detected signals. It was shown that the simulation agrees with the experimental results. In addition, experimental results of the SER analysis of acetone on $M_C = 2$ level modulation, a theoretical analysis was made on the $M_C = 4$ and $M_C = 8$ level modulation along with a theoretical comparison of $M_C = 2$, which produced similar results to the experiment. A binary asymmetric channel was used to model the channel capacity and determine the optimum symbol rate for this particular macro molecular communications system. It was shown

that the macro-scale molecular communication can be modelled and simulated using a variation of the advection-diffusion equation. In addition, parameters such as advective flow aids in terms of reducing the SER more than increasing the diffusivity coefficient and the distance at which transmission takes place has a detrimental effect on the channel capacity of the system. An in-depth analysis into Mo-ISI was carried and by using the model developed in Chapter 4 it was shown that the model is able to replicate the experimental results. From the model equations were derived that allow calculations of the ISI in a given transmission. Based on the model discussed in Chapter 4, the bit distribution of the transmission is studied for three parameters and their effects were discussed. The Following Chapter will focus on the multiple chemical transmission of molecular communication.

Chapter 7

Multi-Chemical Transmission

7.1 Introduction

Molecular communication is an alternative to the present transmission techniques, using particles instead of waves. This change in the propagation methods opens novel modulation methods not present in EM communication such as the characteristics of the particle being transmitted. Every chemical, molecule and compound have specific properties that make them unique and by exploiting this, the throughput and the channel capacity of the molecular communication can be increased. However, to test multiple chemical transmission, a sensor that can distinguish chemicals by a specific property must be used. As described in Chapter 3, a Membrane-Inlet Mass Spectrometer (MIMS) with a Quadrupole Mass Analyser is used as the receiver. Mass spectrometers (MS) have the ability to analyse and distinguish multiple chemicals simultaneously which makes it a suitable detector for use in this application [250].

The novel contributions of the Chapter are as follows;

- **Multi-Chemical Transmission:** An experimental proof-of-transmission along with theoretical comparison was conducted with additional analysis of multiple-chemical noise.
- **Molecular Quadrature Amplitude Modulation (MQAM):** Influenced by its EM counterpart, theoretical analysis was done on this modulation scheme with analysis on the parameters of the communication for SER and MI.
- **Chemical Time Offset Keying (ChToK):** A modulation method is proposed based on the relative position of signals in a given time-frame.
- **Chemical Ratio Keying (ChRK):** A modulation method is proposed based on the amplitude of the chemicals relative to each other in a given symbol period.

In the simulations conducted in the chapter, it is assumed that the transmission possesses Additive White Gaussian Noise (AWGN) ($\mathcal{N}(\mu_N, \sigma_N^2)$) based on the single chemical noise analysis in [9] and the multi noise analysis conducted in this study. Finally, it is assumed that there are no interferences between carriers.

TABLE 7.1: Parameters for multi-chemical transmission study.

Experimental Parameter	Symbol	Value	Unit
Tracked signal flow ion	m/z	$31^1, 43^2$	Da
Signal flow	q	8	ml/min
Carrier flow	Q	750	ml/min
Transmission distance	x_d	2.5 ± 0.1	cm
Acetone Detection delay [45]	t_d	20	s
Environment pressure	P_E	1 ± 0.003	bar
Carrier flow pressure	P_F	1	bar
Vacuum pump pressure	P_V	1.95×10^{-6}	torr
Environment temperature	T_E	297.35 ± 1.5	K
Diffusivity in air ³	D	$0.15^1, 0.124^2$	cm ² /s
Theoretical Parameter	Symbol	Value	Unit
Injected mass	M_0	$1^1, 3.6^2$	ng
Advective flow in x -axis	u_x	0.04	cm/s
Advective flow in y -axis & z -axis	u_y & u_z	0	cm/s
Transmission distance	x_d	2.5	cm
Detector radius	R_D	0.3	cm
Longitudinal diffusivity	D_L	$0.15^1, 0.124^2$	cm ² /s
Radial diffusivity	D_T	$0.005^1, 0.003^2$	cm ² /s
Noise mean & variance	μ_N, σ_N^2	1.21, 0.096	pA, W/ion

¹ Methanol ² Acetone ³ Normal air and Temperature

7.2 Multi Chemical Transmission

An experiment was undertaken to test the possibility of sending two chemical species simultaneously. To detect and analyse multiple chemicals simultaneously, a mass spectrometer (MS) was used which its inner workings were described in detail in Chapter 3. The signal chemicals were chosen as acetone with tracked ion of m/z 43 and methanol with tracked ion of m/z 31. The experimental parameters used in the experiment can be seen in Table 7.1.

The experimental result of the transmission along with the theoretical comparison can be observed in Figure 7.1a. As can be seen, two signal chemicals (acetone & methanol) were transmitted simultaneously. However it must be noted that there is a difference in the amplitude from the captured particle of two chemical species. This can be caused by numerous effects such as the particles interaction with the detector inlet (i.e., PDMS membrane), the presence of another messenger particles interaction, the ionisation efficiency of the samples inside the detector. In this transmission, acetone produced a higher signal current than methanol. However, the retrieved signal of methanol (31 Da) has experienced considerable amount of distortion compared to acetone (43 Da).

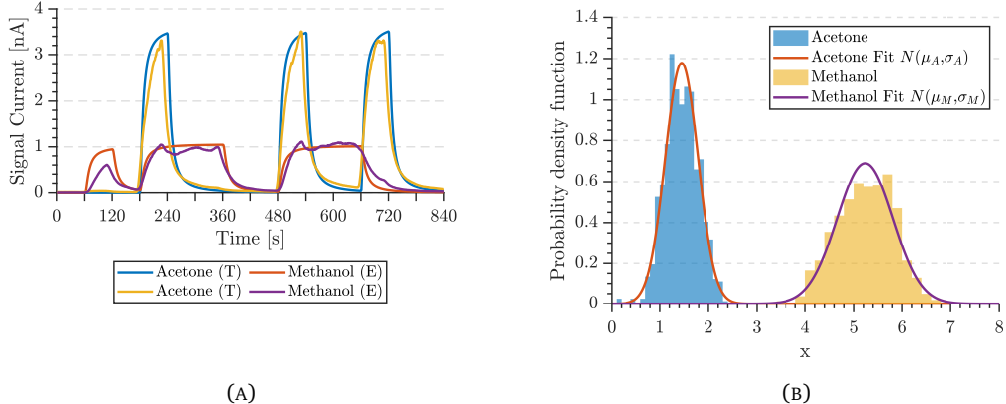


FIGURE 7.1: (A) Experimental results along with theoretical results of multi-chemical transmission. (Equations used in modelling: Eq. 4.11c and Eq. 4.14c) (B) Experimental along with theoretical fitting of multi-chemical noise.

The mathematical model presented in Chapter 4, Section 4.2.1 and its comparison to experimental data can be seen in Figure 7.1a. As can be seen, the model shows agreement with the experimental data. To quantify the agreement with experimental data to the theoretical model Pearson correlation is used [353]:

$$\rho_{E,T} = \frac{\text{cov}(E, T)}{\sigma_E \sigma_T}, \quad (7.1)$$

where E is the experimental data and T is the theoretical data. Based on the equation, Acetone produced a correlation coefficient of $\rho = 0.96$ and Methanol produced a correlation coefficient of $\rho = 0.94$ showing that the model shows validity in analysing and predicting multiple chemical transmission. A final comment needs to be made in the initial pulsation of the methanol signal. This “transient” behaviour can be caused by the complex interactions of the membrane and the chemicals. After the initial interaction the signal becomes easily predictable by the model developed and presented in Chapter 4.

7.3 Multi Chemical Noise

One of the important limitations in a communication system is the disturbances in the environment which influences the transmission. The noise in molecular communications can be caused by numerous effects. These include particles present in the environment, minute pressure differences in the inlet of the detector, temperature and pressure of the environment etc.. A study was done in [9] that shows experimentally that the noise of a single chemical in the environment effecting the transmission is AWGN. In this experiment, the presence of multiple chemicals noise is conducted to analyse the noise in a multi-channel transmission. The experimental parameters can be seen in Table 7.2.

The results can be seen in Figure 7.1b. As can be seen the results show a strong relation to Gaussian distribution for both mass-to-charge values. To quantify the goodness-of-fit, Kolmogorov-Smirnov test is used [352]. The equation of this test is given below:

TABLE 7.2: parameters for multi-chemical noise study.

Experimental Parameter	Symbol	Value	Unit
Tracked acetone ion	m/z	43	Da
Tracked methanol ion	m/z	38	Da
Environment pressure	P_E	1.005	bar
Carrier flow pressure	P_F	1	bar
Vacuum pump pressure	P_V	2.85×10^{-6}	torr
Environment temperature	T_E	291.85	K
Diffusivity of acetone in air ¹	D	0.124	cm^2/s
Diffusivity of methanol in air ¹	D	0.15	cm^2/s

¹ Normal air and temperature

$$D_n = \sup_x |F_n(x) - F(x)|, \quad (7.2)$$

Based on the test, the result for acetone is $D_n = 0.0267$ and for methanol is $D_n = 0.0448$, which shows that the noise data is drawn from a Gaussian distribution with a significance level of $\alpha = 0.05$. From these results it can be seen that each chemical possesses a different noise mean (μ_N) and variance (σ_N^2). In addition, from Figure 7.1a it can be seen that the amplitude of signal reaches different values for different chemicals show that each chemical has a different signal-to-noise ratio (SNR). The multi-chemical noise measured can be given as:

$$\mu_A = 1.45 \times 10^{-3}, \quad \sigma_A = 0.33 \times 10^{-3}, \quad (7.3a)$$

$$\mu_M = 5.23 \times 10^{-3}, \quad \sigma_M = 0.57 \times 10^{-3}. \quad (7.3b)$$

7.4 Molecular Quadrature Amplitude Modulation (MQAM)

By using more than a single chemical species to transmit information, the amount of bits encoded in a given symbol can be increased, which in turn increases the channel capacity (C) of the transmission.

In this section a molecular analogy of quadrature amplitude modulation (QAM) is developed, whereby coding a bit value into the amplitude value of more than one chemical, increases the number of bits in a symbol.

The amount of elements that can be coded to a molecular amplitude can be expressed by the cardinality (i.e., number of elements in a set) of the input set with following equation:

$$\text{card}(M) = \phi^{\text{Ch}}, \quad (7.4)$$

where ϕ is the number of modulated levels on the chemicals and Ch is the number of distinguishable chemicals used in the transmission of information. Based on this, the channel

capacity of an n block transmission with memory effects can be written using the following generalised equation [86]:

$$C \triangleq \lim_{n \rightarrow \infty} \sup \frac{1}{n} I(X^n; Y^n). \quad (7.5)$$

In the above equation $I(X^n; Y^n)$ represents the mutual information between the input alphabet X and the output Y with the following identity [82]:

$$I(X^n; Y^n) = H(Y^n) - H(Y^n|X^n), \quad (7.6)$$

where $H(Y^n)$ is the Shannon entropy of the probability vector Y and $H(Y^n|X^n)$ is the conditional entropy of Y given X .

As mentioned previously, an advantage of molecular communication over conventional EM communications is the ability to increase the amount of carrier signals in a given channel. For example, in the experimental analysis shown in Figure 7.1a, it was shown that it is possible to transmit multiple chemicals at the same time. These chemicals have the possibility of transmitting information with negligible interference.

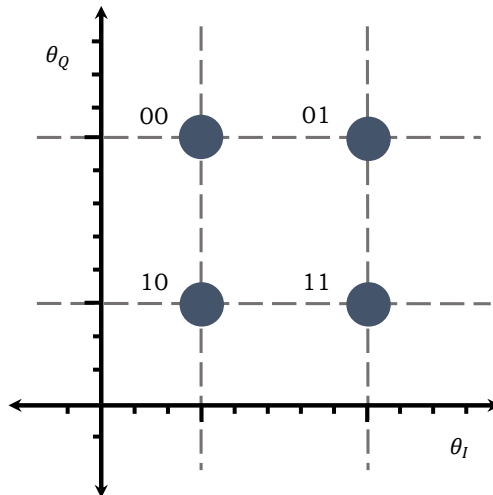


FIGURE 7.2: A constellation diagram for use in molecular quadrature amplitude modulation (MQAM).

Based on these experimental results shown in Figure 7.1a and Figure 7.1b a theoretical analysis was carried out on multiple chemical transmission. In this analysis, two chemicals were chosen as information carriers and assumed to cause no interference to each other. One chemical is given the designation θ_Q and the second chemical is defined as θ_I . Two levels of mass were chosen ($\theta_Q = \theta_I = 1$, $\theta_Q = \theta_I = 2$) for encoding information. The constellation diagram used in the simulation can be seen in Figure 7.2. Based on these descriptions the SER and the MI can be seen in Figure 7.3a and Figure 7.3b respectively.

As can be seen, the maximum information (compared to Shannon's Law [85]) sees a considerable increase with each chemical species introduced, however the errors produced

TABLE 7.3: Theoretical parameters of molecular quadrature amplitude modulation (MQAM).

Theoretical Parameter	Symbol	Value	Unit
Injected mass	M_0	1	ng
Transmission distance	x_d	2.5	cm
Advective flow in x -axis	u_x	0.1	cm/s
Advective flow in y -axis & z -axis	u_y & u_z	0	cm/s
Longitudinal diffusivity	D_L	0.1	cm ² /s
Radial diffusivity	D_T	1×10^{-3}	cm ² /s
Symbol duration	T_S	20	s
Detector radius	R_D	0.3	cm

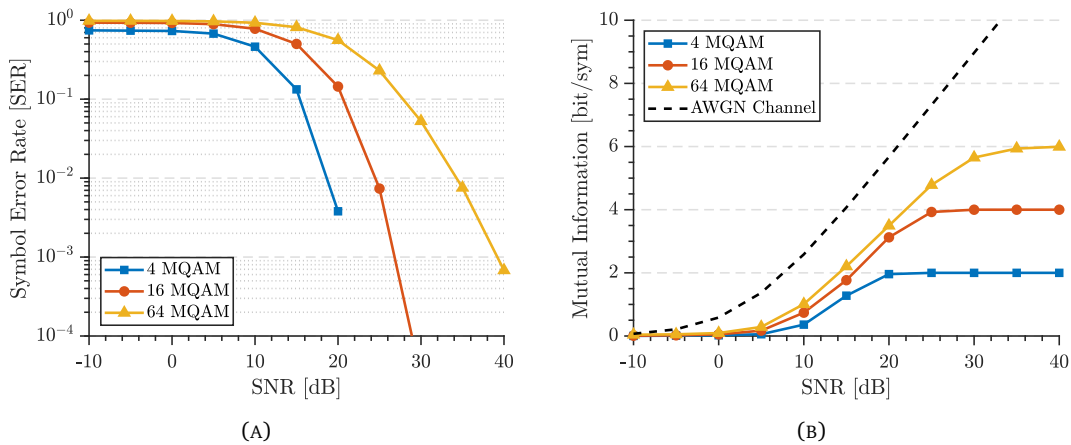


FIGURE 7.3: (A) Simulation results of the SER of MQAM transmission. (B) Simulation results of the MI of MQAM transmission.

from the constellation experiences a considerable increase as well. This is due to the increase of symbols that can interfere with their neighbouring symbol values.

The upper bound symbol-error rate (SER) for the MQAM method with AWGN present in the transmission can be given as:

$$P_s \leq 1 - \left(1 - \left(1 - \frac{1}{\sqrt{M_C}} \right) \text{erfc} \left(\sqrt{\frac{3 \log_2 M_C}{2(M_C - 1)} \left(\frac{E_b}{N_0} \right)} \right) \right), \quad (7.7)$$

where M_C is the number of constellations in the modulation and E_b is the energy per bit (W). The following subsection will focus on the effect of the three parameters (longitudinal diffusion, advective flow and transmission distance) on the MI and SER of the MQAM. The values used in the theoretical study can be seen in Table 7.3.

7.4.1 Advective Flow

The effect of the advective flow (u_x) on the modulation can be seen in Figure 7.4a. As it can be seen, the increase of flow has a profound effect on the position of the detected mass values (θ_I, θ_Q). Lower velocity values have shown that the detected bit values are scattered away

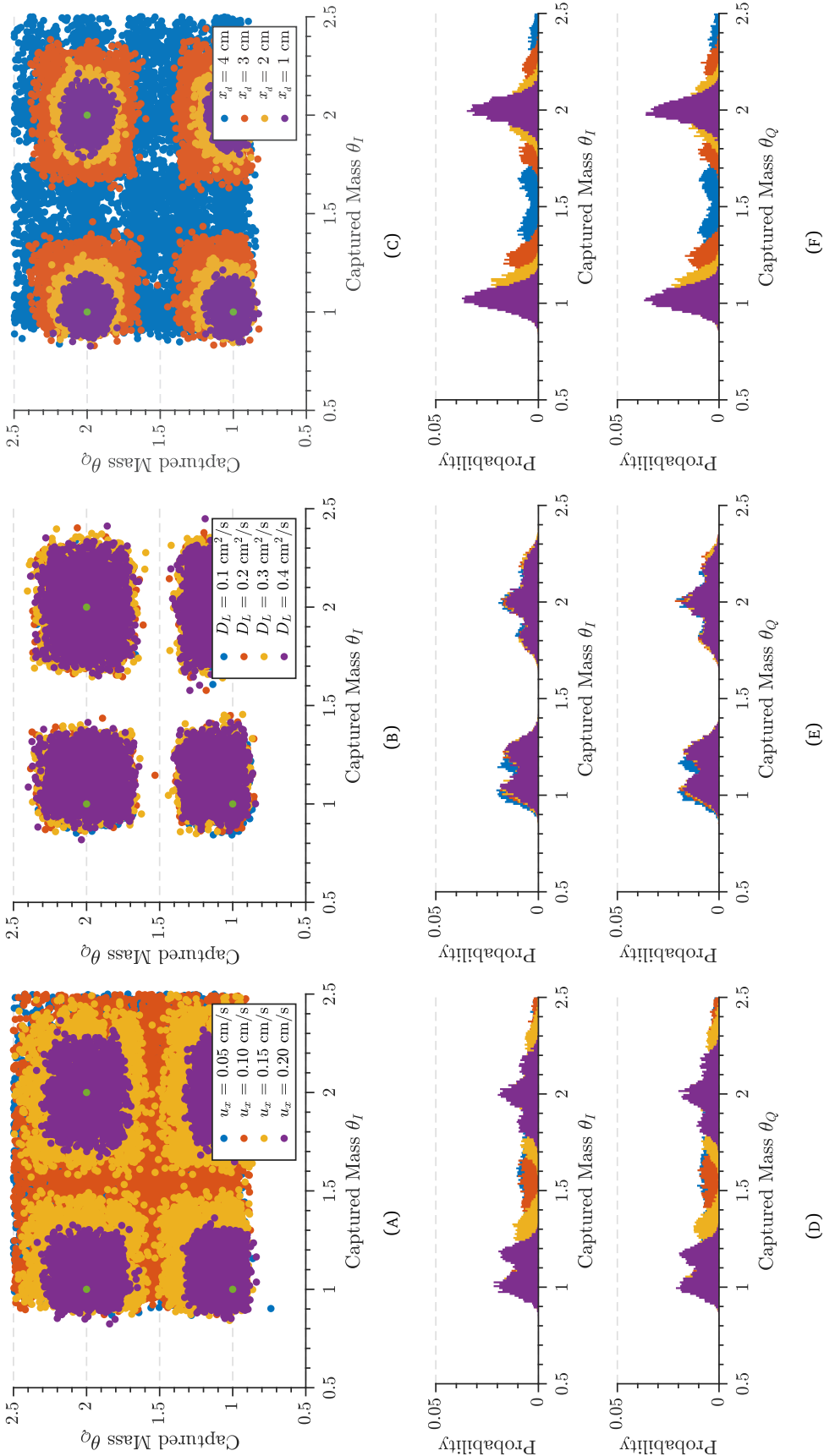


FIGURE 7.4: Simulation results of molecular communication using molecular quadrature amplitude modulation (MQAM): (A) Constellation diagram of MQAM with different advective flow rates. (B) Constellation diagram of MQAM with longitudinal diffusivity rates. (C) Distribution of received θ_I and θ_Q masses with different advective flow rates. (D) Distribution of received θ_I and θ_Q masses with different transmission distance rates. (E) Distribution of received θ_I and θ_Q masses with different longitudinal diffusivity rates. (F) Distribution of received θ_I and θ_Q masses with different transmission distance rates. [Ideal R_X value (●)]

from the ideal R_X value. Increasing the flow rate, decreases the variance of the detected mass values and begins concentrating the values closer to the ideal R_X value. The distribution of masses with different advective flow can be seen in Figure 7.4d.

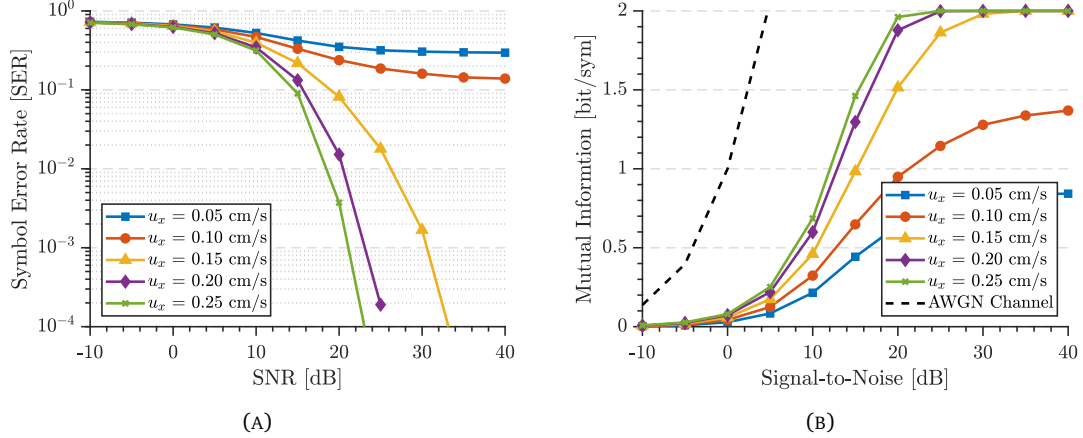


FIGURE 7.5: (A) Simulation results of the SER of MQAM transmission for different advective flows.
(B) Simulation results of the MI of MQAM transmission for different advective flows.

The theoretical analysis of $M_C = 4$ analysis for different advective flows can be seen in Figure 7.5a for SER and Figure 7.5b for MI. As mentioned, advective flow plays a positive role in increasing the MI and decreasing the SER encountered during transmission.

7.4.2 Coefficient of Diffusivity

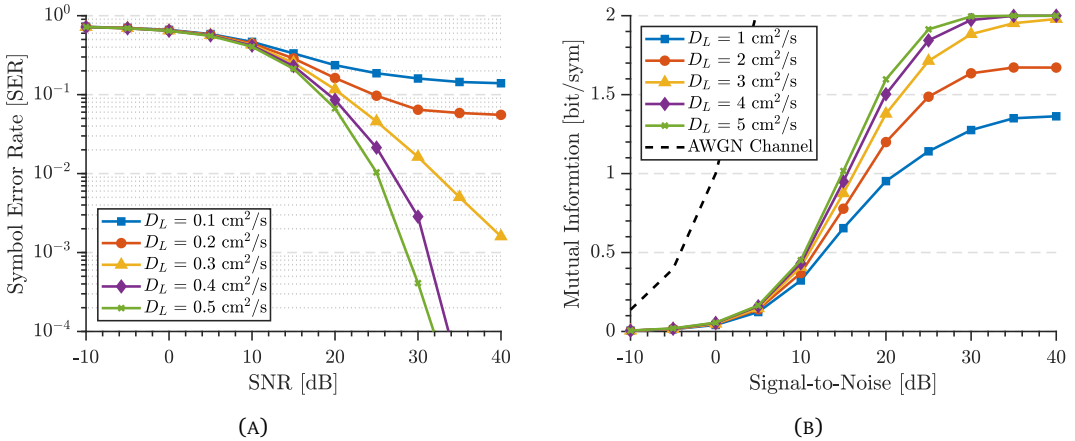


FIGURE 7.6: (A) Simulation results of the SER of MQAM transmission for different longitudinal diffusion.
(B) Simulation results of the MI of MQAM transmission for different longitudinal diffusion.

Diffusivity plays a negligible effect on the transmission as a whole which can be observed in Figure 7.4b and the received mass distribution can be seen in Figure 7.4e. While the effect is necessary for transmission without external energy, when an active transport is present, the effect of diffusivity does not play a primary role on the clarity of the detected bits. This is likely due to the dominance of the advective flow over the diffusivity of the transmitted

chemicals. This effect can also be observed in SER and MI in Figure 7.6b and Figure 7.6a respectively.

7.4.3 Transmission Distance

The effect of the transmission distance on the bit detection can be seen in Figure 7.4c and on received mass distribution can be seen in Figure 7.4e. As can be seen when transmission distance (x_d) is increased, the divergence of the received bits from the ideal R_X value also increases. In addition, as distance is decreased, the concentration of received bits approach closer to the ideal R_X value. Unlike the advective flow this behaviour is detrimental to the communication. This effect can also be observed in SER and MI in Figure 7.7a and Figure 7.7b respectively.

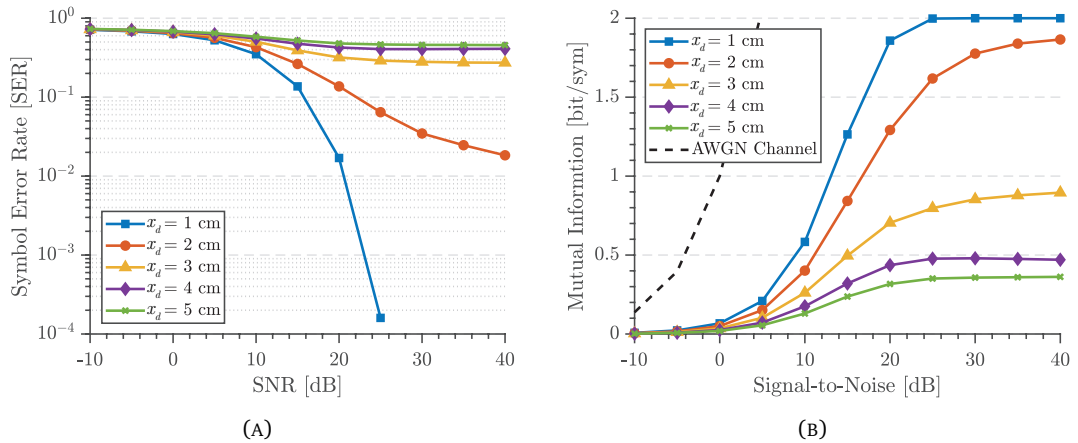


FIGURE 7.7: (A) Simulation results of the SER of MQAM transmission for different transmission distance. (B) Simulation results of the MI of MQAM transmission for different transmission distance.

7.5 Chemical Time Offset Keying (ChToK)

An alternative way of modulating the signal is to add relative relations between each signal. As it is in EM communication, an implementation of Phase Shift Keying (PSK) is implemented into molecular communication in this study along with experimental test. The diagram of this modulation can be seen in Figure 7.8 where T is the period of the pulse of a chemical (s), δT is the time frame which the chemical can be shifted (s) and T_F is the duration of the frame (s). Therefore the cardinality of the modulation can be represented as:

$$\text{card}(M) = \left(\frac{T_F}{\delta T} \right)^{\text{Ch}}. \quad (7.8)$$

If number of modulated levels (ϕ) are also implemented into the modulation, the equation can be rewritten as:

$$\text{card}(M) = \left(\phi \left(\frac{L}{\delta T} \right) \right)^{\text{Ch}}. \quad (7.9)$$

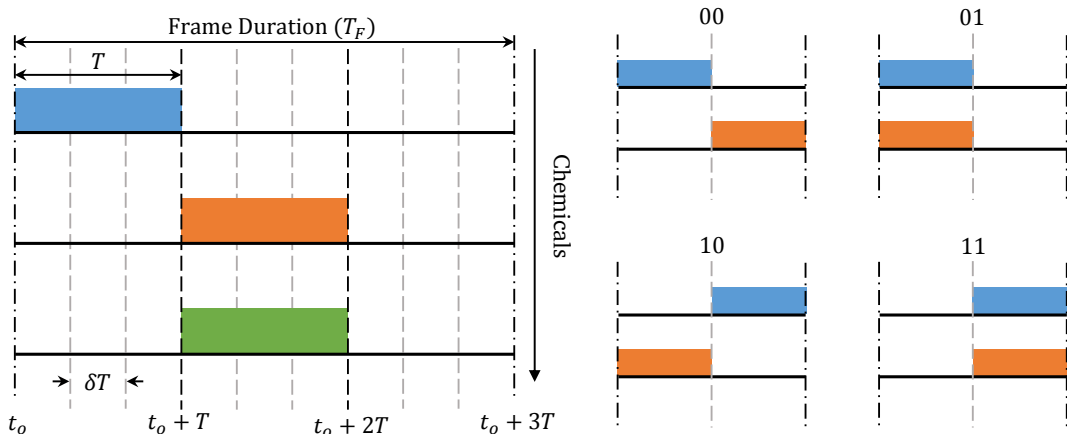


FIGURE 7.8: Diagram representing the chemical shift keying (ChSK).

This modulation, as can be seen has four parameters that can be used to increase the number of bits transmitted. By introducing more chemicals to the modulation scheme, more information can be encoded to a single pulse of chemical mixture. This modulation could also be used for secure communication as the modulation can be established to be time sensitive which can be used to transmit information in a secure manner. This, however opens up additional problems that are needed to be overcome, the primary one being the synchronisation between the transmitter and the receiver. In addition due to the chemicals' diffusivity, physical limits are imposed on the time unit δT (i.e., Limit of Detection, Limit of Quantification, Sampling Rate).

The sampling rate is determined by the sensor being used. For the QMA used in the study, the sampling rate is determined by the mass range being scanned. For long mass ranges (50-1050) the maximum scan rate is 8.3 Hz however, as the MIMS can only analyse the samples that have a lower mass than 200 Da, the scan rate can be increased up to 28.14 Hz for use in multi-chemical communication.

7.5.1 Experimental Analysis

An experimental transmission of ChToK was done with the experimental parameters are shown in Table 7.4. The experimental results of the ChToK can be seen in Figure 7.9. The ASCII letter “x” was transmitted by using Acetone and Methanol as signal chemicals, where in a given time frame, if the peak of the acetone appears first compared to methanol, it is given the symbol 0, and symbol 1 is given for the inverse case.

It can be observed that the signal amplitude of each chemical reach different peaks. This can be caused by various effects, such as inlet interactivity with chemicals, chemicals own interactivity or chemicals inherent properties. In each chemical period T , there are two distinguishable peaks, leading or lagging relative to Acetone. Figure 7.10 is shown for the validation of the mathematical model in predicting the modulated signal for the transmission

TABLE 7.4: Parameters for chemical time offset keying transmission study.

Experimental Parameter	Symbol	Value	Unit
Tracked signal flow ion	m/z	$31^1, 43^2$	Da
Signal flow	q	8	ml/min
Carrier flow	Q	750	ml/min
Acetone detection delay [45]	t_d	20	s
Transmission distance	x_d	2.5 ± 0.1	cm
Detector radius	R_D	0.3	cm
Environment pressure	P_E	1 ± 0.003	bar
Carrier flow pressure	P_F	1	bar
Vacuum pump pressure	P_V	1.95×10^{-6}	torr
Environment temperature	T_E	297.35 ± 1.5	K
Diffusivity in air ³	D	$0.15^1, 0.124^2$	cm^2/s
Theoretical Parameter	Symbol	Value	Unit
Advective flow in x -axis	u_x	0.02	cm/s
Advective flow in y -axis & z -axis	u_y & u_z	0	cm/s
Transmission distance	x_d	2.5	cm
Detector radius	R_D	0.3	cm
Longitudinal diffusivity	D_L	$0.15^1, 0.124^2$	cm^2/s
Radial diffusivity	D_T	$0.001^{1,1}$	cm^2/s
Noise mean & variance	μ_N, σ_N^2	1.21, 0.096	pA, W/ion

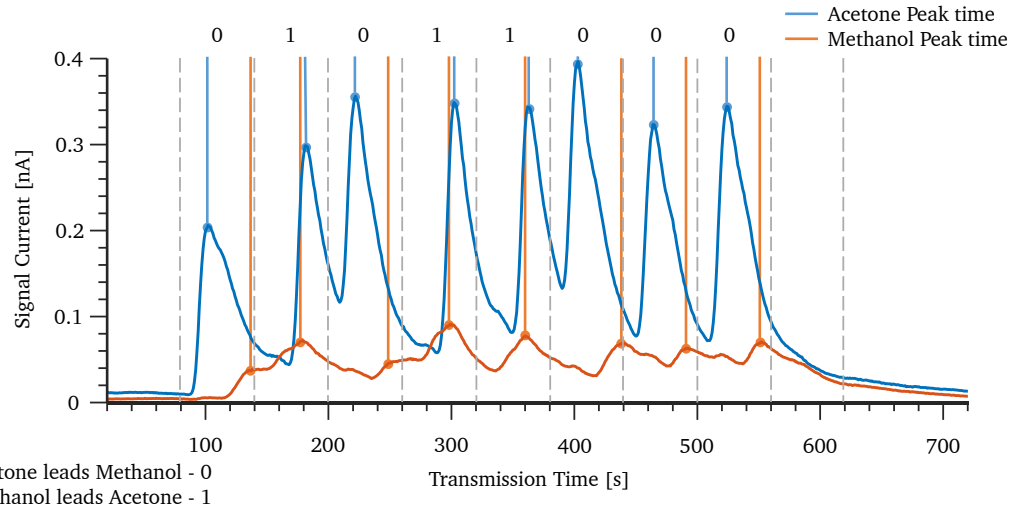
¹ Methanol ² Acetone ³ Normal air and temperature

FIGURE 7.9: Experimental transmission of acetone and methanol using ChToK.

of acetone chemical. As can be seen the mathematical model, described in Chapter 4, shows agreement ($\rho = 0.96$) with the experimentally transmitted signal.

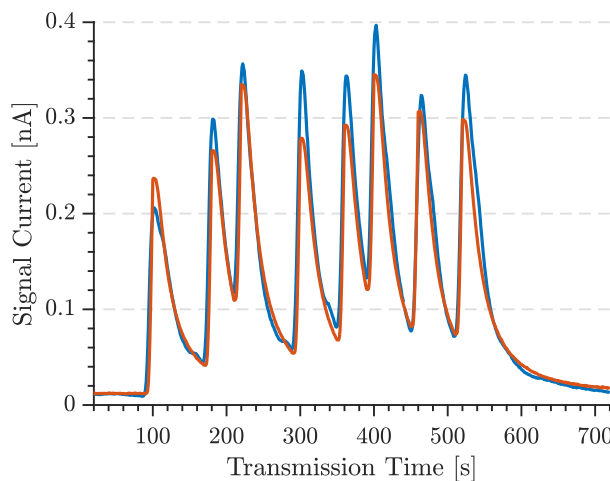


FIGURE 7.10: Experimental transmission of the acetone (—) along with the theoretical comparison (—). (Equations used in modelling: Eq. 4.11c and Eq. 4.14c)

7.6 Chemical Ratio Modulation (CRM)

One of the defining aspects of molecular communication is, as mentioned previously, the possibility of transmitting multiple chemicals simultaneously. This approach allows implementation of novel modulation approaches that may not be common in EM communications. One such being the use of multiple chemical ratios to transmit information. Here information is encoded based on the ratio between two or more chemicals transmitting simultaneously. A diagram that represents the chemical ratio keying can be seen in Figure 7.11.

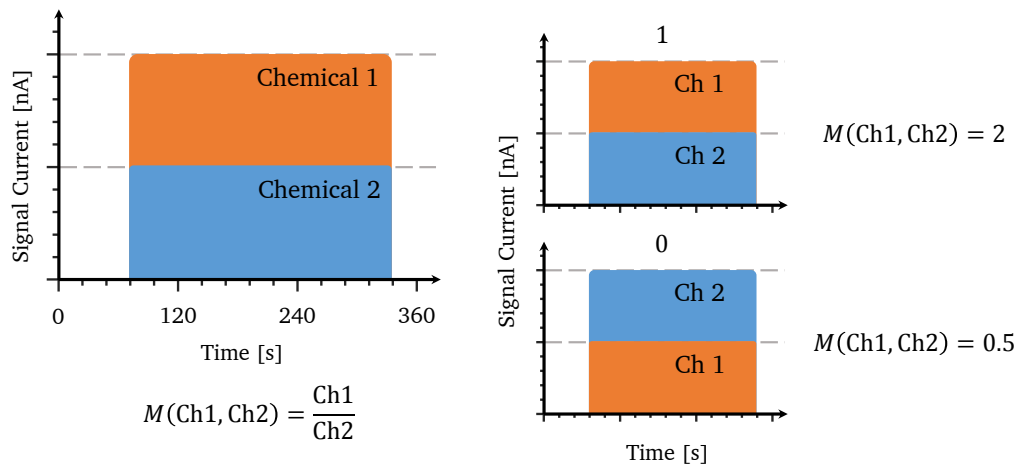


FIGURE 7.11: Diagram representing the chemical ratio keying (CRK).

7.6.1 Calculation of the modulation matrix

To mathematically define the modulation, two chemicals (ϕ_A , ϕ_B) are used. Let ϕ_A and ϕ_B be the chemicals with the following set:

$$\phi_A = \{\phi_{A0}, \phi_{A1}, \phi_{A2}, \dots, \phi_{Ai}\}, \quad \phi_A \subseteq \mathbb{N}, \quad (7.10a)$$

$$\phi_B = \{\phi_{B0}, \phi_{B1}, \phi_{B2}, \dots, \phi_{Bj}\}, \quad \phi_B \subseteq \mathbb{N}. \quad (7.10b)$$

In this context the ratio is defined as the division of the chemicals:

$$M(i, j) = \frac{\phi_{Ai}}{\phi_{Bj}}. \quad (7.11)$$

The matrix that gives the possible combinations of modulations is given as:

$$M_{i,j} = \begin{bmatrix} \frac{\phi_{A1}}{\phi_{B1}} & \frac{\phi_{A1}}{\phi_{B2}} & \frac{\phi_{A1}}{\phi_{B3}} & \cdots & \frac{\phi_{A1}}{\phi_{Bj}} \\ \frac{\phi_{A2}}{\phi_{B1}} & \frac{\phi_{A2}}{\phi_{B2}} & \frac{\phi_{A2}}{\phi_{B3}} & \cdots & \frac{\phi_{A2}}{\phi_{Bj}} \\ \vdots & \vdots & \vdots & \ddots & \vdots \\ \frac{\phi_{Ai}}{\phi_{B1}} & \frac{\phi_{i1}}{\phi_{B2}} & \frac{\phi_{Ai}}{\phi_{B3}} & \cdots & \frac{\phi_{Ai}}{\phi_{Bj}} \end{bmatrix}. \quad (7.12)$$

However, this matrix will possess values that are equal in terms of ratio (i.e., 4/2, 6/3, 8/4, ...) which are not suitable for use in modulation and may cause confusion in decoding the transmitted messages. The individuality of the ratios lies in the numbers that are co-primes. Two integers ϕ_A , ϕ_B are co-prime if the only positive integer (factor) that divides both of them is 1. Any ratio between two co-primes will produce a unique value in which information can be encoded given enough precision by the detector and the transmitter. To calculate the amount of combinations that can be generated, the Riemann-Zeta function is used with the following identity:

$$\zeta(s) = \sum_{n=1}^{\infty} \frac{1}{n^s}. \quad (7.13)$$

The relation of the above function to the problem in hand is as follows. Let the sum definition of $\zeta(s)$ be the following expression:

$$\zeta(s) = 1 + \frac{1}{2^s} + \frac{1}{3^s} + \frac{1}{4^s} + \frac{1}{5^s} + \cdots, \quad \Re(s) > 1, \quad (7.14)$$

From this series, to remove any number that is divisible by 2 ($2|n$) Eq. (7.15) is subtracted from (7.14):

$$\frac{1}{2^s} \zeta(s) = \frac{1}{2^s} + \frac{1}{4^s} + \frac{1}{6^s} + \frac{1}{8^s} + \frac{1}{10^s} + \cdots. \quad (7.15)$$

The below equation represents the reciprocal of probability of s amount of numbers not having a common divisor of 2:

TABLE 7.5: Particular values of the Riemann-Zeta function.

Parameter	Function	Closed Form	Value	OEIS
$\zeta(2)^1$	$1 + \frac{1}{2^2} + \frac{1}{3^2} + \dots$	$\frac{\pi^2}{6}$	1.6449 ...	A013661
$\zeta(3)^2$	$1 + \frac{1}{2^3} + \frac{1}{3^3} + \dots$	—	1.2020 ...	A002117
$\zeta(4)$	$1 + \frac{1}{2^4} + \frac{1}{3^4} + \dots$	$\frac{\pi^4}{90}$	1.0823 ...	A013662
$\zeta(5)$	$1 + \frac{1}{2^5} + \frac{1}{3^5} + \dots$	—	1.0369 ...	A013663
$\zeta(6)$	$1 + \frac{1}{2^6} + \frac{1}{3^6} + \dots$	$\frac{\pi^6}{945}$	1.0173 ...	A013664

¹ Known in literature as the Basel problem² Known in literature as the Apéry's constant

$$\left(1 - \frac{1}{2^s}\right)\zeta(s) = 1 + \frac{1}{3^s} + \frac{1}{5^s} + \frac{1}{7^s} + \frac{1}{9^s} + \dots. \quad (7.16)$$

This action is carried out to remove the common divisor of 3 ($3|n$):

$$\frac{1}{3^s} \left(1 - \frac{1}{2^s}\right)\zeta(s) = \frac{1}{3^s} + \frac{1}{9^s} + \frac{1}{15^s} + \frac{1}{21^s} + \frac{1}{27^s} + \dots. \quad (7.17)$$

If this process is continued *ad infinitum* the following expression is obtained:

$$\dots \left(1 - \frac{1}{11^s}\right) \left(1 - \frac{1}{7^s}\right) \left(1 - \frac{1}{5^s}\right) \left(1 - \frac{1}{3^s}\right) \left(1 - \frac{1}{2^s}\right) \zeta(s) = 1. \quad (7.18)$$

The above expression gives the reciprocal probability of s amount of numbers having no common divisors aside from 1 (i.e., co-prime):

$$\zeta(s) = \sum_{n=1}^{\infty} \frac{1}{n^s} = \prod_{p \text{ prime}} \frac{1}{1 - p^{-s}}. \quad (7.19)$$

The right hand expression given in Eq. (7.19) is described as the Euler product which is an infinite product indexed by prime numbers. This connection allows the quantification and the calculation of the unique values of the modulation with high accuracy. While there are no closed form for odd values for Riemann-Zeta function, the closed form function for the even numbers can be expressed as:

$$\zeta(2n) = (-1)^{n+1} \frac{B_{2n}(2\pi)^{2n}}{2(2n)!}, \quad (7.20)$$

where B_{2n} is the Benoulli number. Particular values of the Riemann-Zeta function for $s = 2 \dots 6$ can be seen in Table 7.5.

Based on the aforementioned equations, the number of individual values in a modulation matrix used can be expressed as:

$$\text{card}(M) = \frac{1}{\zeta(s)} \prod_{i=1}^{i=s} \phi_i. \quad (7.21)$$

TABLE 7.6: Experimental parameters for chemical ratio keying (ChRK).

Experimental Parameter	Symbol	Value	Unit
Tracked ion	m/z	$43^1, 42^2, 57^3$	Da
Carrier flow	Q	1000	ml/min
Detection delay [45]	t_d	$15^1, 14^2, 20^1$	s
Diffusivity in air	D	$0.124^1, 0.07^1,$ 0.11^3	cm^2/s
Inner tube diameter	ϕ_{in}	19.80	mm
Outer tube diameter	ϕ_{out}	24.25	mm

¹ Acetone ² Cyclopentane ³ n-Hexane

In the above-given example, two chemicals were used. The amount of modulated values are therefore can be approximated as:

$$\phi_A \phi_B \zeta(2) = \phi_A \phi_B \frac{\pi^2}{6}. \quad (7.22)$$

Comparison of actual individual values to estimated ones along with estimation error can be seen in Figure 7.12a and Figure 7.12b respectively.

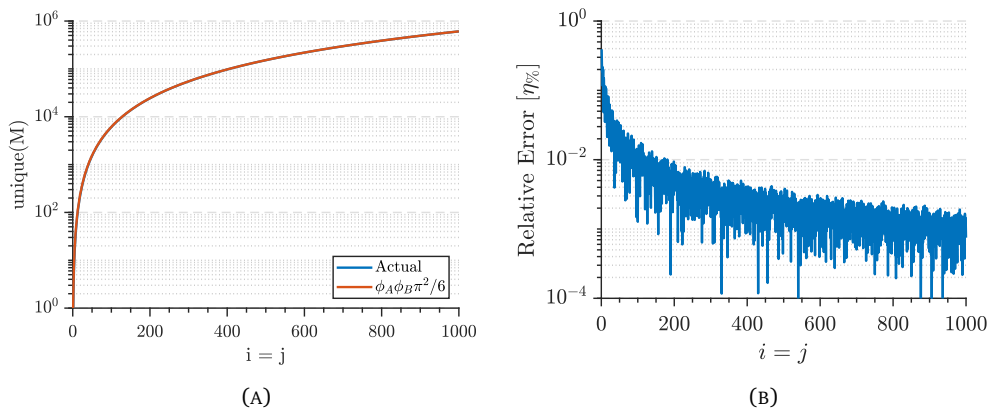


FIGURE 7.12: (A) Comparison of the unique values of the ratio modulation (—) comparison to the function $\phi_A \phi_B \frac{\pi^2}{6}$. (—)(B) Relative error ($\eta\%$) of the $\phi_A \phi_B \frac{\pi^2}{6}$ approximation.

To test the proposed modulation scheme, an experiment was conducted with the parameters given in Table 7.6.

7.6.2 Experimental Analysis

In this setup, a clear acrylic tube is used to initiate a long distance transmission to show the resilience of the modulation to signal attenuation.

The experimental results can be seen collectively in Figure 7.14. From (a) to (d) the effect of attenuation for three chemicals by increasing distance can be observed. Decrease of signal strength is to be expected. However, it must be noted that each chemical experiences attenuation differently making some chemicals better at transmitting long distances than

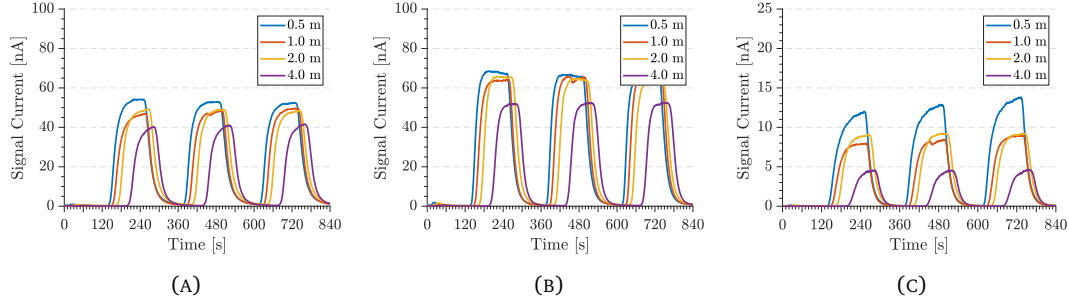


FIGURE 7.13: (A) Experimental transmission with increasing distance of (A) acetone (B) cyclopentane (C) n-hexane.

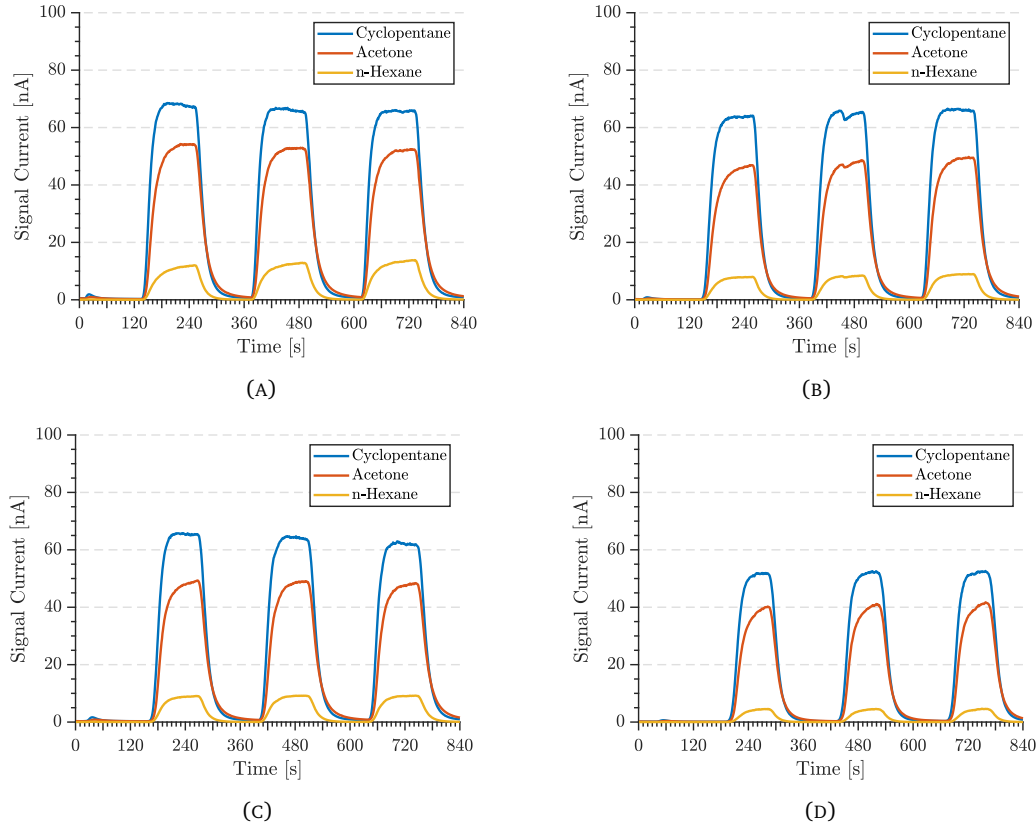


FIGURE 7.14: Experimental results of chemical ratio keying (ChRK) by using three different chemicals: acetone, cyclopentane and n-hexane. The figures above show the signal strength with increasing distance: (A) 0.5 m, (B) 1.0 m, (C) 2.0 m and (D) 4.0 m.

others. This effect can be seen in Figure 7.15a for their measured values and in Figure 7.15b for their values relative to 0.5 m measurement.

As can be seen in Figure 7.15b, the chemicals experience different attenuation rates. While Cyclopentane and Acetone experience similar attenuation, n-Hexane experiences higher attenuation compared to the other two chemicals. This difference can be caused by the unique parameters of the chemical species used for sending the pulse. In addition each chemical achieves a different maximum amplitude which can also be caused by the ionisation of samples, and their weight. The ratio of the two chemicals (Cyclopentane/Acetone) can be

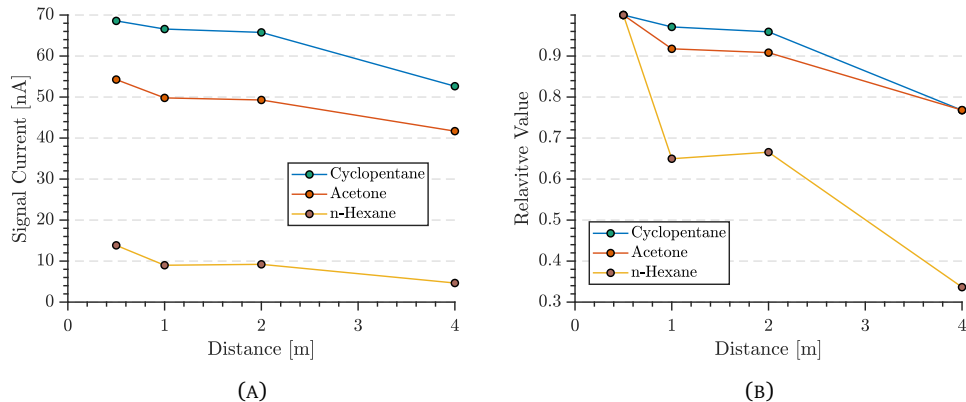


FIGURE 7.15: Experimental ratio values from the ratio modulation study: (A) Signal amplitudes of the three transmitted chemicals relative to distance. (B) Amplitude values of chemicals relative to 0.5 m signal current values.

observed in Figure 7.16a. Unlike the signal amplitude, the ratio value experiences less of a change, making it a better option to transmit information over long distances. However, the stability of the ratio value depends on the chosen chemical combinations. As can be seen from the Figure 7.16a and 7.16b, some combinations can produce ratios that are maintained over distance whereas some ratios, seen in Figure 7.16b, are not suitable for ratio modulation usage.

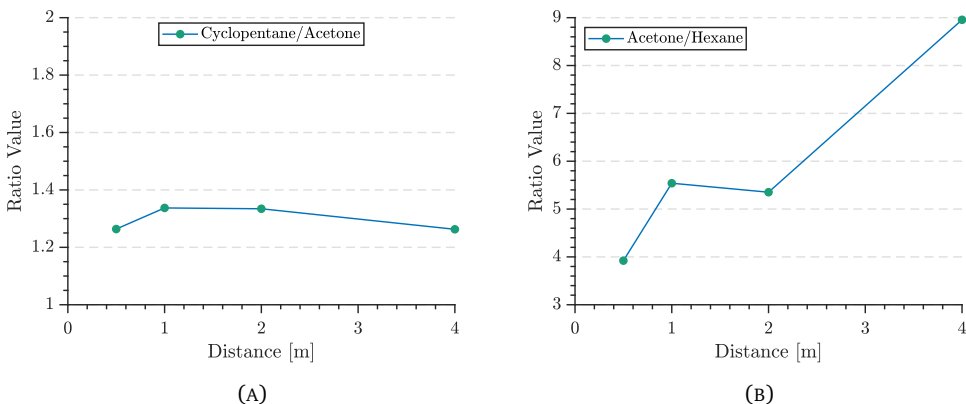


FIGURE 7.16: Experimental ratio values from the ratio modulation study: (A) cyclopentane/acetone, (B) acetone/n-hexane.

7.7 Conclusion

In this chapter, an experimental and analytical study was done on the possibility of transmitting multiple chemicals at the same time. To achieve this, an odour gas generator was used to generate and transmit chemicals. For detector, a quadrupole mass spectrometer was utilised as a detector. The ability of the mass spectrometer, to distinguish and analyse multiple chemicals concurrently, makes the MS an invaluable tool for multi-molecular communications. To mathematically validate the experiments, 3D Advection-Diffusion Equation

is used. Experimentally a multi-chemical transmission was done and shown to have strong agreement with mathematical model developed in this study. Experimentally the noise of the multi-chemical system was analysed and shown to behave as an Additive White Gaussian Noise with distinct values for the mean and variance for each chemical. Based on the mathematical model, a molecular version of QAM is developed in this study for macro-scale molecular communication and its properties are analysed. This chapter also proposed and experimented two types of molecular communication for use in macro-scale ratio modulation and phase shift keying. These modulation methods and the use of multiple chemical show that it is possible to greatly increase the achievable mutual information rate of the system which can create new application purposes for molecular communication and shows that there is still a possibility of increasing the throughput of the communication.

Chapter 8

Summary and Future-Work

In this thesis, an overview of macro-scale molecular communication was undertaken. Macro-scale molecular communication is described as an alternative branch of communication engineering, where the applications and the challenges greatly differ from its micro-scale counterpart. Molecular communication at the macro-scale can be used for infrastructure monitoring or communication in underwater or underground environments where EM waves would prove inefficient due to environmental energy absorption.

In Chapter 2 a comprehensive review on the topic of molecular communication is done. The review includes the concept of molecular communications. A detailed description of the differences between macro and micro-scale communication is given. The information theory of the communication is discussed and a brief section on information security is given. A detailed analysis on different types of propagation used in modelling molecular communication is shown for two types of propagation elements: diffusion and advection-diffusion. Moreover, a review on different types of modulation methods proposed and simulated for molecular communications are compared with additional discussion on the ISI, error correction and the receivers. Receiver for molecular communications, both experimental and theoretical are reviewed along with the experimental setups and proposed applications throughout the literature. The review on the field concludes with the simulation platforms and the standardisation efforts made for molecular communications

Throughout Chapter 2 it was shown that majority of the literature focuses on the theoretical aspect of molecular communication with micro-scale being the considered range. Therefore, two major gaps are identified in the literature: theoretical and experimental studies of molecular communication at the macro-scale. Subsequent chapters focused on different aspects of macro-scale molecular communication with experimental studies conducted to validate the mathematical models developed in the thesis.

In Chapter 3 a detailed description of the experimental setup is given that is used in the experiments conducted in Chapters 5, 6 and 7. To generate chemical pulses based on the digital information and transmit them into the transmission medium, an odour generator (OG) was utilised and an evaporation chamber (EC) was used to transmit the signal chemicals into the odour generator. The properties of the chemicals used in the thesis are given which are: acetone, methyl alcohol, cyclopentane and n-hexane. To detect the transmitted

chemicals, a membrane inlet mass spectrometer (MIMS) with a quadrupole mass analyser (QMA) was used. One of the defining features of the MIMS is its use of a membrane to separate chemicals at the inlet which is discussed in this chapter. The chapter concludes with detailed information regarding the operational use and the theoretical aspects of the detector.

In Chapter 4 the mathematical model that is used throughout the thesis is described. The model is based on the advection-diffusion equation (ADE). The developed model is used in describing and understanding the macro-molecular propagation and the particles interaction with the membrane. The model is developed for two environments: Open boundary (Cartesian coordinates) and cylindrical boundary (cylindrical coordinates). In open boundary a decay (λ_D) is implemented to simulate the effect of decay and in closed boundary, method of mirror images is used to simulate the boundary in a pipe. Due to the effect of the boundary, the diffusion is calculated based on Taylor-Aris dispersion which the derivation can be seen in Appendix B. Based on the equation, a simulation model was developed and given in detail for both aforementioned environments.

In Chapter 5, the parameter analysis of molecular communication in macro-scale is experimented and studied. The parameters in question are: environmental noise, signal flow, carrier flow, bit duration, open-distance transmission and closed-distance transmission. These aforementioned particles were analysed based on their signal amplitude, signal energy, signal-to-noise and signal shape. The noise present in the communication is analysed and modelled as additive white Gaussian noise (AWGN) present at the detector. The mathematical model derived in Chapter 4 is used to describe and predict the behaviour of the parameters. It was shown that the model accurately predicts the parameters behaviour and its signal shapes.

In Chapter 6, modulation methods on macro-scale molecular communications is studied. M_C -ary modulation of levels 2, 4, 8 and symbol periods of 30s, 60s, 90s were investigated. An experimental transmission of a chemical message (“*Call me Ishmael*”) is conducted. To better understand the effect of leftover chemicals on the background noise (Mo-ISI) transmissions were investigated. All the aforementioned experiments were additionally analysed by the theoretical model developed in Chapter 4. Based on the empirical evidence gathered a model was developed to predict the residual background signal after a transmission is terminated and additional calculations were done on the optimal symbol period of a chemical pulse. Experimental investigations were carried out on the SER performance of the communication and the channel behaviour is defined as a Binary Asymmetric Channel (BAC). Based on the channel definition and the model, theoretical calculations were initiated for channel capacity and SER performance for the following parameters: symbol duration, coefficient of diffusion, transmission distance and advective flow. The chapter concludes with a theoretical study on the bit distribution on the four aforementioned parameters.

In Chapter 7, to improve the throughput of the communication, multiple chemicals were employed and experimented. A proof-of-concept transmission of multiple chemical was investigated. The environmental noise characteristics of multiple-chemical transmission was

also undertaken and was shown to demonstrate Gaussian behaviour with different mean and variance for each chemical. Three types of modulation methods were then developed. The first one is based on quadrature amplitude modulation (QAM) named molecular-QAM (MQAM). Theoretical analysis were done on the channel capacity and the SER performance with additional analysis on the scattering distributions. The second modulation method is based on the relative time difference between distinguishable chemical signals and an experimental transmission was conducted based on this proposed modulation method. A Final modulation method was experimented based on the ratios of the propagating chemicals and was shown to be possible for use in long range molecular communications.

8.1 Future Research Directions

The field of molecular communication in the macro-scale is still in its infancy in regards to its understanding and its exploitation. Based on the research done in this thesis there are a few areas in which the work presented here can be carried out.

8.1.1 Different Receivers

In Chapter 3 the MS with a membrane inlet (MIMS) was used as the receiver. MS are an industry standard in detecting and quantifying chemical species. However, the response rate of the sensor can be better. Therefore, alternative chemical sensor can be employed that can be better choice for fast-transmission molecular communication.

In Chapter 2 alternative sensors for macro-scale molecular communication were discussed. One of these being electronics noses. These machines, intended to detect odours or flavours, can be used as a detector for the communication. However, to decrease the cost of the setup, cheaper alternatives can be sought after, for example Tin-Oxide (SnO_2) sensors. The behaviour of these sensors in the macro-scale are yet to be fully understood and further studies can show the optimal cost-effective use of these sensors for different environments.

Additional future-work can be focused on designing a molecular antenna to detect the direction in which the message is coming and if possible, triangulate the source of the transmission.

8.1.2 Turbulent Environments

In Chapter 4 a mathematical description of a molecular communication in macro-scale in isotropic environment was developed. In future, the mathematical model can be defined for describing the environments where turbulence ($\text{Re} > 4000$) plays a prominent role. Turbulence is defined as a fluid motion with chaotic changes in pressure and flow velocity and is encountered in everyday phenomena such as fast flowing rivers, smokes from a chimney and majority of the fluid flows occurring in nature. The complex motion of the fluid with rapid changes in its properties make it a challenge to understand and still is an unsolved problem in physics.

Since the majority of fluid flow in nature happens on $\text{Re} > 4000$, an understanding of this motion would open new possibilities of implementing macro-scale molecular communication to already existing propagation methods.

8.1.3 Complex Geometries

In Chapter 5 the parameters of macro-scale molecular communications were analysed. The closed distance transmission was experimented and mathematically modelled. However, only a straight cylindrical geometry (i.e., pipe) was considered. Geometries that have curvature would increase the complexity of the solution and analytical solutions to these geometries may not exist and only approximations can be made. Different types of methods can be used to achieve this, such as asymptotic analysis or centre manifold theorem. Derivation of these complex geometries may open up macro-molecular communication to new applications such as drug-delivery for in-vivo systems or molecular communication in riverbeds.

8.1.4 Secure Chemical Communications

In Chapter 7 communication throughput was shown to be able to be increased by the use of multiple chemical propagation. The prospect opens up new possibilities for implementing known technologies (i.e., security) to be implemented.

8.1.5 Novel Modulation Methods

In Chapter 7 it was shown that novel modulation methods can be developed that have the potential to increase the communication throughput or its reliability. Future-work on this topic is to analyse other modulation methods that also exploit multiple chemical transmission. One approach is the optimisation of the ratio modulation discussed in Chapter 7. While it was shown that it is possible to send chemicals with their ratios staying relatively stable, the choice of the chemicals that are capable of accomplishing this task needs to be chosen carefully. Understanding the chemicals properties may yield better combinations which may increase the range and the throughput of the modulation scheme.

Appendix A

Derivation of the Thin-Film Solution

The diffusion equation is a linear one, and a solution can, therefore, be obtained by adding several other solutions. An elementary solution ("building block") that is particularly useful is the solution to an instantaneous, localised release in an infinite domain initially free of the substance.

Mathematically, the problem is stated as follows:

- Environment domain is assumed infinite ($-\infty < x < \infty$)
- Diffusion is assumed to be constant ($\partial D / \partial t = 0$)
- Localised release ($c(x, t_0) = M_0 \delta(x)$)

Since the substance will take an infinite time to reach the infinitely far ends of the domain, the following limits are imposed.

$$\lim_{x \rightarrow +\infty} c(x, t) = \lim_{x \rightarrow -\infty} c(x, t) = 0. \quad (\text{A.1})$$

In the above, M_0 is the total mass of the substance released per unit cross-sectional area, and $\delta(x)$ is the Dirac function. Physically, the behaviour as displayed in Figure A.1 is anticipated. The pollutant patch gradually spreads on both sides of the release location, with a commensurate decrease in the maximum center value. Curves at later times appear similar to those at earlier times, only being flatter and wider. Anticipating such similarity in the solution, the following equation and the transform parameter is written;

$$c(x, t) = t^{-\alpha_D} F(\gamma) \quad \text{with} \quad \gamma = \frac{x^2}{4Dt}, \quad (\text{A.2})$$

where $t^{-\alpha_D}$ represents the decay of the maximum concentration value attained at $x = 0$. Since decay has to decrease the concentration α_D parameter is a positive value ($\alpha_D \geq 0$). $F(\gamma)$ is the shape factor of the solution, to give similar curve profile given in Figure A.1.

The exponent present in the distance (x^2) is chosen to represent the second order derivative of the diffusion PDE. The same rule applies to the t parameter present in the $F(\gamma)$. The D factor is the make the function dimensionless. The factor 4 is introduced to simplify the mathematical process of derivation.

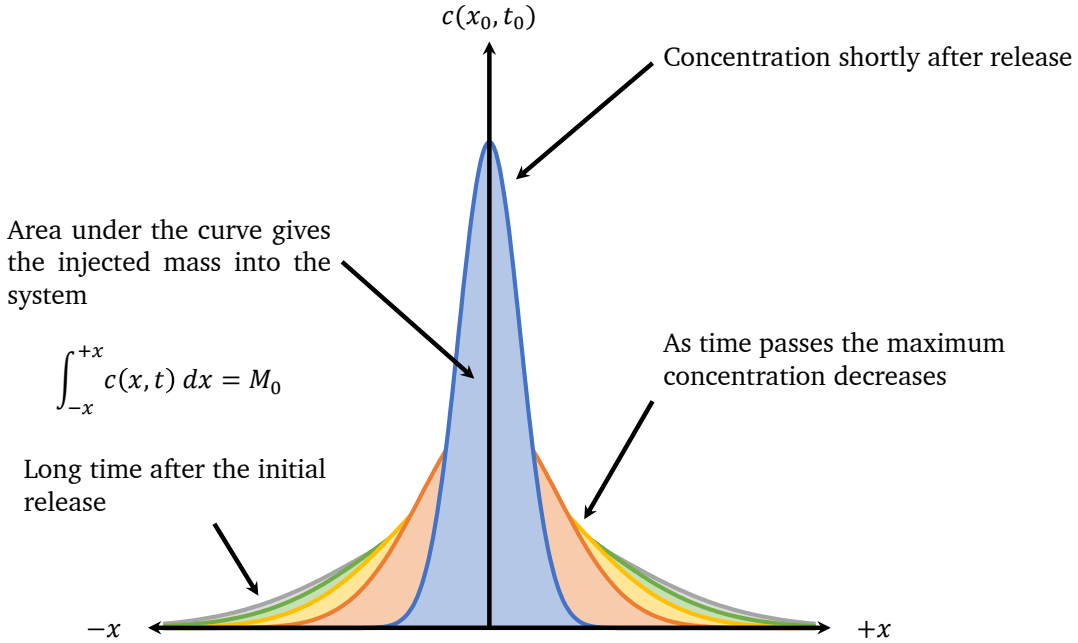


FIGURE A.1: Diffusion process in time of a localized mass injection. As the mass concentration distributes along the x -axis, the area under the curve is preserved

By introducing the proposed solution in Eq. (A.2) to the PDE shown in Eq. (2.11a).

$$\frac{\partial c}{\partial t} = -\alpha_D t^{-\alpha_D-1} F(\gamma) + t^{-\alpha_D} \frac{\partial F}{\partial \gamma} \frac{\partial \gamma}{\partial t} = -\alpha_D t^{-\alpha_D-1} F(\gamma) - \gamma t^{-\alpha_D-1} \frac{\partial F}{\partial \gamma}, \quad (\text{A.3a})$$

$$\frac{\partial c}{\partial x} = t^{-\alpha_D} \frac{\partial F}{\partial \gamma} \frac{\partial \gamma}{\partial x} = \frac{x t^{-\alpha_D-1}}{2D} \frac{\partial F}{\partial \gamma}, \quad (\text{A.3b})$$

$$\frac{\partial^2 c}{\partial x^2} = \frac{t^{-\alpha_D-1}}{2D} \frac{\partial F}{\partial \gamma} + \frac{x t^{-\alpha_D-1}}{2D} \frac{\partial^2 F}{\partial \gamma^2} \frac{\partial \gamma}{\partial x} = \frac{t^{-\alpha_D-1}}{2D} \frac{\partial F}{\partial \gamma} + \frac{t^{-\alpha_D-1}}{D} \gamma \frac{\partial^2 F}{\partial \gamma^2}. \quad (\text{A.3c})$$

After deriving the new element, substitution of $\partial c / \partial t$ and $\partial^2 c / \partial x^2$ in the diffusion equation yields:

$$-\alpha_D t^{-\alpha_D-1} F(\gamma) - \gamma t^{-\alpha_D-1} \frac{\partial F}{\partial \gamma} = \frac{t^{-\alpha_D-1}}{2} \frac{\partial F}{\partial \gamma} + \gamma t^{-\alpha_D-1} \frac{\partial^2 F}{\partial \gamma^2}. \quad (\text{A.4})$$

The time factors cancel out due to the definition of γ , and the partial-differential equation is reduced to an ordinary differential equation, with variable γ :

$$\gamma \frac{\partial}{\partial \gamma} \left(\frac{\partial F}{\partial \gamma} + F \right) + \frac{1}{2} \left(\frac{\partial F}{\partial \gamma} + 2\alpha_D F \right) = 0. \quad (\text{A.5})$$

To decrease the complexity of the solution and thereby making the group in the parenthesis identical, α_D is chosen as 0.5.

$$\frac{\partial F}{\partial \gamma} + F(\gamma) = 0, \quad (\text{A.6})$$

which the solution is,

$$F(\gamma) = G \exp(-\gamma), \quad (\text{A.7})$$

where G is an arbitrary constant of integration. By putting Eq. (A.2) to Eq. (A.7) the solution can be written as;

$$c(x, t) = \frac{G}{\sqrt{t}} \exp\left(-\frac{x^2}{4Dt}\right). \quad (\text{A.8})$$

While the initial boundary condition are met with this equation, the G needs to be defined. This can be achieved by imposing a conservation of mass to the equation.

$$\int_{-\infty}^{+\infty} c(x, t) dx = \int_{-\infty}^{+\infty} c(x, t_0) dx = M_0. \quad (\text{A.9})$$

This condition defines the constant G as;

$$G = \frac{M_0}{\sqrt{4\pi D}}. \quad (\text{A.10})$$

The solution can be finally written as;

$$C(x, t) = \frac{M_0}{\sqrt{4\pi Dt}} \exp\left(-\frac{x^2}{4Dt}\right) \quad \blacksquare. \quad (\text{A.11})$$

Appendix B

Derivation of the Taylor-Aris Dispersion

It is considered that the flow inside a straight cylindrical pipe is steady, driven by a constant pressure gradient (i.e, Poiseuille flow). The average velocity over the pipe cross-section can be given as:

$$u(r) = 2\bar{u} \left(1 - \frac{r^2}{R^2} \right), \quad (\text{B.1})$$

where:

$$\bar{u} = \frac{1}{\pi R^2} \int_0^{2\pi} d\theta \int_0^R r u dr. \quad (\text{B.2})$$

In these equations \bar{u} denotes the average quantity of the velocity flowing through the pipe. If it is assumed that an axisymmetric distribution of material $c(r, z, t)$ is released into the flow, the evolution of the propagation is described by the ADE in cylindrical form.

$$\frac{\partial c}{\partial t} + u(r) \frac{\partial c}{\partial z} = D_m \left(\frac{\partial^2 c}{\partial z^2} + \frac{1}{r} \frac{\partial}{\partial r} \left(r \frac{\partial c}{\partial r} \right) \right). \quad (\text{B.3})$$

Since no particle can leave the system, the boundary conditions are must satisfy $\partial c / \partial r = 0$ at $r = R$. By separating c using Reynold's decomposition method, c is separated into its cross-sectional average and r variable parts.

$$c(r, z, t) = \bar{c}(z, t) + c'(r, z, t), \quad (\text{B.4})$$

where:

$$\bar{c} = \frac{2}{R^2} \int_0^R r c dr. \quad (\text{B.5})$$

since the average of deviation is zero ($\bar{c}' = 0$) the equation can be written as:

$$\frac{\partial \bar{c}}{\partial t} + \frac{\partial c'}{\partial t} + u(r) \left(\frac{\partial \bar{c}}{\partial z} + \frac{\partial c'}{\partial z} \right) = D_m \left(\frac{\partial^2 \bar{c}}{\partial z^2} + \frac{\partial^2 c'}{\partial z^2} + \frac{1}{r} \frac{\partial}{\partial r} \left(r \frac{\partial c'}{\partial r} \right) \right). \quad (\text{B.6})$$

Taking the cross-sectional average of Eq. (B.6) yields the following simplification taking into account that $\partial c'/\partial t = 0$ on $r = R$.

$$\frac{\partial \bar{c}}{\partial t} + \overline{u(r)} \frac{\partial \bar{c}}{\partial z} + \overline{u(r) \frac{\partial c'}{\partial z}} = D_m \frac{\partial^2 \bar{c}}{\partial z^2}. \quad (\text{B.7})$$

The the mean concentration \bar{c} depends on the average advection of the r -varying part of c (i.e., $c'(r, z, t)$), which is calculated by subtracting Eq. (B.7) from Eq. (B.6) reveals the r -varying component of Eq. (B.6),

$$\frac{\partial c'}{\partial t} + (u(r) - \bar{u}) \frac{\partial \bar{c}}{\partial z} + u \frac{\partial c'}{\partial z} - \overline{u \frac{\partial c'}{\partial z}} = D_m \nabla^2 c'. \quad (\text{B.8})$$

Based on this equation, an approximation is made whereby after a time of in the order $t = R^2/D_m$ the radial diffusion to have almost smoothed out variation in the r -axis. Thus for $t \sim \mathcal{O}(R^2/D_m)$, it is expected for $\bar{c} \gg c'$. In addition, the gradients in the r -direction are greater than those in the z -direction. Therefore the primary balance is:

$$(u(r) - \bar{u}) \frac{\partial \bar{c}}{\partial z} \simeq \frac{D_m}{r} \frac{\partial}{\partial r} \left(r \frac{\partial c'}{\partial r} \right), \quad (\text{B.9})$$

Introducing Eq. (B.1) into (B.9), the following expression is derived.

$$\frac{\partial}{\partial r} \left(r \frac{\partial c'}{\partial r} \right) = \frac{\bar{u}}{D_m} \frac{\partial \bar{c}}{\partial z} \left(r - \frac{2r^3}{R^2} \right). \quad (\text{B.10})$$

As shown in the Reynold's decomposition of c in Eq. (B.4), \bar{c} is independent from r , so Eq. (B.10) can be integrated twice over,

$$c' = \frac{\bar{u}}{D_m} \frac{\partial \bar{c}}{\partial z} \left(\frac{r^2}{4} - \frac{r^4}{8R^2} + A + B \ln r \right). \quad (\text{B.11})$$

Since c' is regular at $r = 0$ B can be declared the value of 0. Furthermore, c' has zero average. This yields:

$$\int_0^R r u' dr = 0, \quad (\text{B.12})$$

This equation give A the value of:

$$A = -\frac{R^2}{12}, \quad (\text{B.13})$$

$$c' = \frac{\bar{u} R_r^2}{24 D_m} \frac{\partial \bar{c}}{\partial z} (6R_r^2 - 3R_r^4 - 2) \quad \text{where} \quad R_r = \frac{r}{R}. \quad (\text{B.14})$$

Equation (4) requires the term $\overline{u(r) \partial c' / \partial z}$, which is

$$\overline{u(r) \frac{\partial c'}{\partial z}} = -\frac{R^2 \bar{u}}{48D_m} \frac{\partial^2 \bar{c}}{\partial z^2}. \quad (\text{B.15})$$

Substituting this result into (B.6), ADE for the mean concentration $\bar{c}(z, t)$ is derived.

$$\frac{\partial \bar{c}}{\partial t} + \bar{u} \frac{\partial \bar{c}}{\partial z} = \left(D_m + \frac{R^2 \bar{u}^2}{48D_m} \right) \frac{\partial^2 \bar{c}}{\partial z^2} = D_{\text{eff}} \frac{\partial^2 \bar{c}}{\partial z^2}. \quad (\text{B.16})$$

Appendix C

Photographs of the Experimental Setups

C.1 Experimental Setup

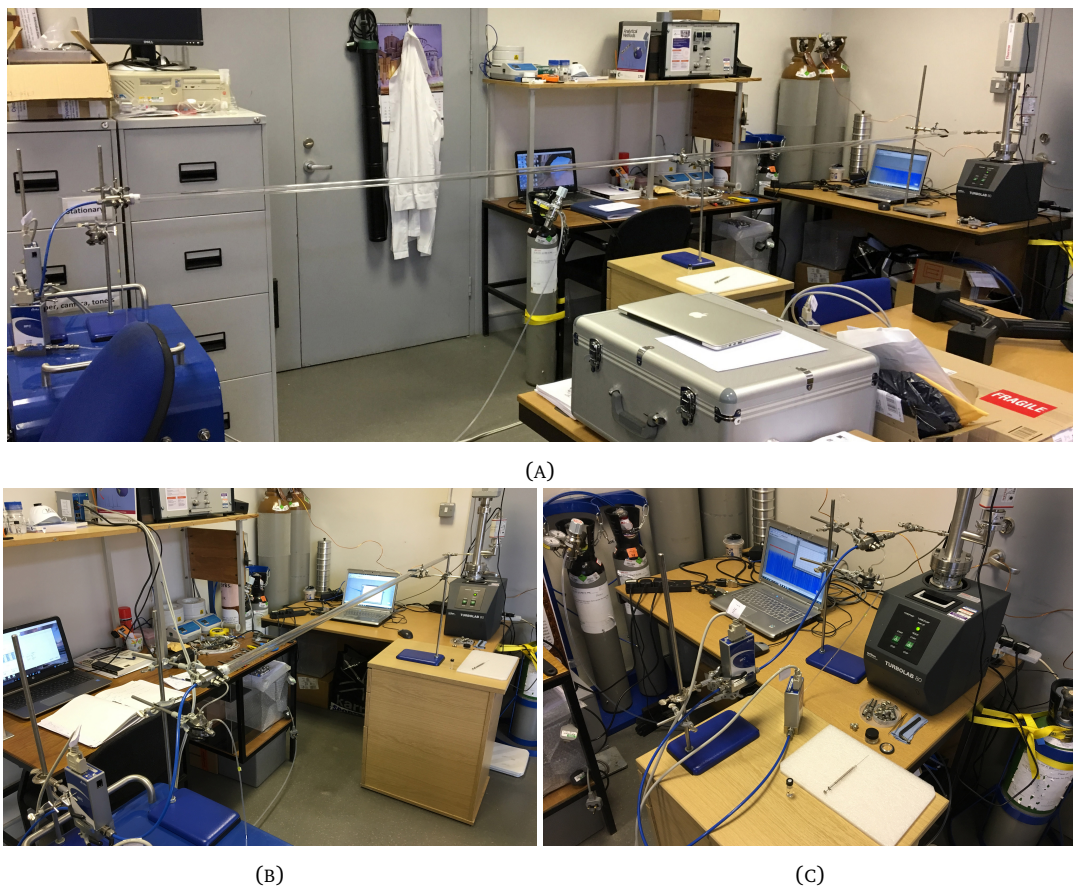


FIGURE C.1: (A), (B)Experimental setup for long distance transmission. (C) Experimental setup for short distance transmission.

C.2 Transmitter

C.2.1 Odour Generator

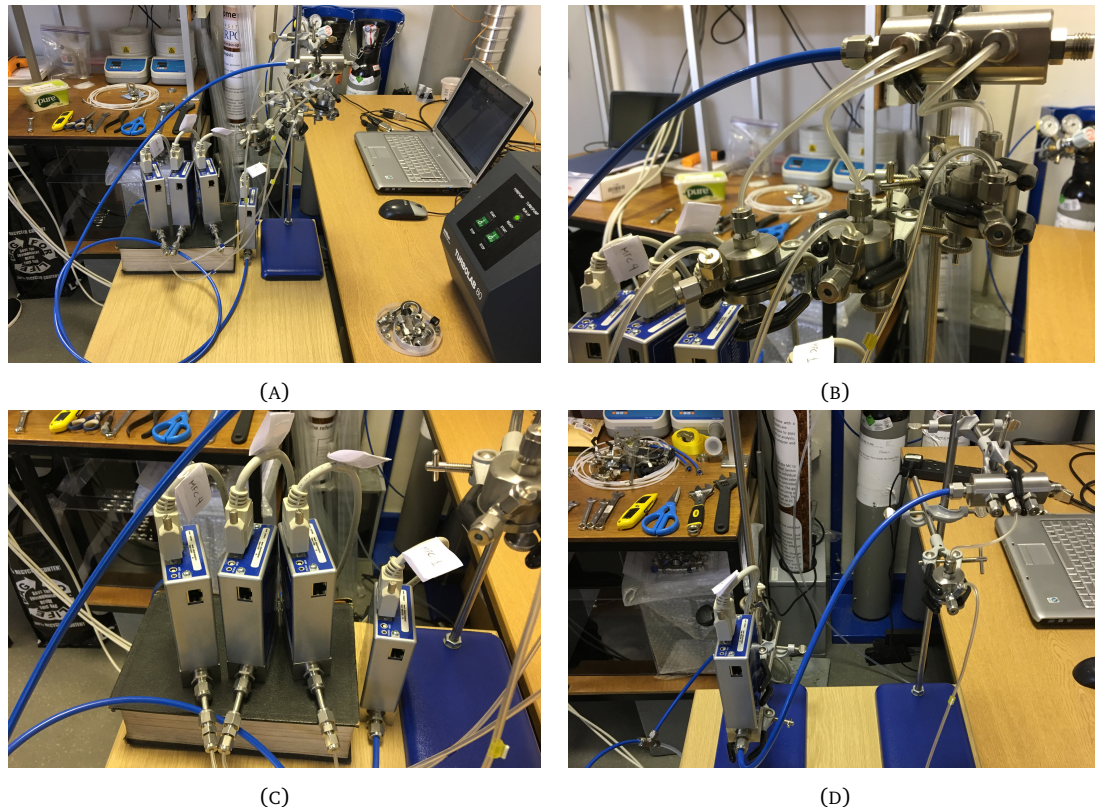


FIGURE C.2: (A) The odour generator with three evaporation chambers and mass flow controllers attached. (B) A close-up of the evaporation chambers connected to the odour generator. (C) A close-up of the mass flow controllers connected to evaporation chambers. (D) An odour generator with a single evaporation chamber and mass flow controller attached.

C.2.2 Evaporation Chamber

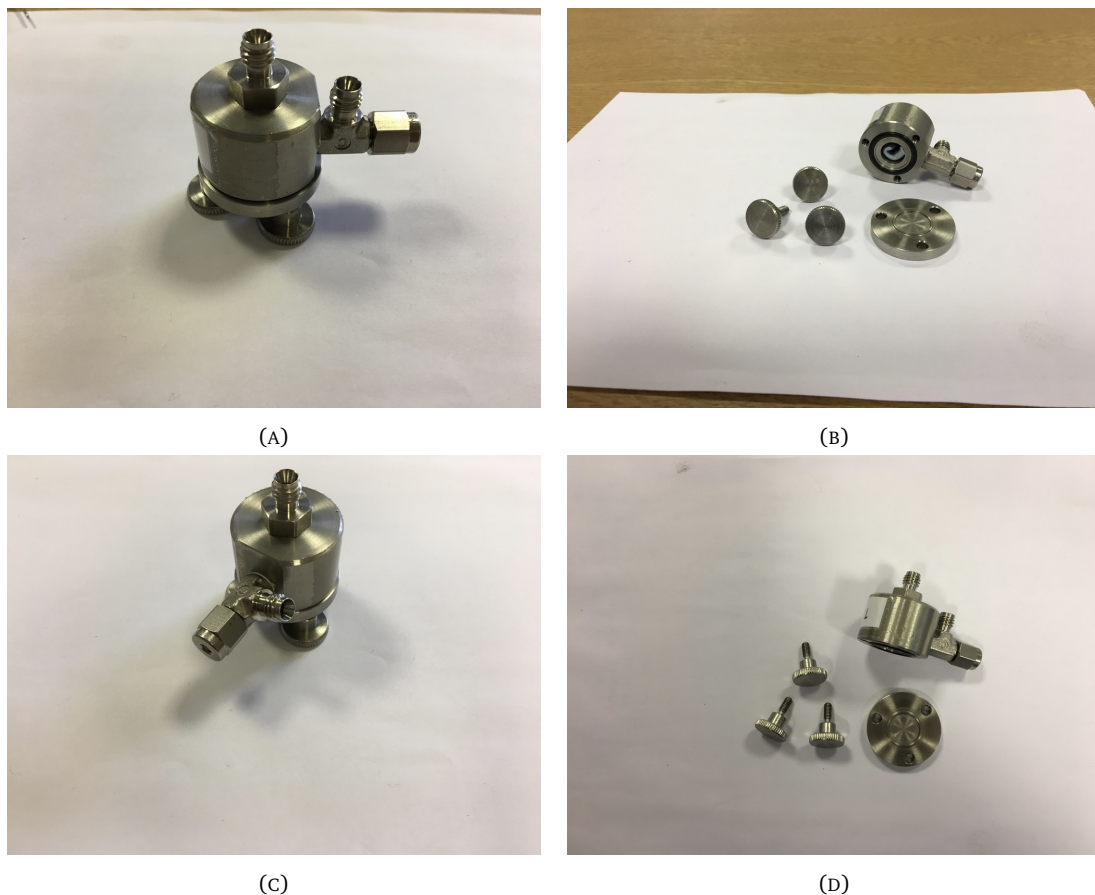


FIGURE C.3: (A) Evaporation chamber. (B) Evaporation chamber disassembled. (C) Evaporation chamber from a different angle. (D) Evaporation chamber disassembled from a different angle.

Appendix D

Derivation of the Optimal Sampling Time for 1D

$$n_x = \left(\frac{x_d - u_x T_{OSP}}{2\sqrt{D_x T_{OSP}}} \right), \quad (\text{D.1})$$

Squaring both sides

$$n_x^2 = \left(\frac{x_d^2 - 2x_d u_x T_{OSP} + u_x^2 T_{OSP}}{4D_x T_{OSP}} \right), \quad (\text{D.2})$$

Multiplying both sides with $4D_x T_{OSP}$,

$$4D_x T_{OSP} n_x^2 = x_d^2 - 2x_d u_x T_{OSP} + u_x^2 T_{OSP}. \quad (\text{D.3})$$

Sides of the equation are switched.

$$x_d^2 - 2x_d u_x T_{OSP} + u_x^2 T_{OSP} = 4D_x T_{OSP} n_x^2, \quad (\text{D.4})$$

Substracting $4D_x T_{OSP} n_x^2$ from both sides,

$$x_d^2 - 2x_d u_x T_{OSP} + u_x^2 T_{OSP} - 4D_x T_{OSP} n_x^2 = 4D_x T_{OSP} n_x^2 - 4D_x T_{OSP} n_x^2, \quad (\text{D.5})$$

Simplifying the equation,

$$u_x^2 T_{OSP} - (2x_d u_x + 4D_x n_x^2) T_{OSP} + x_d^2 = 0, \quad (\text{D.6})$$

The above equation is in the form of $ax^2 + bx + c = 0$ and therefore the solution to these form of equation are;

$$T_{1D_{max,min}} = \frac{-b \pm \sqrt{b^2 - 4ac}}{2a}, \quad (\text{D.7})$$

For $a = u_x^2$, $b = -2x_d u_x - 4D_x n_x^2$ and $c = x_d^2$ the solution becomes;

$$T_{1D_{max,min}} = \frac{-(-2x_d u_x - 4D_x n_x^2) \pm \sqrt{(-2x_d u_x - 4D_x n_x^2)^2 - 4u_x^2 x_d^2}}{2u_x^2}, \quad (\text{D.8})$$

The following steps are simplifications for the aforementioned equation.

$$T_{1D_{max,min}} = \frac{2x_d u_x + 4D_x n_x^2 \pm \sqrt{(-2x_d u_x - 4D_x n_x^2)^2 - 4u_x^2 x_d^2}}{2u_x^2}, \quad (\text{D.9})$$

The part $(-2x_d u_x - 4D_x n_x^2)^2$ is opened;

$$T_{1D_{max,min}} = \frac{2x_d u_x + 4D_x n_x^2 \pm \sqrt{(4x_d^2 u_x^2 + 16x_d u_x D_x n_x^2 + 16D_x^2 n_x^4) - 4u_x^2 x_d^2}}{2u_x^2}, \quad (\text{D.10})$$

The equation is simplified;

$$T_{1D_{max,min}} = \frac{2x_d u_x + 4D_x n_x^2 \pm \sqrt{16x_d u_x D_x n_x^2 + 16D_x^2 n_x^4}}{2u_x^2}, \quad (\text{D.11})$$

$16n_x^2$ is taken out of the squareroot.

$$T_{1D_{max,min}} = \frac{2x_d u_x + 4D_x n_x^2 \pm 4n_x \sqrt{x_d u_x D_x + D_x^2 n_x^2}}{2u_x^2}, \quad (\text{D.12})$$

$$T_{1D_{max,min}} = \frac{x_d u_x + 2D_x n_x^2 \pm 2n_x \sqrt{x_d u_x D_x + D_x^2 n_x^2}}{u_x^2}, \quad (\text{D.13})$$

$$T_{1D_{max,min}} = \frac{x_d u_x + 2D_x n_x^2 \pm 2n_x \sqrt{D_x (D_x n_x^2 + x_d u_x)}}{u_x^2}, \quad (\text{D.14})$$

Bibliography

- [1] S. Shah, A. Raghavachari, C. Lo, and R. Marculescu, “Molecular communication with dna cellular storage system,” in *Proceedings of the 4th ACM International Conference on Nanoscale Computing and Communication*, pp. 1–6, 2017. [doi:10.1145/3109453.3109467](https://doi.org/10.1145/3109453.3109467).
- [2] B. A. Bilgin, E. Dinc, and O. B. Akan, “Dna-based Molecular Communications,” *IEEE Access*, vol. 6, pp. 73119–73129, 2018. [doi:10.1109/ACCESS.2018.2882555](https://doi.org/10.1109/ACCESS.2018.2882555).
- [3] M. Stengl, “Pheromone Transduction in Moths,” *Frontiers in Cellular Neuroscience*, vol. 4, p. 133, 2010. [doi:10.3389/fncel.2010.00133](https://doi.org/10.3389/fncel.2010.00133).
- [4] E. C. Friedberg, “DNA Damage and Repair,” *Nature*, vol. 421, no. 6921, p. 436, 2003. [doi:10.1038/nature01408](https://doi.org/10.1038/nature01408).
- [5] M. Statheropoulos, G. Pallis, K. Mikedi, S. Giannoukos, A. Agapiou, A. Pappa, A. Cole, W. Vautz, and C. P. Thomas, “Dynamic Vapor Generator that Simulates Transient Odor Emissions of Victims Entrapped in the Voids of Collapsed Buildings,” *Analytical Chemistry*, vol. 86, no. 8, pp. 3887–3894, 2014. [doi:10.1021/ac404175e](https://doi.org/10.1021/ac404175e).
- [6] H. A. Wheeler, “Fundamental Limitations of Small Antennas,” *Proceedings of the Institute of Radio Engineers (IRE)*, vol. 35, no. 12, pp. 1479–1484, 1947. [doi:10.1109/JRPROC.1947.226199](https://doi.org/10.1109/JRPROC.1947.226199).
- [7] B. L. Bassler, “How Bacteria Talk to Each Other: Regulation of Gene Expression by Quorum Sensing,” *Current opinion in microbiology*, vol. 2, no. 6, pp. 582–587, 1999. [doi:10.1016/S1369-5274\(99\)00025-9](https://doi.org/10.1016/S1369-5274(99)00025-9).
- [8] D. T. McGuiness, S. Giannoukos, A. Marshall, and S. Taylor, “Parameter Analysis in Macro-Scale Molecular Communications using Advection-Diffusion,” *IEEE Access*, vol. 6, pp. 46706–46717, 2018. [doi:10.1109/ACCESS.2018.2866679](https://doi.org/10.1109/ACCESS.2018.2866679).
- [9] D. T. McGuiness, S. Giannoukos, A. Marshall, and S. Taylor, “Experimental Results on the Open-Air Transmission of Macro-Molecular Communication using Membrane Inlet Mass Spectrometry,” *IEEE Communications Letters*, vol. 22, no. 12, pp. 2567–2570, 2018. [doi:10.1109/LCOMM.2018.2875445](https://doi.org/10.1109/LCOMM.2018.2875445).

- [10] D. T. McGuiness, S. Giannoukos, A. Marshall, and S. Taylor, “Modulation Analysis in Macro-Molecular Communications,” *IEEE Access*, vol. 7, pp. 11049–11065, 2019. [doi:10.1109/ACCESS.2019.2892850](https://doi.org/10.1109/ACCESS.2019.2892850).
- [11] T. Nakano, A. W. Eckford, and T. Haraguchi, *Molecular Communication*. Cambridge University Press, 1st ed., 2013. ISBN-13: 978-1139149693.
- [12] W. Guo, C. Mias, N. Farsad, and J.-L. Wu, “Molecular versus Electromagnetic Wave Propagation Loss in Macro-Scale Environments,” *IEEE Transactions on Molecular, Biological and Multi-Scale Communications*, vol. 1, no. 1, pp. 18–25, 2015. [doi:10.1109/TMBMC.2015.2465517](https://doi.org/10.1109/TMBMC.2015.2465517).
- [13] M. Stojanovic, “Acoustic (Underwater) Communications,” in *Wiley Encyclopedia of Telecommunications*, Wiley Online Library, 1st ed., 2003. ISBN-13: 978-0471219286.
- [14] P. Tyack, “Acoustic Communication Under the Sea,” in *Animal acoustic communication*, pp. 163–220, Springer, 1st ed., 1998. ISBN-13: 978-3642762208.
- [15] D. E. Kroodsma and E. H. Miller, *Ecology and Evolution of Acoustic Communication in Birds*. Cornell University Press, 1st ed., 1996. ISBN-13: 978-0801482212.
- [16] M. Stojanovic and J. Preisig, “Underwater Acoustic Communication Channels: Propagation Models and Statistical Characterization,” *IEEE Communications Magazine*, vol. 47, no. 1, pp. 84–89, 2009. [doi:10.1109/MCOM.2009.4752682](https://doi.org/10.1109/MCOM.2009.4752682).
- [17] R. A. Freitas, *Nanomedicine, Volume I: Basic Capabilities*. CRC Press, 1st ed., 1999. ISBN-13: 978-1570596803.
- [18] I. F. Akyıldız, F. Brunetti, and C. Blázquez, “Nanonetworks: A New Communication Paradigm,” *Computer Networks*, vol. 52, no. 12, pp. 2260–2279, 2008. [doi:10.1016/j.comnet.2008.04.001](https://doi.org/10.1016/j.comnet.2008.04.001).
- [19] W. Davis, T. Yang, E. Caswell, and W. Stutzman, “Fundamental Limits on Antenna Size: a New Limit,” *IET Microwaves, Antennas & Propagation*, vol. 5, no. 11, pp. 1297–1302, 2011. [doi:10.1049/iet-map.2010.0604](https://doi.org/10.1049/iet-map.2010.0604).
- [20] Y. Tanaka, S. Haruyama, and M. Nakagawa, “Wireless Optical Transmissions with White Colored LED for Wireless Home Links,” in *11th International Symposium on Personal, Indoor and Mobile Radio Communications (PIMRC)*, vol. 2, pp. 1325–1329, IEEE, 2000. [doi:10.1109/PIMRC.2000.881634](https://doi.org/10.1109/PIMRC.2000.881634).
- [21] M. U. Mahfuz, D. Makrakis, and H. T. Mouftah, “On the Characterization of Binary Concentration-Encoded Molecular Communication in Nanonetworks,” *Nano Communication Networks*, vol. 1, no. 4, pp. 289–300, 2010. [doi:10.1016/j.nancom.2011.01.001](https://doi.org/10.1016/j.nancom.2011.01.001).

- [22] N. Farsad, H. B. Yilmaz, A. Eckford, C.-B. Chae, and W. Guo, “A Comprehensive Survey of Recent Advancements in Molecular Communication,” *IEEE Communications Surveys & Tutorials*, vol. 18, no. 3, pp. 1887–1919, 2016. [doi:10.1109/COMST.2016.2527741](https://doi.org/10.1109/COMST.2016.2527741).
- [23] B. Alberts, A. Johnson, J. Lewis, M. Raff, K. Roberts, and P. Walter, *Molecular Biology of the Cell*. Garland Science, 5th ed., 2008. ISBN-13: 978-0815341062.
- [24] W. C. Agosta, *Chemical Communication: The Language of Pheromones*. Scientific American Library, 1st ed., 1992. ISBN-13: 978-0716750369.
- [25] A. W. Eckford, “Nanoscale Communication with Brownian Motion,” in *41st Annual Conference on Information Sciences and Systems (CISS)*, pp. 160–165, IEEE, 2007. [doi:10.1109/CISS.2007.4298292](https://doi.org/10.1109/CISS.2007.4298292).
- [26] C. O. Brant, K. Li, N. S. Johnson, and W. Li, “A Pheromone Outweighs Temperature in Influencing Migration of Sea Lamprey,” *Royal Society open science*, vol. 2, no. 5, p. 150009, 2015. [doi:10.1098/rsos.150009](https://doi.org/10.1098/rsos.150009).
- [27] T. Nakano, T. Suda, M. Moore, R. Egashira, A. Enomoto, and K. Arima, “Molecular Communication for Nanomachines Using Intercellular Calcium Signaling,” in *5th IEEE Conference on Nanotechnology*, pp. 478–481, IEEE, 2005.
- [28] E. Gul, B. Atakan, and O. B. Akan, “NanoNS: A Nanoscale Network Simulator Framework for Molecular Communications,” *Nano Communication Networks*, vol. 1, no. 2, pp. 138–156, 2010. [doi:10.1016/j.nancom.2010.08.003](https://doi.org/10.1016/j.nancom.2010.08.003).
- [29] M. S. Leeson and M. D. Higgins, “Forward Error Correction for Molecular Communications,” *Nano Communication Networks*, vol. 3, no. 3, pp. 161–167, 2012. [doi:10.1016/j.nancom.2012.09.001](https://doi.org/10.1016/j.nancom.2012.09.001).
- [30] B. Alberts, D. Bray, K. Hopkin, A. Johnson, J. Lewis, M. Raff, K. Roberts, and P. Walter, *Essential Cell Biology*. Garland Publishing, 3rd ed., 2009. ISBN-13: 978-0815341307.
- [31] E. L. Cussler, *Diffusion: Mass Transfer in Fluid Systems (Cambridge Series in Chemical Engineering)*. Cambridge University Press, 3rd ed., 2009. ISBN-13: 978-0521871211.
- [32] L. P. Giné and I. F. Akyıldız, “Molecular Communication Options for Long Range Nanonetworks,” *Computer Networks*, vol. 53, no. 16, pp. 2753–2766, 2009. [doi:10.1016/j.comnet.2009.08.001](https://doi.org/10.1016/j.comnet.2009.08.001).
- [33] R. P. Feynman, R. B. Leighton, and M. Sands, *The Feynman Lectures on Physics*, vol. 1. Basic books, The New Millennium ed., 2011. ISBN-13: 978-0465023820.
- [34] W. Hundsdorfer and J. G. Verwer, *Numerical Solution of Time-Dependent Advection-Diffusion-Reaction Equations*, vol. 33. Springer Science & Business Media, 1st ed., 2013. ISBN-13: 978-3540034407.

- [35] G. Csanady, *Turbulent Diffusion in the Environment*, vol. 3. Springer Netherlands, 1st ed., 1973. ISBN-13: 978-9401025270.
- [36] T. Nakano, T. Suda, T. Koujin, T. Haraguchi, and Y. Hiraoka, “Molecular Communication Through Gap Junction Channels: System Design, Experiments and Modeling,” in *2nd Bio-Inspired Models of Network, Information and Computing Systems (BIMNICS)*, pp. 139–146, IEEE, 2007. doi:[10.1109/BIMNICS.2007.4610100](https://doi.org/10.1109/BIMNICS.2007.4610100).
- [37] Y. Chahibi, I. F. Akyildiz, and I. Balasingham, “Propagation Modeling and Analysis of Molecular Motors in Molecular Communication,” *IEEE Transactions on NanoBio-science*, vol. 15, no. 8, pp. 917–927, 2016. doi:[10.1109/TNB.2016.2620439](https://doi.org/10.1109/TNB.2016.2620439).
- [38] N. Farsad, W. Guo, and A. W. Eckford, “Tabletop Molecular Communication: Text Messages Through Chemical Signals,” *PLoS ONE*, vol. 8, no. 12, p. e82935, 2013. doi:[10.1371/journal.pone.0082935](https://doi.org/10.1371/journal.pone.0082935).
- [39] S. Basu, Y. Gerchman, C. H. Collins, F. H. Arnold, and R. Weiss, “A Synthetic Multicellular System for Programmed Pattern Formation,” *Nature*, vol. 434, no. 7037, p. 1130, 2005. doi:[10.1038/nature03461](https://doi.org/10.1038/nature03461).
- [40] C. Ming-Tang and R. Weiss, “Artificial Cell-Cell Communication in Yeast *Saccharomyces Cerevisiae* Using Signaling Elements from *Arabidopsis Thaliana*,” *Nature Biotechnology*, vol. 23, no. 12, p. 1551, 2005. doi:[10.1038/nbt1162](https://doi.org/10.1038/nbt1162).
- [41] L. You, R. S. Cox III, R. Weiss, and F. H. Arnold, “Programmed Population Control by Cell-Cell Communication and Regulated Killing,” *Nature*, vol. 428, no. 6985, p. 868, 2004. doi:[10.1038/nature02491](https://doi.org/10.1038/nature02491).
- [42] D. Harel, L. Carmel, and D. Lancet, “Towards an Odor Communication System,” *Computational Biology and Chemistry*, vol. 27, no. 2, pp. 121–133, 2003. doi:[10.1016/S1476-9271\(02\)00092-0](https://doi.org/10.1016/S1476-9271(02)00092-0).
- [43] M. Mukai, K. Maruo, J.-i. Kikuchi, Y. Sasaki, S. Hiyama, Y. Moritani, and T. Suda, “Propagation and Amplification of Molecular Information Using a Photoresponsive Molecular Switch,” *Supramolecular Chemistry*, vol. 21, no. 3-4, pp. 284–291, 2009. doi:[10.1080/10610270802468439](https://doi.org/10.1080/10610270802468439).
- [44] Y. Sasaki, Y. Shioyama, W.-J. Tian, J.-i. Kikuchi, S. Hiyama, Y. Moritani, and T. Suda, “A Nanosensory Device Fabricated on a Liposome for Detection of Chemical Signals,” *Biotechnology and Bioengineering*, vol. 105, no. 1, pp. 37–43, 2010. doi:[10.1002/bit.22521](https://doi.org/10.1002/bit.22521).
- [45] S. Giannoukos, A. Marshall, S. Taylor, and J. Smith, “Molecular Communication over Gas Stream Channels using Portable Mass Spectrometry,” *Journal of The American Society for Mass Spectrometry*, vol. 28, no. 11, pp. 2371–2383, 2017. doi:[10.1007/s13361-017-1752-6](https://doi.org/10.1007/s13361-017-1752-6).

- [46] D. T. McGuiness, A. Marshall, S. Taylor, and S. Giannoukos, “Asymmetrical Inter-Symbol Interference in Macro-Scale Molecular Communications,” in *5th International Conference on Nanoscale Computing and Communication (NANOCOM)*, pp. 1–6, ACM, 2018. [doi:10.1145/3233188.3233194](https://doi.org/10.1145/3233188.3233194).
- [47] S. Giannoukos, D. T. McGuiness, A. Marshall, J. Smith, and S. Taylor, “a Chemical Alphabet for Macromolecular Communications,” *Analytical Chemistry*, vol. 90, no. 12, pp. 7739 –7746, 2018. [doi:10.1021/acs.analchem.8b01716](https://doi.org/10.1021/acs.analchem.8b01716).
- [48] D. Hymel and B. R. Peterson, “Synthetic Cell Surface Receptors for Delivery of Therapeutics and Probes,” *Advanced Drug Delivery Reviews*, vol. 64, no. 9, pp. 797–810, 2012. [doi:10.1016/j.addr.2012.02.007](https://doi.org/10.1016/j.addr.2012.02.007).
- [49] H. Shankaran, H. Resat, and H. S. Wiley, “Cell Surface Receptors for Signal Transduction and Ligand Transport: a Design Principles Study,” *PLoS Computational Biology*, vol. 3, no. 6, p. e101, 2007. [doi:10.1371/journal.pcbi.0030101](https://doi.org/10.1371/journal.pcbi.0030101).
- [50] M. Cole, J. Gardner, Z. Rácz, S. Pathak, T. Pearce, J. Challiss, D. Markovic, A. Guererro, L. Muñoz, G. Carot, B. Hansson, S. Olsson, L. Kübler, J. G. E. Gardeniers, N. Dimov, and W. Bula, “Biomimetic Insect Infochemical Communication System,” in *IEEE SENSORS*, pp. 1358–1361, IEEE, 2009. [doi:10.1109/ICSENS.2009.5398416](https://doi.org/10.1109/ICSENS.2009.5398416).
- [51] T. D. Wyatt, *Pheromones and Animal Behaviour: Communication by Smell and Taste*. Cambridge university press, 1st ed., 2009. ISBN-13: 978-0511615061.
- [52] G. M. Patel, G. C. Patel, R. B. Patel, J. K. Patel, and M. Patel, “Nanorobot: a Versatile Tool in Nanomedicine,” *Journal of Drug Targeting*, vol. 14, no. 2, pp. 63–67, 2006. [doi:10.1080/10611860600612862](https://doi.org/10.1080/10611860600612862).
- [53] A. Murshid and J. Presley, “ER-to-Golgi Transport and Cytoskeletal Interactions in Animal Cells,” *Cellular and Molecular Life Sciences*, vol. 61, no. 2, pp. 133–145, 2004. [doi:10.1007/s00018-003-3352-9](https://doi.org/10.1007/s00018-003-3352-9).
- [54] H. C. Berg and D. A. Brown, “Chemotaxis in *Escherichia coli* Analysed by Three-Dimensional Tracking,” *Nature*, vol. 239, no. 5374, pp. 500–504, 1972. [doi:10.1038/239500a0](https://doi.org/10.1038/239500a0).
- [55] S. Qiu, W. Haselmayr, B. Li, C. Zhao, and W. Guo, “Bacterial Relay for Energy-Efficient Molecular Communications,” *IEEE Transactions on NanoBioscience*, vol. 16, no. 7, pp. 555 – 562, 2017. [doi:10.1109/TNB.2017.2741669](https://doi.org/10.1109/TNB.2017.2741669).
- [56] F. Bogazzi, L. Bartalena, S. Brogioni, A. Burelli, L. Manetti, M. L. Tanda, M. Gasperi, and E. Martino, “Thyroid Vascularity and Blood Flow are not Dependent on Serum Thyroid Hormone Levels: Studies in Vivo by Color Flow Doppler Sonography,” *European Journal of Endocrinology*, vol. 140, no. 5, pp. 452–456, 1999. [doi:10.1530/eje.0.1400452](https://doi.org/10.1530/eje.0.1400452).

- [57] Y. Hiraoka, T. Haraguchi, T. Koujin, T. Suda, A. Enomoto, M. Moore, T. Nakano, Tadashi, Y. Hiraoka, T. Haraguchi, T. Koujin, T. Suda, A. Enomoto, M. Moore, T. Nakano, and Tadashi, “A Cell-Based Molecular Communication Network,” in *1st Bio-Inspired Models of Network, Information and Computing Systems*, pp. 1–1, 2006. [doi:10.1109/BIMNICS.2006.361807](https://doi.org/10.1109/BIMNICS.2006.361807).
- [58] M. Heil and R. Karban, “Explaining Evolution of Plant Communication by Air-borne Signals,” *Trends in Ecology & Evolution*, vol. 25, no. 3, pp. 137–144, 2010. [doi:10.1016/j.tree.2009.09.010](https://doi.org/10.1016/j.tree.2009.09.010).
- [59] D. Demiray, A. Cabellos-Aparicio, E. Alarcón, D. T. Altilar, I. Llatser, L. Felicetti, G. Reali, and M. Femminella, “DIRECT: a Model for Molecular Communication Nanonetworks Based on Discrete Entities,” *Nano Communication Networks*, vol. 4, no. 4, pp. 181–188, 2013. [doi:10.1016/j.nancom.2013.08.004](https://doi.org/10.1016/j.nancom.2013.08.004).
- [60] R. K. Vander Meer, M. D. Breed, K. E. Espelie, and M. L. Winston, *Pheromone Communication in Social Insects: Ants, Wasps, Bees and Termites (Westview Studies in Insect Biology)*. Westview Press, 1st ed., 1997. ISBN-13: 978-0813389769.
- [61] T. D. Wyatt, “Fifty Years of Pheromones,” *Nature*, vol. 457, no. 7227, pp. 262–263, 2009. [doi:10.1038/457262a](https://doi.org/10.1038/457262a).
- [62] F. Stajano, N. Hoult, I. Wassell, P. Bennett, C. Middleton, and K. Soga, “Smart Bridges, Smart Tunnels: Transforming Wireless Sensor Networks from Research Prototypes into Robust Engineering Infrastructure,” *Ad Hoc Networks*, vol. 8, no. 8, pp. 872–888, 2010. [doi:10.1016/j.adhoc.2010.04.002](https://doi.org/10.1016/j.adhoc.2010.04.002).
- [63] P. Couvreur and C. Vauthier, “Nanotechnology: Intelligent Design to Treat Complex Disease,” *Pharmaceutical Research*, vol. 23, no. 7, pp. 1417–1450, 2006. [doi:10.1007/s11095-006-0284-8](https://doi.org/10.1007/s11095-006-0284-8).
- [64] A. E. Forooshani, S. Bashir, D. G. Michelson, and S. Noghanian, “A Survey of Wireless Communications and Propagation Modeling in Underground Mines,” *IEEE Communications Surveys & Tutorials*, vol. 15, no. 4, pp. 1524–1545, 2013. [doi:10.1109/SURV.2013.031413.00130](https://doi.org/10.1109/SURV.2013.031413.00130).
- [65] O. Veiseh, J. W. Gunn, and M. Zhang, “Design and Fabrication of Magnetic Nanoparticles for Targeted Drug Delivery and Imaging,” *Advanced Drug Delivery Reviews*, vol. 62, no. 3, pp. 284–304, 2010. [doi:10.1016/j.addr.2009.11.002](https://doi.org/10.1016/j.addr.2009.11.002).
- [66] D. T. McGuiness, V. Selis, and A. Marshall, “Molecular-Based Nano-Communication Network: A Ring Topology Nano-Bots for In-Vivo Drug Delivery Systems,” *IEEE Access*, vol. 7, pp. 12901–12913, 2019. [doi:10.1109/ACCESS.2019.2892816](https://doi.org/10.1109/ACCESS.2019.2892816).
- [67] S. P. Leary, C. Y. Liu, and M. L. Apuzzo, “Toward the Emergence of Nanoneurosurgery: Part III—Nanomedicine: Targeted Nanotherapy, Nanosurgery, and Progress Toward

- the Realization of Nanoneurosurgery,” *Neurosurgery*, vol. 58, no. 6, pp. 1009–1026, 2006. [doi:10.1227/01.NEU.0000217016.79256.16](https://doi.org/10.1227/01.NEU.0000217016.79256.16).
- [68] R. A. Russell, “an Odour Sensing Robot Draws Inspiration from the Insect World,” in *2nd International Conference on Bioelectromagnetism (ICBEM)*, pp. 49–50, IEEE, 1998. [doi:10.1109/ICBEM.1998.666389](https://doi.org/10.1109/ICBEM.1998.666389).
- [69] S. Kazadi, R. Goodman, D. Tsikata, D. Green, and H. Lin, “an Autonomous Water Vapor Plume Tracking Robot using Passive Resistive Polymer Sensors,” *Autonomous Robots*, vol. 9, no. 2, pp. 175–188, 2000. [doi:10.1023/A:1008970418316](https://doi.org/10.1023/A:1008970418316).
- [70] H. Ishida, T. Nakamoto, T. Moriizumi, T. Kikas, and J. Janata, “Plume-Tracking Robots: A New Application of Chemical Sensors,” *The Biological Bulletin*, vol. 200, no. 2, pp. 222–226, 2001. [doi:10.2307/1543320](https://doi.org/10.2307/1543320).
- [71] A. Lilienthal, A. Zell, M. Wandel, and U. Weimar, “Sensing Odour Sources in Indoor Environments without a Constant Airflow by a Mobile Robot,” in *International Conference on Robotics and Automation (ICRA)*, vol. 4, pp. 4005–4010, IEEE, 2001. [doi:10.1109/ROBOT.2001.933243](https://doi.org/10.1109/ROBOT.2001.933243).
- [72] S. Larionova, N. Almeida, L. Marques, and A. T. de Almeida, “Olfactory Coordinated Area Coverage,” *Autonomous Robots*, vol. 20, no. 3, pp. 251–260, 2006. [doi:10.1007/s10514-006-7099-7](https://doi.org/10.1007/s10514-006-7099-7).
- [73] W. Li, J. A. Farrell, S. Pang, and R. M. Arrieta, “Moth-Inspired Chemical Plume Tracing on an Autonomous Underwater Vehicle,” *IEEE Transactions on Robotics*, vol. 22, no. 2, pp. 292–307, 2006. [doi:10.1109/TRO.2006.870627](https://doi.org/10.1109/TRO.2006.870627).
- [74] P. Sousa, L. Marques, and A. T. de Almeida, “Toward Chemical-Trail Following Robots,” in *7th International Conference on Machine Learning and Applications (ICMLA)*, pp. 489–494, IEEE, 2008. [doi:10.1109/ICMLA.2008.133](https://doi.org/10.1109/ICMLA.2008.133).
- [75] D. Martinez, O. Rochel, and E. Hugues, “a Biomimetic Robot For Tracking Specific Odors in Turbulent Plumes,” *Autonomous Robots*, vol. 20, no. 3, pp. 185–195, 2006. [doi:10.1007/s10514-006-7157-1](https://doi.org/10.1007/s10514-006-7157-1).
- [76] A. D. C. de Albornoz, A. B. Rodríguez, A. L. Lopez, and A. R. G. Ramirez, “a Microcontroller-Based Mobile Robotic Platform for Odor Detection,” in *ISSNIP Biosignals and Biorobotics Conference: Biosignals and Robotics for Better and Safer Living (BRC)*, pp. 1–6, IEEE, 2012. [doi:10.1109/BRC.2012.6222183](https://doi.org/10.1109/BRC.2012.6222183).
- [77] A. Cavalcanti, T. Hogg, B. Shirinzadeh, and H. C. Liaw, “Nanorobot Communication Techniques: a Comprehensive Tutorial,” in *9th International Conference on Control, Automation, Robotics and Vision (ICARCV)*, pp. 1–6, IEEE, 2006. [doi:10.1109/ICARCV.2006.345457](https://doi.org/10.1109/ICARCV.2006.345457).

- [78] G. Von Maltzahn, J.-H. Park, K. Y. Lin, N. Singh, C. Schwöppe, R. Mesters, W. E. Berdel, E. Ruoslahti, M. J. Sailor, and S. N. Bhatia, “Nanoparticles that Communicate *in vivo* to Amplify Tumour Targeting,” *Nature materials*, vol. 10, no. 7, p. 545, 2011. [doi:10.1038/nmat3049](https://doi.org/10.1038/nmat3049).
- [79] Y. Kuwana, S. Nagasawa, I. Shimoyama, and R. Kanzaki, “Synthesis of the Pheromone-Oriented Behaviour of Silkworm Moths by a Mobile Robot with Moth Antennae as Pheromone Sensors,” *Biosensors and Bioelectronics*, vol. 14, no. 2, pp. 195–202, 1999. [doi:10.1016/S0956-5663\(98\)00106-7](https://doi.org/10.1016/S0956-5663(98)00106-7).
- [80] A. H. Purnamadjaja and R. A. Russell, “Pheromone Communication in a Robot Swarm: Necrophoric Bee Behaviour and its Replication,” *Robotica*, vol. 23, no. 6, pp. 731–742, 2005. [doi:10.1017/S0263574704001225](https://doi.org/10.1017/S0263574704001225).
- [81] A. H. Purnamadjaja and R. A. Russell, “Bi-directional Pheromone Communication Between Robots,” *Robotica*, vol. 28, no. 1, pp. 69–79, 2010. [doi:10.1017/S0263574709005591](https://doi.org/10.1017/S0263574709005591).
- [82] T. M. Cover and J. A. Thomas, *Elements of Information Theory*. Wiley-Blackwell, 2nd ed., 2006. ISBN-13: 978-0471241959.
- [83] A. Gohari, M. Mirmohseni, and M. Nasiri-Kenari, “Information Theory of Molecular Communication: Directions and Challenges,” *IEEE Transactions on Molecular, Biological and Multi-Scale Communications*, vol. 2, no. 2, pp. 120–142, 2016. [doi:10.1109/TMBMC.2016.2640284](https://doi.org/10.1109/TMBMC.2016.2640284).
- [84] V. Jamali, A. Ahmadzadeh, N. Farsad, and R. Schober, “SCW Codes for Optimal CSI-free Detection in Diffusive Molecular Communications,” in *International Symposium on Information Theory (ISIT)*, pp. 3190–3194, IEEE, 2017. [doi:10.1109/ISIT.2017.8007118](https://doi.org/10.1109/ISIT.2017.8007118).
- [85] C. E. Shannon, “a Mathematical Theory of Communication,” *Bell system technical journal*, vol. 27, no. 3, pp. 379–423, 1948. [doi:10.1002/j.1538-7305.1948.tb01338.x](https://doi.org/10.1002/j.1538-7305.1948.tb01338.x).
- [86] S. Verdú and T. S. Han, “a General Formula for Channel Capacity,” *IEEE Transactions on Information Theory*, vol. 40, no. 4, pp. 1147–1157, 1994. [doi:10.1109/18.335960](https://doi.org/10.1109/18.335960).
- [87] R. Blahut, “Computation of Channel Capacity and Rate-Distortion Functions,” *IEEE Transactions on Information Theory*, vol. 18, no. 4, pp. 460–473, 1972. [doi:10.1109/TIT.1972.1054855](https://doi.org/10.1109/TIT.1972.1054855).
- [88] S. Arimoto, “an Algorithm for Computing the Capacity of Arbitrary Discrete Memoryless Channels,” *IEEE Transactions on Information Theory*, vol. 18, no. 1, pp. 14–20, 1972. [doi:10.1109/TIT.1972.1054753](https://doi.org/10.1109/TIT.1972.1054753).
- [89] R. Gallager, *Information Theory and Reliable Communication*, vol. 1. Springer, 1970. ISBN-13: 978-3211811450.

- [90] M. Turan, M. Ş. Kuran, H. B. Yılmaz, I. Demirkol, and T. Tuğcu, “Channel Model of Molecular Communication via Diffusion in a Vessel-Like Environment Considering a Partially Covering Receiver,” in *International Black Sea Conference on Communications and Networking (BlackSeaCom)*, pp. 1–5, IEEE, 2018. [doi:10.1109/BlackSeaCom.2018.8433703](https://doi.org/10.1109/BlackSeaCom.2018.8433703).
- [91] S. M. Mustam, S. K. Syed Yusof, and S. Nejatian, “Multilayer Diffusion-based Molecular Communication,” *Transactions on Emerging Telecommunications Technologies*, vol. 28, no. 1, pp. 2161–3915, 2017. [doi:10.1002/ett.2935](https://doi.org/10.1002/ett.2935).
- [92] Y. Murin, N. Farsad, M. Chowdhury, and A. Goldsmith, “Exploiting Diversity in One-Shot Molecular Timing Channels via Order Statistics,” *IEEE Transactions on Molecular, Biological and Multi-Scale Communications*, vol. 4, no. 1, pp. 14–26, 2018. [doi:10.1109/TMBMC.2018.2889644](https://doi.org/10.1109/TMBMC.2018.2889644).
- [93] A. Ahmadzadeh, V. Jamali, and R. Schober, “Statistical Analysis of Time-Variant Channels in Diffusive Mobile Molecular Communications,” in *Global Communications Conference (GLOBECOM)*, pp. 1–7, IEEE, 2017. [doi:10.1109/GLOCOM.2017.8254237](https://doi.org/10.1109/GLOCOM.2017.8254237).
- [94] Y. Sun, *Channel Modelling of Blood Capillary-based Molecular Communication*. PhD thesis, University of Essex, 2018.
- [95] H. Ramezani, T. Khan, and O. B. Akan, “Information Theoretical Analysis of Synaptic Communication for Nanonetworks,” in *Conference on Computer Communications (INFOCOM)*, pp. 2330–2338, IEEE, 2018. [doi:10.1109/INFOCOM.2018.8486255](https://doi.org/10.1109/INFOCOM.2018.8486255).
- [96] J. W. Kwack, H. B. Yilmaz, N. Farsad, C.-B. Chae, and A. Goldsmith, “Two Way Molecular Communications,” in *5th International Conference on Nanoscale Computing and Communication (NANOCOM)*, pp. 1–5, ACM, 2018. [doi:10.1145/3233188.3233199](https://doi.org/10.1145/3233188.3233199).
- [97] H. G. Bafghi, A. Gohari, M. Mirmohseni, G. Aminian, and M. Nasiri-Kenari, “Diffusion-Based Molecular Communication with Limited Molecule Production Rate,” *IEEE Transactions on Molecular, Biological and Multi-Scale Communications*, vol. 4, no. 2, pp. 61–72, 2018. [doi:10.1109/TMBMC.2019.2895815](https://doi.org/10.1109/TMBMC.2019.2895815).
- [98] L. Galluccio, A. Lombardo, G. Morabito, S. Palazzo, C. Panarello, and G. Schembra, “Capacity of a Binary Droplet-based Microfluidic Channel with Memory and Anticipation for Flow-induced Molecular Communications,” *IEEE Transactions on Communications*, vol. 66, no. 1, pp. 194–208, 2018. [doi:10.1109/TCOMM.2017.2755649](https://doi.org/10.1109/TCOMM.2017.2755649).
- [99] N. Farsad, C. Rose, M. Médard, and A. Goldsmith, “Capacity of Molecular Channels with Imperfect Particle-intensity Modulation and Detection,” in *International Symposium on Information Theory (ISIT)*, pp. 2468–2472, IEEE, 2017. [doi:10.1109/ISIT.2017.8006973](https://doi.org/10.1109/ISIT.2017.8006973).

- [100] A. Etemadi, P. Azmi, H. Arjmandi, and N. Mokari, “Compound Poisson Noise Sources in Diffusion-Based Molecular Communication,” *IEEE Transactions on Communications*, vol. 67, no. 6, pp. 4104–4116, 2019. [doi:10.1109/TCOMM.2019.2899092](https://doi.org/10.1109/TCOMM.2019.2899092).
- [101] K. Srinivas, A. W. Eckford, and R. S. Adve, “Molecular Communication in Fluid Media: the Additive Inverse Gaussian Noise Channel,” *IEEE Transactions on Information Theory*, vol. 58, no. 7, pp. 4678–4692, 2012. [doi:10.1109/TIT.2012.2193554](https://doi.org/10.1109/TIT.2012.2193554).
- [102] S. R. Islam, F. Ali, H. Moon, and K.-S. Kwak, “Secure Channel for Molecular Communications,” in *International Conference on Information and Communication Technology Convergence (ICTC)*, pp. 1–4, IEEE, 2017. [doi:10.1109/ICTC.2017.8190929](https://doi.org/10.1109/ICTC.2017.8190929).
- [103] V. Loscri, C. Marchal, N. Mitton, G. Fortino, and A. V. Vasilakos, “Security and Privacy in Molecular Communication and Networking: Opportunities and Challenges,” *IEEE Transactions on NanoBioscience*, vol. 13, no. 3, pp. 198–207, 2014. [doi:10.1109/TNB.2014.2349111](https://doi.org/10.1109/TNB.2014.2349111).
- [104] R. G. Thorne, S. Hrabětová, and C. Nicholson, “Diffusion of Epidermal Growth Factor in Rat Brain Extracellular Space Measured by Integrative Optical Imaging,” *Journal of Neurophysiology*, vol. 92, no. 6, pp. 3471–3481, 2004. [doi:10.1152/jn.00352.2004](https://doi.org/10.1152/jn.00352.2004).
- [105] C. Mucignat-Caretta, *Neurobiology of Chemical Communication (Frontiers in Neuroscience)*. CRC Press, 1st ed., 2014. ISBN-13: 978-1466553415.
- [106] J. Sallée, K. Speer, R. Morrow, and R. Lumpkin, “an Estimate of Lagrangian Eddy Statistics and Diffusion in the Mixed Layer of the Southern Ocean,” *Journal of Marine Research*, vol. 66, no. 4, pp. 441–463, 2008. [doi:10.1357/002224008787157458](https://doi.org/10.1357/002224008787157458).
- [107] P. G. Black, S. J. Buchan, and R. L. Cohen, “The Tropical Cyclone Eyewall Mesovortex: A Physical Mechanism Explaining Extreme Peak Gust Occurrence in TC Olivia, 4 April 1996 on Barrow Island, Australia,” in *Offshore Technology Conference*, pp. 1–5, Offshore Technology Conference, 1999. [doi:10.4043/10792-MS](https://doi.org/10.4043/10792-MS).
- [108] B. Steigerwald, “Jupiter’s little red spot growing stronger,” NASA, 2007. [Retrieved February 8, 2019] https://www.nasa.gov/centers/goddard/news/topstory/2006/little_red_spot.html.
- [109] T. A. Schroer and M. P. Sheetz, “Two Activators of Microtubule-based Vesicle Transport,” *The Journal of Cell Biology*, vol. 115, no. 5, pp. 1309–1318, 1991. [doi:10.1083/jcb.115.5.1309](https://doi.org/10.1083/jcb.115.5.1309).
- [110] E. Barta, S. Sideman, and J. B. Bassingthwaigte, “Facilitated Diffusion and Membrane Permeation of Fatty Acid in Albumin Solutions,” *Annals of Biomedical Engineering*, vol. 28, no. 3, pp. 331–345, 2000. [doi:10.1114/1.274](https://doi.org/10.1114/1.274).
- [111] M. Demir and H. Salman, “Bacterial Thermotaxis by Speed Modulation,” *Biophysical Journal*, vol. 103, no. 8, pp. 1683–1690, 2012. [doi:10.1016/j.bpj.2012.09.005](https://doi.org/10.1016/j.bpj.2012.09.005).

- [112] M. J. Sanderson, “Intercellular Waves of Communication,” *Physiology*, vol. 11, no. 6, pp. 262–269, 1996. [doi:10.1152/physiologyonline.1996.11.6.262](https://doi.org/10.1152/physiologyonline.1996.11.6.262).
- [113] M. Delling, P. G. DeCaen, J. F. Doerner, S. Febvay, and D. E. Clapham, “Primary Cilia are Specialized Calcium Signalling Organelles,” *Nature*, vol. 504, no. 7479, p. 311, 2013. [doi:10.1038/nature12833](https://doi.org/10.1038/nature12833).
- [114] M. B. Elowitz, M. G. Surette, P.-E. Wolf, J. B. Stock, and S. Leibler, “Protein Mobility in the Cytoplasm of *Escherichia coli*,” *Journal of Bacteriology*, vol. 181, no. 1, pp. 197–203, 1999. [PubMed PMID: 9864330](#).
- [115] K. Weiß, A. Neef, Q. Van, S. Kramer, I. Gregor, and J. Enderlein, “Quantifying the Diffusion of Membrane Proteins and Peptides in Black Lipid Membranes with 2-Focus Fluorescence Correlation Spectroscopy,” *Biophysical Journal*, vol. 105, no. 2, pp. 455–462, 2013. [doi:10.1016/j.bpj.2013.06.004](https://doi.org/10.1016/j.bpj.2013.06.004).
- [116] J. M. Berg, J. L. Tymoczko, J. Gregory J. Gatto, and L. Stryer, *Biochemistry*. WH Freeman, 8th ed., 2002. [ISBN-13: 978-1464126109](#).
- [117] S. Kadloor, R. S. Adve, and A. W. Eckford, “Molecular Communication using Brownian Motion with Drift,” *IEEE Transactions on NanoBioscience*, vol. 11, no. 2, pp. 89–99, 2012. [doi:10.1109/TNB.2012.2190546](https://doi.org/10.1109/TNB.2012.2190546).
- [118] T. Pichugina, T. Sugawara, A. Kaykov, W. Schierding, K. Masuda, J. Uewaki, R. Grand, J. R. Allison, R. A. Martienssen, P. Nurse, M. Ueno, and J. M. O’Sullivan, “A Diffusion Model for the Coordination of DNA Replication in *Schizosaccharomyces pombe*,” *Scientific Reports*, vol. 6, p. 18757, 2016. [doi:10.1038/srep18757](https://doi.org/10.1038/srep18757).
- [119] H. C. Berg, *Random Walks in Biology*. Princeton University Press, 1st ed., 1993. [ISBN-13: 978-0691000640](#).
- [120] J. T. Edward, “Molecular Volumes and the Stokes-Einstein Equation,” *Journal of Chemical Education*, vol. 47, no. 4, p. 261, 1970. [doi:10.1021/ed047p261](https://doi.org/10.1021/ed047p261).
- [121] N. Kosov, “Elementary Kinetic Theory of Diffusion in Gases,” *Journal of Engineering Physics*, vol. 42, no. 2, pp. 181–192, 1982. [doi:10.1007/BF00827267](https://doi.org/10.1007/BF00827267).
- [122] D. Ben-Avraham and S. Havlin, *Diffusion and Reactions in Fractals and Disordered Systems*. Cambridge university press, 1st ed., 2005. [ISBN-13: 978-0521617208](#).
- [123] P. S. Nobel, *Physicochemical & Environmental Plant Physiology*. Academic press, 4th ed., 1999. [ISBN-13: 978-0123741431](#).
- [124] D. Voet, J. G. Voet, and C. W. Pratt, *Fundamentals of Biochemistry: Life at the Molecular Level*. John Wiley & Sons, 4th ed., 2012. [ISBN-13: 978-1118129180](#).

- [125] S. M. Clifford and D. Hillel, “Knudsen Diffusion: the Effect of Small Pore Size and Low Gas Pressure on Gaseous Transport in Soil,” *Soil Science*, vol. 141, no. 4, pp. 289–297, 1986. [doi:10.1097/00010694-198604000-00006](https://doi.org/10.1097/00010694-198604000-00006).
- [126] S.-J. Sheu, “Some Estimates of the Transition Density of a Nondegenerate Diffusion Markov Process,” *The Annals of Probability*, vol. 19, no. 2, pp. 538–561, 1991. [doi:10.1214/aop/1176990440](https://doi.org/10.1214/aop/1176990440).
- [127] S. M. Ross, *Stochastic Processes*. Wiley, 2nd ed., 1995. ISBN-13: 978-0471120629.
- [128] J. Berthier and P. Silberzan, *Microfluidics for Biotechnology*. Artech House, 2nd ed., 2009. ISBN-13: 978-1596934436.
- [129] B. Øksendal, *Stochastic Differential Equations: an Introduction with Applications (Universitext)*. Springer-Verlag Berlin Heidelberg, 6th ed., 2014. ISBN-13: 978-3540047582.
- [130] D. S. Lemons and A. Gythiel, “Paul Langevin’s 1908 Paper “on the Theory of Brownian Motion”[“Sur la Théorie du Mouvement Brownien,” cr acad. sci.(paris) 146, 530–533 (1908)],” *American Journal of Physics*, vol. 65, no. 11, pp. 1079–1081, 1997. [doi:10.1119/1.18725](https://doi.org/10.1119/1.18725).
- [131] C. T. Chou, “Extended Master Equation Models for Molecular Communication Networks,” *IEEE Transactions on NanoBioscience*, vol. 12, no. 2, pp. 79–92, 2013. [doi:10.1109/TNB.2013.2237785](https://doi.org/10.1109/TNB.2013.2237785).
- [132] M. Pierobon and I. F. Akyıldız, “Noise Analysis in Ligand-Binding Reception for Molecular Communication in Nanonetworks,” *IEEE Transactions on Signal Processing*, vol. 59, no. 9, pp. 4168–4182, 2011. [doi:10.1109/TSP.2011.2159497](https://doi.org/10.1109/TSP.2011.2159497).
- [133] M. Pierobon and I. F. Akyıldız, “Capacity of a Diffusion-Based Molecular Communication System with Channel Memory and Molecular Noise,” *IEEE Transactions on Information Theory*, vol. 59, no. 2, pp. 942–954, 2013. [doi:10.1109/TIT.2012.2219496](https://doi.org/10.1109/TIT.2012.2219496).
- [134] F. Zabini, “Spatially Distributed Molecular Communications: an Asynchronous Stochastic Model,” *IEEE Communications Letters*, vol. 22, no. 7, pp. 1326–1329, 2018. [doi:10.1109/LCOMM.2018.2826018](https://doi.org/10.1109/LCOMM.2018.2826018).
- [135] J. Crank, *The Mathematics of Diffusion (Oxford Science Publications)*. Oxford University Press, 2nd ed., 1979. ISBN-13: 978-0198534112.
- [136] I. M. Gel’fand and G. E. Shilov, *Generalized Functions, Volume 2: Spaces of Fundamental and Generalized Functions*, vol. 378. AMS Chelsea Publishing, 1st ed., 1968. ISBN-13: 978-1-4704-2659-0.
- [137] S. Redner, *a Guide to First-Passage Processes*. Cambridge University Press, 2001. ISBN-13: 978-0521652483.

- [138] H. B. Yilmaz, A. C. Heren, T. Tuğcu, and C.-B. Chae, “Three-dimensional Channel Characteristics for Molecular Communications with an Absorbing Receiver,” *IEEE Communications Letters*, vol. 18, no. 6, pp. 929–932, 2014. [doi:10.1109/LCOMM.2014.2320917](https://doi.org/10.1109/LCOMM.2014.2320917).
- [139] I. Llatser, E. Alarcón, and M. Pierobony, “Diffusion-based Channel Characterization in Molecular Nanonetworks,” in *Conference on Computer Communications Workshops (INFOCOM WKSHPS)*, pp. 467–472, IEEE, 2011. [doi:10.1109/INFCOMW.2011.5928858](https://doi.org/10.1109/INFCOMW.2011.5928858).
- [140] L. P. Kadanoff, *Statistical Physics: Statics, Dynamics and Renormalization*. World Scientific Publishing Co Inc., 1st ed., 2000. ISBN-13: 978-9810237585.
- [141] B. Atakan and O. B. Akan, “Deterministic Capacity of Information Flow in Molecular Nanonetworks,” *Nano Communication Networks*, vol. 1, no. 1, pp. 31–42, 2010. [doi:10.1016/j.nancom.2010.03.003](https://doi.org/10.1016/j.nancom.2010.03.003).
- [142] L. S. Meng, P. C. Yeh, K. C. Chen, and I. F. Akyildiz, “MIMO Communications Based on Molecular Diffusion,” in *Global Communications Conference (GLOBECOM)*, pp. 5380–5385, IEEE, 2012. [doi:10.1109/GLOCOM.2012.6503976](https://doi.org/10.1109/GLOCOM.2012.6503976).
- [143] R. M. Ziff, S. N. Majumdar, and A. Comtet, “Capture of Particles Undergoing Discrete Random Walks,” *The Journal of Chemical Physics*, vol. 130, no. 20, p. 204104, 2009. [doi:10.1063/1.3137062](https://doi.org/10.1063/1.3137062).
- [144] S. Wang, W. Guo, S. Qiu, and M. D. McDonnell, “Performance of Macro-scale Molecular Communications with Sensor Cleanse Time,” in *21st International Conference on Telecommunications (ICT)*, pp. 363–368, IEEE, 2014. [doi:10.1109/ICT.2014.6845140](https://doi.org/10.1109/ICT.2014.6845140).
- [145] G. B. Thomas, M. D. Weir, J. Hass, and F. R. Giordano, *Thomas' Calculus*. Pearson, 14th ed., 2017. ISBN-13: 978-0134438986.
- [146] J. Pedlosky, *Geophysical Fluid Dynamics*. Springer-Verlag New York, 2th ed., 1987. ISBN-13: 978-0387963877.
- [147] S. Chandrasekhar, “Stochastic Problems in Physics and Astronomy,” *Reviews of Modern Physics*, vol. 15, no. 1, p. 1, 1943. [doi:10.1103/RevModPhys.15.1](https://doi.org/10.1103/RevModPhys.15.1).
- [148] T. Stocker, *Introduction to Climate Modelling*. Springer-Verlag Berlin Heidelberg, 1st ed., 2011. ISBN-13: 978-3-642-00772-9.
- [149] O. K. Jensen and B. A. Finlayson, “Solution of the Transport Equations using a Moving Coordinate System,” *Advances in Water Resources*, vol. 3, no. 1, pp. 9–18, 1980. [doi:10.1016/0309-1708\(80\)90014-7](https://doi.org/10.1016/0309-1708(80)90014-7).

- [150] J.-S. Chen, Y.-H. Liu, C.-P. Liang, C.-W. Liu, and C.-W. Lin, “Exact Analytical Solutions for Two-dimensional Advection–Dispersion Equation in Cylindrical Coordinates Subject to Third-type Inlet Boundary Condition,” *Advances in Water Resources*, vol. 34, no. 3, pp. 365–374, 2011. [doi:10.1016/j.advwatres.2010.12.008](https://doi.org/10.1016/j.advwatres.2010.12.008).
- [151] A. D. Poliarikas, *Transforms and Applications Handbook (Electrical Engineering Handbook)*. CRC press, 3rd ed., 2010. ISBN-13: 978-1420066524.
- [152] N. A. Gershenfeld, *The Nature of Mathematical Modeling*. Cambridge University Press, 1st ed., 1998. ISBN-13: 978-0521570954.
- [153] R. Courant and D. Hilbert, *Methods of Mathematical Physics: Partial Differential Equations, Volume 2*. John Wiley & Sons, 1st ed., 2008. ISBN-13: 978-3527617241.
- [154] M. Zoofaghari and H. Arjmandi, “Diffusive Molecular Communication in Biological Cylindrical Environment,” *IEEE Transactions on NanoBioscience*, vol. 18, no. 1, pp. 74–83, 2018. [doi:10.1109/TNB.2018.2885051](https://doi.org/10.1109/TNB.2018.2885051).
- [155] A. Goel, A. Ridley, and D. S. Bernstein, “Estimation of the Eddy Diffusion Coefficient Using Total Electron Content Data,” in *Annual American Control Conference (ACC)*, pp. 3298–3303, IEEE, 2018. [doi:10.23919/ACC.2018.8431184](https://doi.org/10.23919/ACC.2018.8431184).
- [156] M. M. Karaman and X. J. Zhou, “A Fractional Motion Diffusion Model for a Twice-refocused Spin-Echo Pulse Sequence,” *NMR in Biomedicine*, p. e3960, 2018. [doi:10.1002/nbm.3960](https://doi.org/10.1002/nbm.3960).
- [157] Y. Shao, S. Ramachandran, S. Arnold, and G. Ramachandran, “Turbulent Eddy Diffusion Models in Exposure Assessment-determination of the Eddy Diffusion Coefficient,” *Journal of Occupational and Environmental Hygiene*, vol. 14, no. 3, pp. 195–206, 2017. [doi:10.1080/15459624.2016.1238476](https://doi.org/10.1080/15459624.2016.1238476).
- [158] A. Sommerfeld, “Ein Beitrag zur hydrodynamischen Erklarung der turbulenten Fluessigkeitsbewegungen [a contribution to the hydrodynamic explanation of the turbulent fluid movements],” *Atti del*, vol. 4, pp. 116–124, 1908. [doi:10.1098/rspa.1954.0130](https://doi.org/10.1098/rspa.1954.0130).
- [159] G. I. Taylor, “Eddy Motion in the Atmosphere,” *Philosophical Transactions of the Royal Society of London. Series A, Containing Papers of a Mathematical or Physical Character*, vol. 215, pp. 1–26, 1915. [doi:10.1098/rsta.1915.0001](https://doi.org/10.1098/rsta.1915.0001).
- [160] H. Carslaw and J. Jaeger, *Conduction of Heat in Solids (Oxford Science Publications)*. Oxford University Press, 2nd ed., 1986. ISBN-13: 978-0198533689.
- [161] M. Abbaszadeh, H. B. Yilmaz, P. J. Thomas, and W. Guo, “Linearity of Sequential Molecular Signals in Turbulent Diffusion Channels,” in *International Conference on Communications (ICC)*, pp. 1–6, 2019. [doi:10.1109/ICC.2019.8761812](https://doi.org/10.1109/ICC.2019.8761812).

- [162] I. Atthanayake, S. Esfahani, P. Denissenko, I. Guymer, P. J. Thomas, and W. Guo, “Experimental molecular communications in obstacle rich fluids,” in *5th International Conference on Nanoscale Computing and Communication (NANOCOM)*, pp. 1–2, ACM, 2018. [doi:10.1145/3233188.3233216](https://doi.org/10.1145/3233188.3233216).
- [163] M. Ş. Kuran, H. B. Yılmaz, T. Tuğcu, and I. F. Akyıldız, “Modulation Techniques for Communication via Diffusion in Nanonetworks,” in *International Conference on Communications (ICC)*, pp. 1–5, IEEE, 2011. [doi:10.1109/icc.2011.5962989](https://doi.org/10.1109/icc.2011.5962989).
- [164] M. Ş. Kuran, H. B. Yılmaz, T. Tuğcu, and I. F. Akyıldız, “Interference Effects on Modulation Techniques in Diffusion Based Nanonetworks,” *Nano Communication Networks*, vol. 3, no. 1, pp. 65–73, 2012. [doi:10.1016/j.nancom.2012.01.005](https://doi.org/10.1016/j.nancom.2012.01.005).
- [165] L. Lin, Q. Wu, M. Ma, and H. Yan, “Concentration-Based Demodulation Scheme for Mobile Receiver in Molecular Communication,” *Nano Communication Networks*, vol. 20, pp. 11–19, 2019. [doi:10.1016/j.nancom.2019.01.003](https://doi.org/10.1016/j.nancom.2019.01.003).
- [166] N.-R. Kim and C.-B. Chae, “Novel Modulation Techniques using Isomers as Messenger Molecules for Nano Communication Networks via Diffusion,” *IEEE Journal on Selected Areas in Communications*, vol. 31, no. 12, pp. 847–856, 2013. [doi:10.1109/JSAC.2013.SUP2.12130017](https://doi.org/10.1109/JSAC.2013.SUP2.12130017).
- [167] G. Ardel, C. Külls, and H. Hellbrück, “Towards intrinsic molecular communication using isotopic isomerism,” *Open Journal of Internet Of Things (OJIOT)*, vol. 4, no. 1, pp. 135–143, 2018.
- [168] M. H. Kabir, S. R. Islam, and K. S. Kwak, “D-MoSK Modulation in Molecular Communications,” *IEEE Transactions on NanoBioscience*, vol. 14, no. 6, pp. 680–683, 2015. [doi:10.1109/TNB.2015.2436409](https://doi.org/10.1109/TNB.2015.2436409).
- [169] R. Mosayebi, A. Gohari, M. Mirmohseni, and M. N. Kenari, “Type Based Sign Modulation for Molecular Communication,” in *Iran Workshop on Communication and Information Theory (IWCIT)*, pp. 1–6, IEEE, 2016. [doi:10.1109/IWCIT.2016.7491618](https://doi.org/10.1109/IWCIT.2016.7491618).
- [170] R. Mosayebi, A. Gohari, M. Mirmohseni, and M. Nasiri-Kenari, “Type-Based Sign Modulation and its Application for ISI Mitigation in Molecular Communication,” *IEEE Transactions on Communications*, vol. 66, no. 1, pp. 180–193, 2018. [doi:10.1109/TCOMM.2017.2754492](https://doi.org/10.1109/TCOMM.2017.2754492).
- [171] N. Garralda, I. Llatser, A. Cabellos-Aparicio, E. Alarcón, and M. Pierobon, “Diffusion-based Physical Channel Identification in Molecular Nanonetworks,” *Nano Communication Networks*, vol. 2, no. 4, pp. 196–204, 2011. [doi:10.1016/j.nancom.2011.07.001](https://doi.org/10.1016/j.nancom.2011.07.001).

- [172] B. Krishnaswamy, C. M. Austin, J. P. Bardill, D. Russakow, G. L. Holst, B. K. Hammer, C. R. Forest, and R. Sivakumar, “Time-Elapse Communication: Bacterial Communication on a Microfluidic Chip,” *IEEE Transactions on Communications*, vol. 61, no. 12, pp. 5139–5151, 2013. [doi:10.1109/TCOMM.2013.111013.130314](https://doi.org/10.1109/TCOMM.2013.111013.130314).
- [173] B. Atakan, S. Galmes, and O. B. Akan, “Nanoscale Communication with Molecular Arrays in Nanonetworks,” *IEEE Transactions on NanoBioscience*, vol. 11, no. 2, pp. 149–160, 2012. [doi:10.1109/TNB.2011.2181862](https://doi.org/10.1109/TNB.2011.2181862).
- [174] B. Tepeku, A. E. Pusane, H. B. Yilmaz, and T. Tuğcu, “Energy Efficient ISI Mitigation for Communication via Diffusion,” in *International Black Sea Conference on Communications and Networking (BlackSeaCom)*, pp. 33–37, IEEE, 2014. [doi:10.1109/BlackSeaCom.2014.6848999](https://doi.org/10.1109/BlackSeaCom.2014.6848999).
- [175] S. Pudasaini, S. Shin, and K. S. Kwak, “Run-length Aware Hybrid Modulation Scheme for Diffusion-based Molecular Communication,” in *14th International Symposium on Communications and Information Technologies (ISCIT)*, pp. 439–442, IEEE, 2014. [doi:10.1109/ISCIT.2014.7011950](https://doi.org/10.1109/ISCIT.2014.7011950).
- [176] M. C. Gürsoy, E. Başar, A. E. Pusane, and T. Tuğcu, “Index Modulation for Molecular Communication via Diffusion Systems,” *IEEE Transactions on Communications*, pp. 1–1, 2019. [doi:10.1109/TCOMM.2019.2898665](https://doi.org/10.1109/TCOMM.2019.2898665).
- [177] M. B. Miller and B. L. Bassler, “Quorum Sensing in Bacteria,” *Annual Reviews in Microbiology*, vol. 55, no. 1, pp. 165–199, 2001. [doi:10.1146/annurev.micro.55.1.165](https://doi.org/10.1146/annurev.micro.55.1.165).
- [178] B. C. Akdeniz, A. E. Pusane, and T. Tuğcu, “Position-based Modulation in Molecular Communications,” *Nano Communication Networks*, vol. 16, pp. 60–68, 2018. [doi:10.1016/j.nancom.2018.01.004](https://doi.org/10.1016/j.nancom.2018.01.004).
- [179] Y.-P. Hsieh, Y.-C. Lee, P.-J. Shih, P.-C. Yeh, and K.-C. Chen, “on the asynchronous Information Embedding for Event-driven Systems in Molecular Communications,” *Nano Communication Networks*, vol. 4, no. 1, pp. 2–13, 2013. [doi:10.1016/j.nancom.2012.11.001](https://doi.org/10.1016/j.nancom.2012.11.001).
- [180] I. Llatser, A. Cabellos-Aparicio, M. Pierobon, and E. Alarcón, “Detection Techniques for Diffusion-based Molecular Communication,” *IEEE Journal on Selected Areas in Communications*, vol. 31, no. 12, pp. 726–734, 2013. [doi:10.1109/JSAC.2013.SUP2.1213005](https://doi.org/10.1109/JSAC.2013.SUP2.1213005).
- [181] B. C. Akdeniz, A. E. Pusane, and T. Tuğcu, “a Novel Concentration-type Based Modulation in Molecular Communication,” in *25th Signal Processing and Communications Applications Conference (SIU)*, pp. 1–4, IEEE, 2017. [doi:10.1109/SIU.2017.7960355](https://doi.org/10.1109/SIU.2017.7960355).
- [182] M. J. Moore, T. Suda, and K. Oiwa, “Molecular Communication: Modeling Noise Effects on Information Rate,” *IEEE Transactions on NanoBioscience*, vol. 8, no. 2, pp. 169–180, 2009. [doi:10.1109/TNB.2009.2025039](https://doi.org/10.1109/TNB.2009.2025039).

- [183] M. Pierobon and I. F. Akyildiz, “a Statistical–Physical Model of Interference in Diffusion-Based Molecular Nanonetworks,” *IEEE Transactions on Communications*, vol. 62, no. 6, pp. 2085–2095, 2014. [doi:10.1109/TCOMM.2014.2314650](https://doi.org/10.1109/TCOMM.2014.2314650).
- [184] G. Aminian, H. Arjmandi, A. Gohari, M. Nasiri-Kenari, and U. Mitra, “Capacity of Diffusion-based Molecular Communication Networks over LTI-Poisson Channels,” *IEEE Transactions on Molecular, Biological and Multi-Scale Communications*, vol. 1, no. 2, pp. 188–201, 2015. [doi:10.1109/TMBMC.2015.2502858](https://doi.org/10.1109/TMBMC.2015.2502858).
- [185] G. Genç, Y. E. Kara, H. B. Yilmaz, and T. Tuğcu, “ISI-aware Modeling and Achievable Rate Analysis of the Diffusion Channel,” *IEEE Communications Letters*, vol. 20, no. 9, pp. 1729–1732, 2016. [doi:10.1109/LCOMM.2016.2586069](https://doi.org/10.1109/LCOMM.2016.2586069).
- [186] H. Arjmandi, M. Movahednasab, A. Gohari, M. Mirmohseni, M. Nasiri-Kenari, and F. Fekri, “ISI-avoiding Modulation for Diffusion-based Molecular Communication,” *IEEE Transactions on Molecular, Biological and Multi-Scale Communications*, vol. 3, no. 1, pp. 48–59, 2017. [doi:10.1109/TMBMC.2016.2640311](https://doi.org/10.1109/TMBMC.2016.2640311).
- [187] A. Noel, K. C. Cheung, and R. Schober, “Improving Receiver Performance of Diffusive Molecular Communication with Enzymes,” *IEEE Transactions on NanoBioscience*, vol. 13, no. 1, pp. 31–43, 2014. [doi:10.1109/TNB.2013.2295546](https://doi.org/10.1109/TNB.2013.2295546).
- [188] M. Ş. Kuran, H. B. Yılmaz, and T. Tuğcu, “A Tunnel-based Approach for Signal Shaping in Molecular Communication,” in *International Conference on Communications Workshops (ICC)*, pp. 776–781, IEEE, 2013. [doi:10.1109/ICCW.2013.6649338](https://doi.org/10.1109/ICCW.2013.6649338).
- [189] A. C. Heren, H. B. Yılmaz, C.-B. Chae, and T. Tuğcu, “Effect of Degradation in Molecular Communication: Impairment or Enhancement?,” *IEEE Transactions on Molecular, Biological and Multi-Scale Communications*, vol. 1, no. 2, pp. 217–229, 2015. [doi:10.1109/TMBMC.2015.2502859](https://doi.org/10.1109/TMBMC.2015.2502859).
- [190] N. Farsad and A. Goldsmith, “a Molecular Communication System using Acids, Bases and Hydrogen Ions,” in *17th International Workshop on Signal Processing Advances in Wireless Communications (SPAWC)*, pp. 1–6, July 2016. [doi:10.1109/SPAWC.2016.7536834](https://doi.org/10.1109/SPAWC.2016.7536834).
- [191] Y. J. Cho, H. B. Yılmaz, W. Guo, and C.-B. Chae, “Effective Inter-symbol Interference Mitigation with a Limited Amount of Enzymes in Molecular Communications,” *Transactions on Emerging Telecommunications Technologies*, vol. 28, no. 7, p. e3106, 2017. [doi:10.1002/ett.3106](https://doi.org/10.1002/ett.3106).
- [192] B. C. Akdeniz, A. E. Pusane, and T. Tuğcu, “Optimal Reception Delay in Diffusion-based Molecular Communication,” *IEEE Communications Letters*, vol. 22, no. 1, pp. 57–60, 2018. [doi:10.1109/LCOMM.2017.2761337](https://doi.org/10.1109/LCOMM.2017.2761337).

- [193] G. Chang, L. Lin, and H. Yan, “Adaptive Detection and ISI Mitigation for Mobile Molecular Communication,” *IEEE Transactions on NanoBioscience*, vol. 17, no. 1, pp. 21–35, 2018. [doi:10.1109/TNB.2017.2786229](https://doi.org/10.1109/TNB.2017.2786229).
- [194] O. A. Dambri and S. Cherkaoui, “Enhancing Signal Strength and ISI-avoidance of Diffusion-based Molecular Communication,” in *14th International Wireless Communications & Mobile Computing Conference (IWCMC)*, pp. 1–6, IEEE, 2018. [doi:10.1109/IWCMC.2018.8450431](https://doi.org/10.1109/IWCMC.2018.8450431).
- [195] H. Arjmandi, A. Gohari, M. N. Kenari, and F. Bateni, “Diffusion-based Nanonetworking: a New Modulation Technique and Performance Analysis,” *IEEE Communications Letters*, vol. 17, no. 4, pp. 645–648, 2013. [doi:10.1109/LCOMM.2013.021913.122402](https://doi.org/10.1109/LCOMM.2013.021913.122402).
- [196] Y. Lu, M. D. Higgins, and M. S. Leeson, *the use of Error Correction Codes within Molecular Communications Systems*. CRC Press, 2018. ISBN-13: 978-1138587984.
- [197] P.-J. Shih, C.-H. Lee, P.-C. Yeh, and K.-C. Chen, “Channel Codes for Reliability Enhancement in Molecular Communication,” *IEEE Journal on Selected Areas in Communications*, vol. 31, no. 12, pp. 857–867, 2013. [doi:10.1109/J SAC.2013.SUP2.12130018](https://doi.org/10.1109/J SAC.2013.SUP2.12130018).
- [198] Y. Lu, X. Wang, M. D. Higgins, A. Noel, N. Neophytou, and M. S. Leeson, “Energy Requirements of Error Correction Codes in Diffusion-based Molecular Communication Systems,” *Nano Communication Networks*, vol. 11, pp. 24–35, 2017. [doi:10.1016/j.nancom.2016.09.003](https://doi.org/10.1016/j.nancom.2016.09.003).
- [199] P.-Y. Ko, Y.-C. Lee, P.-C. Yeh, C.-h. Lee, and K.-C. Chen, “a New Paradigm for Channel Coding in Diffusion-based Molecular Communications: Molecular Coding Distance Function,” in *Global Communications Conference (GLOBECOM), 2012 IEEE*, pp. 3748–3753, IEEE, 2012. [doi:10.1109/GLOCOM.2012.6503700](https://doi.org/10.1109/GLOCOM.2012.6503700).
- [200] M. S. Leeson and M. D. Higgins, “Error Correction Coding for Molecular Communications,” in *International Conference on Communications (ICC)*, pp. 6172–6176, IEEE, 2012. [doi:10.1109/ICC.2012.6364980](https://doi.org/10.1109/ICC.2012.6364980).
- [201] C. Bai, M. S. Leeson, and M. D. Higgins, “Minimum Energy Channel Codes for Molecular Communications,” *IET Electronics Letters*, vol. 50, no. 23, pp. 1669–1671, 2014. [doi:10.1049/el.2014.3345](https://doi.org/10.1049/el.2014.3345).
- [202] Y. Lu, M. D. Higgins, and M. S. Leeson, “Comparison of Channel Coding Schemes for Molecular Communications Systems,” *IEEE Transactions on Communications*, vol. 63, no. 11, pp. 3991–4001, 2015. [doi:10.1109/TCOMM.2015.2480752](https://doi.org/10.1109/TCOMM.2015.2480752).
- [203] M. B. Dissanayake, Y. Deng, A. Nallanathan, M. Elkashlan, and U. Mitra, “Interference Mitigation in Large-scale Multiuser Molecular Communication,” *IEEE Transactions on Communications*, vol. 67, pp. 4088–4103, 2019. [doi:10.1109/TCOMM.2019.2897568](https://doi.org/10.1109/TCOMM.2019.2897568).

- [204] V. Jamali, A. Ahmadzadeh, N. Farsad, and R. Schober, “Constant-composition Codes for Maximum Likelihood Detection without CSI in Diffusive Molecular Communications,” *IEEE Transactions on Communications*, vol. 66, no. 5, pp. 1981–1995, 2018. [doi:10.1109/TCOMM.2018.2796612](https://doi.org/10.1109/TCOMM.2018.2796612).
- [205] L. Shi and L.-L. Yang, “Error Performance Analysis of Diffusive Molecular Communication Systems with On-Off Keying Modulation,” *IEEE Transactions on Molecular, Biological and Multi-Scale Communications*, vol. 3, no. 4, pp. 224–238, 2017. [doi:10.1109/TMBMC.2018.2856778](https://doi.org/10.1109/TMBMC.2018.2856778).
- [206] N. Abadi, A. A. Gohari, M. Mirmohseni, and M. Nasiri-Kenari, “Zero-error Codes for Multi-type Molecular Communication in Random Delay Channel,” in *2018 Iran Workshop on Communication and Information Theory (IWCIT)*, pp. 1–6, IEEE, 2018. [doi:10.1109/IWCIT.2018.8405050](https://doi.org/10.1109/IWCIT.2018.8405050).
- [207] B. Krishnaswamy and R. Sivakumar, “Amplitude-width Encoding for Error Correction in Bacterial Communication Networks,” in *5th International Conference on Nanoscale Computing and Communication (NANOCOM)*, p. 25, ACM, 2018. [doi:10.1145/3233188.3233212](https://doi.org/10.1145/3233188.3233212).
- [208] A. O. Kişi, A. E. Pusane, and T. Tuğcu, “a Comparative Analysis of Channel Coding for Molecular Communication,” in *26th Signal Processing and Communications Applications Conference (SIU)*, pp. 1–4, IEEE, 2018. [doi:10.1109/SIU.2018.8404368](https://doi.org/10.1109/SIU.2018.8404368).
- [209] R. Chien, “Cyclic Decoding Procedures for Bose-Chaudhuri-Hocquenghem Codes,” *IEEE Transactions on Information Theory*, vol. 10, no. 4, pp. 357–363, 1964. [doi:10.1109/TIT.1964.1053699](https://doi.org/10.1109/TIT.1964.1053699).
- [210] S. B. Wicker and V. K. Bhargava, *Reed-Solomon Codes and their Applications*. John Wiley & Sons, 1st ed., 1999. ISBN-13: 978-0780353916.
- [211] T. Nakano, M. J. Moore, F. Wei, A. V. Vasilakos, and J. Shuai, “Molecular Communication and Networking: Opportunities and Challenges,” *IEEE Transactions on NanoBio-science*, vol. 11, no. 2, pp. 135–148, 2012. [doi:10.1109/TNB.2012.2191570](https://doi.org/10.1109/TNB.2012.2191570).
- [212] H.-H. Yen, X. Wang, and D. Wang, “QoS Aware Molecular Activation and Communication Scheme in Molecular Nanoscale Sensor Networks,” in *18th International Conference on e-Health Networking, Applications and Services (Healthcom)*, pp. 1–6, IEEE, 2016. [doi:10.1109/HealthCom.2016.7749503](https://doi.org/10.1109/HealthCom.2016.7749503).
- [213] A. Erofeev, P. Gorelkin, A. Garanina, A. Alova, M. Efremova, N. Vorobyeva, C. Edwards, Y. Korchev, and A. Majouga, “Novel Method for Rapid Toxicity Screening of Magnetic Nanoparticles,” *Scientific Reports*, vol. 8, no. 1, p. 7462, 2018. [doi:10.1038/s41598-018-25852-4](https://doi.org/10.1038/s41598-018-25852-4).
- [214] R. Bogue, “Nanosensors: a Review of Recent Research,” *Sensor Review*, vol. 29, no. 4, pp. 310–315, 2009. [doi:10.1108/02602280910986539](https://doi.org/10.1108/02602280910986539).

- [215] M. Egan, T. Q. Duong, and M. Di Renzo, “Biological Circuits for Detection in MoSK-Based Molecular Communication,” *IEEE Access*, vol. 7, pp. 21094–21102, 2019. [doi:10.1109/ACCESS.2019.2897173](https://doi.org/10.1109/ACCESS.2019.2897173).
- [216] A. Marcone, M. Pierobon, and M. Magarini, “Parity-Check Coding Based on Genetic Circuits for Engineered Molecular Communication Between Biological Cells,” *IEEE Transactions on Communications*, vol. 66, no. 12, pp. 6221–6236, 2018. [doi:10.1109/TCOMM.2018.2859308](https://doi.org/10.1109/TCOMM.2018.2859308).
- [217] S. Balasubramaniam, N. T. Boyle, A. Della-Chiesa, F. Walsh, A. Mardinoglu, D. Botvich, and A. Prina-Mello, “Development of Artificial Neuronal Networks for Molecular Communication,” *Nano Communication Networks*, vol. 2, no. 2, pp. 150–160, 2011. [doi:10.1016/j.nancom.2011.05.004](https://doi.org/10.1016/j.nancom.2011.05.004).
- [218] A. Noel, Y. Deng, D. Makrakis, and A. Hafid, “Active versus Passive: Receiver Model Transforms for Diffusive Molecular Communication,” in *Global Communications Conference (GLOBECOM)*, pp. 1–6, IEEE, 2016. [doi:10.1109/GLOCOM.2016.7841566](https://doi.org/10.1109/GLOCOM.2016.7841566).
- [219] L.-S. Meng, P.-C. Yeh, K.-C. Chen, and I. F. Akyıldız, “on Receiver Design for Diffusion-based Molecular Communication,” *IEEE Transactions on Signal Processing*, vol. 62, no. 22, pp. 6032–6044, 2014. [doi:10.1109/TSP.2014.2359644](https://doi.org/10.1109/TSP.2014.2359644).
- [220] A. Noel, K. C. Cheung, and R. Schober, “Optimal Receiver Design for Diffusive Molecular Communication with Flow and Additive Noise,” *IEEE Transactions on NanoBioscience*, vol. 13, no. 3, pp. 350–362, 2014. [doi:10.1109/TNB.2014.2337239](https://doi.org/10.1109/TNB.2014.2337239).
- [221] H. Arjmandi, A. Ahmadzadeh, R. Schober, and M. N. Kenari, “Ion Channel based Bio-synthetic Modulator for Diffusive Molecular Communication,” *IEEE Transactions on NanoBioscience*, vol. 15, no. 5, pp. 418–432, 2016. [doi:10.1109/TNB.2016.2557350](https://doi.org/10.1109/TNB.2016.2557350).
- [222] M. Pierobon and I. F. Akyıldız, “A Physical end-to-end Model for Molecular Communication in Nanonetworks,” *IEEE Journal on Selected Areas in Communications*, vol. 28, no. 4, 2010. [doi:10.1109/JSAC.2010.100509](https://doi.org/10.1109/JSAC.2010.100509).
- [223] U. A. Chude-Okonkwo, R. Malekian, and B. Maharaj, “Diffusion-controlled Interface Kinetics-inclusive System-theoretic Propagation Models for Molecular Communication Systems,” *EURASIP Journal on Advances in Signal Processing*, vol. 2015, no. 1, p. 89, 2015. [doi:10.1186/s13634-015-0275-1](https://doi.org/10.1186/s13634-015-0275-1).
- [224] G. D. Ntouni and G. K. Karagiannidis, “Comparison of Amplitude Detection Techniques for Passive Receivers in Molecular Communications,” in *6th International Conference on Modern Circuits and Systems Technologies (MOCAST)*, pp. 1–4, IEEE, 2017. [doi:10.1109/MOCAST.2017.7937650](https://doi.org/10.1109/MOCAST.2017.7937650).
- [225] C. T. Chou, “Impact of Receiver Reaction Mechanisms on the Performance of Molecular Communication Networks,” *IEEE Transactions on Nanotechnology*, vol. 14, pp. 304–317, March 2015. [doi:10.1109/TNANO.2015.2393866](https://doi.org/10.1109/TNANO.2015.2393866).

- [226] M. Movahednasab, M. Soleimanifar, A. Gohari, M. Nasiri-Kenari, and U. Mitra, “Adaptive Transmission Rate with a Fixed Threshold Decoder for Diffusion-based Molecular Communication,” *IEEE Transactions on Communications*, vol. 64, no. 1, pp. 236–248, 2016. [doi:10.1109/TCOMM.2015.2501823](https://doi.org/10.1109/TCOMM.2015.2501823).
- [227] B. C. Akdeniz, A. E. Pusane, and T. Tuğcu, “2-D Channel Transfer Function for Molecular Communication with an Absorbing Receiver,” in *Symposium on Computers and Communications (ISCC)*, pp. 938–942, IEEE, 2017. [doi:10.1109/ISCC.2017.8024646](https://doi.org/10.1109/ISCC.2017.8024646).
- [228] W. Haselmayr, D. Efrosinin, and W. Guo, “Normal Inverse Gaussian Approximation for Arrival Time Difference in Flow-induced Molecular Communications,” *IEEE Transactions on Molecular, Biological and Multi-Scale Communications*, vol. 3, no. 4, pp. 259–264, 2017. [doi:10.1109/TMBMC.2018.2887237](https://doi.org/10.1109/TMBMC.2018.2887237).
- [229] G. Ardestiri, A. Jamshidi, and A. Keshavarz-Haddad, “Performance Analysis of Decode and Forward Relay Network in Diffusion based Molecular Communication,” in *Iranian Conference on Electrical Engineering (ICEE)*, pp. 1992–1997, May 2017. [doi:10.1109/IranianCEE.2017.7985383](https://doi.org/10.1109/IranianCEE.2017.7985383).
- [230] Z. Luo, L. Lin, W. Guo, S. Wang, F. Liu, and H. Yan, “One Symbol Blind Synchronization in SIMO Molecular Communication Systems,” *IEEE Wireless Communications Letters*, vol. 7, no. 4, pp. 530–533, 2018. [doi:10.1109/LWC.2018.2793197](https://doi.org/10.1109/LWC.2018.2793197).
- [231] M. Egan, T. C. Mai, T. Duong, and M. Di Renzo, “Coordination via Advection Dynamics in Nanonetworks with Molecular Communication,” in *International Conference on Communications (ICC)*, pp. 1–6, IEEE, 2018. [doi:10.1109/ICC.2018.8422573](https://doi.org/10.1109/ICC.2018.8422573).
- [232] L. Lin, J. Zhang, M. Ma, and H. Yan, “Time Synchronization for Molecular Communication with Drift,” *IEEE Communications Letters*, vol. 21, no. 3, pp. 476–479, 2017. [doi:10.1109/LCOMM.2016.2628903](https://doi.org/10.1109/LCOMM.2016.2628903).
- [233] N. Farsad and A. Goldsmith, “Sliding Bidirectional Recurrent Neural Networks for Sequence Detection in Communication Systems,” in *International Conference on Acoustics, Speech and Signal Processing (ICASSP)*, pp. 2331–2335, IEEE, 2018. [doi:10.1109/ICASSP2018.8462140](https://doi.org/10.1109/ICASSP2018.8462140).
- [234] N. Farsad and A. Goldsmith, “Neural Network Detection of Data Sequences in Communication Systems,” *IEEE Transactions on Signal Processing*, vol. 66, pp. 5663–5678, Nov 2018. [doi:10.1109/TSP2018.2868322](https://doi.org/10.1109/TSP2018.2868322).
- [235] X. Qian and M. Di Renzo, “Receiver Design in Molecular Communications: an Approach based on Artificial Neural Networks,” in *15th International Symposium on Wireless Communication Systems (ISWCS)*, pp. 1–5, IEEE, 2018. [doi:10.1109/ISWCS.2018.8491088](https://doi.org/10.1109/ISWCS.2018.8491088).

- [236] T. C. Mai, M. Egan, T. Q. Duong, and M. Di Renzo, “Event Detection in Molecular Communication Networks with Anomalous Diffusion,” *IEEE Communications Letters*, vol. 21, no. 6, pp. 1249–1252, 2017. [doi:10.1109/LCOMM.2017.2669315](https://doi.org/10.1109/LCOMM.2017.2669315).
- [237] A. Shahbazi and A. Jamshidi, “Pre-coding Technique for Adaptive Threshold Detectors in Diffusion-based Molecular Communications,” in *4th International Conference on Computer and Technology Applications (ICCTA)*, pp. 59–63, IEEE, 2018. [doi:10.1109/CATA.2018.8398656](https://doi.org/10.1109/CATA.2018.8398656).
- [238] H. Yan, G. Chang, Z. Ma, and L. Lin, “Derivative-based Signal Detection for High Data Rate Molecular Communication System,” *IEEE Communications Letters*, vol. 22, no. 9, pp. 1782–1785, 2018. [doi:10.1109/LCOMM.2018.2853617](https://doi.org/10.1109/LCOMM.2018.2853617).
- [239] M. U. Riaz, H. Awan, and C. T. Chou, “using Spatial Partitioning to Reduce Receiver Signal Variance in Diffusion-based Molecular Communication,” in *5th International Conference on Nanoscale Computing and Communication*, p. 12, ACM, 2018. [doi:10.1145/3233188.3233192](https://doi.org/10.1145/3233188.3233192).
- [240] A. Shahbazi and A. Jamshidi, “Improving Adaptive Receivers Performance in Molecular Communication via Diffusion,” *IET NanoBiotechnology*, vol. 13, no. 4, pp. 441–448, 2019. [doi:10.1049/iet-nbt.2018.5129](https://doi.org/10.1049/iet-nbt.2018.5129).
- [241] K. Persaud and G. Dodd, “Analysis of Discrimination Mechanisms in the Mammalian Olfactory System using a Model Nose,” *Nature*, vol. 299, no. 5881, pp. 352–355, 1982. [doi:10.1038/299352a0](https://doi.org/10.1038/299352a0).
- [242] J. W. Gardner and P. N. Bartlett, *Electronic Noses: Principles and Applications*. Oxford University Press, USA, 1st ed., 1999. ISBN-13: 978-0198559559.
- [243] A. D’Amico, C. Di Natale, R. Paolesse, A. Macagnano, E. Martinelli, G. Pennazza, M. Santonico, M. Bernabei, C. Roscioni, G. Galluccio, R. Bono, E. F. Agrò, and S. Rullo, “Olfactory Systems for Medical Applications,” *Sensors and Actuators B: Chemical*, vol. 130, no. 1, pp. 458–465, 2008. [doi:10.1016/j.snb.2007.09.044](https://doi.org/10.1016/j.snb.2007.09.044).
- [244] I. A. Casalinuovo, D. Di Pierro, M. Coletta, and P. Di Francesco, “Application of Electronic Noses for Disease Diagnosis and Food Spoilage Detection,” *Sensors*, vol. 6, no. 11, pp. 1428–1439, 2006. [doi:10.3390/s6111428](https://doi.org/10.3390/s6111428).
- [245] K. C. Persaud, “Medical Applications of Odor-sensing Devices,” *The International Journal of Lower Extremity Wounds*, vol. 4, no. 1, pp. 50–56, 2005. [doi:10.1177/1534734605275139](https://doi.org/10.1177/1534734605275139).
- [246] M. Peris and L. Escuder-Gilabert, “a 21st Century Technique for Food Control: Electronic Noses,” *Analytica Chimica Acta*, vol. 638, no. 1, pp. 1–15, 2009. [doi:10.1016/j.aca.2009.02.009](https://doi.org/10.1016/j.aca.2009.02.009).

- [247] S. Ampuero and J. Bosset, “the Electronic Nose Applied to Dairy Products: a Review,” *Sensors and Actuators B: Chemical*, vol. 94, no. 1, pp. 1–12, 2003. [doi:10.1016/S0925-4005\(03\)00321-6](https://doi.org/10.1016/S0925-4005(03)00321-6).
- [248] E. Schaller, J. O. Bosset, and F. Escher, “‘electronic Noses’ and their Application to Food,” *LWT-Food Science and Technology*, vol. 31, no. 4, pp. 305–316, 1998. [doi:10.1006/fstl.1998.0376](https://doi.org/10.1006/fstl.1998.0376).
- [249] A. Wilson and M. Baietto, “Applications and Advances in Electronic-Nose Technologies,” *Sensors*, vol. 9, no. 7, pp. 5099–5148, 2009. [doi:10.3390/s90705099](https://doi.org/10.3390/s90705099).
- [250] E. de Hoffmann and V. Stroobant, *Mass Spectrometry*. Wiley, 3rd ed., 2007. **ISBN-13:** 978-0-470-03310-4.
- [251] B. Clerckx and C. Oestges, *MIMO Wireless Networks: Channels, Techniques and Standards for Multi-antenna, Multi-user and Multi-cell Systems*. Academic Press, 2nd ed., 2013. **ISBN-13:** 978-0123850553.
- [252] B.-H. Koo, C. Lee, H. B. Yilmaz, N. Farsad, A. Eckford, and C.-B. Chae, “Molecular MIMO: from Theory to Prototype,” *IEEE Journal on Selected Areas in Communications*, vol. 34, no. 3, pp. 600–614, 2016. [doi:10.1109/JSAC.2016.2525538](https://doi.org/10.1109/JSAC.2016.2525538).
- [253] B. H. Koo, H. B. Yilmaz, C.-B. Chae, and A. Eckford, “Detection Algorithms for Molecular MIMO,” in *International Conference on Communications (ICC)*, pp. 1122–1127, IEEE, 2015. [doi:10.1109/ICC.2015.7248473](https://doi.org/10.1109/ICC.2015.7248473).
- [254] N. Tavakkoli, P. Azmi, and N. Mokari, “Performance Evaluation and Optimal Detection of Relay-assisted Diffusion-based Molecular Communication with Drift,” *IEEE Transactions on NanoBioscience*, vol. 16, no. 1, pp. 34–42, 2017. [doi:10.1109/TNB.2016.2626313](https://doi.org/10.1109/TNB.2016.2626313).
- [255] R. Mosayebi, V. Jamali, N. Ghoroghchian, R. Schober, M. Nasiri-Kenari, and M. Mehrabi, “Cooperative Abnormality Detection via Diffusive Molecular Communications,” *IEEE Transactions on NanoBioscience*, vol. 16, no. 8, pp. 828–842, 2017. [doi:10.1109/TNB.2017.2775704](https://doi.org/10.1109/TNB.2017.2775704).
- [256] M. Kuscu and O. B. Akan, “Maximum Likelihood Detection with Ligand Receptors for Diffusion-based Molecular Communications in Internet of bio-Nano Things,” *IEEE Transactions on NanoBioscience*, vol. 17, no. 1, pp. 44–54, 2018. [doi:10.1109/TNB.2018.2792434](https://doi.org/10.1109/TNB.2018.2792434).
- [257] S. M. Rouzegar and U. Spagnolini, “Channel Estimation for Diffusive MIMO Molecular Communications,” *European Conference on Networks and Communications (EuCNC)*, pp. 1–5, June 2017. [doi:10.1109/EuCNC.2017.7980701](https://doi.org/10.1109/EuCNC.2017.7980701).
- [258] C. Lee, H. B. Yilmaz, C.-B. Chae, N. Farsad, and A. Goldsmith, “Machine Learning based Channel Modeling for Molecular MIMO Communications,” in *18th International*

- Workshop on Signal Processing Advances in Wireless Communications (SPAWC)*, pp. 1–5, IEEE, 2017. [doi:10.1109/SPAWC.2017.8227765](https://doi.org/10.1109/SPAWC.2017.8227765).
- [259] M. A. Mangoud, M. Lestas, and T. Saeed, “Molecular Motors MIMO Communications for Nanonetworks Applications,” in *Wireless Communications and Networking Conference (WCNC)*, pp. 1–5, IEEE, 2018. [doi:10.1109/WCNC.2018.8377406](https://doi.org/10.1109/WCNC.2018.8377406).
- [260] B. Yin and M. Peng, “Performance analysis of cooperative relaying in diffusion-based molecular communication,” in *International Conference on Computing, Networking and Communications (ICNC)*, pp. 752–756, IEEE, 2018. [doi:10.1109/WCSP2017.8171166](https://doi.org/10.1109/WCSP2017.8171166).
- [261] L. Grebenstein, J. Kirchner, R. S. Peixoto, W. Zimmermann, W. Wicke, A. Ahmadzadeh, V. Jamali, G. Fischer, R. Weigel, A. Burkowski, and R. Schober, “Biological Optical-to-Chemical Signal Conversion Interface: a Small-Scale Modulator for Molecular Communications,” in *5th International Conference on Nanoscale Computing and Communication (NANOCOM)*, pp. 1–6, ACM, 2018. [doi:10.1145/3233188.3233203](https://doi.org/10.1145/3233188.3233203).
- [262] N.-R. Kim, N. Farsad, C. Lee, A. W. Eckford, and C.-B. Chae, “an Experimentally Validated Channel Model for Molecular Communication Systems,” *IEEE Access*, vol. 7, pp. 81849 – 81858, 2019. [doi:10.1109/ACCESS.2018.2889683](https://doi.org/10.1109/ACCESS.2018.2889683).
- [263] N. Farsad, D. Pan, and A. Goldsmith, “a Novel Experimental Platform for in-vessel Multi-chemical Molecular Communications,” in *Global Communications Conference (GLOBECOM)*, pp. 1–6, IEEE, 2017. [doi:10.1109/GLOCOM.2017.8255058](https://doi.org/10.1109/GLOCOM.2017.8255058).
- [264] H. Unterweger, J. Kirchner, W. Wicke, A. Ahmadzadeh, D. Ahmed, V. Jamali, C. Alexiou, G. Fischer, and R. Schober, “Experimental Molecular Communication Testbed based on Magnetic Nanoparticles in Duct Flow,” in *19th International Workshop on Signal Processing Advances in Wireless Communications (SPAWC)*, pp. 1–5, IEEE, 2018. [doi:10.1109/GLOCOM.2017.8255058](https://doi.org/10.1109/GLOCOM.2017.8255058).
- [265] J. Zaloga, C. Janko, J. Nowak, J. Matuszak, S. Knaup, D. Eberbeck, R. Tietze, H. Unterweger, R. P. Friedrich, S. Duerr, R. Heimke-Brinck, E. Baum, I. Cicha, F. Dörje, S. Odenbach, S. Lyer, G. Lee, and C. Alexiou, “Development of a Lauric Acid/Albumin Hybrid Iron Oxide Nanoparticle System with Improved Biocompatibility,” *International Journal of Nanomedicine*, vol. 9, p. 4847, 2014. [doi:10.2147/IJN.S68539](https://doi.org/10.2147/IJN.S68539).
- [266] H. Zhai, Q. Liu, A. V. Vasilakos, and K. Yang, “Anti-ISI Demodulation Scheme and its Experiment-based Evaluation for Diffusion-based Molecular Communication,” *IEEE Transactions on NanoBioscience*, vol. 17, no. 2, pp. 126–133, 2018. [doi:10.1109/TNB.2018.2797689](https://doi.org/10.1109/TNB.2018.2797689).
- [267] C. Lee, B. Koo, N.-R. Kim, B. Yilmaz, N. Farsad, A. Eckford, and C.-B. Chae, “Molecular MIMO communication link,” in *Conference on Computer Communications Workshops (INFOCOM WKSHPS)*, pp. 13–14, IEEE, 2015. [doi:10.1109/INFCOMW.2015.7179319](https://doi.org/10.1109/INFCOMW.2015.7179319).

- [268] C. Lee, B. Koo, N.-R. Kim, H. B. Yilmaz, N. Farsad, A. Eckford, and C.-B. Chae, “Demo: Molecular MIMO with Drift,” in *21st Annual International Conference on Mobile Computing and Networking (MobiCoM)*, pp. 201–203, ACM, 2015. [doi:10.1145/2789168.2789181](https://doi.org/10.1145/2789168.2789181).
- [269] N. A. Abbasi, D. Lafci, and O. B. Akan, “Controlled Information Transfer Through an *in vivo* Nervous System,” *Scientific Reports*, vol. 8, no. 1, p. 2298, 2018. [doi:10.1038/s41598-018-20725-2](https://doi.org/10.1038/s41598-018-20725-2).
- [270] Y. Moritani, S. Hiyama, and T. Suda, “Molecular Communication for Health Care Applications,” in *4th International Conference on Pervasive Computing and Communications Workshops (PERCOMW)*, pp. 5–pp, IEEE, 2006. [doi:10.1109/PERCOMW.2006.97](https://doi.org/10.1109/PERCOMW.2006.97).
- [271] O. B. Akan, H. Ramezani, T. Khan, N. A. Abbasi, and M. Kuscu, “Fundamentals of Molecular Information and Communication Science,” *Proceedings of the IEEE*, vol. 105, no. 2, pp. 306–318, 2017. [doi:10.1109/JPROC.2016.2537306](https://doi.org/10.1109/JPROC.2016.2537306).
- [272] R. Mosayebi, W. Wicke, V. Jamali, A. Ahmadzadeh, R. Schober, and M. Nasiri-Kenari, “Advanced Target Detection via Molecular Communication,” in *IEEE Global Communications Conference (GLOBECOM)*, pp. 1–7, 2018. [doi:10.1109/GLOCOM.2018.8647734](https://doi.org/10.1109/GLOCOM.2018.8647734).
- [273] Z. Sakkaff, A. Immaneni, and M. Pierobon, “Applying Molecular Communication Theory to Estimate Information Loss in Cell Signal Transduction: an Approach based on Cancer Transcriptomics,” in *5th International Conference on Nanoscale Computing and Communication*, p. 16, ACM, 2018. [doi:10.1145/3233188.3233202](https://doi.org/10.1145/3233188.3233202).
- [274] M. L. Simpson, G. S. Sayler, J. T. Fleming, and B. Applegate, “Whole-cell biocomputing,” *Trends in Biotechnology*, vol. 19, no. 8, pp. 317–323, 2001. [doi:10.1016/S0167-7799\(01\)01691-2](https://doi.org/10.1016/S0167-7799(01)01691-2).
- [275] D. Noble, “Opinion: the Rise of Computational Biology,” *Nature Reviews Molecular Cell Biology*, vol. 3, no. 6, p. 459, 2002. [doi:10.1038/nrm810](https://doi.org/10.1038/nrm810).
- [276] T. C. Collier and C. Taylor, “Self-Organization in Sensor Networks,” *Journal of Parallel and Distributed Computing*, vol. 64, no. 7, pp. 866–873, 2004. [doi:10.1016/j.jpdc.2003.12.004](https://doi.org/10.1016/j.jpdc.2003.12.004).
- [277] M. D. Peysakhov and W. C. Regli, “Ant Inspired Server Population Management in a Service based Computing Environment,” in *Swarm Intelligence Symposium (SIS)*, pp. 357–364, IEEE, 2005. [doi:10.1109/SIS.2005.1501643](https://doi.org/10.1109/SIS.2005.1501643).
- [278] M. T. Barros, “Ca²⁺-signaling-based Molecular Communication Systems: Design and Future Research Directions,” *Nano Communication Networks*, vol. 11, pp. 103–113, 2017. [doi:10.1016/j.nancom.2017.02.001](https://doi.org/10.1016/j.nancom.2017.02.001).

- [279] G. Muzio, M. Kuscu, and O. B. Akan, “Selective Signal Detection with Ligand Receptors under Interference in Molecular Communications,” in *19th International Workshop on Signal Processing Advances in Wireless Communications (SPAWC)*, pp. 1–5, IEEE, 2018. [doi:10.1109/SPAWC.2018.8445876](https://doi.org/10.1109/SPAWC.2018.8445876).
- [280] S. Yuan, J. Wang, and M. Peng, “Performance Analysis of Reversible Binding Receptor based Decode-and-Forward Relay in Molecular Communication Systems,” *IEEE Wireless Communications Letters*, vol. 7, no. 5, pp. 880–883, 2018. [doi:10.1109/LWC.2018.2834525](https://doi.org/10.1109/LWC.2018.2834525).
- [281] D. P. Martins, K. Leetanasaksakul, M. T. Barros, A. Thamchaipenet, W. Donnelly, and S. Balasubramaniam, “Molecular Communications Pulse-based Jamming Model for Bacterial Biofilm Suppression,” *IEEE Transactions on Nanobioscience*, 2018. [doi:10.1109/TNB.2018.2871276](https://doi.org/10.1109/TNB.2018.2871276).
- [282] G. L. Adonias, M. T. Barros, L. Doyle, and S. Balasubramaniam, “utilising EEG Signals for Modulating Neural Molecular Communications,” in *5th International Conference on Nanoscale Computing and Communication (NANOCOM)*, p. 39, ACM, 2018. [doi:10.1145/3233188.3236333](https://doi.org/10.1145/3233188.3236333).
- [283] L. Felicetti, M. Femminella, and G. Reali, “Establishing Digital Molecular Communications in Blood Vessels,” in *1st International Black Sea Conference on Communications and Networking (BlackSeaCom)*, pp. 54–58, IEEE, 2013. [doi:10.1109/BlackSeaCom.2013.6623381](https://doi.org/10.1109/BlackSeaCom.2013.6623381).
- [284] Y. Sun, K. Yang, and Q. Liu, “Channel Capacity Modelling of Blood Capillary-based Molecular Communication with Blood Flow Drift,” in *4th International Conference on Nanoscale Computing and Communication*, p. 19, ACM, 2017. [doi:10.1145/3109453.3109454](https://doi.org/10.1145/3109453.3109454).
- [285] M. Kuscu and O. B. Akan, “Modeling Convection-Diffusion-Reaction Systems for Microfluidic Molecular Communications with Surface-based Receivers in Internet of Bio-Nano Things,” *PLoS one*, vol. 13, no. 2, p. e0192202, 2018. [doi:10.1371/journal.pone.0192202](https://doi.org/10.1371/journal.pone.0192202).
- [286] M. Turan, B. C. Akdeniz, M. Ş. Kurancı, H. B. Yılmaz, I. Demirkol, A. E. Pusane, and T. Tuğcu, “Transmitter Localization in Vessel-like Diffusive Channels using Ring-shaped Molecular Receivers,” *IEEE Communications Letters*, 2018. [doi:10.1109/LCOMM.2018.2871456](https://doi.org/10.1109/LCOMM.2018.2871456).
- [287] M. Cole, J. Gardner, S. Pathak, T. Pearce, and Z. Rácz, “Towards a Biosynthetic Infochemical Communication System,” *Procedia Chemistry*, vol. 1, no. 1, pp. 305–308, 2009. [doi:10.1016/j.proche.2009.07.076](https://doi.org/10.1016/j.proche.2009.07.076).

- [288] L. Muñoz, N. Dimov, G. Carot-Sans, W. P. Bula, A. Guerrero, and H. J. Gardeniers, “Mimicking Insect Communication: Release and Detection of Pheromone, Biosynthesized by an Alcohol Acetyl Transferase Immobilized in a Microreactor,” *PloS one*, vol. 7, no. 11, p. e47751, 2012. [doi:10.1371/journal.pone.0047751](https://doi.org/10.1371/journal.pone.0047751).
- [289] S. B. Olsson, L. S. Kuebler, D. Veit, K. Steck, A. Schmidt, M. Knaden, and B. S. Hansson, “a Novel Multicomponent Stimulus Device for use in Olfactory Experiments,” *Journal of neuroscience methods*, vol. 195, no. 1, pp. 1–9, 2011. [doi:10.1016/j.jneumeth.2010.09.020](https://doi.org/10.1016/j.jneumeth.2010.09.020).
- [290] R. A. Russell, *Odour Detection by Mobile Robots*. World Scientific, 1st ed., 1999. ISBN: 978-981-02-3791-2.
- [291] M. Cole, Z. Racz, J. W. Gardner, and T. C. Pearce, “a Novel Biomimetic Infochemical Communication Technology: From Insects to Robots,” in *IEEE Sensors*, pp. 1–4, IEEE, 2012. [doi:10.1109/ICSENS.2012.6411357](https://doi.org/10.1109/ICSENS.2012.6411357).
- [292] J. Steuer, “Defining Virtual Reality: Dimensions Determining Telepresence,” *Journal of Communication*, vol. 42, no. 4, pp. 73–93, 1992. [doi:10.1111/j.1460-2466.1992.tb00812.x](https://doi.org/10.1111/j.1460-2466.1992.tb00812.x).
- [293] M. Chastrette, “Data Management in Olfaction Studies,” *SAR and QSAR in Environmental Research*, vol. 8, no. 3-4, pp. 157–181, 1998. [doi:10.1080/10629369808039139](https://doi.org/10.1080/10629369808039139).
- [294] R. C. Araneda, A. D. Kini, and S. Firestein, “The Molecular Receptive Range of an Odorant Receptor,” *Nature Neuroscience*, vol. 3, no. 12, p. 1248, 2000. [doi:10.1038/81774](https://doi.org/10.1038/81774).
- [295] J. Banks, J. S. Carson, B. L. Nelson, and D. M. Nicol, *Discrete Event System Simulation*. Pearson, 5th ed., 2005. ISBN-13: 978-0136062127.
- [296] L. Felicetti, M. Femminella, and G. Reali, “A Simulation Tool for Nanoscale Biological Networks,” *Nano Communication Networks*, vol. 3, no. 1, pp. 2–18, 2012. [doi:10.1016/j.nancom.2011.09.002](https://doi.org/10.1016/j.nancom.2011.09.002).
- [297] M. Femminella, G. Reali, and A. V. Vasilakos, “A Molecular Communications Model for Drug Delivery,” *IEEE Transactions on NanoBioscience*, vol. 14, no. 8, pp. 935–945, 2015. [doi:10.1109/TNB.2015.2489565](https://doi.org/10.1109/TNB.2015.2489565).
- [298] P. Masek, J. Hosek, D. Kovac, and J. Miklica, “On Simulation Techniques for Modeling of Molecular-Based Nanodevices’ Communication in Human Body Environment,” in *38th International Conference on Telecommunications and Signal Processing (TSP)*, 2015. [doi:10.1109/TSP2015.7296339](https://doi.org/10.1109/TSP2015.7296339).

- [299] I. Llatser, I. Pascual, N. Garralda, A. Cabellos-Aparicio, M. Pierobon, E. Alarcón, and J. Solé-Pareta, “Exploring the Physical Channel of Diffusion-Based Molecular Communication by Simulation,” in *IEEE Global Telecommunications Conference (GLOBECOM)*, pp. 1–5, IEEE, 2011. [doi:10.1109/GLOCOM.2011.6134028](https://doi.org/10.1109/GLOCOM.2011.6134028).
- [300] I. Llatser, D. Demiray, A. Cabellos-Aparicio, D. T. Altilar, and E. Alarcón, “N3Sim: Simulation Framework for Diffusion-Based Molecular Communication Nanonetworks,” *Simulation Modelling Practice and Theory*, vol. 42, pp. 210–222, 2014. [doi:10.1016/j.smpat.2013.11.004](https://doi.org/10.1016/j.smpat.2013.11.004).
- [301] R. Geyer, M. Stelzner, F. Büther, and S. Ebers, “BloodVoyagerS: Simulation of the Work Environment of Medical Nanobots,” in *Proceedings of the 5th ACM International Conference on Nanoscale Computing and Communication*, pp. 1–6, ACM, 2018. [doi:10.1145/3233188.3233196](https://doi.org/10.1145/3233188.3233196).
- [302] Y. Jian, B. Krishnaswamy, C. M. Austin, A. O. Bicen, J. E. Perdomo, S. C. Patel, I. F. Akyıldız, C. R. Forest, and R. Sivakumar, “NanoNS3: Simulating Bacterial Molecular Communication Based Nanonetworks in Network Simulator 3,” in *Proceedings of the 3rd ACM International Conference on Nanoscale Computing and Communication*, pp. 1–7, ACM, 2016. [doi:10.1145/2967446.2967464](https://doi.org/10.1145/2967446.2967464).
- [303] G. Wei, P. Bogdan, and R. Marculescu, “Efficient Modeling and Simulation of Bacteria-Based Nanonetworks with BNSim,” *IEEE Journal on Selected Areas in Communications*, vol. 31, no. 12, pp. 868–878, 2013. [doi:10.1109/JSAC.2013.SUP2.12130019](https://doi.org/10.1109/JSAC.2013.SUP2.12130019).
- [304] A. Akkaya, G. Genç, and T. Tuğcu, “HLA Based Architecture for Molecular Communication Simulation,” *Simulation Modelling Practice and Theory*, vol. 42, pp. 163–177, 2014. [doi:10.1016/j.smpat.2013.12.012](https://doi.org/10.1016/j.smpat.2013.12.012).
- [305] Y. Deng, A. Noel, W. Guo, A. Nallanathan, and M. Elkashlan, “3D Stochastic Geometry Model for Large-Scale Molecular Communication Systems,” in *IEEE Global Communications Conference (GLOBECOM)*, pp. 1–6, IEEE, 2016. [doi:10.1109/GLOCOM.2016.7841486](https://doi.org/10.1109/GLOCOM.2016.7841486).
- [306] A. Noel and A. W. Eckford, “Asynchronous Peak Detection for Demodulation in Molecular Communication,” in *IEEE International Conference on Communications (ICC)*, pp. 1–6, IEEE, 2017. [doi:10.1109/ICC.2017.7996904](https://doi.org/10.1109/ICC.2017.7996904).
- [307] A. Noel, K. C. Cheung, and R. Schober, “Multi-Scale Stochastic Simulation for Diffusive Molecular Communication,” in *IEEE International Conference on Communications (ICC)*, pp. 1109–1115, IEEE, 2015. [doi:10.1109/ICC.2015.7248471](https://doi.org/10.1109/ICC.2015.7248471).
- [308] A. Noel, K. C. Cheung, and R. Schober, “On the Statistics of Reaction-Diffusion Simulations for Molecular Communication,” in *Proceedings of the 2nd Annual International Conference on Nanoscale Computing and Communication*, pp. 1–6, ACM, 2015. [doi:10.1145/2800795.2800821](https://doi.org/10.1145/2800795.2800821).

- [309] H. B. Yilmaz and C.-B. Chae, “Simulation Study of mMolecular Communication Systems with an Absorbing Receiver: Modulation and ISI Mitigation Techniques,” *Simulation Modelling Practice and Theory*, vol. 49, pp. 136–150, 2014. [doi:10.1016/j.simpat.2014.09.002](https://doi.org/10.1016/j.simpat.2014.09.002).
- [310] Y. Chahibi, M. Pierobon, S. O. Song, and I. F. Akyildiz, “A molecular communication system model for particulate drug delivery systems,” *IEEE Transactions on Biomedical Engineering*, vol. 60, no. 12, pp. 3468–3483, 2013. [doi:10.1109/TBME.2013.2271503](https://doi.org/10.1109/TBME.2013.2271503).
- [311] S. F. Bush, J. L. Paluh, G. Piro, V. S. Rao, R. V. Prasad, and A. W. Eckford, “Defining Communication at the Bottom,” *IEEE Transactions on Molecular, Biological and Multi-Scale Communications*, vol. 1, no. 1, pp. 90–96, 2015. [doi:10.1109/TMBMC.2015.2465513](https://doi.org/10.1109/TMBMC.2015.2465513).
- [312] D. T. Gillespie, “Exact Stochastic Simulation of Coupled Chemical Reactions,” *The Journal of Physical Chemistry*, vol. 81, no. 25, pp. 2340–2361, 1977. [doi:10.1021/j100540a008](https://doi.org/10.1021/j100540a008).
- [313] S. Balasubramaniam and P. Lio’, “Multi-hop Conjugation Based Bacteria Nanonetwoks,” *IEEE Transactions on nanobioscience*, vol. 12, no. 1, pp. 47–59, 2013. [doi:10.1109/TNB.2013.2239657](https://doi.org/10.1109/TNB.2013.2239657).
- [314] Y. Wang, A. Noel, and N. Yang, “A Novel A Priori Simulation Algorithm for Absorbing Receivers in Diffusion-Based Molecular Communication Systems,” 2019. [doi:10.1109/TNB.2019.2910556](https://doi.org/10.1109/TNB.2019.2910556).
- [315] F. Dinç, L. Thiele, and B. C. Akdeniz, “The Effective Geometry Monte Carlo Algorithm: Applications to Molecular Communication,” *Physics Letters A*, vol. 383, no. 22, pp. 2594–2603, 2019. [doi:10.1016/j.physleta.2019.05.029](https://doi.org/10.1016/j.physleta.2019.05.029).
- [316] F. Dinç, M. Medvidović, and L. Thiele, “Effective Geometry Monte Carlo: A Fast and Reliable Simulation Framework for Molecular Communication,” *IEEE Access*, vol. 7, pp. 28635–28650, 2019. [doi:10.1109/ACCESS.2019.2902316](https://doi.org/10.1109/ACCESS.2019.2902316).
- [317] X. Bao, J. Lin, and W. Zhang, “Channel Modeling of Molecular Communication via Diffusion with Multiple Absorbing Receivers,” *IEEE Wireless Communications Letters*, vol. 8, no. 3, pp. 809 – 812, 2019. [doi:10.1109/LWC.2019.2894354](https://doi.org/10.1109/LWC.2019.2894354).
- [318] P. Stroobant, L. Felicetti, W. Tavernier, D. Colle, M. Femminella, G. Reali, and M. Pickavet, “Fast Simulation of Interacting Carriers in Nanosimulators,” in *5th International Conference on Nanoscale Computing and Communication*, p. 18, ACM, 2018. [doi:10.1145/3233188.3233200](https://doi.org/10.1145/3233188.3233200).
- [319] T. J. Cain, “The Application of GPU to Molecular Communication Studies,” Master’s thesis, Eastern Washington University, 2018.

- [320] N. Varshney, A. K. Jagannatham, and P. K. Varshney, “On Diffusive Molecular Communication with Mobile Nanomachines,” in *52nd Annual Conference on Information Sciences and Systems (CISS)*, pp. 1–6, IEEE, 2018. [doi:10.1109/CISS.2018.8362192](https://doi.org/10.1109/CISS.2018.8362192).
- [321] Y. Deng, A. Noel, W. Guo, A. Nallanathan, and M. Elkashlan, “Analyzing Large-Scale Multiuser Molecular Communication via 3-d Stochastic Geometry,” *IEEE Transactions on Molecular, Biological and Multi-Scale Communications*, vol. 3, no. 2, pp. 118–133, 2017. [doi:10.1109/TMBMC.2017.2750145](https://doi.org/10.1109/TMBMC.2017.2750145).
- [322] C. Harper, M. Pierobon, and M. Mazarini, “Estimating Information Exchange Performance of Engineered Cell-to-Cell Molecular Communications: a Computational Approach,” in *IEEE INFOCOM 2018-IEEE Conference on Computer Communications*, pp. 729–737, IEEE, 2018. [doi:10.1109/INFOCOM.2018.8485834](https://doi.org/10.1109/INFOCOM.2018.8485834).
- [323] M. R. Bhatnagar and Ankit, “M-ary Poisson Reception in Molecular Communication,” *Micro & Nano Letters*, vol. 13, no. 4, pp. 509–513, 2018. [doi:10.1049/mnl.2017.0665](https://doi.org/10.1049/mnl.2017.0665).
- [324] W. Guo, Y. Deng, H. B. Yilmaz, N. Farsad, M. Elkashlan, A. Eckford, A. Nallanathan, and C.-B. Chae, “SMIET: Simultaneous Molecular Information and Energy Transfer,” *IEEE Wireless Communications*, vol. 25, no. 1, pp. 106–113, 2018. [doi:10.1109/MWC.2017.1600308](https://doi.org/10.1109/MWC.2017.1600308).
- [325] Y. Zhou, Y. Chen, R. D. Murch, R. Wang, and Q. Zhang, “Simulation Framework for Touchable Communication on NS3Sim,” *Nano communication networks*, vol. 16, pp. 26–36, 2018. [doi:10.1016/j.nancom.2018.03.002](https://doi.org/10.1016/j.nancom.2018.03.002).
- [326] Z. Xie, J. Hall, I. P. McCarthy, M. Skitmore, and L. Shen, “Standardization Efforts: The Relationship Between Knowledge Dimensions, Search Processes and Innovation Outcomes,” *Technovation*, vol. 48, pp. 69–78, 2016. [doi:10.1016/j.technovation.2015.12.002](https://doi.org/10.1016/j.technovation.2015.12.002).
- [327] L. Felicetti, S. S. Assaf, M. Femminella, G. Reali, E. Alarcon, and J. Sole-Pareta, “The Molecular Communications Markup Language (MolComML),” *Nano communication networks*, vol. 16, pp. 12–25, 2018. [doi:10.1016/j.nancom.2018.03.001](https://doi.org/10.1016/j.nancom.2018.03.001).
- [328] M. Hucka, A. Finney, H. M. Sauro, H. Bolouri, J. C. Doyle, H. Kitano, A. P. Arkin, B. J. Bornstein, D. Bray, A. Cornish-Bowden, A. A. Cuellar, S. Dronov, E. D. Gilles, M. Ginkel, V. Gor, I. I. Goryanin, W. J. Hedley, T. C. Hodgman, J.-H. Hofmeyr, P. J. Hunter, N. S. Juty, J. L. Kasberger, A. Kremling, U. Kummer, N. L. Novère, L. M. Loew, D. Lucio, P. Mendes, E. Minch, E. D. Mjolsness, Y. Nakayama, M. R. Nelson, P. F. Nielsen, T. Sakurada, J. C. Schaff, B. E. Shapiro, T. S. Shimizu, H. D. Spence, J. Stelling, K. Takahashi, M. Tomita, J. Wagner, and J. Wang, “The Systems Biology Markup Language (SBML): a Medium for Representation and Exchange of Biochemical Network Models,” *Bioinformatics*, vol. 19, no. 4, pp. 524–531, 2003. [doi:10.1093/bioinformatics/btg015](https://doi.org/10.1093/bioinformatics/btg015).

- [329] M. Turan, M. Ş. Kuran, H. B. Yılmaz, C.-B. Chae, and T. Tuğcu, “MOL-eye: A New Metric for the Performance Evaluation of a Molecular Signal,” in *Wireless Communications and Networking Conference (WCNC), 2018 IEEE*, pp. 1–6, IEEE, 2018. [doi:10.1109/WCNC.2018.8377049](https://doi.org/10.1109/WCNC.2018.8377049).
- [330] L. Felicetti, M. Femminella, G. Realì, T. Nakano, and A. V. Vasilakos, “TCP-like Molecular Communications,” *IEEE Journal on Selected Areas in Communications*, vol. 32, no. 12, pp. 2354–2367, 2014. [doi:10.1109/JSAC.2014.2367653](https://doi.org/10.1109/JSAC.2014.2367653).
- [331] M. C. Gürsoy, A. E. Pusane, and T. Tuğcu, “Molecule-as-a-frame: A Frame Based Communication Approach for Nanonetworks,” *Nano communication networks*, vol. 16, pp. 45–59, 2018. [doi:10.1016/j.nancom.2018.02.005](https://doi.org/10.1016/j.nancom.2018.02.005).
- [332] S. Mishra, C. Ghanshyam, N. Ram, S. Singh, R. Bajpai, and R. Bedi, “Alcohol Sensing of Tin Oxide Thin Film Prepared by Sol-Gel Process,” *Bulletin of Materials Science*, vol. 25, no. 3, pp. 231–234, 2002. [doi:10.1007/BF02711159](https://doi.org/10.1007/BF02711159).
- [333] S. Giannoukos, B. Brkić, S. Taylor, A. Marshall, and G. F. Verbeek, “Chemical Sniffing Instrumentation for Security Applications,” *Chemical Reviews*, vol. 116, no. 14, pp. 8146–8172, 2016. [doi:10.1021/acs.chemrev.6b00065](https://doi.org/10.1021/acs.chemrev.6b00065).
- [334] R. Johnson, R. G. Cooks, T. Allen, M. Cisper, and P. Hemberger, “Membrane Introduction Mass Spectrometry: Trends and Applications,” *Mass Spectrometry Reviews*, vol. 19, no. 1, pp. 1–37, 2000. [doi:10.1002/\(SICI\)1098-2787\(2000\)19:1<1::AID-MAS1>3.0.CO;2-Y](https://doi.org/10.1002/(SICI)1098-2787(2000)19:1<1::AID-MAS1>3.0.CO;2-Y).
- [335] K. Demeestere, J. Dewulf, B. De Witte, and H. Van Langenhove, “Sample Preparation for the Analysis of Volatile Organic Compounds in Air and Water Matrices,” *Journal of Chromatography A*, vol. 1153, no. 1-2, pp. 130–144, 2007. [doi:10.1016/j.chroma.2007.01.012](https://doi.org/10.1016/j.chroma.2007.01.012).
- [336] S. Giannoukos, B. Brkić, S. Taylor, and N. France, “Membrane Inlet Mass Spectrometry for Homeland Security and Forensic Applications,” *Journal of the American Society for Mass Spectrometry*, vol. 26, no. 2, pp. 231–239, 2015. [doi:10.1007/s13361-014-1032-7](https://doi.org/10.1007/s13361-014-1032-7).
- [337] H. Strathmann, “Membrane Separation Processes: Current Relevance and Future Opportunities,” *AIChE Journal*, vol. 47, no. 5, pp. 1077–1087, 2001. [doi:10.1002/aic.690470514](https://doi.org/10.1002/aic.690470514).
- [338] S. Giannoukos, B. Brkić, S. Taylor, and N. France, “Monitoring of Human Chemical Signatures using Membrane Inlet Mass Spectrometry,” *Analytical chemistry*, vol. 86, no. 2, pp. 1106–1114, 2013. [doi:10.1021/ac403621c](https://doi.org/10.1021/ac403621c).

- [339] B. Brkić, S. Giannoukos, N. France, R. Murcott, F. Siviero, and S. Taylor, “Optimized DLP Linear Ion Trap for a Portable Non-Scanning Mass Spectrometer,” *International Journal of Mass Spectrometry*, vol. 369, pp. 30–35, 2014. [doi:10.1016/j.ijms.2014.06.004](https://doi.org/10.1016/j.ijms.2014.06.004).
- [340] S. Giannoukos, B. Brkić, and S. Taylor, “Analysis of Chlorinated Hydrocarbons in Gas Phase using a Portable Membrane inlet Mass Spectrometer,” *Analytical Methods*, vol. 8, no. 36, pp. 6607–6615, 2016. [doi:10.1039/C6AY00375C](https://doi.org/10.1039/C6AY00375C).
- [341] S. Giannoukos, A. Agapiou, and S. Taylor, “Advances in Chemical Sensing Technologies for VOCs in Breath for Security/Threat Assessment, Illicit Drug Detection, and Human Trafficking Activity,” *Journal of Breath Research*, vol. 12, no. 2, p. 027106, 2018. [doi:10.1088/1752-7163/aa95dd](https://doi.org/10.1088/1752-7163/aa95dd).
- [342] S. Giannoukos, M. J. A. Joseph, and S. Taylor, “Portable Mass Spectrometry for the Direct Analysis and Quantification of Volatile Halogenated Hydrocarbons in the Gas Phase,” *Analytical Methods*, vol. 9, no. 6, pp. 910–920, 2017. [doi:10.1039/C6AY03257E](https://doi.org/10.1039/C6AY03257E).
- [343] W. Paul and H. Steinwedel, “Ein neues Massenspektrometer ohne Magnetfeld [a New Mass Spectrometer without Magnetic Field],” *Zeitschrift für Naturforschung A*, vol. 8, no. 7, pp. 448–450, 1953. [doi:10.1515/zna-1953-0710](https://doi.org/10.1515/zna-1953-0710).
- [344] C. E. Baukal Jr, V. Gershstein, and X. J. Li, *Computational Fluid Dynamics in Industrial Combustion*. CRC press, 1st ed., 2000. **ISBN-13:** 978-0849320002.
- [345] B. R. Kusse and E. A. Westwig, *Mathematical Physics: Applied Mathematics for Scientists and Engineers*. John Wiley & Sons, 2nd ed., 2010. **ISBN-13:** 978-3527406722.
- [346] L. C. Andrews, *Special Functions of Mathematics for Engineers*. Oxford University Press, 2nd ed., 1997. **ISBN-13:** 978-0819483713.
- [347] J. M. Stockie, “the Mathematics of Atmospheric Dispersion Modeling,” *Siam Review*, vol. 53, no. 2, pp. 349–372, 2011. [doi:10.1137/10080991X](https://doi.org/10.1137/10080991X).
- [348] M. Çağlar, “Velocity Fields with Power-law Spectra for Modeling Turbulent Flows,” *Applied Mathematical Modelling*, vol. 31, no. 9, pp. 1934–1946, 2007. [doi:10.1016/j.apm.2006.08.001](https://doi.org/10.1016/j.apm.2006.08.001).
- [349] F. P. Incropera, A. S. Lavine, T. L. Bergman, and D. P. DeWitt, *Fundamentals of Heat and Mass Transfer*. Wiley, 6th ed., 2006. **ISBN-13:** 978-0471457282.
- [350] R. F. Probstein, *Physicochemical Hydrodynamics: an Introduction*. John Wiley & Sons, 2nd ed., 2003. **ISBN-13:** 978-0471458302.
- [351] D. Frenkel and B. Smit, *Understanding Molecular Simulation: from Algorithms to Applications*, vol. 1. Academic Press, 2nd ed., 2001. **ISBN-13:** 978-0122673511.

- [352] W. W. Daniel, *Applied Nonparametric Statistics*. Houghton Mifflin, 2nd ed., 1980. [ISBN-13: 978-0534381943](#).
- [353] R. E. Walpole, R. H. Myers, S. L. Myers, and K. Ye, *Probability and Statistics for Engineers and Scientists, MyLab Statistics Update*. Pearson, 9th ed., 2016. [ISBN-13: 978-0134115856](#).
- [354] M. Abramowitz and I. A. Stegun, *Handbook of Mathematical Functions: with Formulas, Graphs, and Mathematical Tables*. Dover Books on Mathematics, revised ed., 1965. [ISBN-13: 978-0486612720](#).
- [355] H. Melville, *Moby-Dick; or, the Whale*. Harper & Brothers, 1851. [ISBN-13: 978-0007925568](#).